MILL ROLL PROFILE CONTROL BY MEANS OF SPRAY COOLING

by

Donovan St. P. Collins, B.Sc., M.Sc.

Thesis submitted in partial

fulfillment for the

CNAA

Degree of Doctor of Philosophy

Dorset Institute

and

Davy McKee (Poole) Ltd.

September, 1989

CONTENTS

APPENDIX E
MEASURED DATA

APPENDIX F
GRAPHS COMPARING MEASURED TEMPERATURES AND THERMAL CAMBERS TO CALCULATED VALUES

APPENDIX G
GRAPHS SHOWING VARIATION OF ROLL SURFACE TEMPERATURE AND ROLL DIAMETRAL EXPANSION WITH HEAT TRANSFER COEFFICIENT

APPENDIX H
GRAPHS SHOWING VARIATION OF STRIP CROWN WITH CHANGES IN SPRAY PATTERNS AND WORK ROLL BENDING FORCE

ACKNOWLEDGEMENTS

The author acknowledges with thanks the guidance and technical assistance given by his supervisors, Dr. P. Atack of Davy McKee (Poole) Ltd., and Dr. K. Tabeshfar of Dorset Institute.

Much helpful discussions and technical advice were also contributed by members of the Technology and Development team at Davy McKee, in particular Mssrs. S. Green and P. Round. The typing of the script was helped greatly by Mrs. M. Larter. The author is very grateful.

This research project was sponsored by the Science and Engineering Research Council - Department of Trade and Industry Teaching Company Scheme.

AUTHORS NOTE

All the work submitted in this thesis is the sole and original work of the author, except where otherwise stated by acknowledgement or by reference.

SUMMARY

A 2-dimensional model of a mill roll temperature distribution and radial thermal expansion is presented. The emphasis is on selective axial coolant distribution as a method of controlling strip profile. The Fourier equations describing heat conduction are solved using the method of finite differences. The following effects are considered: (i) The temperature distribution within the roll and strip just prior to entry to the roll bite. (ii) The heat generated in the strip due to deformation. (iii) The heat generated by friction between the strip and the roll. (iv) The temperature distribution of the strip and roll after each pass. (v) The heat conducted into the roll when in contact with the strip. (vi) The heat removed from the roll by the coolant, the air and the back-up rolls . The model also takes account of the geometry of the roll. This complexity means that different models for the roll and strip temperature distributions are required. The model evaluates individual heat transfer coefficients along the axis of the roll in order to simulate the effectiveness of each spray zone in removing heat from the roll. A simplified method of evaluating roll thermal cambers, derived from the model, is presented. The model shows good agreement between predicted and measured roll thermal cambers.

The model is linked to a strip profile prediction model and used to investigate the effects of changing spray patterns and roll bend on profile. It was found that changing spray pattern has a significant effect on strip profile. It was concluded that: (i) Level spray patterns gave the best shape. (ii) Edge sprays sensitivity is important. (ii) Over-cooling outside the strip provides good parabolic shape. (iv) A change to exit side spray levels has a significant effect on strip profile. (v) Exit side sprays

only has a tendency of rolling out the middle of the slab (i.e. a flat middle). (vi) All level sprays on the exit side of the roll only produce a distorted profile on the strip. It was also found that for any given change in roll thermal camber, there is a corresponding change in strip profile. The two changes can be related by a linear factor. The value of this factor has been investigated and found to be product and mill dependent.

CHAPTER 1

INTRODUCTION

During the rolling of a hot aluminium slab, its cross-sectional area is reduced by a succession of passes through two steel or iron work rolls, rotating in opposite directions. In a four-high mill the work rolls are supported by two back-up rolls of larger diameters (as in fig. 1.1). The mills may be arranged in a tandem train where the thickness of the metal is reduced successively in two or more stands. Rolling of the slab can also be carried out in the single stand of a reversing mill by forcing the metal to travel firstly in one direction, then in the other direction . Coolant flowing over the rolls removes heat imparted to the rolls due to contact with the hot strip and friction between strip and rolls. The product from the hot mill may be further rolled in a cold mill.

The markets for flat-rolled aluminium products include can stocks, car and other commercial vehicle body panels and household aluminium foil. The clients demand that the rolled product be of high quality, in particular, exhibits no sheet defects, such as surface buckles, and be of acceptable surface finish. The producers of these products themselves demand, due to the present economic conditions, continually greater efficiencies in production. The

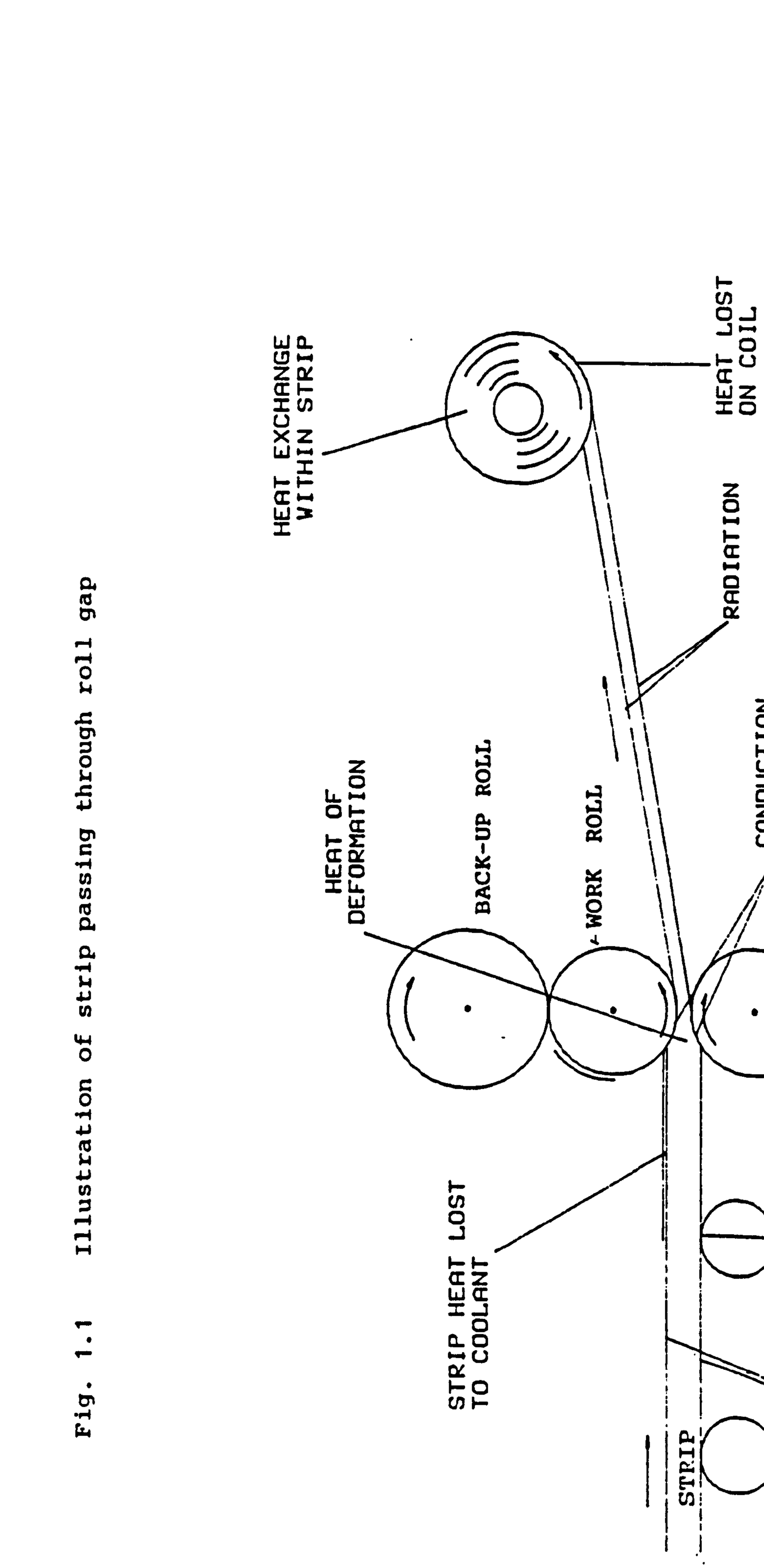
Illustration of strip passing through roll gap
HEAT EXCHANGE WITHIN STRIP
HEAT LOST ON COIL
HEAT OF DEFORMATION
BACK-UP ROLL
WORK ROLL
CONDUCTION BETWEEN ROLLS AND STRIP
RADIATION
STRIP HEAT LOST TO COOLANT
HEAT LOST TO ROLLERS
STRIP
ROLLER
HEAT LOST VIA CONVECTION TO AIR

Fig. 1.1

simultaneous demands of producers and end-users require the accomplishment of the extremely difficult task of producing aluminium strip to narrow dimensional tolerances, tight flatness, temperature and metallurgical specifications at very high rolling speeds. These difficulties are compounded when it is understood that the constraints above apply to products which may differ in alloy types, widths, thicknesses and coil weights, and, on occasions, in product batches of less than ten coils. Thus, when "steady-state" rolling conditions are not achieved, a large number of process variables have to be re-adjusted from product to product to ensure acceptable product quality. Some of these variables are strip entry and exit temperatures and thicknesses, work roll temperatures, mill power consumption, lubricant and coolant flows and strip tensions. Former industrial practices involved adhering to rigid rolling patterns to ensure good quality products. The many process variables proving impossible to control manually to meet the stated criteria, have pushed the rolling industry towards the installation of automatic monitoring and adaptive computer control systems in order to produce strips of acceptable shape.

Shape, as a measure of product quality, is defined by Bryant et al.[97] as the "departure from flatness of the rolled strip (that is, the degree of buckling), and is caused by non-uniform transverse stress distributions at the roll gap exit" when laid flat under zero tension conditions. If residual stresses are large enough to cause visible buckling of the strip, then the term "manifest shape" is applicable and during rolling may be influenced by changing the mean tension in the strip. The term "latent shape" applies when the tension stresses are insufficient to cause visible buckling. Figure 1.2 illustrates some typical flatness problems including tight edge and quarter buckles.

Fig. 1.2 Strip Flatness Defects

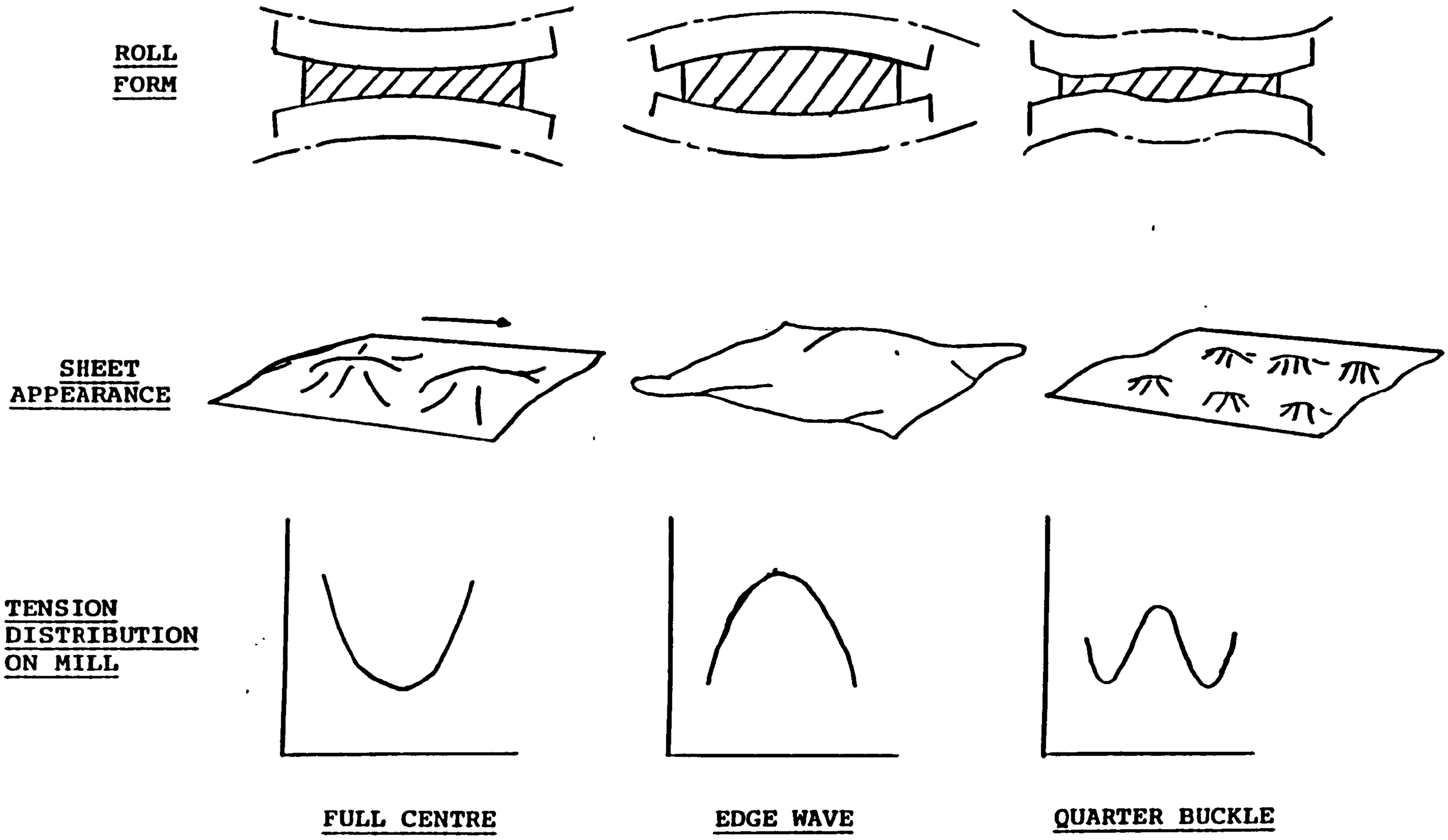

The transverse gauge distribution, termed profile (see fig. 1.3), which is of interest to this study, has a significant effect on strip shape. The highly complex interactions in the pre-set roll-gap between elastic deformation and deflection of the rolls, plastic deformation of the strip, roll wear and the heat transfer between the strip, rolls and the external environments are the final contributors to the shape of the end product.

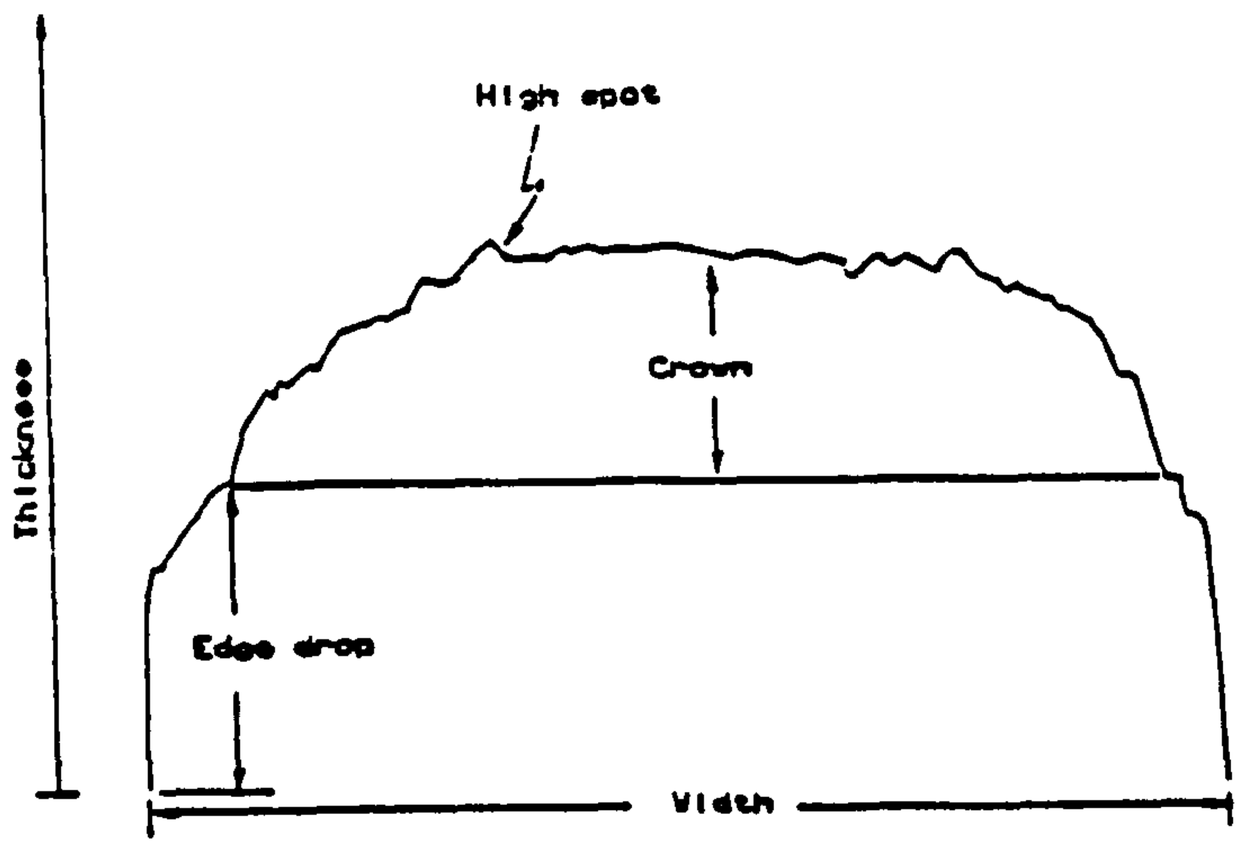

Fig. 1.3 Illustration of strip showing profile (crown, edge drop and high spots).

It is accepted in the rolling industry that in order to produce high quality flat cold-rolled strip, the degree of crown in the hot strip has to be minimised. Indeed, can makers in particular are demanding zero crown so that consistency in their production processes can be achieved. It is therefore essential that hot strip mills are capable of producing low strip profile. A hot mill with this capability will have an important market advantage, so the significance of adopting a profile control policy and control system becomes apparent.

Deflection of the work rolls is partly compensated for by using larger back-up rolls. Further restriction and control

of elastic roll bending is provided by the use of external bending jacks, and by careful roll grinding. Dynamic mill scheduling control also has an important part to play in the achievement of high quality strip and consistency of product. These methods, among others, offer a wide range of control, but an important additional method, control of the roll thermal expansion by selective coolant application, has been relatively neglected by the rolling industry. It is in this area that this study is undertaken. Roll thermal camber, or the difference in transverse expansion of the work rolls, is readily admitted as a serious cause of bad shape.

At present selective spray control in hot rolling is handicapped by inaccurate dynamic measurements of strip shape. This is because the technical difficulties are formidable, due mainly to the operating environment. A shape detector for a hot strip mill must operate during high temperatures (in the range of 300 ^{o}C - 500 ^{o}C for hot aluminium rolling; and between 800 ^{o}C - 1000 ^{o}C in steel mills). The sensor needs to be shock resistant, easy to install and maintain, and require accuracies of the order of 1 μm. The continuing basis towards higher rolling speed will therefore amplify the difficulties of controlling roll thermal camber.

The temperature distribution, and thence the thermal expansion can, however, be simulated by mathematical models, and are important since they can be used to predict the complete temperature history of the rolls. Such information can be used to determine the coolant distribution on-line in real-time control systems, or off-line in simulation and optimisation studies of schedule and plant design.

Engineering science is continually faced with the problem of improving the mathematical models used in the design and evaluation of equipment and processes; hot aluminium

rolling is no exception. This can often be achieved by the eradication of simplifying assumptions. Elimination of assumptions frequently leads to the elucidation of an unrecognized problem, formulation of a corrective theory and an enhancement of the state of the art. Often, too, the solution of the mathematical equations involved becomes increasingly difficult.

The problem of predicting the transient temperature behaviour in the work rolls is to derive an acceptably accurate analytical model for a cylinder of finite length, rotating at high speeds, and subjected to heat transfer over its surface. An accurate model can suggest simplified methods of calculations.

The aim of this work is to provide a unified theory of the spray cooling of mill rolls and its effect on strip profile and to present a functional control algorithm for on-line process control during rolling. To achieve this objective it is proposed to:-

1. Solve the time dependent heat conduction equation in cylindrical co-ordinates using the finite difference techniques. The boundary conditions will be based on conditions experienced by mill rolls.

2. Calculate the variation of radial expansion along the roll axis based on the temperature distribution throughout the rolls.

3. Check the thermal camber model against mill data. This includes on site data collection and processing.

4. Use the time dependent heat conduction equations to predict the angular distribution of temperature in a roll subjected to spray cooling.

5. Use the mathematical models to investigate the effect of various types of spray cooling on the angular temperature distribution and thermal camber of mill rolls.

6. Develop a mathematical model of spray cooling and correlate it with experimental data gathered from an in-house test rig.

Following this introductory chapter, a discussion on the literature related to this work can be found in Chapter 2. A detailed mathematical analysis of the roll temperature function is presented in Chapter 3. Supporting models of roll thermal expansion and roll bite heat transfer are given in appendix B and C, respectively. Analytical solutions to the roll temperature equations for simple heat transfer conditions, such as constant boundary conditions, can be found in appendix A. Appendix D gives a description of the structure of the computer algorithms based on the models mentioned above. The method of data collection at actual rolling mills is given in Chapter 4. Chapter 5 shows the comparison between actual plant data and predicted results from the modelling programs. The complexity of the roll thermal camber model is reduced to simpler forms in Chapter 6. The linking of the thermal camber model and a strip profile prediction model is presented in Chapter 7. The conclusions from this study are set out in Chapter 8

CHAPTER 2

LITERATURE SURVEY

2.1 INTRODUCTION

It was pointed out in the previous chapter that strip profile has a significant effect on the final strip flatness of the cold-rolled product. Consequently, it has become of vital necessity for the producer of hot aluminium products to monitor and control aluminium strip profile. Some of the available actuators such as roll bending, roll grinding, dynamic mill scheduling and tension levelling have also been mentioned. These combined methods have, to some degree, contributed to reducing the problem of profile control, but the control of roll thermal camber is agreed to be vital, if total success in combating this problem is to be achieved. Studies[43,39,72,30] have shown that as a contribution to bad shape, thermal camber affects the roll gap to a similar extent as roll bending and roll flattening. This establishes the requirement of an understanding of the mechanisms affecting the control of roll thermal behaviour.

Thermal camber arises through uneven cooling of the work rolls. Severe buckling can develop if a correct coolant control strategy is not employed. A viable coolant control

strategy must embrace the maintenance of the optimum roll and strip temperature distribution along the entire roll-strip contact length. The consequence of which will be the optimization of roll shape, strip profile, flatness and surface quality. It can be appreciated that temperature control during the entire process cycle can only be achieved by an exact degree of selective axial coolant distribution on the work rolls as a means of controlling local roll radial expansion. It follows then that before a reliable control strategy can be implemented, the problem of dynamic temperature measurement or prediction must be solved.

The solution to the problem of controlling thermal camber through correct coolant application can best be tackled through the development of a reliable mathematical model of the transient temperature behaviour of the rolls, and determining exactly the ability of the coolant sprays to remove heat from the rolls, that is, the governing heat transfer coefficient of the cooling fluid. Thus, if the thermal camber could be calculated, when added to the other profile control actuators, it would be possible to adjust rolling schedules on the basis of a few intermittent temperature measurements to constantly re-calibrate the model. If a reliable roll temperature model could be established to give a "primary standard", a simplified method or model could be realised and be used in control software.

The modelling of strip and roll temperature is a complex heat transfer problem which must consider[70]

1. The temperature distribution within the roll and strip just prior to entry to the roll bite.

2. The heat generated in the strip due to deformation.

3. The heat generated by friction between the strip and the roll.

4. The temperature distribution of the strip and roll after each pass.

5. The heat conducted into the roll when in contact with the strip.

6. The heat removed from the roll by the coolant, the air and the back-up rolls .

This complexity means that different models for the roll and strip temperature distribution are required. This study is primarily concerned with the former problem, although it is evident that the two issues cannot be entirely separated. For an effective knowledge of the roll coolant strategy, an exact knowledge of the coolant heat transfer characteristic is also required. The latter problem will be examined in section 2.4 and in Chapter 3.

Several workers have produced models of the roll thermal behaviour. These models are all based on generalised forms of Fourier's heat conduction equation. The models differ in complexities according to the number of simplifying assumptions made. The more important contributions will now be examined.

2.2 ROLL TEMPERATURE MODELS

Peck, et al.[12] (1954) presented the first genuine thermal and mechanical analysis of the roll. This arose from an interest in the failure of iron work rolls caused by thermal stresses. The types of failures that were of interest to these workers involved breaks in the roll. The problem was examined from a "cause" and "effect" stand-

point in which the causes involved the temperatures of the hot sheet and coolant, roll speed and the heat equivalent of work done by the rolls. Effect was deemed mainly to be the temperature pattern of the roll and the normal and shearing stresses on corresponding surfaces due to the unequal temperatures. This was a cold rolling study.

The mathematical model for heat conduction presented by Peck and his co-workers assumed no axial heat conduction. It was further assumed that the heat transferred to the roll due to contact with the strip was removed by uniform circumferential cooling. The heat input was approximated by a line source. Circumferential heat flow was neglected because it was assumed that contact with the heat source was brief compared to the roll speed and that the zone of high temperature on the roll was thin in comparison to the roll circumference. An average and uniform deformation through the arc of contact was assumed based on an average strip velocity, which with frictional heating was factored in by a complex graphical method from an experimental knowledge of roll torque. The roll surface temperature distribution was considered constant. Based on the above discussions, the authors presented the equation below for a one dimensional bar insulated on its sides:

$$\frac{\partial T}{\partial t} = \frac{k}{\rho C_p} \cdot \frac{\partial^2 T}{\partial r^2} \qquad (2.2.1)$$

where:

t = time

r = radial direction

T = temperature

k = coefficient of thermal conductivity

ρ = roll density

C_p = heat capacity at constant pressure.

The determination of the temperature stresses were based on the following equation:

$$\frac{\partial^4\phi}{\partial r^4}+2\frac{\partial^4\phi}{\partial r^2\partial y^2}+\frac{\partial^4\phi}{\partial y^4}=\frac{\alpha E}{1-\mu}\left[\frac{\partial^2 T}{\partial r^2}+\frac{\partial^2 T}{\partial y^2}\right] \qquad (2.2.2)$$

where

ϕ = stress function

α = coefficient of linear expansion

E = Modulus of Elasticity

μ = Poisson's Ratio

r, y = radial and axial direction, respectively

The authors considered the equations above suitable for hot rolling operations, and solved them by the method of finite differences because it was thought that the number of variables was excessive for analytical solutions. The solution of eqn.(2.2.1) visualised the roll as shown in fig.(2.2.1).

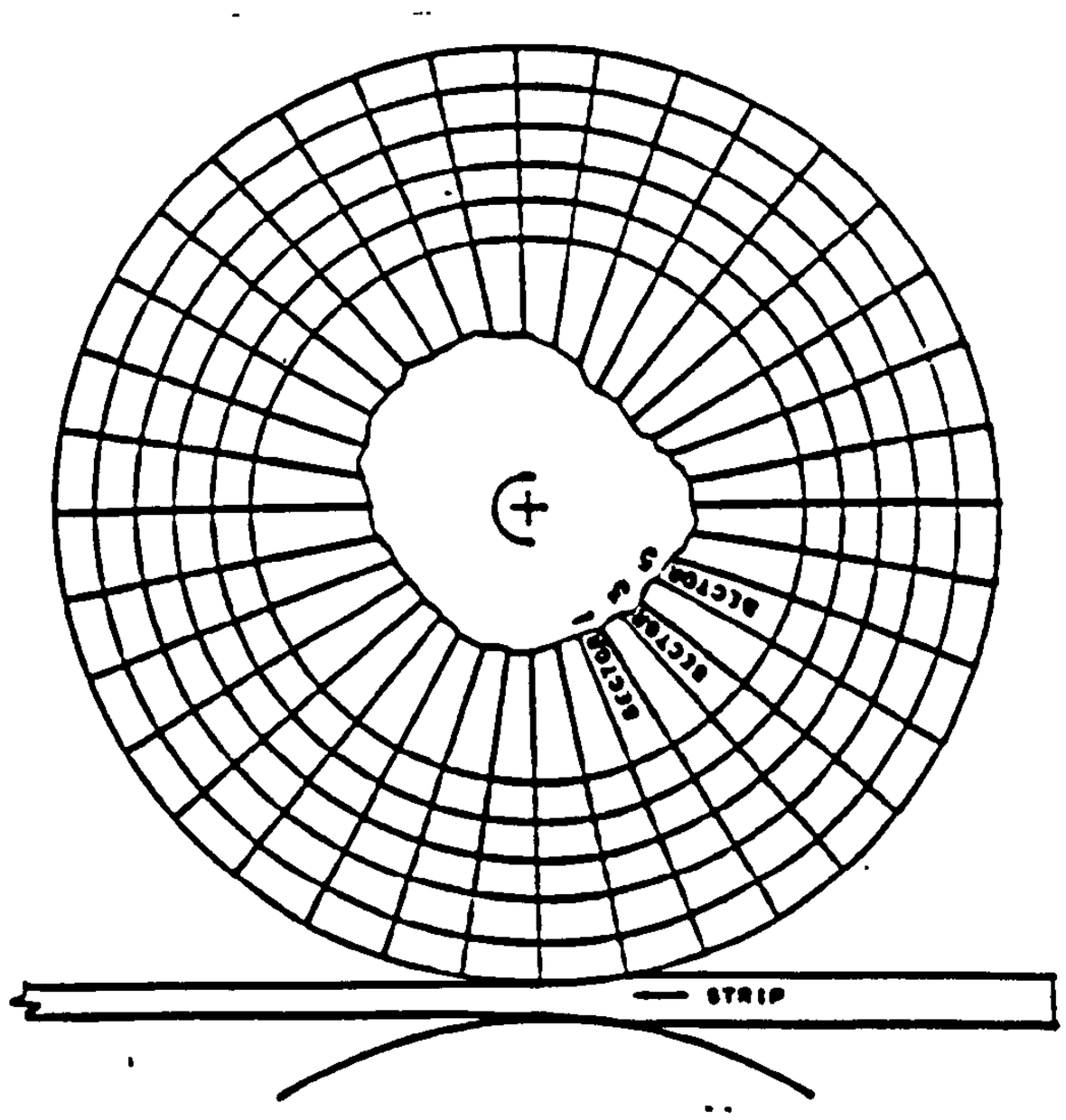

Fig. 2.2.1 Division of the roll into 36 sections for Peck's temperature studies

Several objections can be made to the Peck model, not least of which is the fact that an analysis was made of the case of partial roll cooling. The strip was not treated explicitly and the work of deformation and frictional heating were crudely handled by the introduction of a complicated graphical method. The method, though, can be considered justifiable if it is desired to study the system of the distribution of stresses in only one section of the roll.

Further progress in the area of roll temperature (and stress) prediction was forwarded by Cerni[14] in 1961 when he presented a two-dimensional transient temperature distribution model. He arrived at the following equation:

$$\frac{1}{\kappa}\frac{\partial T^*}{\partial t}=\nabla^2 T^* \qquad (2.2.3)$$

where:

$T^*(r,\theta,t)$ = temperature at any point on the roll (r,θ) as in fig.(2.2.2).

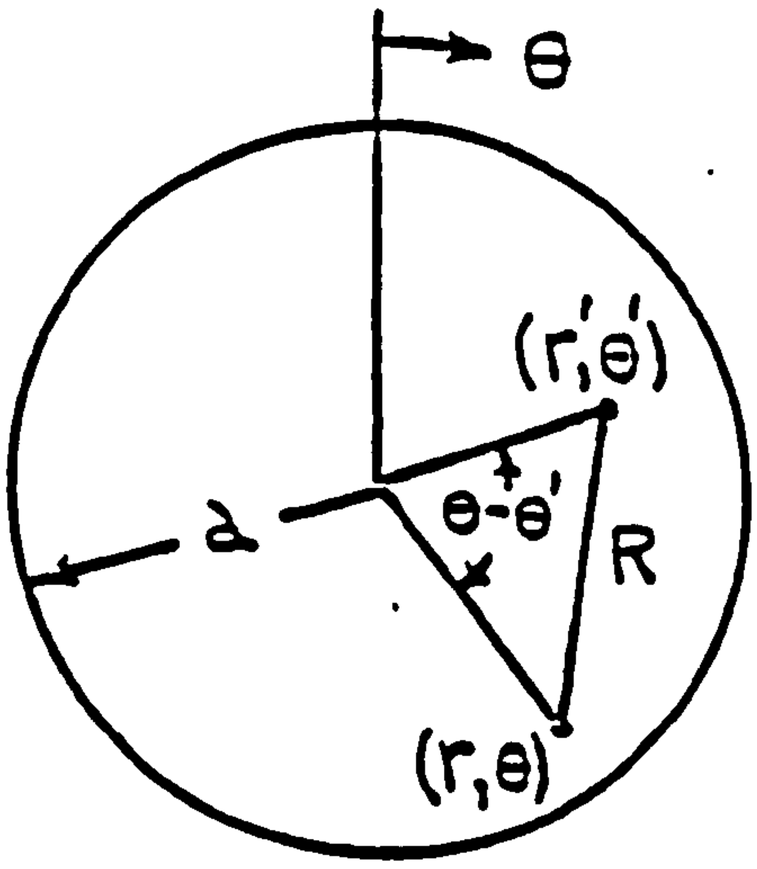

Fig. 2.2.2- Diagram of stationary roll of radius a with an instantaneous line source of heat placed at position (r',θ')

Cerni considered the roll to be stationary, of radius R with an instantaneous unit line source of heat placed at

position (r',θ'). Cerni considered the following boundary conditions:

$$T^*(r,\theta,0) = 0$$

$$T^*(0,\theta,t) \text{ finite}$$

$$T^*(r,\theta,t) \text{ periodic in } \theta$$

$$-k\frac{\partial T^*_{(R,\theta,t)}}{\partial r} = hT^*_{(R,\theta,t)} \qquad (2.2.4)$$

where h = coefficient of heat transfer

He assumed that there was no axial heat flow, that the heat flux to the roll is uniform over the arc of contact, that there were no heat losses to the bearings, and that the heat flux decays exponentially with time. Cerni resorted to a technique used by Jaeger[3] for a rotating line source on a cylinder to solve eqn.(2.2.3) analytically.

Although Cerni's work was more involved than Peck et al.[12] it could likewise be objected to because of the omission of axial conduction which meant it was a sectional study only. The work does not provide the flexibility needed to study cooling in depth (which is understandable, since the computing techniques then available, ensured that these solutions had to estimate the effects).

The next major contribution in developing a mathematical model capable of predicting work roll temperatures came from Pawelski[29] in 1971. He presented a one dimensional model of the temperature field in a roll suitable for hot and cold rolling. He assumed that no heat was conducted axially, and that conduction occurred only in a radial direction, whilst at the surface heat was transferred circumferentially by convection. Therefore, in the roll body heat transfer is governed by the equation:

$$\frac{\partial T}{\partial t} = \kappa\left[\frac{\partial^2 T}{\partial r^2} + \frac{1}{r}\cdot\frac{\partial T}{\partial r}\right] \qquad (2.2.5)$$

It was further assumed that the roll is long enough for thermal equilibrium to be achieved, so that, considered from the spatial context, a stable temperature field should exist. It follows then that only a section of the roll will vary in temperature, restricted to a thin surface layer for the usual situation of very rapid roll revolutions. Below this layer Pawelski considered that the temperature is close to that of the roll core, and for such a situation radial conduction is also limited to the surface layer. Hence, eqn. (2.2.5) can be modified to give:

$$\frac{\partial T}{\partial t} = \kappa\left[\frac{\partial^2 T}{\partial r^2} + \frac{1}{R}\cdot\frac{\partial T}{\partial r}\right] \qquad (2.2.6)$$

Making the substitution

$$r = R - Z \qquad (2.2.7)$$

to generate the equation

$$\frac{\partial T}{\partial t} = \left[\frac{\partial^2 T}{\partial z^2} - \frac{1}{R}\cdot\frac{\partial T}{\partial z}\right] \qquad (2.2.8)$$

means that the heat flow in the Z direction is opposite to the direction of r. For a boundary condition it was assumed that the periodical changes in temperature of a surface element is known. Pawelski presented the solution of eqn. (2.2.8) to be

$$T = \sum_{j=0}^{\infty} e^{-B_j x}\left[M_j \cos(j\phi - B_j x) + N_j \sin(j\phi - B_j x)\right] \qquad (2.2.9)$$

where $\phi = \omega t$

ω = angular velocity of roll

$$B_j = \sqrt{\frac{\omega j}{2\kappa}}$$

and M_j , N_j are arbitrary constants

For x = 0, eqn. (2.2.9) yields

$$T_o = \sum_{j=0}^{\infty} \left(M_j \cos(j\phi) + N_j \sin(j\phi) \right) \qquad (2.2.10)$$

where T_0 is the surface temperature and is to be assumed known.

Pawelski examined the special case for

$$T_o = e^{-H\phi} \qquad 0 \le \phi \le 2\pi \qquad (2.2.11)$$

for which T_0 is the "related excess temperature" T_u/T_{max}. The "excess temperature", T_u, is the difference in temperature compared with the temperature at the entrance to the roll gap. The increase in temperature in the roll gap is T_{umax}. Fig. 2.2.4 is a plot of the function $T_0(\phi)$ for different values of the exponent H.

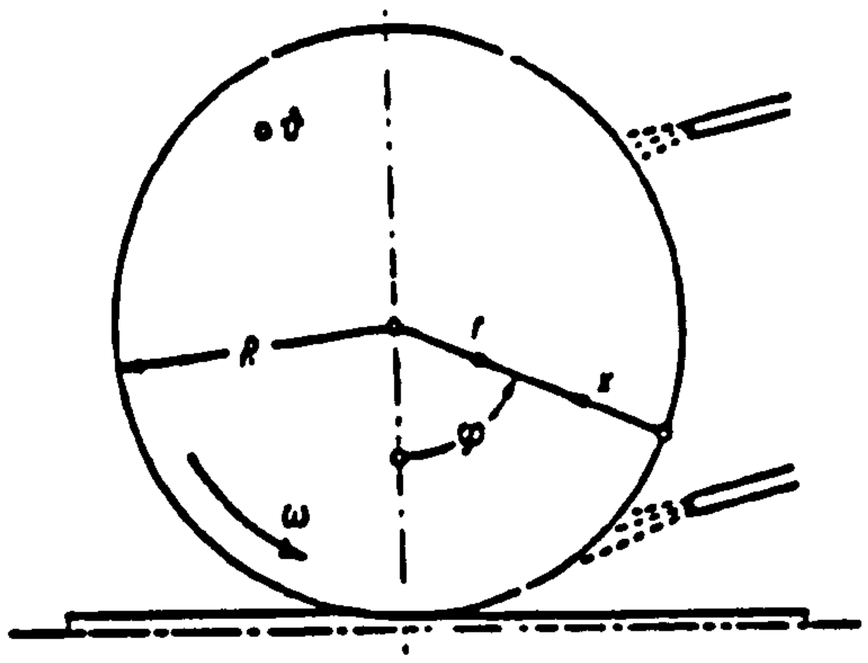

Fig. 2.2.3

Fig.2.2.3 Diagram of roll for Pawelski's model.

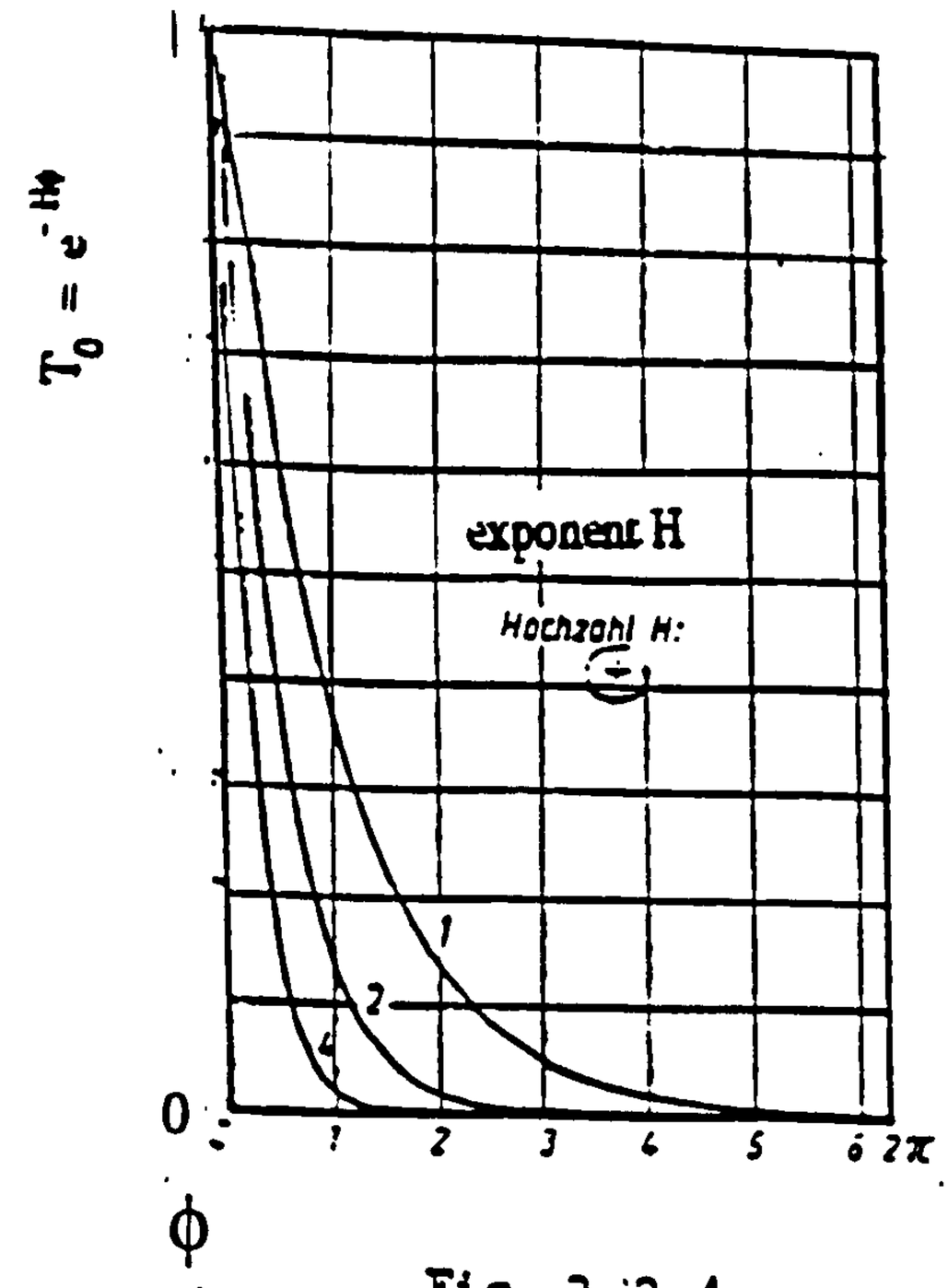

Fig. 2.2.4

Fig.2.2.4 Related excess temp. v heat transfer coefficient (eqn. 2.2.11)

In fig.2.2.4 the position of the clearance between the rolls is at the points $\phi = 0$ or 2π so that the related excess temperature increases instantaneously from 0 to 1 (because of the assumption of negligible circumferential conduction of heat). In the next revolution T_0 is equal to zero once more due to cooling, the exponent H being a measure of the speed of reduction of temperature.

Hence, the Fourier series which results from the conditions discussed above is stated as:

$$T_0 = \frac{1}{2\pi H}\left(1 - e^{-2\pi H}\right)\left[1 + 2H\sum_{j=1}^{\infty}\frac{1}{H^2 + j^2}.\left(H\cos j\phi + j\sin j\phi\right)\right] \qquad (2.2.12)$$

and for which the temperature distribution in the roll is:

$$T = \frac{1}{2\pi H}\left(1 - e^{-2\pi H}\right).\left(1 + 2H\sum_{j=1}^{\infty}\frac{e^{-B_j x}}{H^2 + j^2}\left[H\cos\left(j\phi - B_j x\right) + j\sin\left(j\phi - B_j x\right)\right]\right) \qquad (2.2.13)$$

As x --> ∞ eqn.(2.2.13) becomes (2.2.14) which is the temperature in the core of the roll.

$$T = \frac{1}{2\pi H}\left(1 - e^{-2\pi H}\right) \qquad (2.2.14)$$

Using eqn. (2.2.13) Pawelski presented an examination of the roll temperature distribution for values of $0 \leq x \leq 3$mm and for $0 \leq \phi \leq 2\pi$, and various values of ω. He found that almost no temperature fluctuation exists below 3mm from the roll surface, and fluctuations decrease in size as the angular velocity is increased. Pawelski also found that the better the cooling, i.e. the larger the value of H, the smaller the penetration depth of the temperature waves, and from which it may be concluded that cooling should be effected as soon as the strip leaves the roll bite.

Although Pawelski did not present a comparison of his model with measured data, his assumptions are reasonable, and hence the model, subject to some important qualifications:

heat conduction in the direction of the roll axis can only be ignored where the temperature gradients across the roll are small, such as the section of the roll covered by the strip. However, at the strip edge there are quite large temperature gradients so that Pawelski's model does not represent that section of the roll. In a general application of the model, the roll barrel could be considered in sections of individual discs, independent of each other, then applying the equations. The assumption of known surface temperature as a boundary condition and the assumption of thermal equilibrium in the roll invalidates the use of the model in real time application. The analytical solution chosen by Pawelski means that it would be limited to a few special cases in order to arrive at values for the arbitrary constants in the Fourier series developed from eqn.(2.2.9). The model could, however, give a qualitative insight into the important parameters influencing roll temperature.

In 1971, Stevens et al.[27] published a paper on roll cooling based on actual roll temperatures for a medium-width steel hot strip mill. These workers were primarily interested in the problems of thermal fatigue which can be an important factor in roll wear and roll breakage. They presented a simplified analysis of the thermal and plastic- elastic behaviour of the roll surface. To predict the roll surface temperature, a one-dimensional transient heat conduction equation was suggested, based on the idea that the conditions in the roll bite may be considered similar to a flow of heat between two semi-infinite bodies, instantaneously coming into contact with a thin insulating layer between them. This leads to the equation

$$\frac{\partial T}{\partial t} = \alpha \frac{\partial T}{\partial r} \qquad (2.2.15)$$

with the boundary conditions:

$$-k\frac{\partial T}{\partial r} = h(T_s - T_R) \qquad (2.2.16)$$

where:

T_s = temperature of the strip

T_R = temperature of roll surface

r = distance from interface

α = thermal diffusivity

The solution of eqn.(2.2.15) gives

$$T_{R_2} = T_{R_1} + (T_{s_1} - T_{R_1})\left[\frac{H\sqrt{\alpha_R}}{Ak_R}\right].\text{erfc}\frac{r}{2\sqrt{\alpha_R t}} - \exp\left[\frac{Ar}{\sqrt{\alpha_R}} + A^2\right].\text{erfc}\left[\frac{r}{2\sqrt{\alpha_R t}} + A\sqrt{t}\right]$$

(2.2.17)

$$\text{where } A = \frac{H}{k_R k_S}\left[k_R\sqrt{\alpha_S} + k_S\sqrt{\alpha_R}\right] \qquad (2.2.18)$$

where:

H = conductance of insulating layer.

Suffices:

1 = initial time

2 = at time t

R = roll

s = strip

For x = 0

$$T_{R_2} = T_{R_1} + (T_{S_1} - T_{R_1}).\frac{H\sqrt{\alpha_R}}{Ak_R} + \left(1 - e^{-H^2 t}.\,\text{erfc}\,A\sqrt{t}\right) \qquad (2.2.19)$$

Stevens et al.[27] reported good agreement with experimental measurements using equation (2.2.19). They concluded that thermal fatigue can be a major factor in the roughing train and early finishing stands. They also reported a temperature fluctuation of between 20 ^{o}C and 500 ^{o}C on each revolution as the roll passed under the spray header and entered the roll gap. Extreme temperature rises were

limited to a thin surface layer at less than 3.5 mm and is essentially constant at a depth below 7 mm of the roll surface.

The work of Stevens et al.[27] was limited in that no fundamental studies of the mechanisms of roll cooling or roll wear were offered. The study was useful in implementing a method for getting actual temperatures, although somewhat involved to be used readily in rolling mills. The study showed the need to design proper cooling systems. They made use of their findings to implement a new cooling system for the mill investigated. However, the work did not examine roll camber and its effect on strip profile.

Following the work of Stevens et al., Parke and Baker[28] in 1972 published a report on roll cooling for a hot strip mill with the objectives of determining the methods through which roll cooling regimes may be evaluated, deciding the best means of roll cooling, and developing guide lines for work roll cooling in hot rolling. To meet these objectives, it was reasoned that a knowledge of the temperature of the roll's surface layers would suffice. These workers reported, for reasons of financial constraints and the impracticability of obtaining roll surface temperatures, a limitation of the study to a computational method.

To study the temperature variations during the rolling cycles, Parker and Baker presented a mathematical model, as well as the computer program, of a central cross-section of a long cylinder rotating through the varying cooling conditions that occurs during rolling. The model assumes fixed boundary conditions in time and predicts temperatures close to the roll surface. Heat transfer to the work rolls is assumed to result from conduction from the roll surface towards the roll interior, at the slab - roll interface (due to the heat of deformations), ambient cooling, radiation from the slab on entrance to and exit from the

roll bite, spray cooling, cooling by water that adheres to and flows along the roll surface, and heat conducted between the back-up and work rolls.

The heat transfer coefficients for the effect of spray cooling are determined by an equation of the form:

$$h = h_0 \frac{(T_R - T_w)^n}{100} \qquad (2.2.20)$$

where:

h = actual heat transfer coefficient

h_o = basic heat transfer coefficient

T_R = roll surface temperature

T_W = water temperature

n = exponent dependent on flow regime

Parke and Baker[28] reported values for h of between 5.5 - 30 kW m^{-2} $^oK^{-1}$ depending on the spray configuration. The exponent n was determined from the literature on the cooling of heated plates. The determination of valid heat transfer coefficient is paramount in any model of the transient roll temperatures, and as such eqn.(2.2.20) is too over-simplified for use in an automatic spray control system. The heat transfer coefficient for spray cooling needs to be modelled as a function of temperature, jet velocity and flow patterns on the roll surface, the nature of the cooling fluid, and any other relevant parameters.

This model divides the roll circumferentially by a series of equally spaced radial lines into wedges. Radial division is through a pattern of concentric circles not necessarily of equal radial distances apart. Nodes result where radial lines intersect the concentric circles. Thus, the temperatures of an element surrounded by a set of nodes are computed, i.e. the temperature change at each node is

computed during the rotation through an angular width. The calculated change in temperature of an element is derived from the quantity of energy required to store the excess energy transferred from the neighbouring elements during the interval, for a rotation through one wedge angle.

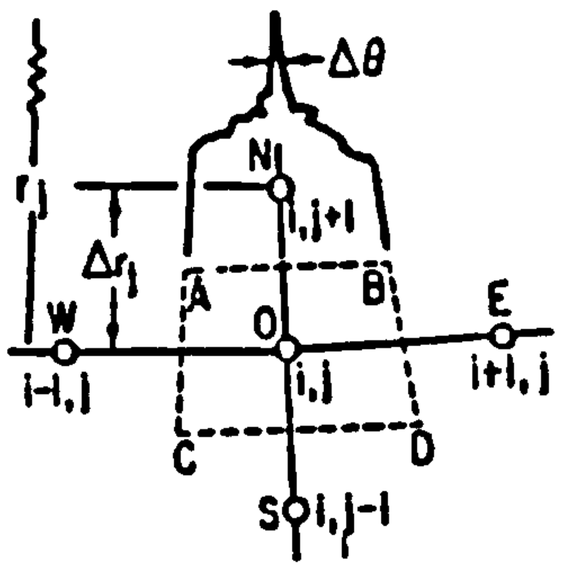

Fig. 2.2.5

The total heat flow through *AB* along *NO* (from *O* to *N*) will be given approximately by $(T_{i,j}-T_{i,j+1})\ (r_j-\Delta r_j/2)\ \Delta\theta\Delta z\ k/\Delta r_j$

Where $T_{i,j}$ is the average temperature measured at *O* and $T_{i,j+1}$ is the average temperature measured at *N* during the time interval $t_k - \Delta t/2 \geq t_k \geq t_k + \Delta t/2$; $\Delta\theta$ is the angular spacing of the radial lines *AC* and *BD* and Δr_j is the distance radially between *N* and *O*; *k* is the coefficient of thermal conductivity.

This computational scheme is useful in performing a detailed calculation of the roll surface temperature, providing the correct heat transfer coefficients are arrived at, but it is too computationally expensive for consideration for on-line applications for spray cooling control. Moreover, only a section of the roll can be considered at any one time, since the model does not assume axial conduction of heat. Although the authors presented much calculated data, they did not measure the roll temperature directly, and hence their model remains untested against good experimental data.

Parke and Baker found that for entry side cooling, heat transfer from the work rolls is greatest immediately the strip leaves the exit side of the roll bite when surface quenching by the back-up rolls occurs, prior to any effect of the cooling sprays. This fact, they reasoned, is due to greater heat flux towards the core of the work and back-up rolls because metal conduction is equivalent to surface film coefficients of heat transfer in the order of 70 kW m^{-2} $^{o}C^{-1}$, or more. These relatively large heat flux rates are due to the steep radial temperature gradients.

Hence, these workers concluded that cooling on the strip entry side is inefficient.

Beeston and Edwards[30] described a comprehensive mathematical model of the cold-rolling process in 1973. Much of this work is applicable to hot rolling with the appropriate modification of some assumptions. These workers assumed a mean heat transfer coefficient and heat input averaged around the roll circumference. Heat conduction to the back-up rolls were assumed negligible as was the cyclic variation in temperature. Hence, Beeston and Edwards[30] were able to employ the Fourier equation for heat conduction within a solid[10], namely,

$$\rho C \frac{\partial \theta}{\partial t} = k \left(\frac{\partial^2 \theta}{\partial r^2} + \frac{1}{r} \frac{\partial \theta}{\partial r} + \frac{\partial^2 \theta}{\partial x^2} \right) + q' \qquad (2.2.21)$$

where:

q' = heat addition to an element per unit volume

ρ = density of work roll

C = specific heat of roll

θ = roll temperature function

k = roll thermal conductivity

x, r = axial and radial coordinates, respectively

Axial symmetry and an equivalent roll length as an approximation to the actual roll length were assumed. This led to the boundary conditions necessary to solve eqn. (2.2.21) using finite difference techniques.

In the same year as the Beeston and Edwards publication[30], Wilmotte and Mignon[32] published their work on thermal camber of work rolls during hot rolling. The mathematical model for the temperature field in the roll is similar to that presented by Beeston and Edwards. Radiative heat

transfer is considered negligible and the heat removed from the work rolls assumed to be by the cooling water, by the air, the back-up rolls and by the bearings. Equivalent heat transfer coefficients are assumed along the roll surface to account for the heat exchanges occurring along these boundaries. Equivalent temperatures are also assumed for the surroundings. The authors resorted to an explicit numerical solution of eqn. (2.2.21)

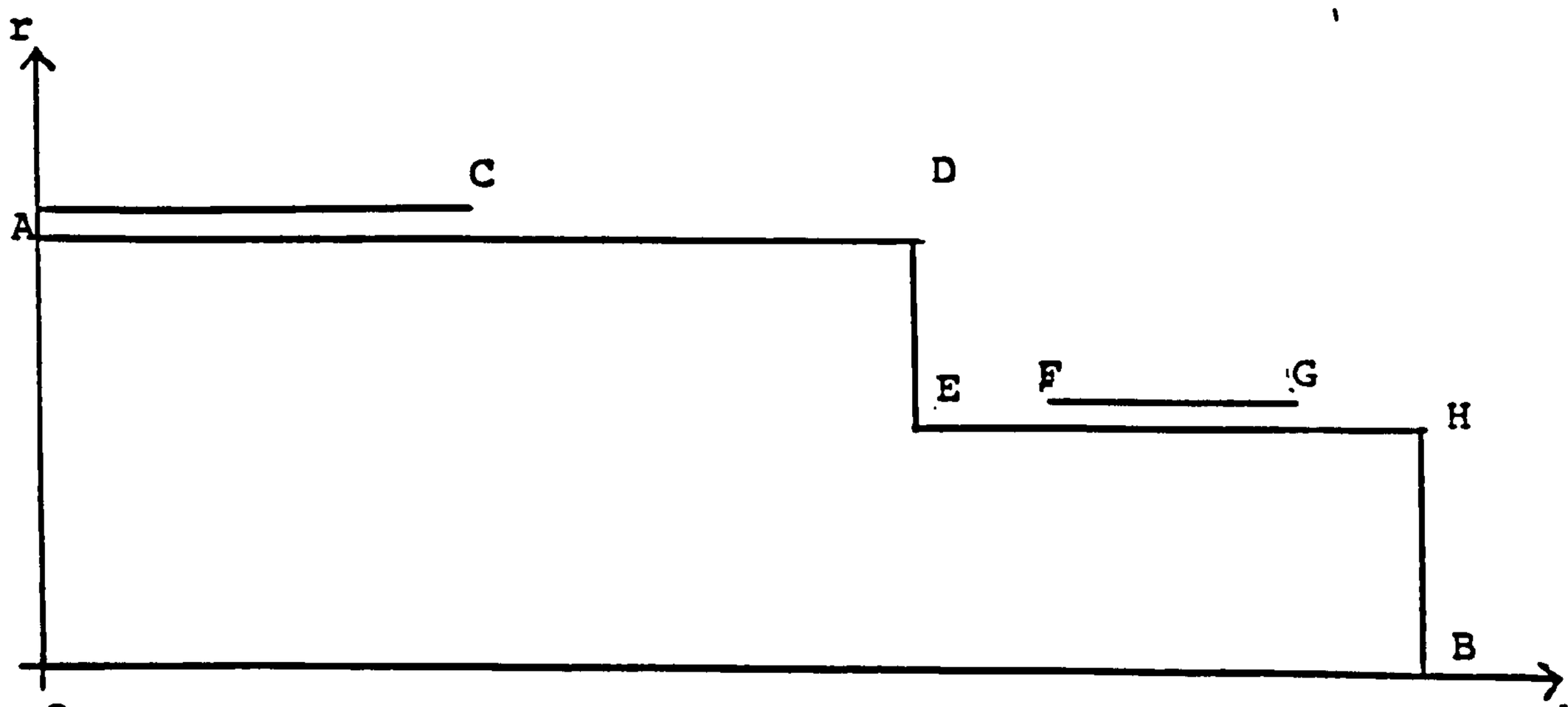

Fig. 2.2.6 Schematic view of roll section and its surroundings

Consider the roll boundaries above.

The boundary conditions were given by Wilmotte and Mignon as follows. Along the roll axes, OA and OB of fig. 2.2.6, respectively

$$\frac{\partial T}{\partial r} = 0 \qquad (2.2.22)$$

and

$$\frac{\partial T}{\partial x} = 0 \qquad (2.2.23)$$

Along ACD, EFGH, there is an equivalent heat transfer coefficient $g^*(x)$, and an equivalent external environment temperature $V^*(x)$, so that

$$-k\frac{\partial T}{\partial x} = g^*_{(x)}(T_{(x)} - V^*_{(x)}) \qquad (2.2.24)$$

and analogously along boundary DE :

$$-k\frac{\partial T}{\partial r} = g^*_{(r)}(T_{(r)} - V^*_{(r)}) \qquad (2.2.25)$$

The characteristics of the equivalent surroundings are as follows

Boundary DEF:

$$g^*_{DEF} = g_a \qquad (2.2.26)$$
$$v^*_{DEF} = v_a$$

Boundary CD:

Any given point along this boundary comes into contact consecutively with air, back-up roll and the coolant. Hence, during one revolution of the roll, the amount of heat exchanged per unit of surface with air is

$$q_a = g_a \int_0^{\tau_a} (T_a - V_a).dt \qquad (2.2.27)$$

where:

τ = time interval

T_a = ambient temperature in contact with the roll

Similar relations apply in respect to the areas in contact with the back-up roll and coolant, i.e., q_{BUR} and q_R, respectively. Hence the total quantity of heat transferred per unit of surface per revolution of the roll is

$$q = g^*_{CD}\left(T_{(x)} - V^*_{CD}\right)\theta \qquad (2.2.28)$$

where:

θ = time for one revolution

Wilmotte and Mignon assumed that the surface temperature $T_{(x)}$ remains constant at T_s for work roll contact with the air, coolant and back-up roll. Similarly the external temperature V^*_{CD} is assumed constant at V_a.

Hence,

$$g^*_{CD} = g_a\frac{\tau_a}{\theta} + g_{BUR}\frac{\tau_{BUR}}{\theta} + g_C\frac{\tau_C}{\theta} \qquad (2.2.29)$$

The authors suggested that the work of Lambert and Economupoulus[109] could be used to determine the heat transfer coefficients, g_a and g_c, whereas the term g_{BUR} can be calculated from an expression proposed by Pawelski[99]:

$$\frac{g_{BUR}\,\tau_{BUR}}{\theta} = m\,\frac{k}{2\pi R_w\sqrt{\kappa_R\,\pi}}\cdot\sqrt{l_c\,\pi} \qquad (2.2.30)$$

where:

κ_R = thermal diffusivity of the roll

l = length

U = linear speed of work rolls

R_w = roll radius

m = constant determined by state of contact between back-up roll and work roll

= 0.3 for imperfect contact

Boundary AC:

The expression for equivalent heat transfer coefficient is given as

$$g^{*}_{AC} = g_a\frac{\tau_a}{\theta} + g_{BUR}\frac{\tau_{BUR}}{\theta} + g_C\frac{\tau_C}{\theta} = g_{eq.} \qquad (2.2.31)$$

and for equivalent temperature

$$V^{*}_{AC} = \left(1-\frac{\tau_g}{\theta}\right)V_a + \frac{\tau_g}{\theta}V' + \frac{\tau_g}{\theta}.\frac{1}{1+\alpha}(V-V') + \frac{1}{\theta}.(V-V')\bullet$$
$$\left(\frac{1}{g^{*}_{eq.}}.\frac{\kappa_{s^D}r}{s} - \frac{1}{1+\alpha}\right)\int_0^{\tau_g}\exp\left(\delta^2\kappa_s t\right)\operatorname{erfc}\left(\delta\sqrt{\kappa_s t}\right).dt \qquad (2.2.32)$$

$$\delta = \frac{\kappa_{s^D}r}{\kappa_s}.\frac{1+\alpha}{\alpha} \qquad (2.2.33)$$

α = coefficient of thermal expansion

V' = temperature of roll before contact: defined as the value of the surface temperature at the middle of the barrel determined for the preceeding interval

s = thickness of oxide layer

suffix

g = roll gap

Reported values of g_a and g_c are given as:

g_a = 1.5 x 10-3 cal mm^{-2} s^{-1} $^oC^{-1}$

g_c = 5.0 x 10-3 cal mm^{-2} s^{-1} $^oC^{-1}$

Good agreement was reported between measured and calculated thermal camber.

Patula[52] in 1981 published an analytical model for the steady-state temperature distribution in a long cylinder rotating at constant speed and subjected to constant surface heat fluxes and convective cooling. Patula assumed that axial heat conduction, because of the long roll assumption, could be neglected; that the cylinder is heated and cooled at various section of the roll surface, thermal properties are uniform and independent of temperature. For this model it was also assumed that steady state temperature existed for any control volume. Based on the above assumptions, eqn. (2.2.34) (refer to fig.2.2.7 below) can be derived[100]:

$$\frac{s}{\kappa R}\cdot\frac{\partial T}{\partial \theta} = \frac{1}{r}\cdot\frac{\partial}{\partial r}\left(r\frac{\partial T}{\partial r}\right) + \frac{1}{r^2}\cdot\frac{\partial^2 T}{\partial \theta^2} \qquad (2.2.34)$$

$$\kappa = \frac{k}{\rho C}$$

where:

s = roll surface speed

k = roll thermal conductivity

κ = $k/\rho C$

θ = angular coordinate

T = temperature difference define as $T_R - T_C$

T_C = coolant temperature

T_R = actual roll temperature

r = radial coordinate

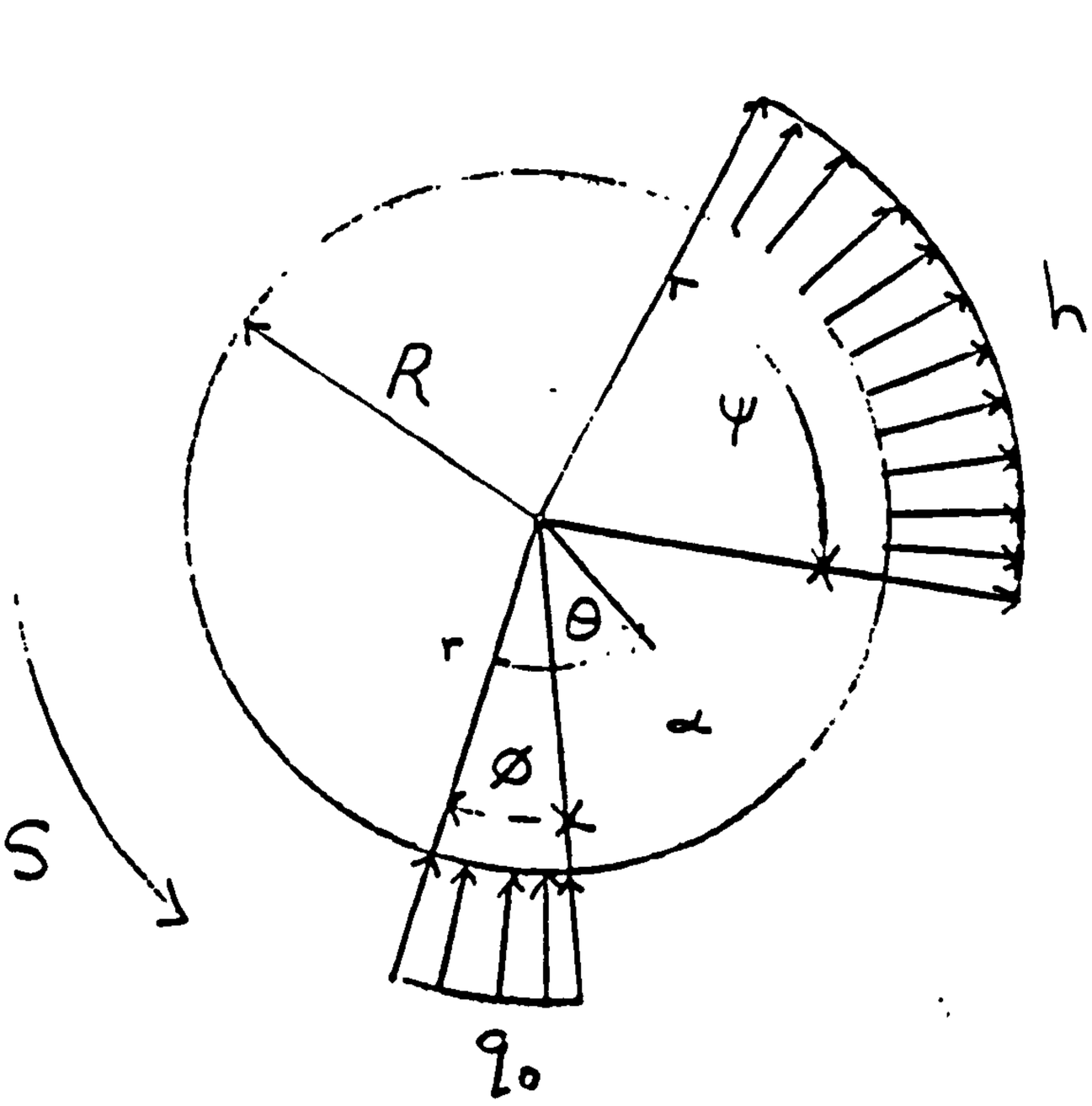

Fig.2.2.7. Schematic diagram of rotating roll showing locations of heat transfer.

The relevant boundary conditions are given as

$$-k\frac{\partial T_{(R,\theta)}}{\partial r} = \begin{cases} -q_0 & ; 0 < \theta < \phi \\ 0 & ; \phi < \theta < \phi + \alpha \\ hT_{(R,\theta)} & ; \phi + \alpha < \theta < \phi + \alpha + \varphi \\ 0 & ; \phi + \alpha + \varphi < \theta < 2\pi \end{cases} \qquad (2.2.35)$$

where α = angular separation between the heat input and the cooling regions (radians)

φ = angle for convective cooling, radians

θ = angle for heat input, (radians)

h = (constant) heat - transfer coefficient

A solution of eqn. (2.2.34) can be reached by consulting Patula's[52] publication. In applying eqn. (2.2.34), the author reported that the penetration of the surface temperature variations is only about 6 per cent of the roll radius under steady state conditions for relatively slow rolling speeds. In particular he found that relocating the sprays had a negligible effect on the roll centre line temperature except for low values of the parameters $[\sqrt{(sR/\kappa}][k/(hR)]$ (it should be greater than 10).

Patula's examination can be considered useful for analysis of the bulk roll temperature and thermal roll crowns, but is limited in not being able to predict the localised thermal displacements or temperatures at the roll surface accurately. The assumption of steady state roll temperature is clearly unreasonable for actual rolling situations.

In the same year as Patula's publication Weber and Unger[53] brought out a paper which detailed the examination of the influence of the barrel length, strip width and roll gap temperature during cold rolling with reference to certain parametric values[101,102]. These

authors modelled the roll temperature with the equation :

$$T_{(r,x)} = T_A + \sum_{m=1}^{\infty} \frac{h}{\zeta_m I_1(\zeta_m R) + h I_0(\zeta_m R)} \int_0^{L_1} v(\zeta)\Theta_m(\zeta_m).d\zeta.\ \Theta_m(x).I_0(r\zeta_m) \qquad (2.2.36)$$

where:

$T_{(r,x)}$ = temperature field

T_A = ambient temperature

L_1 = half modified roll barrel length

h = mean relative heat transfer coefficient on the cylinder jacket

ξ_m = proper value

I_1 = modified Bessel function of the first kind, zero order

I_0 = modified Bessel function of the second kind, 1st order

n = coefficient of transverse expansion

θ = characteristic function

ϵ = integration variable

Based on the application of eqn. (2.2.36) these workers concluded that the temperature variation within the width of the strip was independent of barrel length, the longer the barrel, but the roll temperature decreases towards the barrel end. They also concluded that with increasing strip width, higher surface temperatures can be expected with otherwise constant conditions. Not surprisingly, they also reported that for increased roll gap temperatures, higher surface and bulk temperatures will result.

Pavlossoglou[57] in 1981 produced a mathematical model for hot flat rolling in the deformation zone, and aimed to predict the temperature profile of the roll and strip in the absence of any cooling. Since this model ignores

cooling by convection, is one dimensional (only radial conduction of heat is considered), and assumes constant centre line temperatures of both the roll and strip, it can be considered unsuitable to the present area of study. In continuation of this work, Pavlossoglou[58] later extended this model to include heat losses due to radiation and convective cooling but not due to a liquid coolant when the rolls are not in contact with the strip. In any event the work did not include any reference to experimental data.

Pallone[72] considered that it was of paramount importance to include axial conduction in any model of the work roll temperature behaviour. Citing the work of Patula[52], Pallone decided that only the bulk roll temperature need be considered in an examination of the roll thermal expansion. Patula had found that only four per cent of the radius experienced any temperature fluctuations under steady-state conditions. Thus, to develop his model Pallone dismissed radial and circumferential heat conduction, and considered that heat input from hot slabs and heat removal by coolant sprays is even at any given cross- section along the circumference of the roll (because of high roll rotational speeds). He further assumed that constant heat transfer coefficients existed between the slab and the roll over the slab width and that between the coolant and the full roll length. In hot rolling, the coolant is not necessarily sprayed over the entire length of the roll, nor is the quantity of coolant evenly distributed across the roll. In addition, Pallone assumed that the heat gained by the roll from the slab is through contact conductance. Finally, he assumed that the roll length can be divided into two regions, namely, where the slab and coolant sprays are active. The above assumptions led him to arrive at the following equations (see fig. 2.2.8):

$$\frac{\partial T_I}{\partial t} = \alpha \frac{\partial^2 T_I}{\partial x^2} + 2\frac{h_T \phi}{\rho C_p \pi d}\left(T_s - T_I\right) - \frac{2h_C \varphi}{\rho C_p \pi d}\left(T_I - T_f\right) \qquad (2.2.37)$$

and for region II

$$\frac{\partial T_{II}}{\partial t} = \alpha \frac{\partial^2 T_{II}}{\partial x^2} - 2 \frac{h_T \varphi}{\rho C_p \pi d} \left(T_{II} - T_f \right) \qquad (2.2.38)$$

At the interface where region I and II meet the boundary conditions are given as

$$\frac{\partial T_I}{\partial x}\left(\frac{w}{2}.t\right) = \frac{\partial T_{II}}{\partial t}\left(\frac{w}{2}.t\right) \qquad (2.2.39)$$

$$T_I\left(\frac{w}{2}.t\right) = T_{II}\left(\frac{w}{2}.t\right) \qquad (2.2.40)$$

where:

w = slab width

C_p = specific heat of work roll

d = work roll diameter

h_c = coefficient of forced convection

h_T = coefficient of thermal contact

T_f = coolant spray temperature

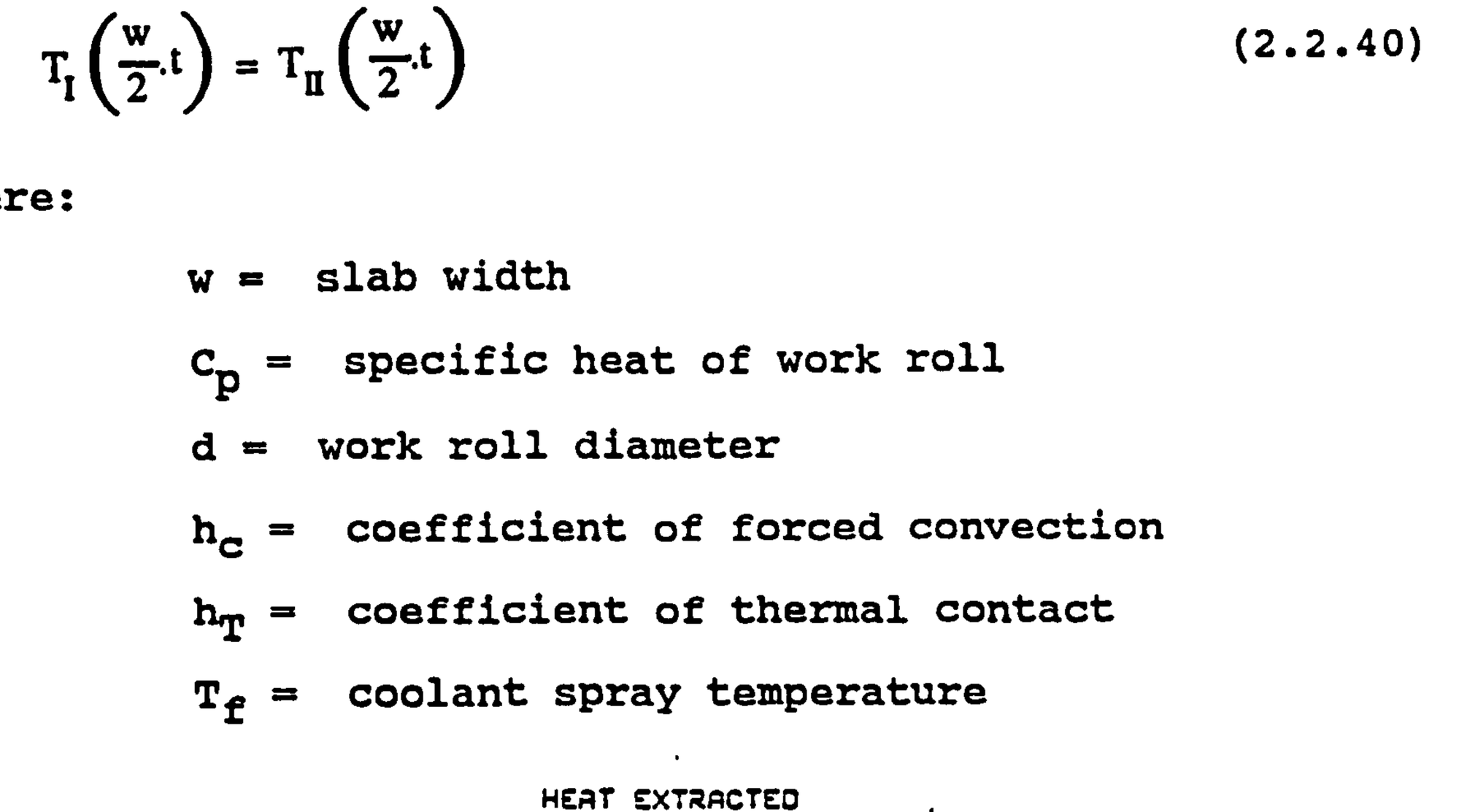

Fig. 2.2.8. Location of heat input and heat loss in work roll

The additional boundary and initial conditions required in order to solve eqn. (2.2.37) are given as

$$\frac{\partial T_I(0,t)}{\partial x} = 0 \qquad (2.2.41)$$

and

$$T_I(x,0) = T_f$$

and corespondingly for eqn. (2.2.38)

$$T_{II}(1/2,t) = T_f$$

and (2.2.42)

$$T_{II}(x,0) = T_f$$

From a solution to the above equations the diametral expansion based on the mean temperature distribution can be derived. It is clear from the analysis that this model is not suitable for the evaluation of roll thermal cambers which is a pre-requisite for effective strip crown control.

Bennon[77] continued the search for an appropriate mathematical model of the transient thermal behaviour of work rolls by developing an implicit three-dimensional, control-volume based, finite difference solution for the Fourier equations of heat conduction in a section of a solid rotating cylinder. He assumed constant thermo-physical material properties and axial symmetry to arrive at the equation:

$$\rho C\frac{\partial T}{\partial t} + \rho C\omega\frac{\partial T}{\partial \theta} = \frac{k}{r}\frac{\partial}{\partial r}\left(r\frac{\partial T}{\partial r}\right) + \frac{k}{r^2}\cdot\frac{\partial^2 T}{\partial \theta^2} + k\frac{\partial^2 T}{\partial x^2} \qquad (2.2.43)$$

where:

θ = circumferential coordinate

ω = angular velocity

The boundary conditions do not stipulate constant heat transfer coefficients but this model can be considered one of the more realistic representation of a typical work roll

environment. It may be that the computing requirements are too great if circumferential temperature variations are considered. The author did not report any comparisons for his calculated results and experimental data.

The latest published attempt at modelling the problem of roll thermal behaviour came from Beaudoin and Woodbury[106] who favoured the use of a finite element model coupled with a finite difference model. However, this analysis is limited to the steady-state but may be considered seriously for its examination of the behaviour at the interface between the strip and roll.

2.3 ROLL THERMAL CAMBER

The importance of the effect of work roll thermal camber on strip profile in hot rolling has been pointed out earlier and in the literature[30,39,43,72]. Thermal camber arises from the process of heat transfer to and from the work rolls. Heat is provided intermittently to the rolls through contact with the hot plate or strip. Additional heat transfer results from the frictional contact in the roll bite where metal and roll surfaces move at different speeds, sliding across each other. Heat is also generated as the strip passes through the roll gap and is deformed. Thus, as the rolls are heated, they expand. The rolls are usually cooler at the sides and hotter in the middle and so develop a "positive" thermal camber.

Heat is removed from the rolls mainly by coolant flowing over the roll surface, but some heat is also extracted by conduction to the cooler roll ends, by convection to the air and by conduction to the back-up rolls. The position of the sprays is important. Putting sprays at the sides would result in the centre heating up more than the sides, thus

increasing the positive thermal camber. Sprays at the centre reduce this positive camber. Localised differences in cooling will also affect the shape of the thermal camber.

An attempt can be made to model the existence of thermal camber by considering the important parameters which affect it. From experience, these parameters are the mill pacing[+], the form of heat transfer to the rolls, the strip width and the conditions of deformation in the roll gap[32]. The thermal camber model must aim to determine the roll surface displacements as a function of time and heat flows at the roll surface.

An exact calculation of thermal camber can be separated into the following stages[30], heat input calculation; solution of the differential equation governing heat conduction for the particular boundary conditions to give the temperature distribution in the roll interior as a function of time; and thermal strain analysis. This procedure is possible because thermal strains have no direct influence on the temperature distribution. However, since the strip shape is a function of the thermal camber, this will result in a change in the heat input distribution across the strip width, and so ensures an indirect link between thermal strains and the temperature distribution.

Finding the thermal camber at any one instant of the rolling operation is very complex, and the fact that the ground camber may subsequently vary at any moment due to

---

[+]Mill pacing deals with controlling the rate at which slabs pass through the mill; and is aimed at specifying the transient slab temperature everywhere in the mill so that metallurgical needs are met. Mill pacing is the subject of other studies32,63 and will not be dealt with here.

wear and thermal effects, adds to the difficulty of predicting camber. The progress of wear is continuous, and allowance is made for this factor by imparting an appropriate shape to the rolls prior to rolling. Contrasting this, the thermal camber is dependent on the rate of rolling and possible incidents causing stoppages.

The earliest models for calculating thermal cambers are extremely elementary in concept, depending on the assumption of a parabolic shape of the work rolls. This method was initially proposed by Mort[113] in 1947 and subsequently emulated by several authors, including Larke[114] (1963) and Hinkforth[115] (1972). It has been evident from actual thermal camber measurements after rolling that this assumption cannot be validated in practice[116,117].

Beeston and Edwards[30] adopted a solution to the radial surface displacement for a heated solid cylinder, originally given by Timoshenko and Goodier[98]. According to Timoshenko and Goodier the surface displacement depends on the moment of the temperature distribution $\theta(x',r^*)$ about the roll centre. Timoshenko and Goodier, by assuming an infinite length roll with temperature distribution $\theta(x',r^*)$, for the areas of the roll with relatively small temperature differences, give an approximation of the roll surface displacements as:

$$u(x') = 2\alpha R\int_0^{\cdot}\theta(x',r')r'\,dr' \qquad (2.3.1)$$

where:

$u(x')$ = roll surface displacement

α = coefficient of thermal expansion

R = roll radius

$r^* = r/R$

Due to axial symmetry

$$u(x') = u(-x')$$

and

$$g(x^*, x') = g(-x^*, -x')$$

It is evident that $y_\theta(x^*)$ need only be solved for $0 \leq x^* \leq 1/R$ and not for the entire roll length.

An even function $(\beta/\sqrt{2\pi})\exp -\frac{1}{2}[\beta(x^* - x')]^2$ was assumed for $g(x^*, x')$. The constant β can be adjusted to give the required results (see Appendix B). Compensation for end effects can be obtained by normalizing the influence function to have unit area , i.e.

$$g(x^*, x') = \frac{\exp\left(-\frac{1}{2}\left[\beta(x^* - x')\right]^2\right)}{\int_{-x_0}^{x_0} \exp\left(-\frac{1}{2}\left[\beta(x^* - x')\right]^2\right).dx'} \qquad (2.3.3)$$

Wilmotte and Mignon[32] gave the same solution to the surface displacement problem as Beeston and Edwards[30], but made no accommodation for error near the strip edge that eqn. (2.3.1) implies.

For the prediction of roll thermal camber, Weber and Unger[53] proposed the equation:

$$\begin{aligned} u(x) = {} & \frac{2(\upsilon-1)^2 Q}{(\upsilon^2+\upsilon-1)R}\int_0^R r\left\{T_{(r,x)} - T_A\right\}.dr + \frac{\upsilon(1-\upsilon)}{\upsilon^2+\upsilon-1}.RQ\left\{T_{(R,x)} - T_A\right\} \\ & + \frac{2\upsilon^3}{(\upsilon^2+\upsilon-1)(\upsilon+1)}.\frac{Q}{R}\int_0^R r\left\{T_{(r,L)} - T_A\right\}.dr \\ & + \frac{\upsilon^2}{(\upsilon^2+\upsilon-1)(\upsilon+1)}.RQ\left[T_{(R,L)} - T_A\right]\left(x\,\varepsilon_{(0,L)}\right) \end{aligned} \qquad (2.3.4)$$

where Q = constant
u(x) = thermal camber relative to the roll radius

Using eqn. (2.3.4) they concluded that thermal camber increases for increasing barrel length for a given distribution of cooling and lubrication. The thermal camber will also increase if cooling is more intense towards the edge of the barrel. These workers also reported that thermal camber is greatest during the rolling of a medium strip width, for various rolling conditions. The same result can be expected from higher roll gap temperatures. Roll camber, they concluded, is greatly influenced by the distribution of coolant over the roll surface.

Pallone[72] proposed the equation:

$$\Delta D = D_o \alpha_E (T_{I,II} - T_f) \qquad (2.3.5)$$

where:

D_o = work roll diameter

$T_{I,II}$, T_f are referred to in eqn. (2.2.37) and (2.2.38)

to represent the diametrical expansion ΔD along the roll axis based on the roll temperature distribution.

2.4 HEAT TRANSFER COEFFICIENT FOR A ROTATING CYLINDER UNDER VARIOUS COOLING CONDITIONS

Even if the mathematical models of the transient work roll temperature and thermal expansion were exact in the sense that all the simplifying assumptions mentioned in the sections above were true, modelling of the complex heat transfer regimes at the roll surface would have to be overcome before any of the remaining parts of the model could be seriously considered for on-line automatic coolant control. A consideration of the environment existing at the roll surface for one revolution for an axial section of the roll during rolling, reveal that on contact with the hot strip the roll experiences a rapid rise in temperature which continues as the strip progresses through the roll bite. (See fig. 2.4.1). Directly the strip exits the roll bite coolant sprays are applied to the roll which will also certainly experience cooling in the air during part of the time the roll takes to travel from strip exit to back-up roll contact. Depending on the efficiency of the exit sprays, quenching of the work rolls by the back-up rolls will occur to some degree. If entry sprays are present more coolant may be applied. Finally, the section of roll being considered will undergo some more cooling in the air before completing the revolution.

An exact knowledge of the individual heat transfer coefficient at each of the cooling regimes would be ideal, although in the context of the model adopted by the author generalised values are sufficient. For models that consider circumferential variation in the roll temperature, the mathematical relationships between the cooling regimes and heat transfer coefficient have to be more exact.

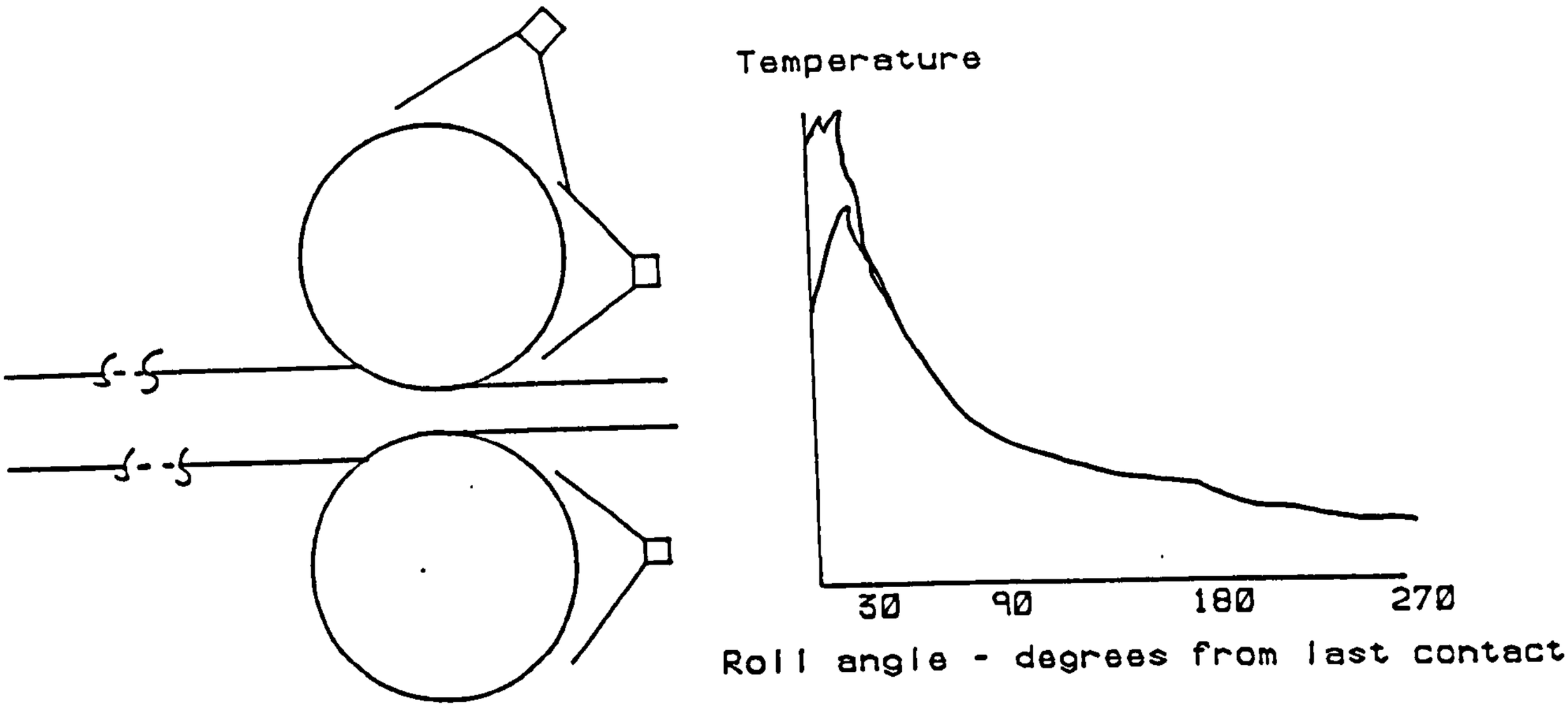

Fig. 2.4.1 Diagram of roll with sprays and strip going through. The back-up rolls are not shown.

In general the literature on spray heat transfer coefficient can be divided broadly into theoretical and experimental investigations. This survey will concentrate on relevant experimental works. Bolle and Moureau[65] have published an extensive literature review of this area of work. They summarised the published results between 1966 and 1973 as in fig. 2.4.2 and table 2.4.1.

The general conclusion from the work of Bolle and Moureau[65] is that experimental heat transfer results show no reliable degree of correlation. This fact, they proposed, is quite likely to be due to the many parameters that can influence heat transfer and differing spray characteristics such as droplet size.

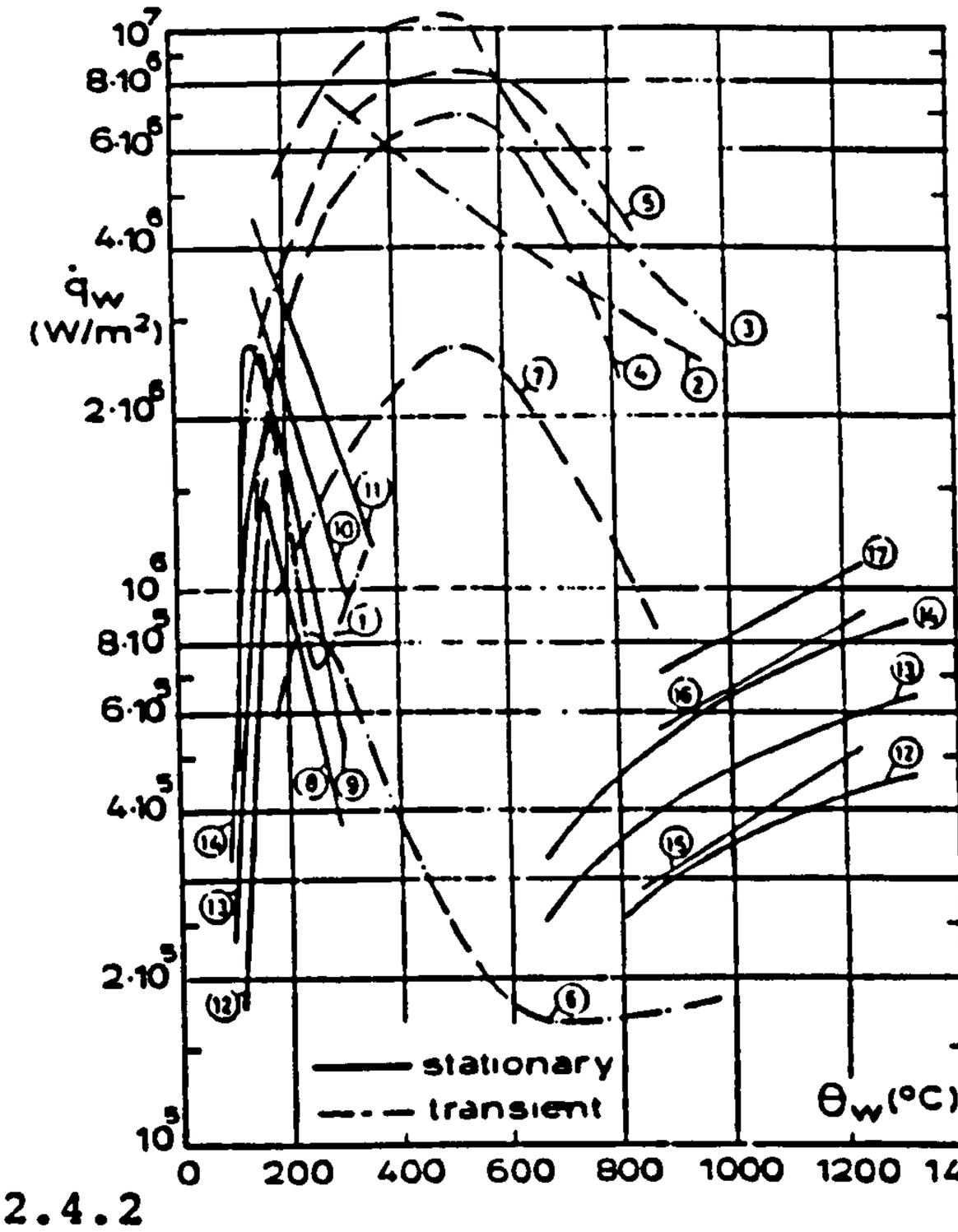

Fig. 2.4.2

Heat flux density at the wall as a function of wall temperature (for the nomenclature of the curves, see Table 2.4.1

Table 2.4.1 Experimental condition of tests

References	General Characteristics of the Tests							Characteristics of the curves of Fig. 4
	Nature of the Hot Wall	Surface Area of the Hot Wall (cm^2)	Temperature of the Spray (°C)	Shape of the Spray and Working pressure, (bar)	Mass velocity of the spray, (kg/m^2 s)	Mean Drop Diameter, (μm)	Mean Drop Velocity, (m/s)	(Number of curve and Main Parameter)
Gaugler (1966)	Horizontal upper face of a copper cylinder plated with chrome	1.2	20	Full cone	0.7-3.7	126-250	16-26	(1) [illegible] = 2 kg/m^2 s
Corman (1966)	Id	Id	Id	Id	57	-	-	(2) [illegible] = 57 kg/m^2 s
Auman et al. (1967)	Horizontal plate made of stainless steel (AISI304)	300	21	Fan	-	-	-	3) -
Lambert and Economopoulos (1970)	Horizontal cylinder made of nickel	3.1	20	1-5	-	-	-	(4) [illegible] = 1 bar (5) [illegible] = 3 bar
Hoogendoorn and den Hond (1974)	Horizontal disk made of stainless steel (AISI321)	269	20	Full cone, 1-10	0.6-25	200-1000	10-30	(6) [illegible] = 0.6 kg/m^2 s (7) [illegible] = 25 kg/m^2 s
Toda (1972)	Horizontal disk made of copper plated with gold	1.8	55, 70, 85, 92, 100	Full cone, 40-150	3.8-32	88-146	42-72	(8) [illegible] = 3.8 kg/m^2 s [illegible] = 42.3m/s, [illegible] = 88x10^{-6} m (9) [illegible] = 4.5 kg/m^2 s [illegible] = 48.9m/s, [illegible] = 146x10^{-6} m (10) [illegible] = 5.0 kg/m^2 s [illegible] = 46.2m/s, [illegible] = 117x10^{-6} m (11) [illegible] = 32 kg/m^2 s [illegible] = 72.4m/s, [illegible] = 117x10^{-6} m
Junk (1972)	Vertical stainless steel tube	83-207	-	Fan 2-6	-	-	-	(12) [illegible] = 2 bar (13) [illegible] = 4 bar (14) [illegible] = 6 bar
Müller and Jeschar (1973)	Vertical stainless steel plate	20-65	20	Fan Full cone. 2-10	0.3-9	-	11-32	(15) [illegible] = 2 bar (16) [illegible] = 7 bar (17) [illegible] = 10 bar

The earliest example found in the literature of an attempt to present mathematical equations for heat transfer coefficients for a rotating cylinder was by Anderson and Saunders[11] (1952). They considered the case of heat transfer from a heated cylinder rotating about its axis in air. These workers deduced a dependency of heat transfer on rotational speed, and also concluded that for this type of heat transfer the Nusselt number was independent of the Reynolds number up to a critical value, beyond which the Nusselt number increased with the Reynolds number. They proposed the expression

$$Nu = 0.14Re^{2/3} \qquad (2.4.1)$$

where:

Re = Reynolds number

Nu = Nusselt number

to relate the heat transfer coefficient to environmental conditions. Anderson and Saunders[11] suggested that this equation is valid for other fluids other than air. Since other workers have proposed other equations for heat transfer coefficients, this generality is highly doubtful, but the form of eqn. (2.4.1) has a general application.

Dropkin and Carmi[96] developed this work when investigating the factors that could be employed to determine the heat transfer coefficient for a horizontal cylinder, rotating in air. They arrived at the relationship

$$\frac{hD}{k} = C^1 \left(\frac{D^3 \rho^2 g}{\mu^2} \right)^x \left(\frac{v^2}{Dg} \right)^y (\Delta\beta)^z \qquad (2.4.2)$$

where:

h = convective heat transfer coefficient

D = outside diameter of cylinder

k = thermal conductivity

ρ = density of air

g = gravitational constant

μ = absolute viscosity

v = surface velocity of cylinder

$\Delta\beta$ = coefficient of volumetric expansion

C_1 = constant

x, y, z = exponents

To evaluate the constant C_1 and the exponents x, y, z, Dropkin and Carmi kept two of the parameters of the right-hand side of equation (2.4.2) constant while varying the remaining parameters. From their experimental results they concluded that up to a certain Reynolds number, rotating the roll has no effect on the heat transfer coefficient. However, above this critical value of the Reynolds value the heat transfer coefficient will increase with increases in the speed of rotation and is also influenced by free convection. They further concluded that there is a region where the heat transfer coefficient is only proportional to the speed of rotation.

For Reynolds number larger than 15,000, Dropkin and Carmi[96] recommended the use of the simplified equation

$$Nu = 0.073 \ (Re)^{0.7} \qquad (2.4.3)$$

and for the region in which the heat transfer coefficient is influenced by rotation of the roll, the equation

$$Nu = 0.095 \ (0.5 \ Re^2 + Gr)^{0.25} \qquad (2.4.4)$$

may be used,

where:

$$Gr = \text{Grashof number} = D^2\rho^2 g\Delta\beta/\mu^2$$

The authors reported good experimental correlation.

Kadinova and Krivizhenko[9] investigated the problem of predicting heat transfer coefficients by examining the cooling efficiency of single round and flat spray nozzles. The experiments were not directly related to cooling of cylindrical rolls, but rather of a flat plate. The factors that they considered important included the shape and structure of the spray, the degree of dispersion, its distance from and orientation with respect to the cooled object. From this investigation they concluded that there is a quantitative dependence of the heat transfer coefficient on the geometrical parameters of the system being investigated. They found that cooling is greatest in the centre of the sprays, gradually decreasing toward the edge of its sprayed area. In addition, they pointed out that the greater the distance between the jet and the cooled object, the higher the flow velocity and amount of water needed to achieve a given cooling rate. Based on these considerations, they modelled the heat transfer characteristics using a form of eqn. (2.4.2), suggesting for a round jet

$$h = 2.47\frac{\lambda}{\delta_s} Re^{0.4} Pr^{0.36} \left(\frac{l}{\delta_s}\right)^{-0.43} \qquad (2.4.5)$$

$$l/d_c = 22 - 38$$

and for a flat jet with $l/\sigma_s = 130$

$$h = 2.47\frac{\lambda}{\sigma_s} Re^{-0.4} Pr^{0.36} \left(\frac{l}{\sigma_s}\right)^{-0.43} \qquad (2.4.5)$$

where:

h = heat transfer coefficient

Re, Pr = Reynolds and Prandtl number, respectively

d_c, δ_s = nozzle diameters of round and flat jets, respectively

l_s, σ_s = distance from plate with round and flat jets, respectively.

In a later investigation Kadinova and Kheifets[26] characterised the effect of the angle, β, of the water stream to the cooled surface. They proposed the generalised equation

$$Nu = cRe^{n} Pr^{0.36} (1/d_c)^{0.4} \beta^{0.27} (d_z/d_c)^{-0.06} \qquad (2.4.7)$$

where the values of the coefficients c and n are characteristics of the nozzle and d_z is the diameter of the spray zone.

In general, the literature on spray cooling reveal that heat transfer coefficient can be characterised by equations of the form of eqn. (2.4.1). The important parameters[26,103,119] to consider are surface temperature, water impingement density, droplet impulse and the proportion of the cooled surface material. The important coefficients based on these variables seem to be highly specific to the system investigated.

2.5 FAST THERMAL CAMBER MODELS

As a pre-requisite to controlling the spray behaviour, it is necessary that the computing time of the roll thermal camber model be as rapid as possible whilst maintaining computational accuracy. This is in order to co-ordinate mill-scheduling and spray behaviour. Thus, the approach to developing a simplified roll thermal camber model is that such a model must closely match the results of the more comprehensive model.

Beeston & Edwards[30] have examined this problem by considering the most computationally time consuming area of thermal camber calculations. Computing time is mostly used during the integration of the heat conduction equations such as eqn. (2.2.21) and eqn. (2.3.1). Hence, these types of equations were replaced by a simpler model for determining the radial displacements axially, U(x), eqn. (2.3.1). They proposed that for work rolls with specified dimensions and physical properties, U(x) can be approximated if considered as a function of strip width, heat input and heat transfer coefficient. The proposed form of the model was therefore:

$$u_0(x) = u_\infty \left[1 - k \left(e^{\frac{x}{\lambda_1}} + e^{-\frac{x}{\lambda_1}} \right) \right] \qquad x \le w \qquad (2.5.1)$$

$$u_0(x) = u_\infty k\lambda_2 \left[e^{\frac{w}{\lambda_1}} - e^{-\frac{w}{\lambda_1}} \right] e^{-\frac{(x-w)}{\lambda_2}} \qquad |x| > w \qquad (2.5.2)$$

$$\text{where } k = \frac{1}{\left[e^{\frac{w}{\lambda_1}}(1+\lambda_2/\lambda_1) + e^{-\frac{w}{\lambda_1}}(1-\lambda_2/\lambda_1) \right]}$$

$$\lambda_1 = \left(\frac{kR}{2H_{r1}} \right)^{\frac{1}{2}}$$

$$\lambda_2 = \left(\frac{kR}{2H_{r_2}} \right)^{\frac{1}{2}}$$

$$H_r(x) = H_{r_1} \qquad |x| \leq w$$

$$H_r(x) = H_{r_2} \qquad |x| > w$$

$$u = \frac{\alpha q}{2\pi H_{r_1}} = \alpha R \Delta\theta$$

w = strip width

R = roll radius

q = specific heat input

H = heat trasfer coefficient

α = coefficient of thermal expansion

x = axial coordinate

Beeston & Edwards[30] reported good agreement between this model and their more accurate model of eqn.(2.3.1) as shown in fig. 2.5.1.

Fig.2.5.1 Simplified model performance by Beeston & Edwards[30].

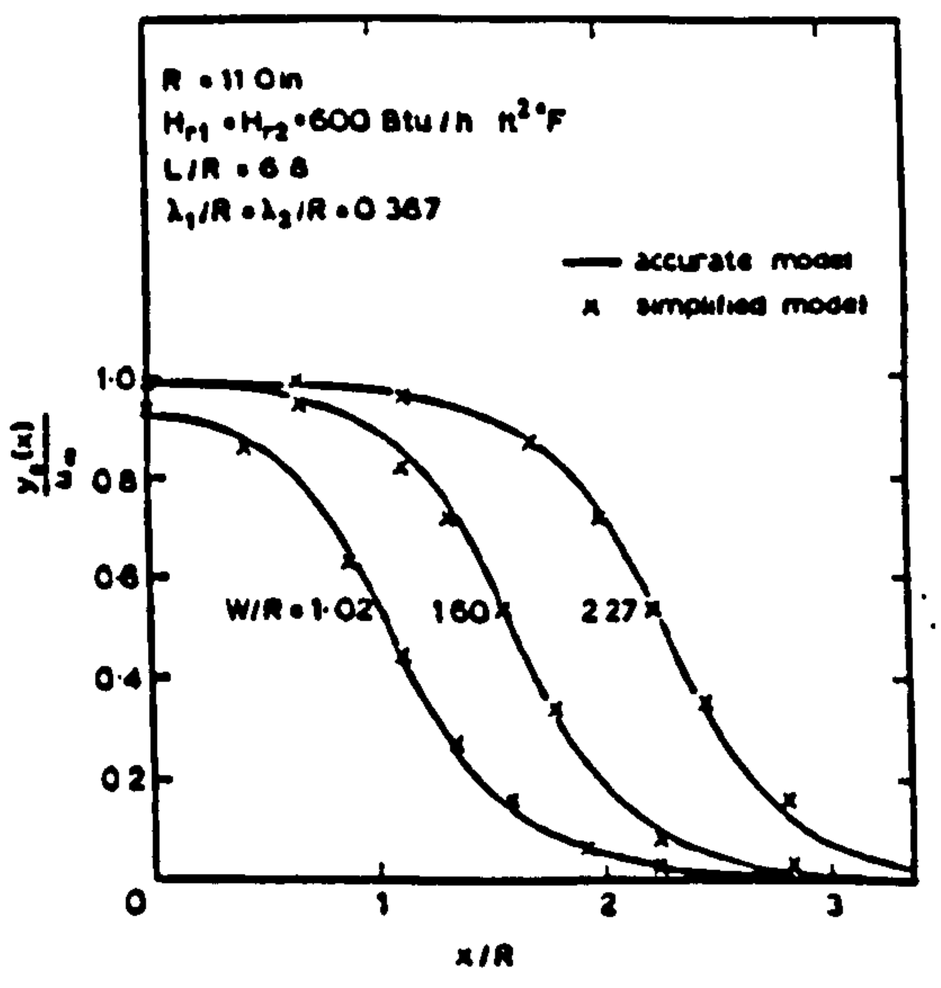

The Beeston & Edwards[30] model represented by eqn. (2.5.1) shows an interesting approach to the development of a simplified model. They admitted the difficulty of determining heat transfer coefficient from an analysis of the parameters of the spray system, and recommended that each mill be calibrated to determine heat transfer.

Oshima et al.[67] have suggested a fast thermal camber model In this model the work roll is divided into three radial layers of equal area. Since the temperature gradients are greatest near the roll surface, division of the roll in this way means that the finite difference mesh points become finer closer to the roll surface, giving a faster approximation to the roll temperature (see fig. 2.5.2).

The model for thermal strain calculations proposed by Ohshima et al. is described by the equation:

$$U_{i,j} = \frac{\alpha(1+\nu)RT_o}{3}\sum_{j=1} T_{(i,j,k)} \qquad (2.5.3)$$

where:

$U_{i,j}$ = surface expansion

α = coefficient of thermal expansion

ν = Poisson's ratio

T_o = reference temperature

The term ν in the above equation reflects the fact that generally in a continuous body expansion cannot proceed freely and stresses caused by heating are set up.

Yamamot et al.[120] have derived simple equations for roll surface temperature and thermal crown by taking the thermal

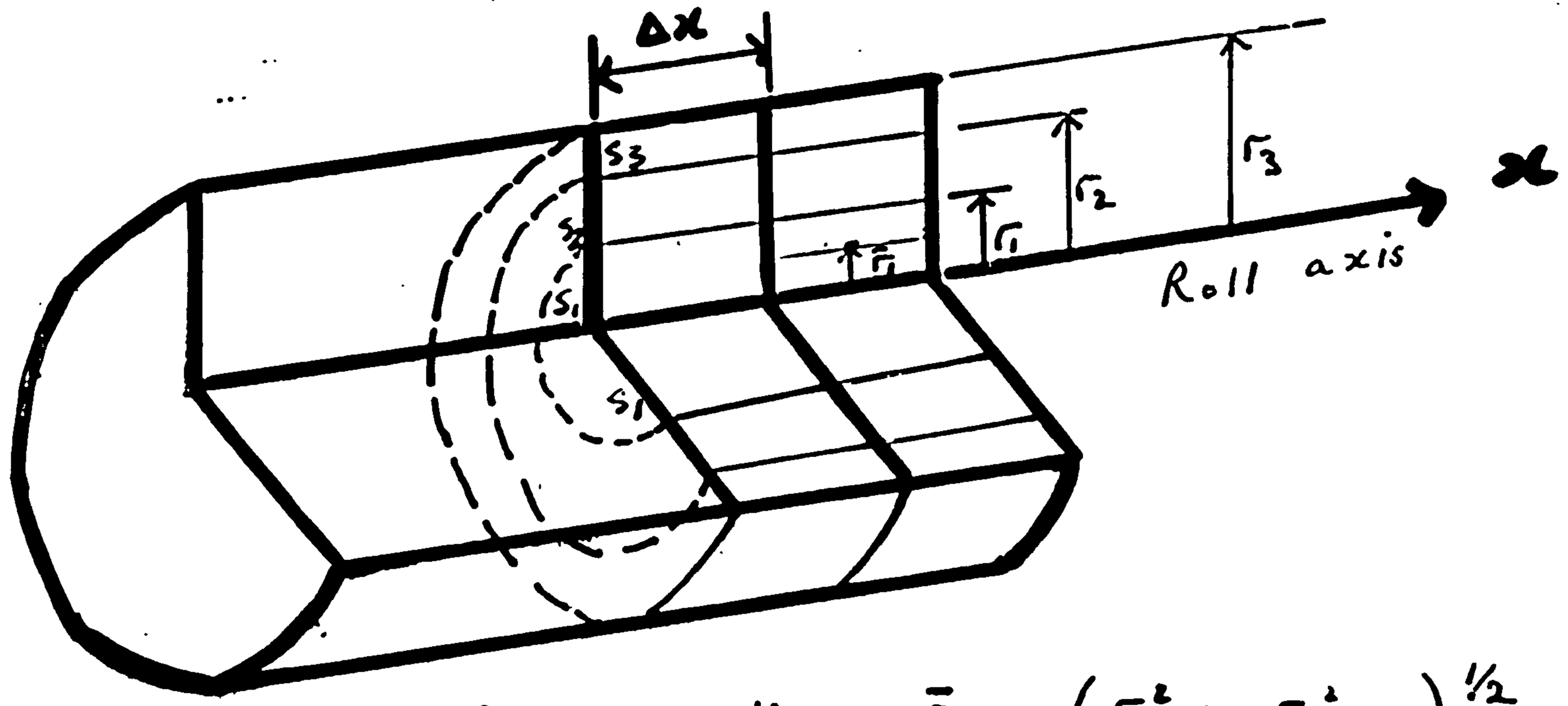

$$\text{Mean radius } \bar{r}_j = \left(\frac{r_j^2 + r_{j-1}^2}{2} \right)^{1/2}$$

$$\text{Section Area } S = S_1 = S_2 = S_3$$

Fig. 2.5.2. Element diagram for Oshima[67] (fast) thermal camber model.

conduction in the axial and radial directions into account. From a simplification of the heat conduction equation, (eqn. 2.2.21), the following equations are obtained for roll surface temperature under spray cooling:

$$T_c(R,x,t) = \frac{T(R,x,0) - T_w}{\frac{1}{b_1 t^{\delta_1}}}\left[1 + \frac{\beta_1(\alpha_c - 6000)}{3000}\right].Y_T + T_w \quad (2.5.4)$$

and for thermal crown:

$$C_c(x,t) = \frac{C(x,0)}{\frac{1}{b_2 t^{\delta_2}}}\left[1 + \frac{\beta_2(\alpha_c - 6000)}{3000}\right].Y_c \quad (2.5.5)$$

where:

$T_o = T_{(R,x,o)}$ = initial roll temperature

$C_o = C_{(x,o)}$ = initial thermal crown

T_w = cooling water temperature

a_c = thermal conductivity of roll surface during water cooling

$Y_T = Y_T(x)$, $Y_c = Y_c(x)$ = compensating coefficient taking heat transfer into account.

b_1, b_2, σ_1, σ_2, β_1, β_2, = constants which make the simple equation agree with the absolute solution.

Yamamot et al.[120] reported good agreement with the more detailed model, but it is apparent that this model cannot account for changes in the spray configuration.

2.6 ROLL BITE TEMPERATURE MODELS

The importance of being able to predict the temperature changes at all points in the mill has already been stated. Modelling of the work roll thermal behaviour has been considered from three separate inter-linked mechanisms,

viz., the heat input calculations, the heat conduction and thermal expansion evaluation. The literature on the latter two considerations have been dealt with in the preceding sections. It is now proposed to review the literature on the heat input section.

It is accepted that during the earlier passes of the hot rolling process the bulk temperature of the hot[56] slab falls gradually, but the slab experiences rapid falls in temperature when its thickness is reduced to below 13mm. It is suggested by Bradley[70] that frictional effects are negligible during the hot rolling process and that nearly all the mill power applied to strip goes into deforming it. During hot rolling, the roll is generally cooler than the slab, and since contact duration is brief, only the surface layer of the slab is chilled because of contact with the rolls.

Bradley, et al.[70], have postulated four separate mechanisms of roll - slab temperature behaviour, namely,

i. The flow of heat from the hot aluminium slab to the (relatively) cold steel roll during the contact phase.

ii. The cooling of the roll and slab in the air or by the coolant sprays.

iii. The internally generated heat produced by the plastic deformation of the slab.

iv. The increase in roll temperature on each rotation when the slab becomes longer than one roll circumference. This affects the heat transfer mechanism of (i).

On considering the amount of heat flowing from the slab to

the rolls, Bradley and his co-workers[70] thought it was important to consider the contact time, but admitted the difficulty of predicting this time without some assumptions. By assuming an average between the entry and exit speeds for a point on the slab in contact with the roll, they proposed that the contact time can be determined from

$$\tau_s = \frac{R\phi T}{\left(L_{in} + L_{out}\right)^{\frac{1}{2}} + R\phi} \qquad (2.6.1)$$

where:

R = roll diameter

L_{in}, L_{out} = slab lengths before and after

T = The total pass time that respectively the slab and roll are in contact

$$\phi = \cos^{-1}\left[1 - \frac{H_1 - H_2}{R}\right]$$

H1, H2 = input and output slab thicknesses, respectively

For the temperatures of the slab and rolls in contact, Bradley et al.[70] proposed the equations:

$$\frac{\partial \theta_1}{\partial t} = \alpha_1 \frac{\partial^2 \theta_1}{\partial x^2} \qquad x < 0 \qquad (2.6.2)$$

$$\frac{\partial \theta_2}{\partial t} = \alpha_2 \frac{\partial^2 \theta_2}{\partial x^2} \qquad x > 0 \qquad (2.6.3)$$

where:

θ_1, θ_2 = slab and roll temperature distance x from the interface at time t

Respectively, α_1, α_2 = thermal diffusivity of roll and strip.

By assuming no thermal contact resistance, then

$$\theta_1 = \theta_2, \qquad x=0,\ t>0 \tag{2.6.4}$$

and continuity considerations imply that:

$$k_1\frac{\partial\theta_1}{\partial x} = k_2\frac{\partial\theta_2}{\partial x}, \qquad x = 0 \tag{2.6.5}$$

where:

k_1, k_2 thermal conductivities of the slab and roll respectively.

On first contact, if all temperatures are measured relative to the roll, then

$$\theta_1 = \theta_2 \ , \ t = o \tag{2.6.6}$$

and

$$\theta_2 = \ 0 \ , \ t = o \tag{2.6.7}$$

to give the boundary and initial conditions.

Laplace transformation techniques can be used to solve the equations for θ_1 and θ_2. This method of solution is doubtful as regards to its applicability since the boundary conditions are continually changing, and the physical parameters are known to display some dependency on temperatures of the magnitudes involved in this part of the rolling process.

Bradley et al.[70] considered that deformation heating can be accounted for by assuming that only a fraction (about 80%) of the energy expended by the mill motors is converted into heat within the slab. The remaining part of the mill power input can be assumed lost in frictional effects at the roll

slab interface. Since this is difficult to quantify, and the frictional effect is indistinguishable from a change in contact resistance, then it is reasonable to assume that all the energy transmitted by the motors appears as deformation heat, evenly distributed throughout the slab.

Hollander[83] paralleled the modelling technique of Bradley et al.[70] but chose a numerical solution based on finite differences.

CHAPTER 3

ROLL TEMPERATURE ANALYSIS

3.1 INTRODUCTION

This chapter contains the complete mathematical analysis of a transient work roll temperature model in two spatial dimensions. The model is developed from an energy balance for the work roll. The partial differential equations generated are solved numerically by replacing the Fourier equations describing heat transfer with finite differences. The resulting set of ordinary differential equations are solved with respect to time.

The exact geometry of the work roll will be considered. Heat input to the work rolls will be considered as a boundary condition which permits the development of a more elegant computer algorithm. Heat transfer coefficients relating the various modes of heat transfer from the roll to its surroundings, will be considered as a single parameter which can vary across the roll. The complete development of the model and the attendant computer algorithm allows the axial elements resulting from this method to have localised heat transfer coefficients . Each element can be switched on and off at set times to examine the effects of spray switching during rolling. Values of this heat transfer coefficient for different spray configurations will be determined initially from a calibration of the roll temperature model. The calibration is performed by matching predicted roll surface temperatures to measured roll surface temperatures at known times during the rolling programme. Another method of determining spray heat transfer cofficient will also be suggested.

The model is used to calculate the temperature changes in the roll during rolling and for a given time after rolling has ended and the coolant is turned off. The thermal expansion is calculated by assuming that the surface displacement depends on the moment of the temperature distribution based on the method suggested by Timoshenko an Goodier[98]. The method is detailed in appendix B.

The roll bite model is detailed in appendix C.

3.2 ROLL TEMPERATURE ANALYSIS

The following assumptions are made in the roll temperature model

(1) Cyclic temperature variations in the tangential direction can be ignored because the period of roll revolution is two orders of magnitude smaller than the response time of the roll thermal camber to a change in rolling conditions. Negligible discrepancies will occur near the roll surface for a depth of approximately 5mm[30].

(2) The roll exhibits uniform physical properties . This assumption implies a non-dependency on temperature.

With reference to fig. 3.2.1:

$$A_{left} = 2\pi r\,\delta r$$

$$A_{right} = 2\pi r\,\delta r$$

$$A_{inside} = 2\pi r\,\delta x$$

$$A_{outside} = 2\pi (r + \delta r)\,\delta x$$

where:

A = cross-sectional area of roll

$Q_x(x)$ = total heat flow rate into element through A_{left}

$Q_x(x + \delta x)$ = total heat out of element through A_{right}

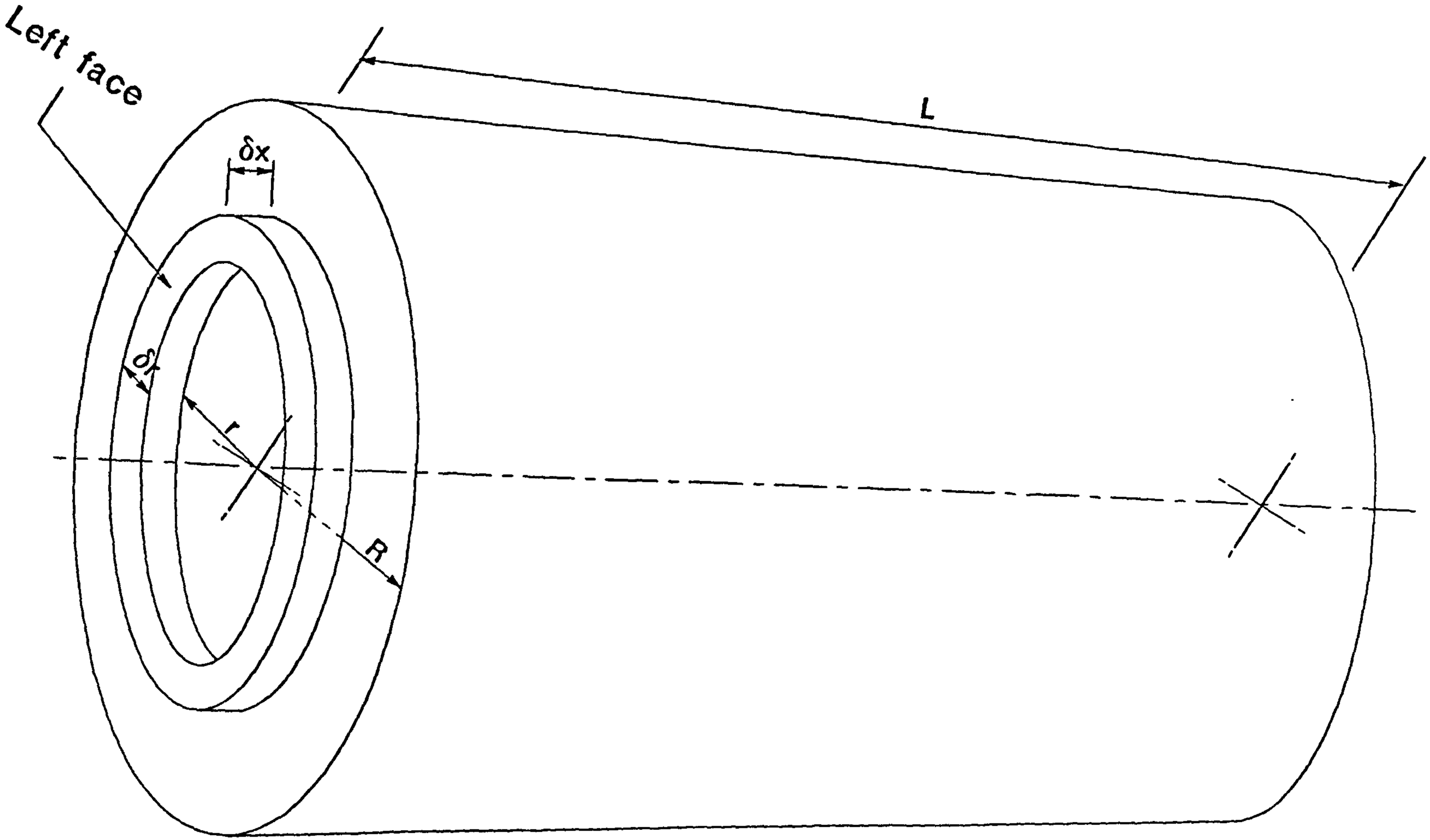

Fig. 3.2.1. View

$Q_r(r)$ = total heat flow rate into element through A_{inside}

$Q_r(r + \delta r)$ = total heat out of element through $A_{outside}$

Q is to be taken as positive in the positive r direction.

Hence a heat balance on the element gives:

$$F(x,r,t) = Q_x(x) - Q_x(x + \delta x) + Q_r(r) - Q_r(r + \delta r) \qquad (3.2.1)$$

where

F = Heat flow rate into element

t = time

Using a Taylor series expansion and neglecting the higher terms, eqn.(3.2.1) becomes:

$$F(x,r,t) = Q_x(x) - \left(Q_x + \left.\frac{\partial Q_x}{\partial x}\right|_{x,r,t} \delta x \right) + Q_r(r) - \left(Q_r(r) + \left.\frac{\partial Q_r}{\partial r}\right|_{r,x,t} .\delta r \right) + \ldots$$

$$= - \left.\frac{\partial Q_x}{\partial x}\right|_{x,r,t} .\delta x - \left.\frac{\partial Q_r}{\partial r}\right|_{r,x,t} .\delta r \qquad (3.2.2)$$

Let the heat content of the element be W, then

$$F(x,r,t).\delta t = W(x,r,t+\delta t) - W(x,r,t)$$

$$= W(x,r,t) + \left.\frac{\partial W}{\partial t}\right|_{x,r,t} .\delta t - W(x,r,t) + \ldots.$$

$$F(x,r,t) = \frac{\partial W}{\partial t} \qquad (3.2.3)$$

Substitute eqn. (3.2.2) into eqn. (3.2.3) to get:

$$-\frac{\partial Q_x}{\partial x}\bigg|_{x,r,t}.\delta x \;-\; \frac{\partial Q_r}{\partial r}\bigg|_{x,r,t}.\delta r \;=\; \frac{\partial W}{\partial t} \qquad (3.2.4)$$

Using the heat conduction equation, we get

$$Q_x(x) = -k\,A_{left}.\frac{\partial T}{\partial x}$$

$$= -k.2\pi\, r\,\delta r.\frac{\partial T}{\partial x}$$

$$Q_r(x,r,t) = -k\,A_{inside}.\frac{\partial T}{\partial r}$$

$$= -k.\,2\pi\, r.\delta x.\frac{\partial T}{\partial r}$$

where:

k = thermal conductivity (W m^{-1} $°K^{-1}$)

T = roll temperature function (°K)

And

$$W_{(x,\ r,\ t)} = C\rho T\ 2\pi r\,\delta r\,\delta x \qquad (3.2.5)$$

where

ρ = density of roll (kg m^{-3})

C = volumetric specific heat capacity (kJ kg^{-1} K^{-1} m^{-3})

$$\frac{\partial}{-\partial x}\left(-k\ 2\pi\, r\,\delta r\frac{\partial T}{\partial x}\right).\delta x - \frac{\partial}{\partial r}\left(-k.2\pi\, r\,\delta x\frac{\partial T}{\partial r}\right).\delta r$$

$$=\frac{\partial}{\partial t}\left(C\rho T.2\pi\, r\,\delta r\,\delta x\right)$$

$$\frac{\partial}{\partial x}\left(rk\frac{\partial T}{\partial x}\right) + \frac{\partial}{\partial r}\left(k\,r\frac{\partial T}{\partial r}\right) = \frac{\partial}{\partial t}(C\rho Tr)$$

$$r\,k\frac{\partial^2 T}{\partial x^2} + k\frac{\partial}{\partial r}\left(r\frac{\partial T}{\partial r}\right) = C\rho r\frac{\partial T}{\partial t}$$

$$k\frac{\partial^2 T}{\partial x^2} + \frac{k}{r}\frac{\partial}{\partial r}\left(r\frac{\partial T}{\partial r}\right) = C\rho\frac{\partial T}{\partial t} \qquad (3.2.6)$$

Expand and re-arrange eqn. (3.2.6) to get

$$\rho C\frac{\partial T}{\partial t} = k\left(\frac{\partial^2 T}{\partial r^2} + \frac{1}{r}\cdot\frac{\partial T}{\partial r} + \frac{\partial^2 T}{\partial x^2}\right) \qquad (3.2.7)$$

THE BOUNDARY CONDITIONS

The existing boundary conditions are (with reference to fig. 3.2.2):

Boundary OA

Since the temperature distribution is symmetrical with respect to the r-axis:

$$\frac{\partial T}{\partial x} = 0 \quad \text{when } x = 0 \qquad (3.2.8)$$

Boundary ED

$$-k\frac{\partial T}{\partial x} = H_{DE}(T - T_{DE}) \qquad (3.2.9)$$

where : H_{DE} = heat transfer coefficient along boundary ED

T_{DE} = external temperature at ED

Boundary BG

when x = L

$$-k\frac{\partial T}{\partial x} = H_e\left(T - T_e(x)\right) \qquad (3.2.10)$$

where: H_e = heat transfer coefficient at BG

$T_e(x)$ = Te = temperature of endplate coolant.

Boundary OB

when r = 0

$$\frac{\partial T}{\partial r} = 0 \qquad (3.2.11)$$

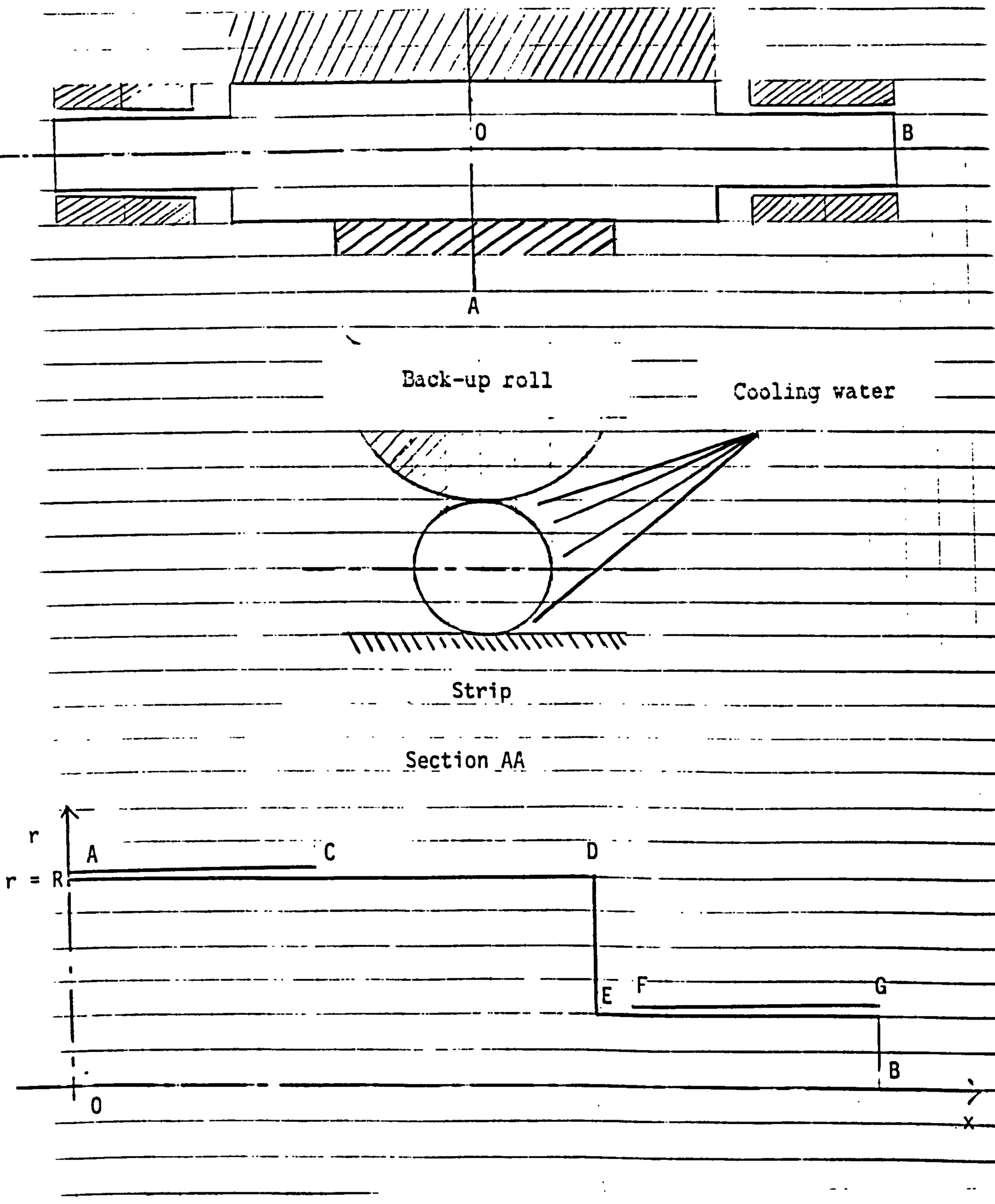

Fig 3.2.2 Schematic view of work roll and its surroundings

(Since there is symmetrical temperature distribution with respect to the x-axis).

Boundary ACD

when r = R

$$-k\frac{\partial T}{\partial r} = H_{r(x)}\left(T - T_{c(x)}\right) - \frac{q'_{(x)}}{2\pi R} \qquad (3.2.12)$$

where $H_{r(x)}$ = heat transfer coefficient at r =R

T = roll temperature function

$T_{c(x)}$ = temperature of coolant

q' = heat input per unit width (W m^{-1})

Boundaries EF and FG

$$-k\frac{\partial T}{\partial r} = H_{r(x)}\left(T - T_{b(x)}\right) - q'_{b(x)} \qquad (3.2.13)$$

where : $T_b(x)$ = external temperature of area EFG

q_b' = heat generated in bearings (W m^{-1})

3.2.1 THE DIMENSIONLESS FORM OF THE HEAT CONDUCTION EQUATIONS

In dimensionless form, eqn. (3.2.6) becomes:

$$\frac{\partial T}{\partial \tau} = \frac{\partial^2 T}{\partial r^{*2}} + \frac{1}{r^*}\cdot\frac{\partial T}{\partial r^*} + \frac{\partial^2 T}{\partial x^{*2}} \qquad (3.2.14)$$

where:

T = roll temperature function

$$\tau = \frac{kt}{\rho C R^2}$$

$$r^* = \frac{r}{R} \qquad (3.2.15)$$

$$x^* = \frac{x}{R}$$

The boundary conditions are:

For x^*:

Boundary OA, $X^* = 0$

$$\frac{\partial T}{\partial x^*} = 0 \qquad (3.2.16)$$

Boundary ED

$$\frac{\partial T}{\partial x^*} = -\frac{RH_{DE}}{k}\left(T - T_{DE}\right) \qquad (3.2.17)$$

Boundary BG

when $X^* = x_0 = L/R$

$$\frac{\partial T}{\partial x^*} = -\frac{RH_e}{k}\left(T - T_e(x)\right) \qquad (3.2.18)$$

For r^* :

Boundary OB:

when $r^* = 0$,

$$\frac{\partial T}{\partial r^*} = 0 \qquad (3.2.19)$$

Boundary ACD

when $r^* = 1$

$$\frac{\partial T}{\partial r^*} = -\frac{RH_r(x)}{k}\left(T - T_c(x)\right) + \frac{Rq'(x)}{2\pi Rk}$$

$$\frac{\partial T}{\partial r^*} = -\frac{RH_r(x)}{k}\left(T - T_c(x)\right) + q^*_{(x)} \qquad (3.2.20)$$

where: $q^* = \dfrac{q'}{2\pi k}$

Boundary EFG:

$$\frac{\partial T}{\partial r^*} = -\frac{RH_r(x)}{k}\left(T - T_b\right) + q^*_b \qquad (3.2.21)$$

3.3 THE HOLLOW CYLINDER CASE

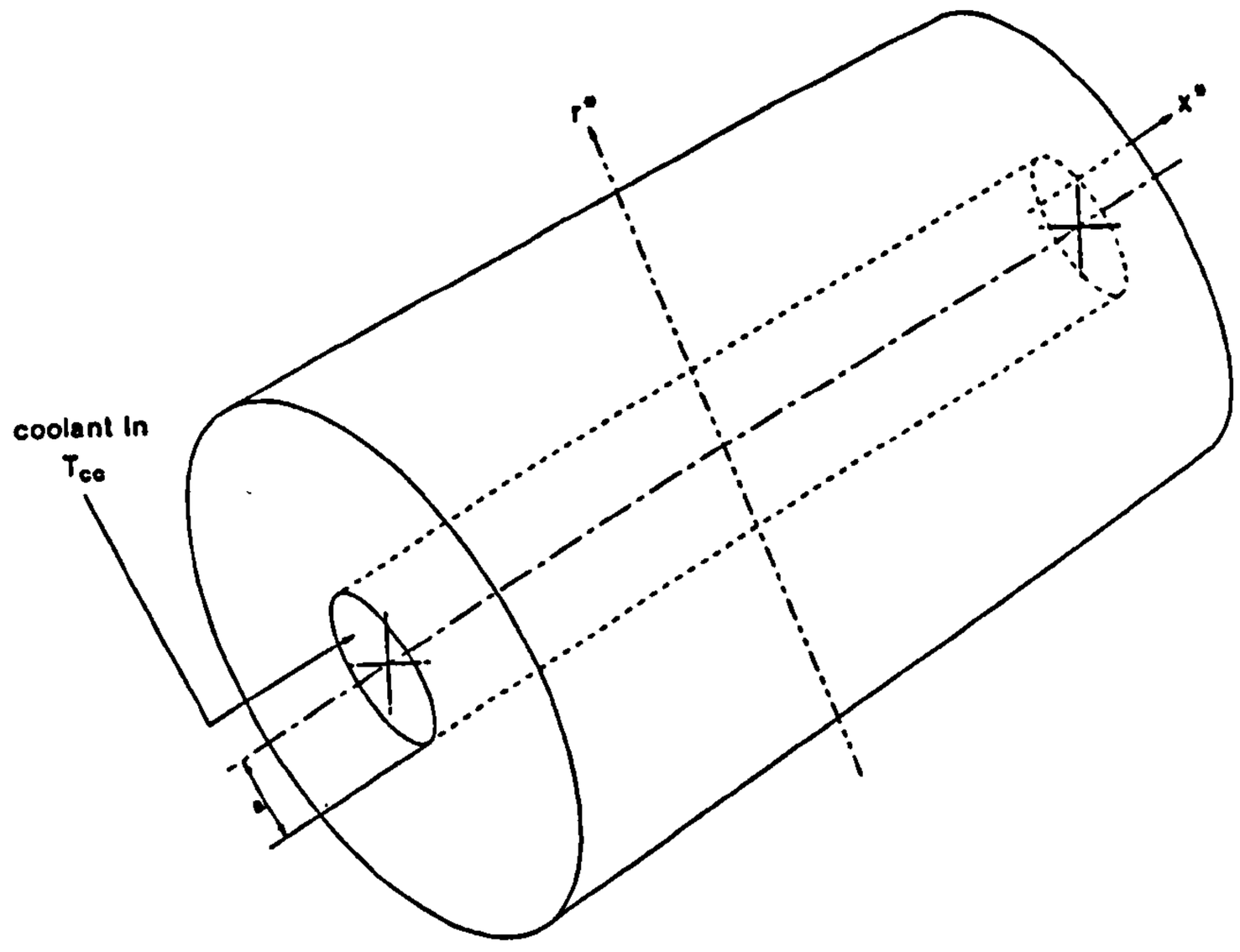

Fig. 3.3.1 Roll with hollow centre.

In some cases of mill operation a cylindrical hole is drilled in the centre of the work roll through which coolant flows in order to remove heat from the centre of the roll. The partial differential equations describing this situation is arrived at by a similar method to that previously described for a solid cylinder. An important change, however arises in the boundary conditions, this being, at $r = r_a$ (fig. 3.3.1)

$$-k\frac{\partial T}{\partial r} = h_{(x)}\left(T_{cc(x)} - T\right) \qquad (3.3.1)$$

where:

$T_{cc(x)}$ = roll coolant temperature function at centre

h(x) = heat transfer coefficient at the centre of the roll

In dimensionless form this becomes

$$\frac{\partial T}{\partial r^*} = \frac{Rh_{(x)}}{k}\left(T - T_{cc}(x)\right) \qquad (3.3.2)$$

3.4 THE FINITE DIFFERENCE REPRESENTATIONS

Equations (3.2.14 - 3.2.21) can be solved numerically by replacing the partial derivatives with finite differences[120,121] and integrating the resulting set of ordinary differential equations with respect to time.

The forward difference representation of eqn. (3.2.14) is given as:

$$\nabla T_{i,j}^{k+1} = \frac{T_{i,j+1}^{k} - 2T_{i,j}^{k} + T_{i,j-1}^{k}}{\Delta r^{*2}} + \frac{1}{r_j^{*}} \cdot \frac{T_{i,j+1}^{k} - T_{i,j-1}^{k}}{2\Delta r^{*}} + \frac{T_{i+1,j}^{k} - 2T_{i,j}^{k} + T_{i-1,j}^{k}}{\Delta x^{*2}} \qquad (3.4.1)$$

where: k = k^{th} time interval

i = i^{th} column of elements

j = j^{th} row of elements

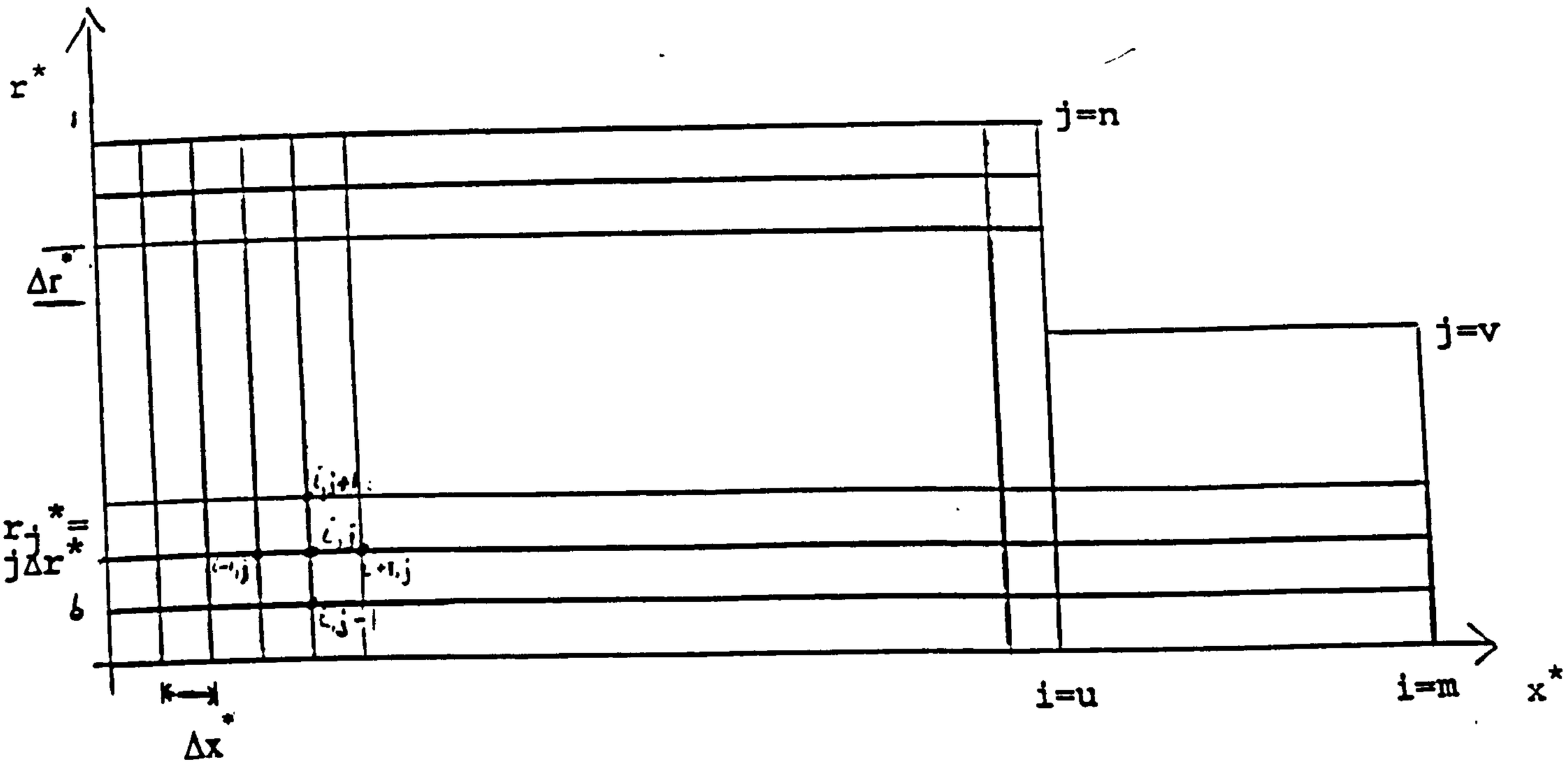

Fig. 3.4.1. Regular network of mesh Δx^*, Δr^*

From fig. 3.4.1, showing the mesh arrangement, it is clear that equation 3.3.1 is unworkable, since the term r^*_j is equal to zero at j equal to zero. However, if eqn. (3.2.6) is examined, we can see that the term $1/r\ (\partial T/\partial r)$, which at $r^* = 0 = r$, $\partial T/\partial r = 0$, is equivalent to zero divided by zero.

Thus, using L' Hopital's rule we get for r = 0

$$\lim_{r\to 0}\left(\frac{1}{r}\cdot\frac{\partial T}{\partial r}\right) = \frac{\partial^2 T}{\partial r^2}$$

So eqn. (3.2.6), for r = 0, can be replaced by

$$\frac{\partial T}{\partial \tau} = 2\frac{\partial^2 T}{\partial r^{*2}} + \frac{\partial^2 T}{\partial x^{*2}} \qquad (3.4.2)$$

and the finite difference form becomes (j = 0):

$$\nabla T_{i,0} = \frac{2\left(T_{i,1} - 2T_{i,0} + T_{i,-1}\right)}{\Delta r^{*2}} + \frac{T_{i+1,0} - 2T_{i,0} + T_{i-1,0}}{\Delta x^{*2}} \qquad (3.4.3)$$

This latter form will be used in the computer algorithm since it has the advantage of ignoring the fictitious nodes at j= -1.

$$\nabla T_{i,0} = \frac{4\left(T_{i,1} - T_{i,0}\right)}{\Delta r^{*2}} + \frac{T_{i+1,0} - 2T_{i,0} + T_{i-1,0}}{\Delta x^{*2}} \qquad (3.4.4)$$

For eqn. (3.3.2), the finite difference form is (b =a/R):

$$\frac{T_{i,b+1} - T_{i,b-1}}{2\Delta r^*} = \frac{Rh_{(x)}\left(T_{i,b} - T_{cc}(x)\right)}{k}$$

$$T_{i,b+1} - T_{i,b-1} = 2\Delta r^* \frac{Rh_{(x)}}{k}\left(T_{i,b} - T_{cc}(x)\right)$$

$$T_{i,b-1} = T_{i,b+1} - 2\Delta r^* \frac{Rh_{(x)}}{k}\left(T_{i,b} - T_{cc}(x)\right)$$

Eqn. (3,2,16) becomes:

$$(\text{when } x^* = 0,\ \frac{\partial T}{\partial x^*} = 0) \Rightarrow$$

$$\frac{T_{i+1,j} - T_{i-1,j}}{2\Delta x^*} = 0$$

$$T_{i+1,j} = T_{i-1,j}, \quad i = 0,\ j = 0, 1, \ldots n \qquad (3.4.6)$$

Eqn. (3.2.17) becomes (boundary DE):

$$\frac{\partial T}{\partial x^*} = -\frac{RH_{DE}}{k}(T - T_{DE}) \quad \Rightarrow$$

$$\frac{T_{i+1,j} - T_{i-1,j}}{2\Delta x^*} = -\frac{RH_{DE}}{k}(T_{ij} - T_{DE})$$

$$T_{i+1,j} = -\frac{2\Delta x^* RH_{DE}}{k}(T_{ij} - T_{DE}) + T_{i-1,j}$$

i=u, j=v, v+1, ... n

(3.4.7)

Eqn. (3.2.18) becomes (boundary BG, $x^* = 0$):

$$\frac{T_{i+1,j} - T_{i-1,j}}{2\Delta x^*} = -\frac{RH_e}{k}\left(T_{i,j} - T_e(x)\right), \qquad i = m,\ j = 0, 1, .. v$$

... (3.4.8)

When $r^* = 0$, $\frac{\partial T}{\partial r^*} = 0$, (boundary OA), the finite difference representation is:

$$T_{i,j+1} = T_{i,j-1}, \qquad j = 0,\ i = 0, 1, \ldots, n \qquad (3.4.9)$$

Eqn.(3.2.20) becomes (boundary ACD), $r^* = 1$,

$$\frac{\partial T}{\partial r^*} = -\frac{RH_r(x)}{k}(T - T_c(x)) + q_x^*$$

$\Rightarrow$

$$\frac{T_{i,j+1} - T_{i,j-1}}{2\Delta r^*} = -\frac{RH_r(x)}{k}(T_{ij} - T_c(x)) + q_i^*$$

where $q_i^* \left\{ \begin{array}{ll} = q_x^*, & j = n \\ = 0, & j < n \end{array} \right\}$

$$T_{i,j+1} = 2\Delta r^* \left[q_i^* - \frac{RH_r(x)}{k}(T_{ij} - T_c) \right] + T_{i,j-1},\ i = 0, 1, .., u;\ j = n$$

(3.4.10)

Eqn.(3.2.21), (boundary EFG), becomes:

$$T_{i,j+1} = 2\Delta r^{*}\left[q_b^{*} - \frac{RH_r(x)}{k}\left(T_{i,j} - T_b\right)\right] + T_{i,j-1},\ i = u, u+1, \ldots m,\ j = v \qquad (3.4.11)$$

3.5 DIVISION OF ROLL INTO ELEMENTS

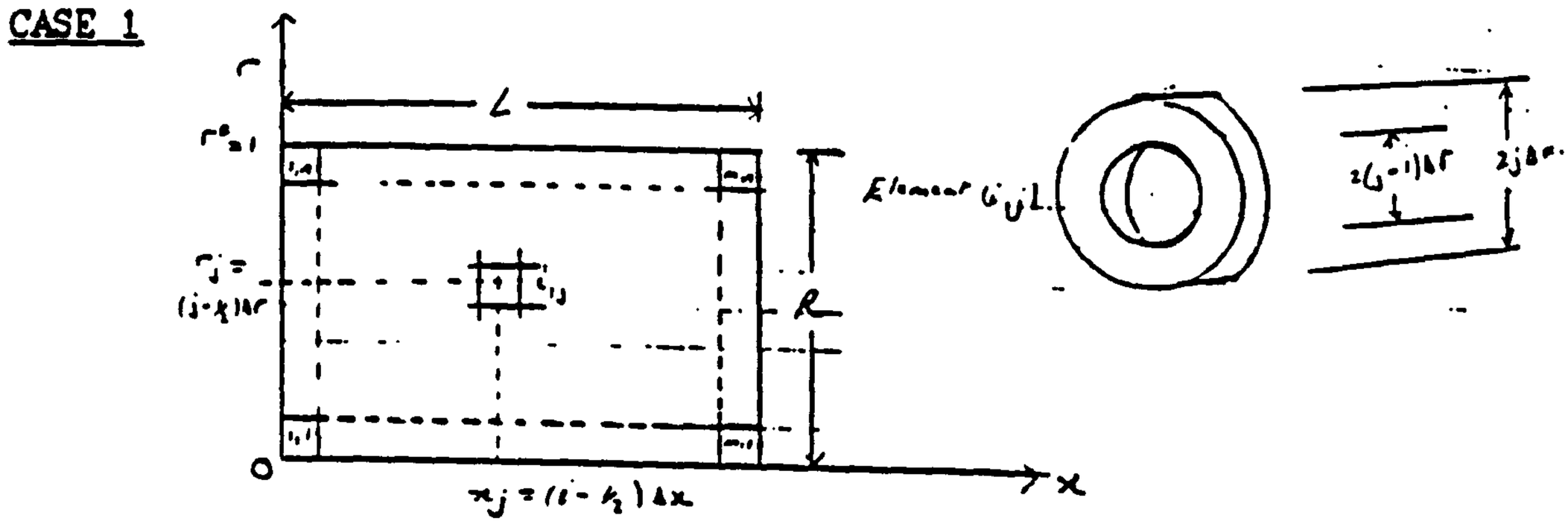

Fig. 3.5.1 Roll element notation.

When the roll is divided according to fig. 3.5.1, the distance r_j lies midway between the radial elements j and j+1. The position x_j is similarly defined. This means that the last radial plane does not coincide with the surface of the roll. From this fact it can be deduced that the actual roll surface temperature will be a little higher than that predicted by the model. The magnitude of the difference will be dependent on the number of radial nodes used, neglecting error terms and inaccurate data.

CASE 2

If the roll is to be divided into n radial elements, the distance between any adjacent two (see fig. 3.4.1) is found simply as

$$\Delta r^{*} = 1/n \qquad (3.5.1)$$

bearing in mind that the number 1 of eqn. (3.5.1) represents the plane at which r* is equal to 1. This method of dividing the roll implies that a plane of nodes will coincide with the surface of the roll as well as with the centre line of the roll.
It is also implicit that

$$r^*_j = j\Delta r^* \qquad (3.5.2)$$

A similar treatment lies behind the positioning of the axial elements, due to the matching of the nodes with the actual spray nozzles.
However, this method of dividing the roll may not account for the position of the coolant sprays. This disadvantage can be negated somewhat by increasing the number of radial nodes, but this in turn results in increased computation times and the need to use more individual heat transfer coefficients.

CASE 3

Fig. 3.5.2 shows the situation in which one of the strings from the node (1,j) is intersected by the boundary OA. The distance between

the node (1,j) and the boundary OA, $\varepsilon\Delta x^*$, where $0 \leq \varepsilon \leq 1$,

is less than the mesh size Δx^*.

The boundary condition existing at $x^* = 0$ is given by eqn. (3.2.16),

$$\frac{\partial T}{\partial x^*} = 0 \qquad (3.2.16)$$

and its finte difference representation by:

$$T_{-1,\,j} = T_{1,\,j} \qquad (3.5.3)$$

since we can make the fictitious distance between i = -1 and i = 0, and the distance between i=0 and i=1, equal, i.e,

$\varepsilon\Delta x^*$. However, since the distance between i = 0 and i = 1,

CASE 3

Fig. 3.5.2. One string intercepted by a curved boundary.

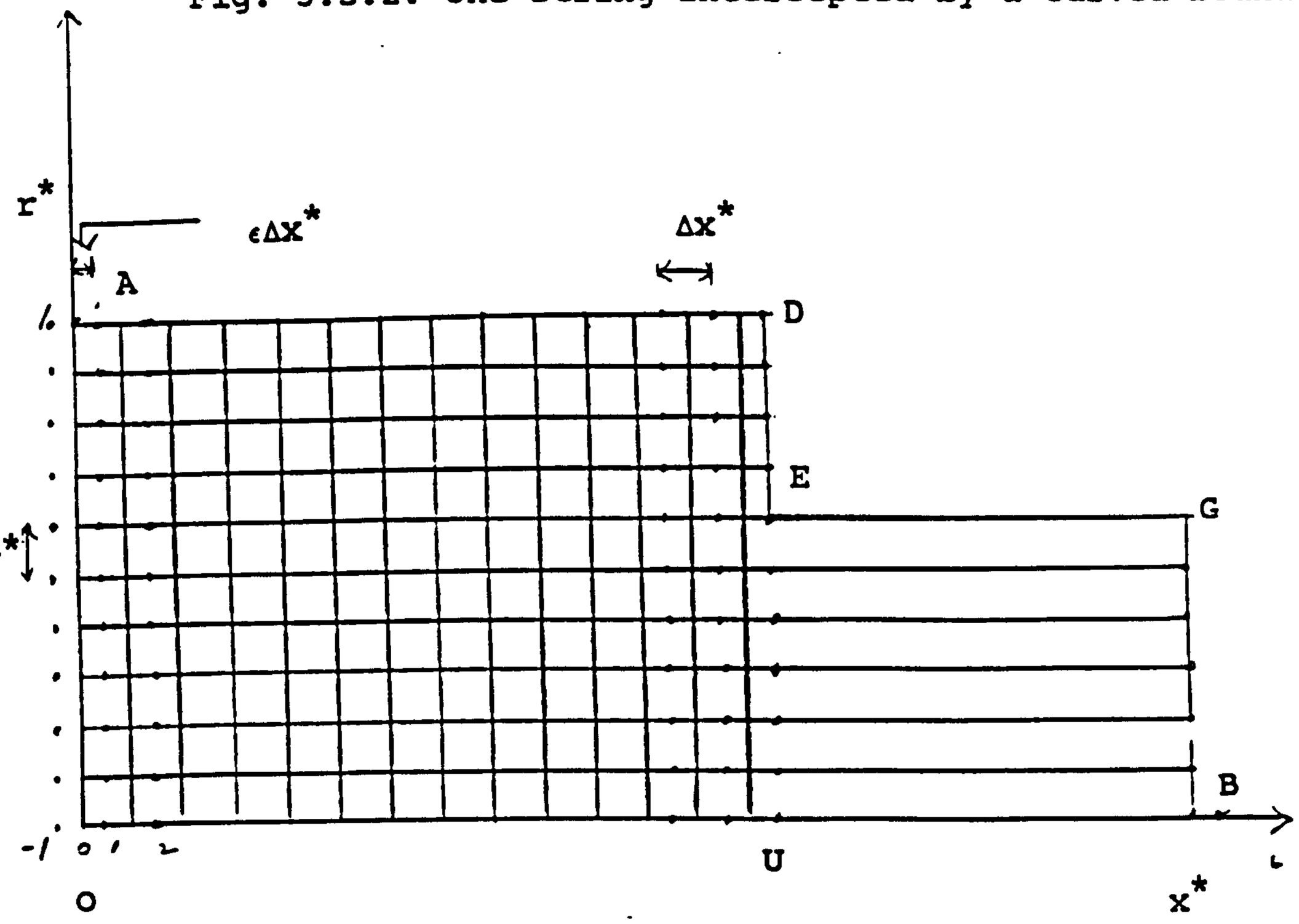

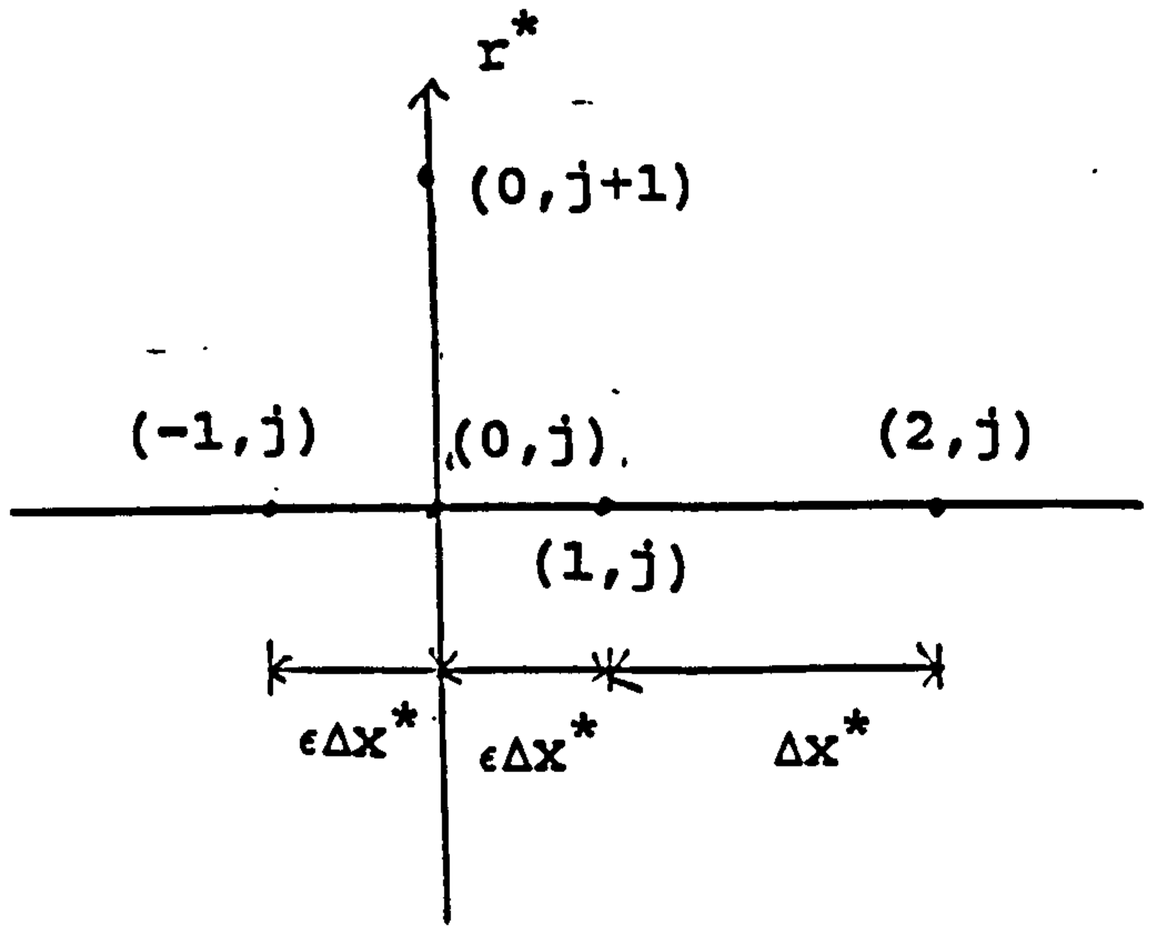

Fig. 3.5.3 Arrangement of nodes near the minor axis of the roll (boundary OA, fig. 3.2.1)

and from i = 1 to i = 2 are not equal we can modify the relevant finite equations of section 3.2 to account for this. Let us examine the position at node (1,j). By a Taylor series expansion of $(-2\varepsilon\Delta x^*)$ and Δx^* we, respectively, obtain:

$$T_{-1,j} = T_{1,j} - 2\varepsilon\Delta x^* \cdot \left.\frac{\partial T}{\partial x^*}\right|_{1,j} + \frac{\left(2\varepsilon\Delta x^*\right)^2}{2!} \cdot \left.\frac{\partial^2 T}{\partial x^{*2}}\right|_{1,j} + \ldots$$

$$T_{2,j} = T_{1,j} + \Delta x^* \cdot \left.\frac{\partial T}{\partial x^*}\right|_{1,j} + \frac{\left(\Delta x^*\right)^2}{2!} \cdot \left.\frac{\partial^2 T}{\partial x^{*2}}\right|_{1,j} + \ldots \quad (3.5.5)$$

Multiply eqn. (3.5.5) by 2ε and add to eqn. (3.5.4) to eliminate ∂T/∂x we get:

$$T_{-1,j} + 2\varepsilon T_{2,j} = T_{1,j} + 2\varepsilon T_{1,j} + \frac{(2\varepsilon)^2\left(\varepsilon x^*\right)^2}{2!} \cdot \left.\frac{\partial^2 T}{\partial x^{*2}}\right|_{1,j} +$$

$$2\varepsilon\frac{(\Delta x^*)^2}{2!} \cdot \left.\frac{\partial^2 T}{\partial x^{*2}}\right|_{1,j}$$

$$\varepsilon(2\varepsilon+1)\left(\Delta x^{*}\right)^{2}.\frac{\partial^{2}T}{\partial x^{*^{2}}} = 2\varepsilon T_{2,j} - T_{1,j}\left(1+2\varepsilon\right) + T_{-1,j}$$

$$\left.\frac{\partial^{2}T}{\partial x^{*^{2}}}\right|_{1,j} = \frac{2\varepsilon T_{2,j} - T_{1,j}\left(1+2\varepsilon\right) + T_{-1,j}}{\varepsilon(2\varepsilon+1)\Delta x^{*^{2}}} \qquad (3.5.6)$$

If $\varepsilon = 1/2$

$$\left.\frac{\partial^{2}T}{\partial x^{*^{2}}}\right|_{1,j} = \frac{T_{2,j} - 2T_{1,j} + T_{-1,j}}{\Delta x^{*^{2}}} \qquad (3.5.7)$$

which is the same form as eqn. (3.4.1). Further, since from eqn. (3.5.3) $T_{-1,j} = T_{1,j}$, then,

$$\left.\frac{\partial^{2}T}{\partial x^{*^{2}}}\right|_{1,j} = \frac{T_{2,j} - T_{1,j}}{\partial x^{*^{2}}} \qquad (3.5.8)$$

For the purpose of the computer algorithm it is now necessary to modify the axial dimensions of the roll to ensure that the boundaries at DE and BG coincide with the nodes at i = u. This will ensure that the boundary conditions are easily approximated by the finite difference equations.

3.6 ERROR TERMS FOR FINITE DIFFERENCES

A Taylor series can be used to determine the error involved in the finite difference approximation for eqn. (3.2.14).

Consider that temperature T is a function of t, x, and r, so that, based on the Taylor theorem, T can be expanded at t + Δt in terms of T at t as:

$$T(t+\Delta t, x, y) = T(t,x,y) + \frac{\partial T}{\partial t}.\Delta t + \frac{1}{2!}.\frac{\partial^2 T}{\partial t^2}.\Delta t^2 + \frac{1}{3!}.\frac{\partial^3 T}{\partial t^3}.\Delta t^3 + \frac{1}{4!}.\frac{\partial^4 T}{\partial t^4}.\Delta t^4$$

. . .

(3.6.1)

Eqn. (3.6.1) can be re-arranged to give

$$\frac{\partial T}{\partial t} = \frac{T(t+\Delta t, x, y) - T(t, x, y)}{\Delta t} + O(\Delta t) \qquad (3.6.2)$$

where O (Δt) is the term containing the first and higher order powers of Δt. Eqn. (3.6.2) is the basis for the forward difference approximation, hence,

$$\frac{\partial T}{\partial t} = \frac{T_{i,j}^{k+1} - T_{i,j}^{k}}{\Delta t} + O(\Delta t) \qquad (3.6.3)$$

which has an accuracy of order Δt. The error is approximately reduced by half for $\Delta t/2$.

Similarly, an expansion of T(t-Δt,x,y) in terms of T at t gives:

$$T(t-\Delta t, x, y) = T(t,x,y) - \frac{\partial T}{\partial t}.\Delta t + \frac{1}{2!}.\frac{\partial^2 T}{\partial t^2}.\Delta t^2 - \frac{1}{3!}.\frac{\partial^3 T}{\partial t^3}.\Delta t^3 + \frac{1}{4!}.\frac{\partial^4 T}{\partial t^4}.\Delta t^4 \qquad (3.6.4)$$

Eqn. (3.6.4) - (3.6.1)

$$\frac{\partial T}{\partial t} = \frac{T(t+\Delta t, x, y) - T(t-\Delta t, x, y)}{2\Delta t} + O(\Delta t)^2 \qquad (3.6.5)$$

which is the basis for the central difference approximation of $\partial T/\partial t$, viz.,

$$\frac{\partial T}{\partial t} = \frac{T_{i,j}^{k+1} - T_{i,j}^{k-1}}{2\Delta t} + O(\Delta t)^2 \qquad (3.6.6)$$

The technique demonstrated above can be applied to the terms in $\partial^2 T/\partial x^2$, $\partial^2 T/\partial r^2$, $\partial T/\partial r$. Hence,

$$\left.\frac{\partial^2 T}{\partial x^2}\right|_{i,j} = \frac{T_{i+1,j}^{k} - 2T_{i,j}^{k} + T_{i-1,j}^{k}}{\Delta x^2} + O(\Delta x)^2 \qquad (3.6.7)$$

$$\left.\frac{\partial^2 T}{\partial r^2}\right|_{i,j} = \frac{T_{i,j+1}^{k} - 2T_{i,j}^{k} + T_{i,j-1}^{k}}{\Delta r^2} + O(\Delta r)^2 \qquad (3.6.8)$$

$$\left.\frac{\partial T}{\partial r}\right|_{i,j} = \frac{T_{i,j+1}^{k} - T_{i,j-1}^{k}}{2\Delta r} + O(\Delta r)^2 \qquad (3.6.9)$$

and

$$\rho C \frac{\partial T}{\partial t} = k\left(\left.\frac{\partial^2 T}{\partial x^2}\right|_{i,j} + \left.\frac{\partial^2 T}{\partial r^2}\right|_{i,j} + \frac{1}{r}\cdot\left.\frac{\partial T}{\partial r}\right|_{i,j}\right) \qquad (3.6.10)$$

leading to

$$\frac{T_{i,j}^{k+1} - T_{i,j}^{k}}{\Delta t} = \frac{k}{\rho c}\left[\frac{T_{i+1,j}^{k} - 2T_{i,j}^{k} + T_{i-1,j}^{k}}{\Delta x^2} + \frac{T_{i,j+1}^{k} - 2T_{i,j}^{k} + T_{i,j-1}^{k}}{\Delta r^2} + \left|\frac{1}{r_j}\left(\frac{T_{i,j+1}^{k} - T_{i,j-1}^{k}}{2\Delta r}\right)\right|\right] + e$$

. (3.6.11)

where : e is the error term of order $(2\Delta r^2 + \Delta x^2 + \Delta t)$

$r_j = j\Delta r$

3.7 STABILITY AND CONVERGENCE CRITERIA

By the explicit method , eqn. (3.6.11) becomes:

$$T_{i,j}^{k+1} - T_{i,j}^{k} = \frac{k\Delta t}{\rho C(\Delta x)^2 (\Delta r)^2} \left\{ \left(T_{i+1,j}^{k} - 2T_{i,j}^{k} + T_{i-1,j}^{k}\right).(\Delta r)^2 + \right.$$

$$\left. \left(T_{i,j+1}^{k} - 2T_{i,j}^{k} + T_{i,j-1}^{k}\right).(\Delta x)^2 + \left(T_{i,j+1}^{k} - T_{i,j-1}^{k}\right)\frac{\Delta x^2}{2j} \right\}$$

$$T_{i,j}^{k+1} = \varepsilon \left\{ \left(T_{i+1,j}^{k} + T_{i-1,j}^{k}\right)(\Delta r)^2 + T_{i,j+1}^{k}\left(1 + \frac{1}{2j}\right)(\Delta x)^2 + \right.$$

$$\left. T_{i,j-1}^{k}\left(1 - \frac{1}{2j}\right)(\Delta x)^2 - 2T_{i,j}^{k}\left(\Delta r^2 + \Delta x^2\right) \right\} + T_{i,j}^{k} \qquad (3.7.1)$$

$$\text{where } \varepsilon = \frac{k\Delta t}{\rho C(\Delta x)^2 (\Delta r)^2}$$

Let θ represent the exact solution of eqn. (3.6.10), and T the numerical solution. Assume that T is without round-off errors for now, such that T and θ differ only in the error caused by replacing eqn. (3.6.10) by eqn. (3.6.11). Let

$e_{i,j}^{k} = \theta_{i,j}^{k} - T_{i,j}^{k}$, at the point

$x = x_i$, $r = r_j$, $t = t_k$. Substituting

$T = \theta - e$ into eqn. (3.7.1) to get

$$e_{i,j}^{\tau+1} = \varepsilon \left\{ \left(e_{i+1,j}^{k} + e_{i-1,j}^{k}\right)(\Delta r)^2 + \right.$$

$$\left. e_{i,j+1}^{k}\left(1 + \frac{1}{2j}\right)(\Delta x)^2 + e_{i,j-1}^{k}\left(1 - \frac{1}{2j}\right)(\Delta x)^2 \right\} +$$

$$e^{k}_{i,j}\left(1 - 2\varepsilon\left(\Delta r^2 + \Delta x^2\right)\right) -$$

$$\varepsilon\left\{\left(\theta^{k}_{i+1,j} + \theta^{k}_{i-1,j}\right)(\Delta r)^2 +\right.$$

$$\left.\theta^{k}_{i,j+1}\left(1+\frac{1}{2j}\right)(\Delta x)^2 + \theta^{k}_{i,j-1}\left(1-\frac{1}{2j}\right)(\Delta x)^2\right\} -$$

$$\theta^{k}_{i,j}\left(1 - 2\varepsilon\left(\Delta r^2 + \Delta x^2\right)\right) + \theta^{k+1}_{i,j} \qquad (3.7.2)$$

A Taylor series expansion gives:

$$\theta^{k}_{i+1,j} = \theta^{k}_{i,j} + \left.\frac{\partial\theta}{\partial x}\right|_{i,j,t_k}\Delta x + \frac{\Delta x^2}{2}\cdot\frac{\partial^2\theta_{\xi_1,j,t_k}}{\partial x^2} + \cdots \quad x_i < \xi_1 < x_{i+1}$$

$$\theta^{k}_{i-1,j} = \theta^{k}_{i,j} - \left.\frac{\partial\theta}{\partial x}\right|_{i,j,t_k}\Delta x + \frac{\Delta x^2}{2}\cdot\frac{\partial^2\theta_{\xi_2,j,t_k}}{\partial x^2} + \cdots \quad x_{i-1} < \xi_2 < x_i$$

$$\theta^{k}_{i,j+1} = \theta^{k}_{i,j} + \left.\frac{\partial\theta}{\partial r}\right|_{i,j,t_k}\Delta r + \frac{\Delta r^2}{2}\cdot\frac{\partial^2\theta_{(i,\pi_1,\tau_k)}}{\partial r^2} + \cdots \quad r_j < \pi_1 < r_{j+1}$$

$$\theta^{k}_{i,\,j-1} = \theta^{k}_{i,\,j} - \left.\frac{\partial\theta}{\partial r}\right|_{i,\,j,\,t_k} \Delta r + \frac{\Delta r^2}{2}\cdot\frac{\partial^2\theta_{(i,\,\pi_2,\,\tau_k)}}{\partial r^2} + \cdots \quad r_{j-1} < \pi_2 < r_j$$

$$\theta^{k+1}_{i,\,j} = \theta^{k}_{i,\,j} + \Delta t.\frac{\partial\theta_{(i,\,j,\,\eta)}}{\partial t} + \ldots \quad t_k < \eta < t_{k+1}$$

Substituting these equations into eqn (3.7.2) gives:

$$e^{\kappa+1}_{i,\,j} = \varepsilon\left\{\left(e^{k}_{i+1,\,j} + e^{k}_{i-1,\,j}\right)(\Delta r)^2 + e^{k}_{i,\,j+1}\left(1+\frac{1}{2j}\right)(\Delta x)^2 + e^{k}_{i,\,j+1}\left(1-\frac{1}{2j}\right)(\Delta x)^2\right\} +$$

$$e^{k}_{i,\,j}\left(1 - 2\varepsilon\left(\Delta r^2 + \Delta x^2\right)\right) -$$

$$\varepsilon\,(\Delta r)^2\,\frac{(\Delta x)^2}{2}\left\{\frac{\partial^2\theta_{(\xi_1,\,j,\,t_k)}}{\partial x^2} + \frac{\partial^2\theta_{(\xi_2,\,j,\,t_k)}}{\partial x^2}\right\} -$$

$$\varepsilon\,(\Delta x)^2\,\frac{(\Delta x)^2}{2}\left\{\left(1+\frac{1}{2j}\right)\frac{\partial^2\theta_{(i,\,\pi_1,\,\tau_k)}}{\partial r^2} + \left(1-\frac{1}{2j}\right)\frac{\partial^2\theta_{(i,\,\pi_2,\,t_k)}}{\partial r^2} + \frac{1}{j\Delta r}\cdot\frac{\partial\theta_{(i,\,j,\,t_k)}}{\partial r}\right\} +$$

$$\Delta t\,\frac{\partial\theta_{(i,\,j,\,\eta)}}{\partial t}$$

$$\text{Since } \varepsilon = \frac{k\Delta t}{\rho C\,(\Delta x)^2\,(\Delta r)^2}$$

$$e_{i,j}^{k+1} = \varepsilon \left\{ \left(e_{i+1,j}^{k} + e_{i-1,j}^{k} \right)(\Delta r)^2 + \right.$$

$$\left. e_{i,j+1}^{k} \left(1 + \frac{1}{2j}\right)(\Delta x)^2 + e_{i,j+1}^{k} \left(1 - \frac{1}{2j}\right)(\Delta x)^2 \right\} +$$

$$e_{i,j}^{k} \left(1 - 2\varepsilon\left(\Delta r^2 + \Delta x^2\right)\right) -$$

$$\frac{k\Delta t}{2\rho C} \left\{ \begin{array}{l} \frac{\partial^2\theta}{\partial x^2}(\xi_1, j, t_k) + \frac{\partial^2\theta}{\partial x^2}(\xi_2, j, t_k) + \frac{2}{r_j}\frac{\partial\theta}{\partial r}(i, j, t_k) + \\ (1 + \frac{1}{2j})\frac{\partial^2\theta}{\partial r^2}(i, \pi_1, t_k) + (1 - \frac{1}{2j})\frac{\partial^2\theta}{\partial r^2}(i, \pi_2, t_k) \end{array} \right\}$$

$$+ \Delta t.\frac{\partial\theta}{\partial t}(i, j, \eta)$$

$$= \varepsilon \left\{ \left(e_{i+1,j}^{k} + e_{i-1,j}^{k} \right)(\Delta r)^2 + \right.$$

$$\left. e_{i,j+1}^{k} \left(1 + \frac{1}{2j}\right)(\Delta x)^2 + e_{i,j+1}^{k} \left(1 - \frac{1}{2j}\right)(\Delta x)^2 \right\} +$$

$$e_{i,j}^{k} \left(1 - 2\varepsilon\left(\Delta r^2 + \Delta x^2\right)\right) +$$

$$\Delta t \left\{ \frac{\partial\theta}{\partial t}(i, j, \eta) - \frac{k}{2\rho C} \left[\begin{array}{l} \frac{\partial^2\theta}{\partial x^2}(\xi_1, j, t_\tau) + \frac{\partial^2\theta}{\partial x^2}(\xi_2, j, t_\tau) + \frac{2}{r_j}\frac{\partial\theta}{\partial r}(i, j, t_k) + \\ (1 + \frac{1}{2j})\frac{\partial^2\theta}{\partial r^2}(i, \pi_1, t_k) + (1 - \frac{1}{2j})\frac{\partial^2\theta}{\partial r^2}(i, \pi_2, t_k) \end{array} \right] \right\}$$

$$t_k \le \eta \le t_{k+1},\ x_{i-1} \le \xi \le x_{i+1},\ r_{j-1} < \pi \le r_{j+1}$$

Let E^τ be the magnitude of the maximum error in the row of calculations for $t = t_k$ and let $M > 0$ be an upper bound for the magnitude for the expression in the second set of

brackets in eqn.(3.7.3).

If $\varepsilon((\Delta r)^2 + (\Delta x)^2) \leq 1/2$, all the coefficients in eqn. (3.7.3) are positive or zero, to give the inequality:

$$\left|e_{i,j}^{k+1}\right| \leq 2\varepsilon(\Delta r)^2 E^k + 2\varepsilon(\Delta x)^2 E^k + E_{i,j}^k\left(1 - 2\varepsilon\left((\Delta r)^2 + (\Delta x)^2\right)\right) + M\Delta t$$

This is true for all $e_{i,j}^{\tau}$ at $t = t_{\tau+1}$, hence,

$$E^{k+1} \leq E^k + M\Delta t$$

Since this is true at each time step,

$$E^{k+1} \leq E^k + M\Delta t \leq E^{k-1} + 2M\Delta t \ldots$$

$$\leq E^0 + (k+1)M\Delta t = E^0 + Mt_{k+1}$$

$$= Mt_{k+1}$$

because at $t = 0$, E^0 is zero since θ is given by the initial conditions.

As $\Delta x \to 0$, $\Delta r \to 0$ and $\Delta t \to 0$ if

$$\frac{k\,\Delta t\,(\Delta r)^2(\Delta x)^2}{\rho C\,(\Delta x)^2(\Delta r)^2} \leq \frac{1}{2}, \text{ and } M \to 0$$

because as Δx, Δr and Δt get smaller,

$$\left\{\frac{\partial\theta_{(i,j,\eta)}}{\partial t} - \frac{k}{2\rho C}\left[\frac{\partial^2\theta_{(\xi_1,j,t_k)}}{\partial x^2} + \frac{\partial^2\theta_{(\xi_2,j,t_k)}}{\partial x^2} + \frac{2}{r_j}\cdot\frac{\partial\theta_{(i,j,t_k)}}{\partial r} + \right.\right.$$

$$\left(1+\frac{1}{2j}\right)\frac{\partial^2\theta_{(i,\pi_1,t_k)}}{\partial r^2}+\left(1-\frac{1}{2j}\right)\frac{\partial^2\theta_{(i,\pi_2,t_k)}}{\partial r^2}\Bigg]\Bigg\} \Longrightarrow$$

$$\left\{\frac{\partial\theta}{\partial t}-\frac{k}{\rho C}\left[\frac{\partial^2\theta}{\partial r^2}+\frac{1}{r}\cdot\frac{\partial\theta}{\partial r}+\frac{\partial^2\theta}{\partial x^2}\right]\right\}$$

$$= 0$$

The last equation follows from eqn. (3.6.10). Hence, it follows the explicit method is convergent for

$$\varepsilon\left((\Delta r)^2+(\Delta x)^2\right)\leq\frac{1}{2}$$

or

$$\frac{k\,\Delta t\,(\Delta r)^2+(\Delta x)^2}{\rho C\,(\Delta x)^2\,(\Delta r)^2}\leq\frac{1}{2},\ \text{because}$$

the errors approach zero as Δt, Δx and Δr are made smaller.

In dimensionless units, the convergence criterion becomes:

$$\frac{\Delta\tau\left[(\Delta r^*)^2+(\Delta x^*)^2\right]}{(\Delta r^*)^2\,(\Delta x^*)^2}\leq\frac{1}{2}$$

3.8 STANDARD (DAVY McKEE) SPRAY BAR ARRANGEMENT

A standard Davy McKee (Poole) Ltd. spray system is configured around the work rolls as shown in fig. 3.8.1. The seven spray levels are achieved through the combination of valves shown in Table 3.8.1. Table 3.8.2 shows how the the levels are defined for each nozzle position.

Fig. 3.8.1. Standard spray bar arrangement.

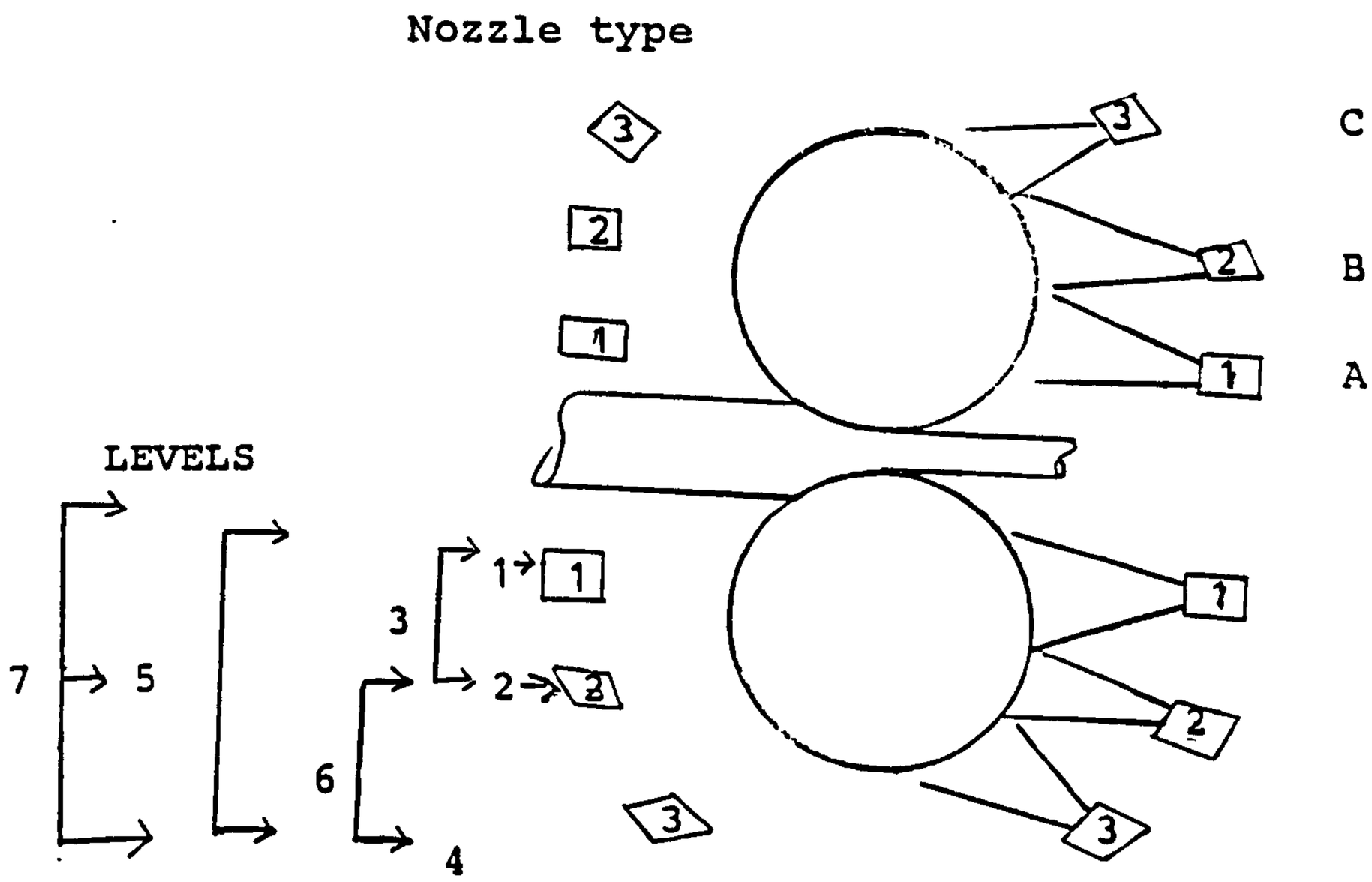

Level	Spray combination
0	no spray
1	A only
2	B only
3	A + B
4	C only
5	A + C
6	B + C
7	A + B + C

Table 3.8.1. Arrangement of nozzles according to levels across the roll length for the roll shown in fig. E7.

Level	No.of type 1 Nozzles	No.of type 2 Nozzles	No.of type 3 Nozzles
1	9	0	0
2	0	9	0
3	9	9	0
4	0	0	9
5	9	0	9
6	0	9	9
7	9	9	9

Table 3.8.2. Definition of levels for each nozzle position.

Level	For each nozzle position No.of type 1 Nozzles	No.of type 2 Nozzles	No.of type 3 Nozzles
1	1	0	0
2	0	1	0
3	1	1	0
4	0	0	1
5	1	0	1
6	0	1	1
7	1	1	1

3.8.2 SPRAY HTC EQUATIONS

Based on a report submitted by F. Robinson[126] on the effect of each relevant parameter, such as coolant flow rate, nozzle diameter, and nozzle angle, on the cooling ability of each type of spray, the following equation was derived[127]:

$$Nu = 42\ Re^{0.4}\ (L/d_c)^{-1.09}(\tan\theta/2)^{-1.2}\ Pr^{0.36} \qquad ...(3.8.1)$$

where

$$Nu = \text{Nusselt number} = hd_c/k$$

Re = Reynolds number = $d_c v/\rho M$

Pr = Pradtl number = $C_p \mu/k = 5.25$

ρ = Coolant density (kg m^{-3})

μ = Fluid dynamic viscosity = 8 x 10^{-4} kg s^{-1} m^{-2}

ν= Kinematic viscosity = μ/ρ = 8 x 10^{-7} m^2 s^{-1}

C_p = Fluid specific heat capacity = 4.2 x 10^{-3} J kg^{-1} $^oK^{-1}$

k = Thermal conductivity = 0.64 W m^{-1} $^oK^{-1}$

d_c = Nozzle diameter (m)

L = Distance of nozzle from surface

θ = Nozzle angle = 15^o for flats and cone type nozzles

Q = Volumetric flow rates (m^3 s^{-1})

h = Heat transfer coefficient due to water spray cooling

v = Spray velocity = $\frac{Q}{\pi}\left(\frac{2}{d_c}\right)^2$ (m s^{-1})

Thus equation (3.8.1) can be simplified to:

$$h = 168306\ Q^{0.4}\ dc^{-0.31}\ L^{-1.09} \qquad (3.8.2)$$

for the special case of Mill B spray system (figs. 3.8.1 and E7).

CHAPTER 4

PLANT MEASUREMENTS

4.1 TEST PROCEDURES AT MILL A

Data collection took place during the period 14 - 18 October, 1985 at Mill A, a single stand reversing mill for rolling aluminium alloys. The procedure used to collect data is outlined below.

For a fixed rolling schedule the following data was gathered:

1. Chart recordings, (see fig. E1), were made of rolling load, current and voltage supplied to drive motors, and roll speed. Normal plant sensors were used to provide inputs to the chart recorders. The rest and rolling times were deduced from the chart recordings. Figure E2 shows a summary of part of the data collected at Mill A. Figure E3 shows a chart detailing the movement of slabs through the mill. Figure E3 reads, for example, that the temperature measurement of the roll was started 200 seconds after completion of the rolling of slab 1. This was followed by a further 205 seconds before rolling of the next slab began. (Seven slabs

were rolled following a rolling change, prior to the start of data gathering).

2. Temperatures were recorded at alternative passes, starting with the first pass, using a hand-held two-pronged K-type chromel-alumel thermo-couple probe. Strip entry temperatures for the passes when the temperatures were not measured were estimated using methods developed at Davy McKee (Poole) Ltd.

3. Coolant zone settings are shown by fig. E4. Coolant, roll end, bearing and ambient temperatures were recorded. No data was available for coolant flowrates, nozzle type or size at Mill A.

4. Roll surface temperatures were measured for the bottom work roll as soon as possible after the mill stopped. The hand-held thermocouple probe was placed on the roll at desired points. These points were located by using a wooden template. The template was marked with test points symmetrical about the roll centre line to a distance of 1000mm from the centre line.

5. Roll cambers were recorded by compressing rods of a soft aluminium alloy in the roll bite for the cold rolls (to measure ground crown) and immediately after rolling a given number of slabs . The aluminium rods were fixed 50mm apart, in an aluminium bar. The difference in indentation of the rods were measured by a micrometer. Subtracting ground camber from rolled camber gave the thermal camber across the roll. Repeatability of the readings were within the range microns. These errors were due to the care required in locating the point of maximum indentation for each rod. The thermal cambers were taken as being relative to the expansion of the roll 800mm from the drive side of the roll centre line.

The measured thermal cambers across the work roll are shown in fig. E5.

4.1.1 OBSERVATIONS ON TEST PROCEDURES AT MILL A

The roll temperature test began within 200 seconds after the coiling pass and took three to five minutes. The temperature of the roll did not appear to change during that time. An unknown quantity of coolant flowed for 224 seconds after the rolling of slab 3 (the third slab rolled after temperature readings commenced). The flow was observed to be less than that during rolling.

4.2 TEST PROCEDURES AT MILL B

Data collection took place on Friday, 7th November, 1986, at Mill B, a single stand hot reversing mill. Data was collected for alloy 3004, a 1.3208m wide strip. The procedure was as follows:

1. Rolling loads, power, times were provided by normal mill sensors and chart recordings.

2. The sprays were set to level 3^{+} on both entry and exit sides of the roll (according to fig. E7). Two coils were rolled.

3. Roll centre and edge temperatures were recorded.

4. Roll cambers were recorded as detailed above. The aluminium rods were placed 4 inches (101.6mm) apart,

---

+ Each spray level corresponds to a specific arrangement of the spray nozzles, and hence to the volume of coolant flow (see pp. 84 - 85).

corresponding to nozzle positions across the roll. The thermal cambers were taken as being relative to the radial expansion at the edge of the roll from the operator side (see fig. E8).

The whole procedure was repeated with sprays set at levels 2 and 1, respectively. The complete list of recorded data is given in fig. E6.

4.3 CALIBRATION OF THERMAL CAMBER MODELS

The thermal camber models were calibrated using the data summarised in Table 4.3.2 below. The physical properties assumed for the work roll and strip are given in Table 4.3.1.

Table 4.3.1 - Roll and strip physical properties.

	Roll	Strip
Thermal conductivity kW m^{-2} $^{o}C^{-1}$	0.045	0.173
Thermal diffusivity m^2 s^{-1}	1.24 x 10^{-5}	6.104 x 10^{-5}

Table 4.3.2. Spray levels during the rolling of 8 coils.

Nozzle No. from roll ℄	1	2	3	4	5	6	7	8	9	No.of coils rolled	℄ Temperature	End Temperature	Neck Temperature
Spray level	7	7	7	3	3	2	1	0	0	1	-	-	-
	3	3	3	3	3	3	3	0	0	2	-	-	-
	3	3	3	3	3	3	3	0	0	3	-	-	-
	3	3	3	3	3	3	3	0	0	4	68	53	49
	2	2	2	2	2	2	2	0	0	5	-	-	-
	2	2	2	2	2	2	2	0	0	6	72	54	49
	1	1	1	1	1	1	1	0	0	7	-	-	-
	1	1	1	1	1	1	1	0	0	8	78	54	49

CHAPTER 5

COMPARISONS BETWEEN MILL MEASUREMENTS AND THE MATHEMATICAL MODELS

5.1 INTRODUCTION

The most important test of the mathematical models for predicting work roll thermal cambers and strip profiles are their abilities to accurately reflect actual data. Data was obtained at two mills during the course of this project, as detailed in Chapter 4.

This section of the thesis will compare measured temperatures and cambers with the results of the thermal camber model of Chapter 3 and that based on the ideas of Oshima et al.[67] detailed in Chapter 2. The former model is termed the "large" model and the latter, the "fast" model, hereafter. The prediction of strip profile using a strip profile model will also be examined in Chapter 7. However, no measured data on strip profile was available.

5.2 COMPARISONS FOR MILL A

Plant data were obtained at Mill A as described in Chapter 4.

5.2.1 ROLL TEMPERATURE MATCHING WITH DATA FROM MILL A

One deficiency of the modelling process is that there is no reliable method of calculating heat transfer coefficients based solely on the spray configuration. In view of this fact, the operating heat transfer coefficients for the modelling of roll thermal camber were obtained by matching the calculated temperatures to the measured temperatures at equivalent points on the actual roll and that of the models. In practice roll temperatures are relatively simple to obtain after the coiling pass with minimum disruption of the rolling program, as discussed in Chapter 4.

5.2.1.1 DETERMINATION OF HEAT TRANSFER COEFFICIENTS

No quantitative data on the spray levels was available at Mill A. The heat transfer coefficients were determined from the combination of overall and ambient heat transfer coefficients which resulted in the nearest match to the measured temperatures. A further criterion was that the value of the ambient heat transfer coefficient must be such that the temperature of the roll calculated for the coiling pass must fall as close as required to the temperature of the roll at the time of measurement. After that, each nozzle ratio can be tuned to match the measured temperatures as closely as desired.

5.2.1.2 MEASURED THERMAL CAMBERS FOR MILL A

Curves of thermal camber development on the work roll against time are shown in fig. E5. The curve marked "1st slab" represents the measured camber across the work roll immediately after the rolling of the first slab. The thermal camber at the centre of the roll was measured at

193 microns and remains close to this value up to a distance of 300mm from the roll centre line where the camber was found to be 190 microns. At the strip edge, 550mm from the centre line, the thermal camber falls to 75 microns, and at 800mm from the centre line to 35 microns. The roll thermal camber was next measured after a further two slabs were rolled, 29 minutes after the first slab, and is shown by fig.E5 by the curve marked "3rd slab". The pattern of this curve is similar to that described above, except that higher thermal cambers were in evidence. The thermal camber at the roll centre line is now 244 microns, falling off to 158 microns at the strip edge, and 43 microns at 800mm from the centre line (on the operator side). After the seventh slab was rolled the thermal camber at the roll centre had risen to 305 microns and 23 microns at 800 mm from the roll centre line.

5.3 COMPARISONS BETWEEN MEASURED AND PREDICTED CAMBERS USING "LARGE" AND "FAST" THERMAL CAMBER MODELS.

Figure E5 clearly indicates the dynamic nature of thermal camber. However, because thermal camber builds up relatively slowly, as fig.E5 shows, we can place some reliance on the data, especially since the method of measurement was so simple and elegant.

5.3.1 H.T.C. = 17.5 Large Model. HTC = 17.5; Poisson's Ratio, ν = 0.33, Fast Model (eqn. 2.5.3).

The temperatures across the roll surface were calculated using the "large" model to closely match the measured temperature after the third slab was rolled (see appendix E for the complete set of data). This resulted in a coolant heat transfer coefficient (H.T.C) of 17.5 kW m^{-2} $^{o}C^{-1}$, 0.1 kW m^{-2} $^{o}C^{-1}$, for the bearings and end plate, 0.06 and 2.5 kW m^{-2} $^{o}C^{-1}$ for the ambient and centre pipe, respectively. These values of heat transfer coefficients were then used

to calculate the temperatures after slab 1 was rolled. Thus if the amount of coolant did not vary too greatly during the period of rolling, then these values should be valid for the entire rolling programme. The "fast" camber model should follow the same reasoning.

Fig. F1, curve 1, shows the measured temperatures across the roll (on the operator side), after slab 1 was rolled. Curves 2 and 3 show the calculated temperatures using the large and fast thermal camber models, respectively. Both models assumed a heat transfer coefficient of 17.5 $kW\ m^{-2}\ {}^{o}C^{-1}$ for the coolant nozzles 1 - 14, and 0.06 $kW\ m^{-2}\ {}^{o}C^{-1}$ at nozzle positions 15 - 17. The close matchings of calculated temperatures for the large model can be clearly seen, but the fast model predicts temperatures 6 ^{o}C higher, up to 400mm from the roll centre line, dropping to a 3 ^{o}C difference at the strip edge. Thereafter the difference in predicted temperatures become less.

The comparison between measured and calculated cambers for the roll after slab 1 was rolled (fig.F2) also show good agreement for the large model. Again the fast model does not compare too well.

Fig. F3 shows similar comparisons between predicted and calculated temperatures, after the third slab was rolled. In this instance both the large and fast camber models predicted higher temperatures than those measured. This is not surprising because this is the case where coolant still flowed on the roll for 224 seconds after rolling. Although the model can simulate this event, no data existed on the coolant flow (which was visibly less than that during rolling); and hence no valid conclusions from a match of calculated and measured temperatures.

For the fast thermal camber model, the calculated cambers of figs. F2, F4 and F6 reflect the case where a value of 0.33 was used for Poisson ratio in eqn.(2.5.3). In this case, the roll ends were assumed to be under constrained expansion. (This assumption is not made in the large camber model, although the normalized coefficients of eqn. B3 were used as a compensation). Hence, combined with the fact that the calculated temperatures were greater with the fast model, using the value of 17.5 kW m^{-2} $^{o}C^{-1}$ for the overall heat transfer coefficient, significant differences in thermal cambers resulted from those measured. Thus, fig. F2 and Table 5.3.2 show a close matching of the calculated cambers to the measured cambers (after slab 1 was rolled), for the large model only (with 50 radial nodes). A maximum difference of 33 microns beyond the strip edge is shown. This fact can be attributed to the lower temperatures predicted in this area by this model and are depicted in fig. F1. (This is because lower roll expansions are therefore predicted). The fast model only partly show good agreement with the measured cambers for the same comparison with measured data. This holds true up to 400 mm from the roll centre line, deteriorating to a difference of 115 microns at the strip edge, and 231 microns, 800mm from the roll centre line (see Table 5.3.2).

Applying the same heat transfer coefficients to account for heat transfer from the roll after slab 1 was rolled, produced matching thermal cambers to within 24 microns between the large camber model (with 50 radial nodes) and the measured data at the strip edge. Thirty four microns difference is shown 800mm from the roll centre line (see fig. F2). However, for the same comparison the fast camber model differs by 50 microns at the strip edge and 115 microns 800mm from the centre line. That is, a difference of 149 microns, 800mm from the centre line between the large and fast camber models. This fact could be expected on examination of fig. F1 showing the larger predicted temperature differences between the models across the roll.

Comparisons of thermal camber of the work roll following the rolling of slab 3, not surprisingly show much more marked deviations. These are attributable to the fact coolant still flowed on the roll after the coiling pass. This could not be modelled correctly due to insufficient data. This demonstrates the necessity of being able to account for the heat transfer regime at all times during rolling.

Good matches with predicted roll temperatures and thermal cambers and those measured are shown in fig. F5 and F6, respectively. This comparison is with reference to the state of the roll after the seventh slab was rolled.

TABLE 5.3.1 SLAB 1. Variations in thermal cambers

Model		HTC (kW m^{-2} $^{o}C^{-1}$)	ν	Thermal Cambers/(μm) at: Roll Centre Line	Strip Edge	800mm from Centre Line
Measured →				193	75	- 35
Large	50 Nodes	17.5		194	99	- 1
Model	3 Nodes	17.5		194	73	- 50
Fast	3 Nodes	17.5	0.33	197	25	-150
Model		17.5	0.0	197	61	- 72
		22.0	0.33	190	49	- 97
		22.0	0.0	194	85	- 23

TABLE 5.3.2 slab 7. Variations in thermal cambers

Model	No. of nodes	HTC (kW m^{-2} $^{o}C^{-1}$)	ν	Thermal Cambers/(μm) at: Roll Centre Line	Strip Edge	800mm from Centre Line
Measured →				305	80	23
Large Model	50 Nodes	17.5		305	50	0
	3 Nodes	17.5		305	73	37
Fast Model	3 Nodes	17.5	0.33	305	43	-208
		17.5	0.00	305	06	- 81
		22.0	0.33	305	98	-114
		22.0	0.00	305	146	- 10

5.3.2 H.T.C. = 17.5 Large Model; HTC = 22.0 , ν = 0.33 Fast Model (eqn 2.5.3).

It was found that an overall coolant heat transfer coefficient of 22 kW m^{-2} $^{o}C^{-1}$ gave a good match between the measured and calculated temperatures using the fast model (see fig. F7) with the data after the 7th slab was rolled. As in section 5.3.1 ν was equal to 0.33 (from eqn. 2.5.3). The Oshima[67] (fast) model again showed large deviations between the measured camber and calculated cambers, as shown in fig. F8. This suggested that free expansion of the roll ends had to be assumed, i.e ν = 0. For the comparative thermal cambers, however, the deviations in calculated to measured cambers had decreased to 32 microns at the strip edge and at 800mm from the roll centre line.

5.3.3 HTC = 17.5 Large Model. HTC = 17.5, ν = 0 Fast Model (Fig. F9)

Since the value of Poisson ratio does not affect the calculated temperatures, the graphs of temperatures v. axial positions using the parameters above, are the same as in F1, F3 and F5 (when Poisson's ratio was equal to 0.33). However, now that free expansion of the roll ends is assumed, the differences in measured to calculated thermal cambers (using the fast model) are now greatly decreased. Fig. F9 now shows that the fast model calculates a thermal camber which differs by 74 microns at the strip edge, and 104 microns 800mm from the roll centre line after a seven slab simulated rolling.

5.3.4 H.T.C. = 17.5 Large Model. H.T.C. = 22.0, ν = 0 Fast Model (fig. F10)

The most suitable heat transfer coefficient for the coolant effects, as accepted by the Oshima (fast) model, was 22.0 kW m^{-2} $^{o}C^{-1}$ and ν was given the value zero for the simulated rolling of slab 7. Figure F7, curve 4, depicts the match between measured and calculated surface temperatures against distance from the roll centre line using the fast model. The resulting cambers shown in Fig. F10 point to good agreement between measured and calculated cambers. The cambers match to within 14 microns, 400mm from the roll centre line, but diverges to 34 microns at the strip edge and 33 microns 800mm from the roll centre line. The measured cambers are 305 microns at the roll centre, 263 and 23 microns, 400mm and 800mm from the roll centre line, respectively.

5.4 COMPARISONS FOR MILL B

In calibrating the "fast" thermal camber model on site, it was found that suitable heat transfer coefficients could be

estimated based on the spray levels by using the following equation derived from a model of the roll angular temperature distribution.

$$h_s = h_b + f*h_n \qquad (5.4.1)$$

where:

h_s = coolant heat transfer coefficient based on spray levels set.

h_b = "base" heat transfer coefficient = 0.8 kW m^{-2} $^oC^{-1}$

h_n = nominal heat transfer coefficient = 3.59

f = multiplication factor based on spray levels. Therefore, based on the configuration of the sprays shown in Table 3.8.1 and on equation (5.4.1), heat transfer coefficients are evaluated and shown in Table 5.4.1.

Table 5.4.1 Factors used to evaluate HTC according to eqn. (5.4.1)

	spray level							
	0	1	2	3	4	5	6	7
f	0	0.94	1.2	1.62	1.18	1.61	1.61	1.86
h_s	0.8	7.549	9.416	12.432	9.272	12.360	12.360	14.155

Figs. F11 - F13 depict the comparisons between measured and calculated temperatures and cambers along the roll axis. In this case. Cambers are taken relative to the end of the roll barrel. Figs. F11, F12 and F13 refer to data after 4, 6 and 8 coils were rolled, respectively, after a roll change. The curves labelled "predicted camber (1)" and "calculated temperature (1)" were obtained by setting the heat transfer coefficient to those given by H(1) on the coolant HTC v distance from roll centre line graphs. These values of heat transfer coefficients are based on the

method in 6.6. Correspondingly, the curves labelled (2) refer to H(2) found from eqn. (5.4.1) and Table 5.4.1.

The values of heat transfer coefficients according to H(1) gave an almost exact match of cambersin each case, although slightly higher temperatures than measured at the roll centre had to be assumed. This could not be said of the method suggested by eqn. (5.4.1).

5.5 DISCUSSION

In all the cases considered, using values of heat transfer coefficients evaluated according to the two methods mentioned above, the match between measured and calculated cambers between the two models differed sharply across the length of the roll. For example, in fig. F19 the difference in measured and calculated camber at 50.8mm from the roll centre line is 30 microns. At the strip edge the difference is 5 microns. Thus if cambers were matched at the centre, a difference of 25 microns would occur at the strip edge.

It is not immediately clear why the "large" and "fast" camber models produced different results for the same conditions. Different values of heat transfer coefficients are required because to the nature of the derivation of these values. In the latter case, it is assumed that the heat transfer conditions across the roll will be the same because the sprays were set to one level. However, it was clear from visual observations that blocked nozzles and leaking pipes resulted in uneven coolant distribution on the rolls. Using only three radial nodes in the fast model predicted greater thermal gradients in the roll from which the thermal cambers are derived. The assumed geometry of the roll was also different in the two models.

The (large) model, using the first set of heat transfer coefficient values, simulates, very closely, the exact

geometry of the rolls. The second set of heat transfer coefficients (22 kW m^{-2} $^{o}C^{-1}$) were derived from a match between the measured and calculated cambers using the fast model which assumed a completely cylindrical roll, much longer than the actual roll, thereby assuming an infinitely long roll in comparison to the width of the strip).

5.5.1 VARYING THE NUMBER OF RADIAL NODES IN THE LARGE MODEL

The large camber model has proved its ability to predict work roll thermal camber to a good degree of acceptability. However, in its original format it suffered from the undesirable fault of demanding a large amount of computing time to complete the time iterations in the finite difference solution of the equations governing heat conduction. The error in each time row of calculation can be shown to be of the order $(2(\Delta r)^2 + (\Delta x)^2 + \Delta t)$ where Δr, Δx and Δt represent the grid spacing in the radial, axial and time dimensions, respectively. Further, the iterative method used is convergent only if

$$\frac{k\,\Delta t\,[\,\Delta r^2 + \Delta x^2\,]}{\rho C \Delta r^2\,\Delta x^2} \leq \frac{1}{2}$$

where k is the thermal conductivity of the roll, ρ is its density and C its volumetric specific heat capacity. Thus, if the time steps used in the iterations are too large, loss of accuracy may result; and if too small, magnification of computational time requirements will increase. A resolution of this dilemma may lie in resorting to an alternative - direction - implicit scheme as proposed by Peaceman and Rachford[125]. This method in its turn requires additional computer memory.

Another solution would be to find a relationship between the minimum number of nodes which could be used and the number of nodes which gave the limiting degree of accuracy. (The accuracy required is in the order of 10μm in 200

compared to measured values). In addition, if the time iterations could be reduced, then the existing explicit iterative computation scheme could fulfil its role in real time computing. Work along the above lines were pursued but no reliable relationship between accuracy and the number of radial divisions of the roll could be found.

It has been found that the minimum value for j was 3, but it may be assumed that the degree of accuracy in the calculations reduces with decreasing number of nodes. This is because the finite difference equations are based on central differences which assume an error of the order discussed above. However, it has been found through trial an error that computational accuracy is always maintained, regardless of the number of radial nodes, if the roll is modelled as a hollow cylinder, with coolant flowing through its centre. The author was unable to establish a valid theoretical justification for this fact. Figure F10, curves 2 and 3, show how performing the computation using 3 radial nodes compares favourably with 50 radial nodes when the roll is assumed to be hollow, and the roll divided according to fig. (3.5.3).

CHAPTER 6

TEMPERATURE - HEAT TRANSFER COEFFICIENT - ROLL THERMAL EXPANSION RELATIONSHIPS

6.1 INTRODUCTION

This chapter will examine some simple mathematical relationships between coolant heat transfer coefficient, work roll surface temperature and diametral expansion of the roll.

The Fourier equation describing the transient thermal behaviour of a solid cylinder is given by the equation :

$$\rho C \frac{\partial T}{\partial t} = k \left(\frac{\partial^2 T}{\partial r^2} + \frac{1}{r} \cdot \frac{\partial T}{\partial r} + \frac{\partial^2 T}{\partial x^2} \right) \qquad (6.1.1)$$

where:

ρ = density of the roll

C = volumetric specific heat capacity

k = roll thermal conductivity

r = radial direction

x = axial direction

T = roll temperature

t = time

In dimensionless form eqn.(6.1.1) becomes:

$$\frac{\partial T}{\partial \tau} = \frac{\partial^2 T}{\partial r^{*2}} + \frac{1}{r^*}\frac{\partial T}{\partial r^*} + \frac{\partial^2 T}{\partial x^{*2}} \qquad (6.1.2)$$

where:

$\tau = kt/(\rho CR^2)$

$r^* = r/R$

R = roll radius

$x^* = x/R$

Eqn.(6.1.2) can be solved numerically by replacing the partial derivatives with finite differences and integrating the resulting set of ordinary differential equations with respect to time. The solution of eqn (6.1.3) require a complete knowledge of the boundary conditions as well as an initial condition, viz. the initial work roll temperature. The boundary condition existing at the roll surface is described by the equation:-

$$\frac{\partial T}{\partial r^*} = -\frac{RH_r(x)}{k}\left(T - T_c(x)\right) + q^*_{(x)} \qquad (6.1.3)$$

where:

$q^* = \frac{q'}{2\pi k}$

q' = Heat input per unit width

T = Roll temperature function

T_c = External temperature (coolant, air, etc)

R = Work roll radius

r = Radial position

r^* = r/R (= 1 at the surface)

x^* = x/R

x = Axial position

$Hr_{(x^*)}$ = Heat transfer coefficient at axial position x^*

k = Roll thermal conductivity.

Thus, eqn (6.1.3) suggests that for a given heat transfer coefficient a related roll surface temperature will exist. The surface temperature, however, constantly varies, depending on the solution of eqn.(6.1.2) and is affected by the heat transferred to the roll. For a given radial position, the surface temperature will vary during each stage of the rolling programme and with spray settings.

Therefore, in order to examine the relationships between surface temperature and heat transfer coefficient, the predicted surface temperatures for a range of values of heat transfer coefficients, spray arrangements, and for different numbers of slabs rolled have been examined.

6.2 HTC - TEMPERATURE RELATIONSHIPS

For this line of investigation, the rolling of several slabs were simulated using the "large" model based on the schedule for the rolling of slab 1 (fig. E2). Figure G1 shows plots of work roll surface temperature against heat transfer coefficient for each nodal position covered by coolant across the roll. There were eleven nodes within the strip width, corresponding to each nozzle location. (This is indicated in fig. G1 and similar figures). Hence curve 12 relates to the first nozzle position outside the strip width.

The spray settings were made equal across the barrel for the length covered by coolant, i.e., ($H_{r(x)}$ of eqn.(6.1.3) was made constant), and the predicted surface temperatures at each node compared with this value of $H_{r(x)}$. The comparison was repeated with a new value of $H_{r(x)}$.

Figure G1 clearly shows that, except for the nodes outside the strip, the predicted surface temperature is governed by an exponential function for the heat transfer coefficient, and the temperatures at nodes 13 - 17 are essentially constant.

Figs. G2, G3 and G4 follow the same theme as above, but for the simulated rolling of 2, 3 and 7, respectively, based on the schedule for slab 1 only. Figs. G5, G6, & G7 are the plots derived from the individual schedules when rolling 2,3 and 7 slabs, respectively. These curves are seen to be almost identical to those of fig. G2, G3 and G4. These figures show that for any node within the strip width with any given coolant distribution the same surface temperature will be reached if the schedules are similar. This applies if the roll does not exhibit large temperature fluctuations from pass to pass due to, say, increase power input to the roll.

To describe these curves mathematically suppose now that we assume some function,

$$T^S = f\ (H_{r(x)}) \qquad (6.2.1)$$

where T^S = roll surface temperature

exists, which by inspection of figs. G1 - G4 can be more explicitly stated as

$$T^S{}_{(x)} = k\ H_r{}^m{}_{(x)} \qquad (6.2.2)$$

where k = a constant

The assumed function of eqn. (6.2.1) makes no reference to the heat input term because this seems adequate for the present exploration. The constant k and the exponent, m, may be evaluated from the relevant curves of figs. G1 - G4, but a simple transformation of eqn.(6.2.2) to the logarithmic form yields:

$$\log_{10} [\ T^{s}_{(x)}\ ] = m \log_{10} [\ H_{r(x)}\ ] + \log_{10} k \qquad (6.2.3)$$

or

$$Y^{T}_{(x)} = m\ X_{(x)} + c \qquad (6.2.4)$$

Eqn. (6.2.4) gives a linear relationship which is more manageable. Using eqn. (6.2.4) plots of representing heat transfer coefficient- temperature relationships of the roll after 1 and seven slabs were rolled, respectively, were transformed to the straight-line forms. These are depicted by figs. G8 & G9, respectively. Eqn. (6.2.4) does not in fact produce a completely linear curve, but two lines can be defined for two ranges of heat transfer coefficients. One line is with HTC $\geq$ 10.05, and the other, HTC $\leq$ 10.05. The value of 10.05 for the heat transfer coefficient is essentially arbitrary but was selected on the basis that the best two straight lines were found for the ranges given. Values of m and c can be evaluated from least squares fits for each nodal positions and a range of heat transfer coefficients.

6.3 INDIVIDUAL PASS DATA. STEPPED FRACTIONAL HTC

For this case, the pattern of heat transfer coefficient used in the computations was stepped up evenly across the roll barrel starting from the roll centre line to the barrel end. That is, if at node 1 the fractional HTC was 0.1 then at node two this would be 0.12, at node 3, 0.13, and so forth (including larger steps). (The model evaluated a coefficient of heat transfer from: actual HTC = overall HTC x fractional HTC). Figs. G10 & G11 show that the relationships between temperature and HTC still hold true after rolling one and 7 slabs, respectively, for uneven distribution of coolant across the roll.

6.4 INDIVIDUAL PASS DATA. RECTANGULAR PULSED PATTERN FOR HTC

In this case the HTC'S were distributed on a pattern of rectangular waves across the roll, as the diagram below illustrates

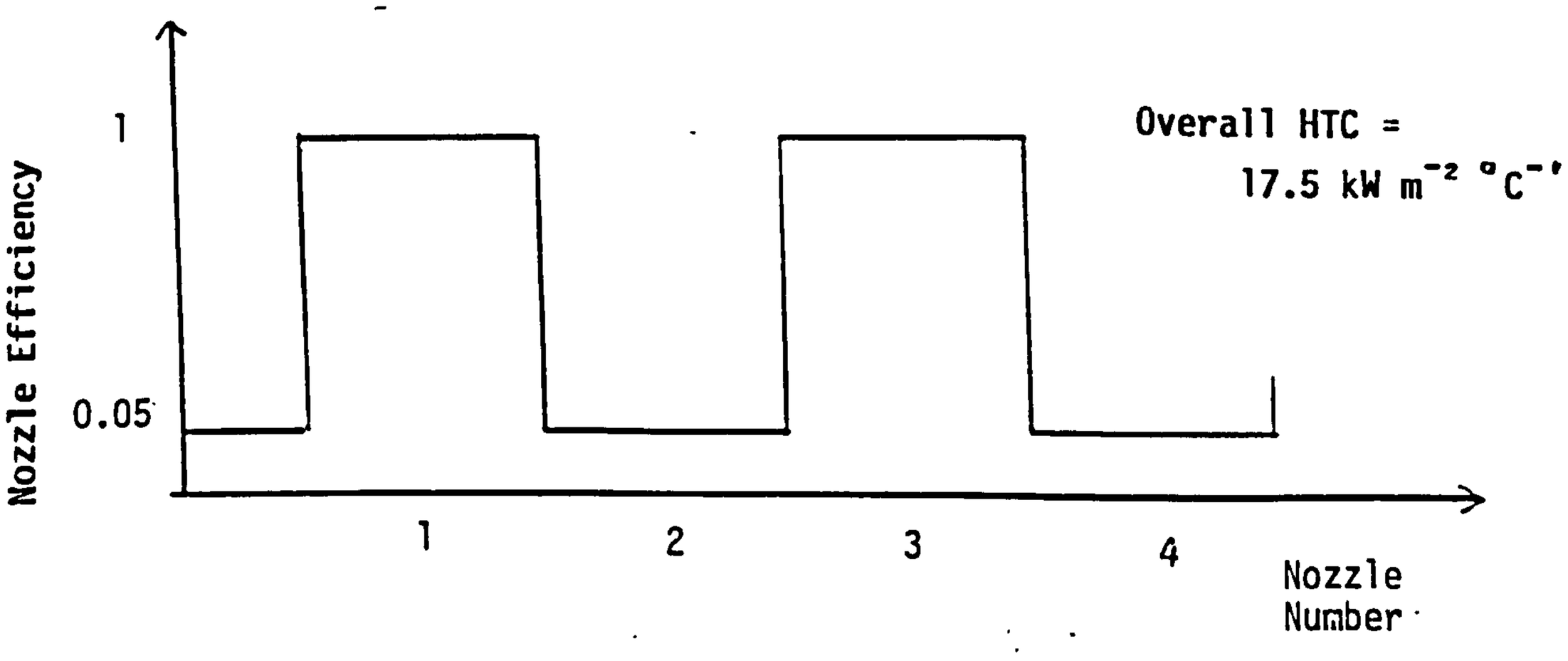

Fig. G12 is an illustration of the plot of roll surface temperature against heat transfer coefficient, distributed as described above, after one slab had been rolled.

6.5 HTC - DIAMETRAL EXPANSION RELATIONSHIPS

Figs G13 and G14 are graphs showing the relationship between heat transfer coefficient and diametral expansion at each axial node for the simulated rolling of one and seven slabs, respectively. Again, it is evident that an exponential function is capable of describing this relationship. Thus, if we let

$$E_{R(x)} = f\ (h_{R(x)}) \qquad (6.5.1)$$

where,

$E_{R(x)}$ = roll diametral expansion at x

$h_{R(x)}$ = heat transfer coefficient at x

Then from examination we can state this function more explicitly as

$$E_R(x) = k\ h_{R(x)}M \qquad (6.5.2)$$

$$\log E_{R(x)} = M.\log h_{R(x)} + \log k$$

$$X_{(x)} = M\ H_{R(x)} + C \qquad (6.5.3)$$

where,

$X_{(x)} = \log E_{R(x)}$

$H_{R(x)} = \log [H_{R(x)}]$

M = gradient

C = intercept

The corresponding plots from figs. G13 and G14 are shown in fig. G15 and G16. A least squares fit can be used to evaluate the gradient and intercept for each line. Once

again, for better accuracy two separate lines can be defined for regions of HTC $\leq$ 10.05 and for HTC $\geq$ 10.05.

6.6 TEMPERATURE AND DIAMETRAL EXPANSION

Fig. G17 show plots of roll diametral expansion against roll surface temperature for a 7 slab simulation using the schedule for slab 1 only. Fig. G18 show the same comparison for 2 slabs but with the individual pass data used as input data to the model. The individual curves of each figure depict the relationship between temperature and roll expansion at each nodal position within the strip width.

It is clear from an examination of the curves that the roll expansion varies linearly with the roll surface temperature and can be described by the equation

$$X_{(x)} = a\ T_{(x)} + b \qquad (6.6.1)$$

However, the gradients of these curves, as well as the intercepts, changes from node to node, and from slab to slab, but not with the arrangement of the sprays as fig. G19 shows. Figure G19 shows the sprays "ramped" when rolling with slab 1 schedule. This suggests that, with automatic spray control in mind, based on a given schedule, these constants (gradients and intercepts) could be evaluated from a slab to slab basis. We could do this by generating a range of heat transfer coefficient in the computerised model so that a range of roll surface temperatures will be predicted along with the roll expansion due to the temperature effects. These will give straight line relationships between the two variables. Straight line relationships also exist between the log of the diametral expansion and log of the heat transfer coefficients, enabling us to evaluate these sets of gradients and intercepts.

6.7 DISCUSSION

We are not really interested in the absolute expansion of the roll at this stage. We are, for now, solely concerned with the relative axial expansion of the roll. So now, what we need is some definition of thermal cambers, and to examine how this camber varies with surface temperature for different positions across the roll, taking into account the number of slabs rolled, and even the number of passes.

Let us assume a definition of thermal camber to be

ΔC_x = (thermal diametral expansion at the roll centre line)
- (thermal diametral expansion at axial position x)

To predict the heat transfer coefficient required by the large model to give a desired camber, we could have a starting value of HTC using eqn. (6.2.4). We could assume a roll surface temperature, and then eqn. (6.5.3) could be used directly with or without further reference to the large model to specify the HTC at each axial location. We could, given a specified (or desired) roll thermal camber, d_i, evaluate the required roll expansion at the centre of the roll using eqn.(6.7.1) below :

$$y_i^{new} = y_1^{old} - d_i \qquad (6.7.1)$$

where y_i = predicted roll expansion at axial position x = i

A further application of eqn. (6.5.3) then gives the required heat transfer coefficient.

The success of the method described above can be seen by reference to fig. F11 - F13 which show roll cambers after

one and seven slabs were rolled, respectively. The values for heat transfer coefficients were arrived at using the equations above with the measured camber assumed to be the desired camber required to achieve a given profile.

CHAPTER 7

STRIP PROFILE PREDICTION

7.1 INTRODUCTION

It is commercially important to produce high quality hot-band because of the inability of subsequent cold rolling operations to remove inherent shape defects. Computer control systems require reliable methods of determining on-line deviations in strip quality. Strip quality can be considered in terms of metallurgical factors, surface defects, shape defects and strip profile.

Profile is defined as (see fig. 8.1.1):

$$\% \text{ crown} = \frac{H - H_x}{H} .100 \qquad (7.1.1)$$

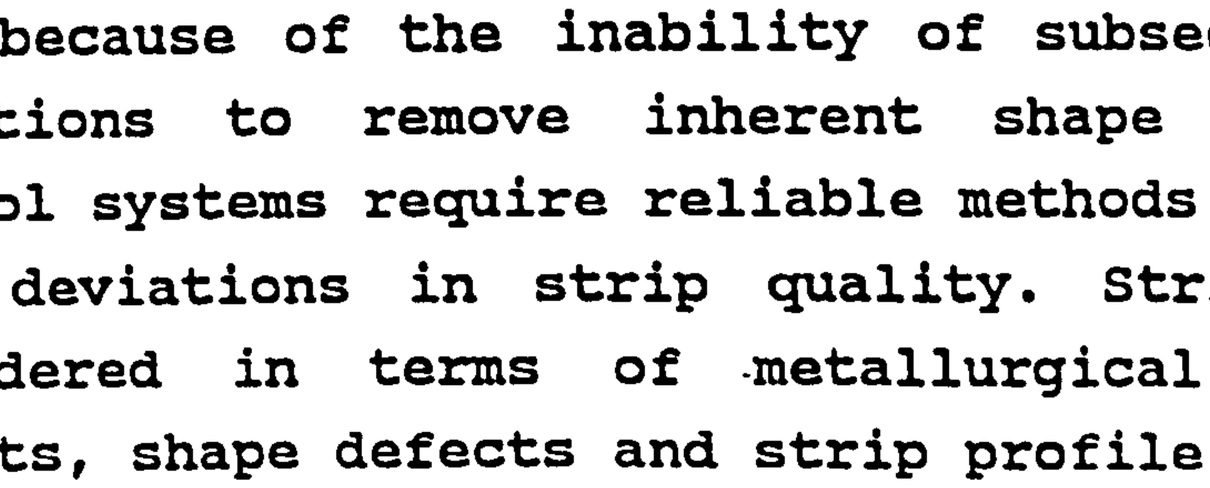

Fig. 7.1.1. Definition of strip crown.

Work roll profile is considered to be the result of the addition of deflections and deformations from the following effects:

1. Work roll flattening next to the strip
2. Work roll/back-up roll flattening
3. Back-up roll bending
4. Back-up shear deflection
5. Ground and thermal crown
6. Poisson deformation of rolls
7. Work roll bending due to end forces on work roll chocks

The mathematical model of roll bending resolves the deflections at discrete points across the strip width. The number of equally spaced points across half the strip width is an input variable. There are five extra points fixed 10mm from the strip edge to aid with computing accuracy in this area. If the strip width is greater than the back-up - work roll contact length, extra points are set at the end of the contact length (see figs 7.1.2 & 7.1.3).

In order to establish a suitable control strategy it is necessary to compare profile output from the profile prediction model[128] with product target profile, varying:-

- coolant levels
- mill start conditions
- products
- interpass - intercoil cooling
- roll bend

From an analysis of the above conditions the most effective strategies for setting coolant pattern and roll bend can be established.

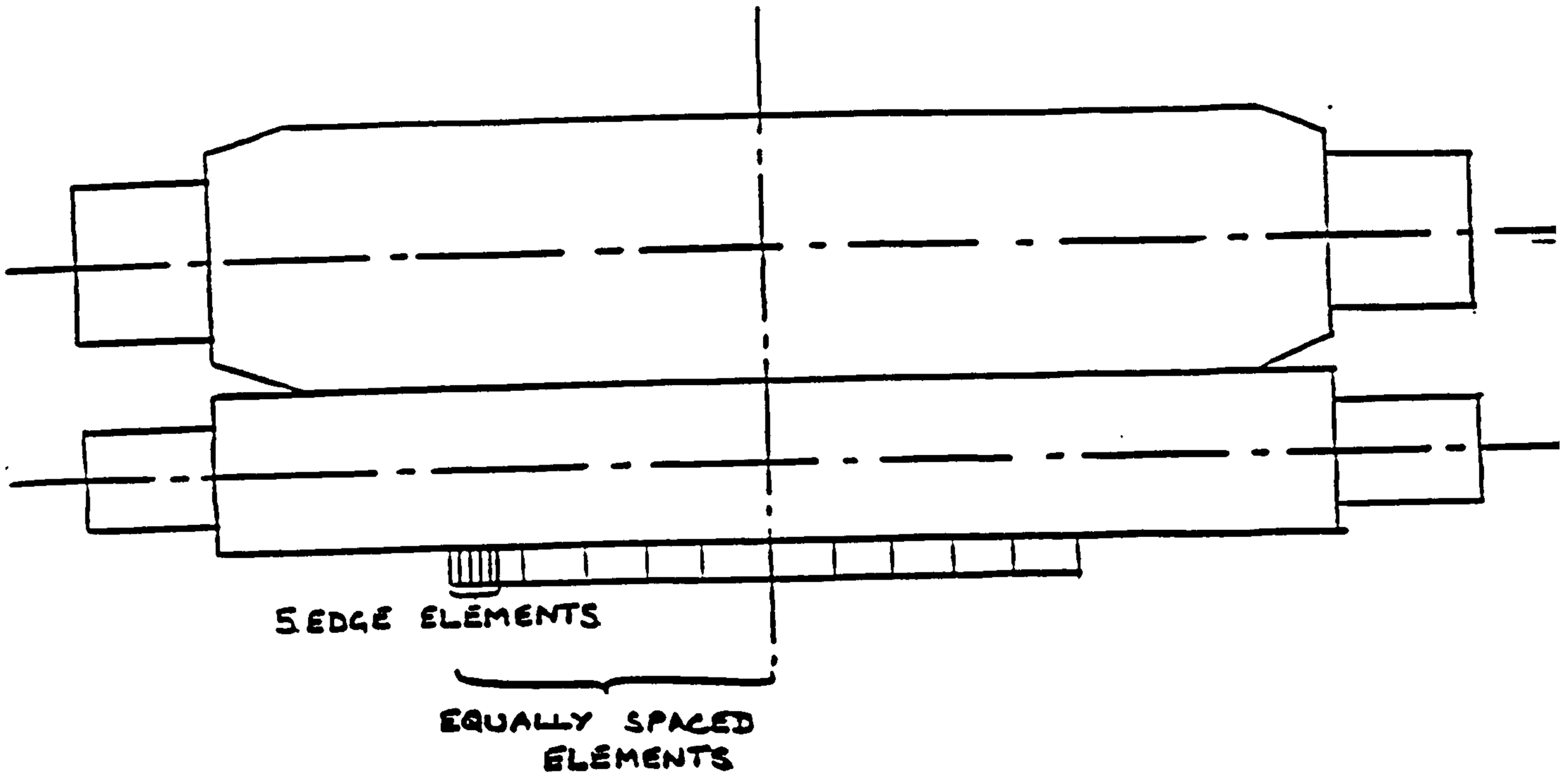

Fig. 7.1.2 Strip Width $\leq$ BUR/WR Contact length

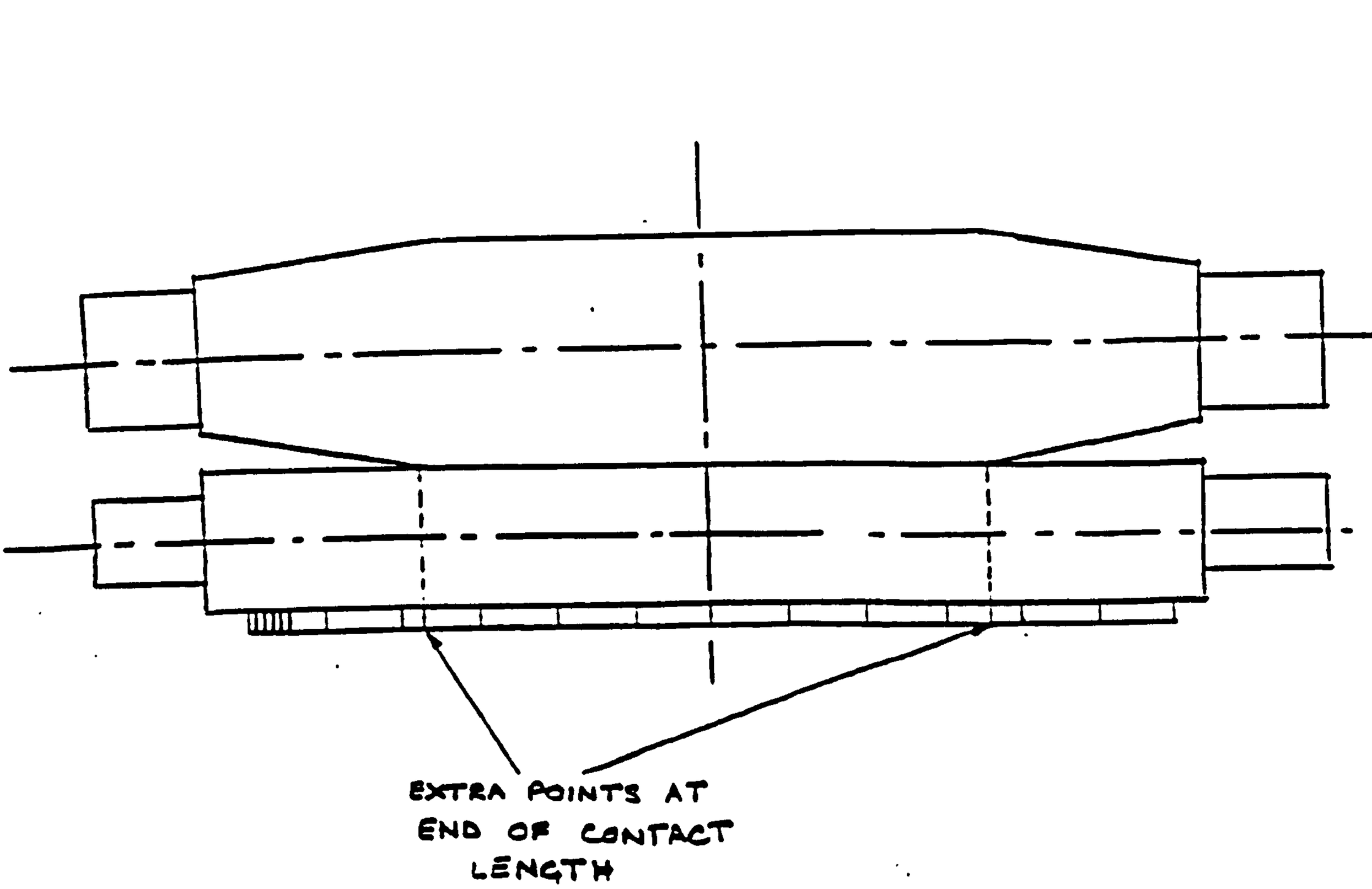

Fig. 7.1.3 Strip Width $>$ Contact length

7.2 TRIALS ON PRODUCT 3004, MILL B DATA

Data for the simulations below were obtained as described in Chapter 4. The heat transfer coefficient at the spray levels used were deduced from the roll temperature measurements. No plant data was available on rolled strip profile, hence, the predictions of strip profile could not be compared with actual measurement.

7.3 EFFECT OF VARYING COOLANT LEVELS ON STRIP PROFILE

Since the number of permutations of spray patterns is very large, the exact number depending on the spray system, only a selected series of patterns could be investigated. The basis for selecting the spray patterns chosen was to simulate normal mill spray settings. Some deviations from customary practice, such as increasing spray levels towards the centre of the strip, were also examined. The predicted thermal cambers for a number of spray patterns can be viewed in appendix H, as directed in Table 7.3.1.

Table 7.3.1 - Location of graphs in appendix H showing predicted thermal cambers for given spray patterns and number of slabs rolled.

Fig.	Spray pattern						Number of slabs rolled
	entry side			exit side			
H1	001	111	111	111	111	100	1
H2	001	111	111	111	111	100	4
H3	003	333	333	333	333	300	1
H4	003	333	333	333	333	300	4

Table 7.3.2 Rolling load (MN) for given passes and slabs for the curves of figs. H5 - H18 (see figure E6 for full data set).

Pass number	Slabs rolled								
	1	2	3	4	5	6	7	8	9
15	10.9	10.8	10.9	11.3	11.3	12.3	12.6	11.6	11.4
16	11.8	11.3	11.4	11.4	11.3	12.1	12.4	11.6	11.6
17	9.9	9.6	9.8	11.1	11.1	11.6	12.0	11.6	11.6
18	7.3	7.1	10.2	10.3	10.4	10.6	10.8	10.7	10.9
19	10.1	10.4	7.0	7.7	7.0	7.1	7.2	6.7	7.1

Roll bend force set at 0.512 MN in each case.

7.3.1 LEVEL SPRAY PATTERNS, EDGE SPRAYS OFF

Figs. H5 and H6 show the changes in strip profile for the last 7 passes of 19 pass schedules when the sprays are set at level 1 within the strip width and turned off outside the strip width. The rolling load is similar at respective passes. Profile is maintained at each pass for the same spray pattern, except where there is a significant change in rolling load.

Figures H7 and H8 are included to show that the argument above holds true at any uniform spray pattern. For figs. H7 and H8 this is level 3.

7.3.2 LEVEL SPRAY PATTERNS, EDGE SPRAYS ON

For the situation where the edge sprays are switched on, changes in strip profile shows at the strip edge. This can be confirmed by figs. H9 and H10 which show strip profiles for the slab numbers indicated with all available sprays switched on at level 1. The first slab rolled seems relatively insensitive to spray pattern changes, but

noticeable differences in profiles are shown by the third slab for the last pass. At the end of a 9 coil simulation, a 0.5% change in profile occurs, compared to the former situation when only the sprays within the strip width were set to level 1 (fig. H11).

7.3.3 LEVEL SPRAY PATTERN WITHIN STRIP WIDTH, EXIT SIDE ONLY

Figures H12 and H13 show the expected crown for a series of simulated rolling conditions in which the sprays are all set at level 1 within the strip width on the exit side of the mill only. This has the effect of producing coils with flat middles, except for the first coil, but the edge effects are amplified compared to sprays set on both sides of the mill. For example, compare figure H5 and H6 in which the latter shows that level 1 sprays are set on both sides of the mill within the strip width. For the simulated run of 9 slabs, (fig. H14)there is a change in profile of +1.3% for a change from exit and entry side sprays to only exit side. Further, this type of spray pattern appears to maintain the same degree of profile from slab to slab, apart from the first coil. In this case strip crown can be reduced to that of the following slabs by reducing the rate of cooling at the roll centre as figs. H15 and H16 indicate. Perhaps, this is not surprising, if the effect of the roll profile is considered for the situation of relatively greater cooling towards the roll centre as described pictorially in figure 7.3.1 below.

Fig. 7.3.1. Effect of cooling roll centre less than the edge on the strip and roll.

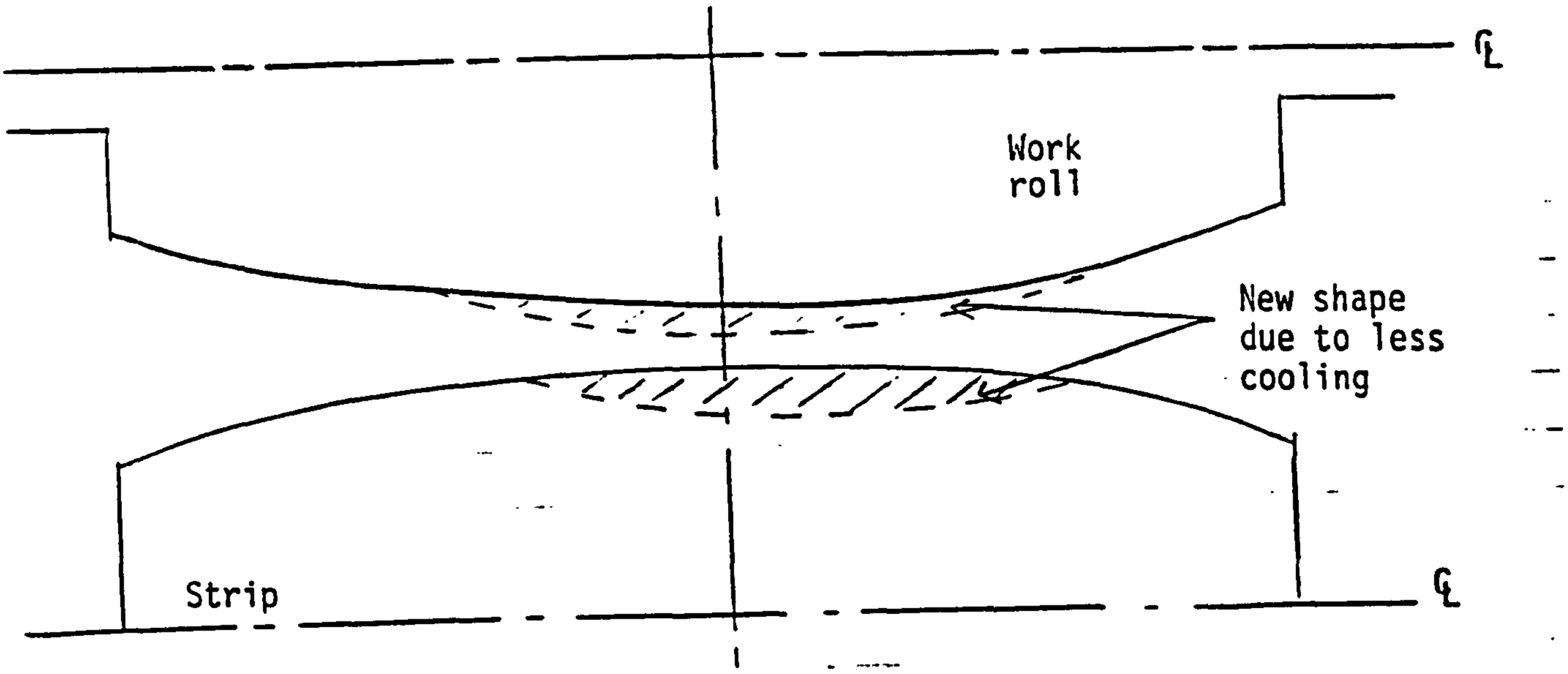

Fig.7.3.2. Effect of cooling roll edge more than the centre on the strip.

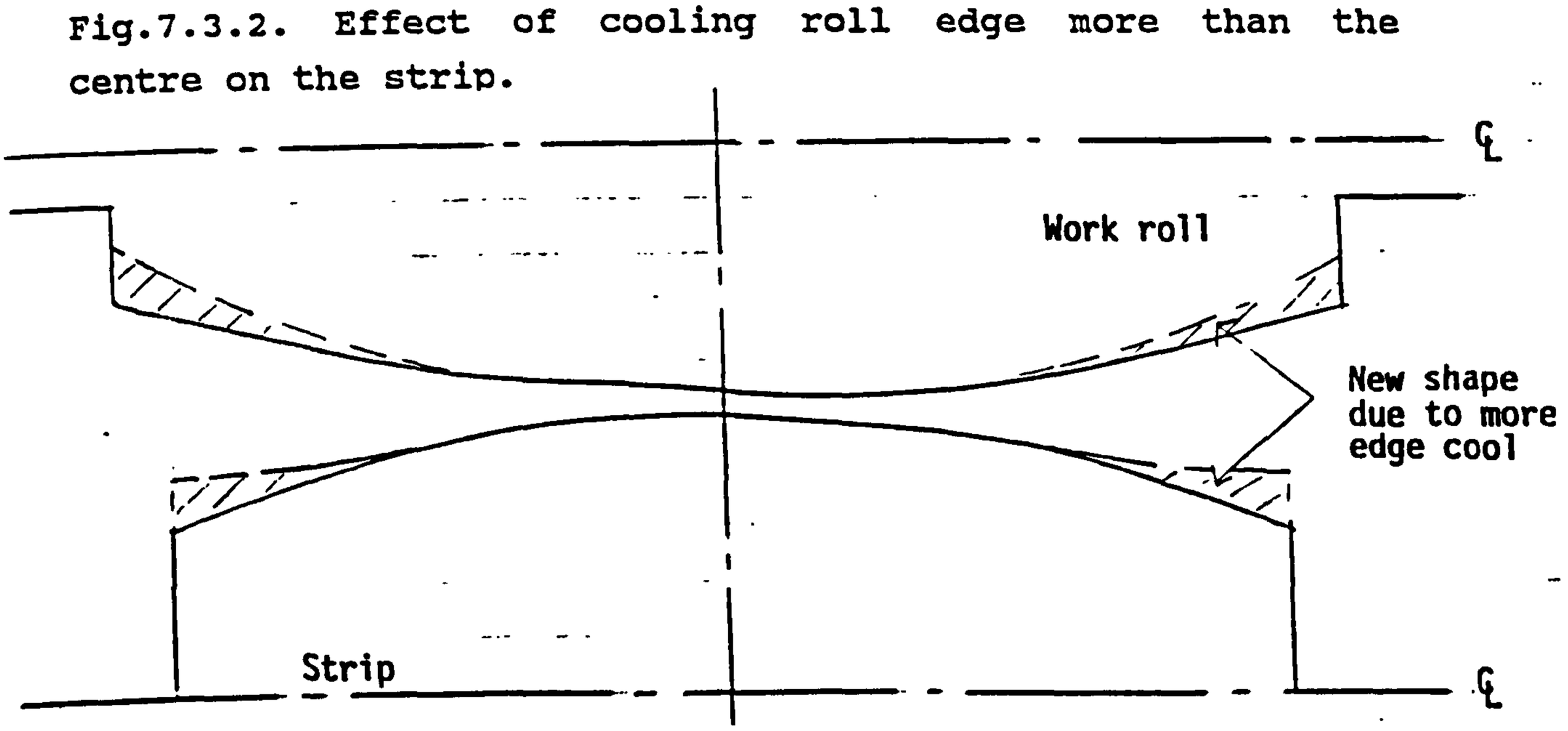

Figs 7.3.1, H15 and H16 show that a reduction in cooling at the centre of the roll will cause the roll to expand more at its centre, decreasing the strip centre thickness. From the definition of (positive) crown given in section 7.1, a reduction in strip centre thickness relative to the edge is equivalent to a reduction in strip crown. More cooling at the edge of the roll is equivalent to an increase in roll

centre thickness as shown in fig.7.3.2.

7.3.4 LEVEL SPRAY PATTERN, INCLUDING EDGE SPRAYS

The strong influence of the edge sprays can be seen in figs. H17 and H18 which illustrate the case for all level 1 sprays switched on across the roll. Compare the shape of these curves with figs. H12 and H14 when all the exit and entry sprays are switched on. In each case, with exit side sprays only, the curves suggest strips with flat middles will be produced. For example, in the case of the 9th slab, last pass, there is a 1% change in predicted profiles between the two conditions of spray levels, all other factors being the same for respective slabs.

7.4 SUMMARY ON THE EFFECTS OF VARYING SPRAY LEVELS

The important conclusions that can be made from the analysis of the data presented in appendix H are as follows.

- Spray pattern changing across the roll has a significant effect on strip profile

- Generally, level spray patterns gave the best shape.

- Edge sprays sensitivity is important. Over-cooling outside the strip provides good parabolic shape.

- A change to exit side spray levels has a significant effect on strip profile.

- Exit side sprays only has a tendency of rolling out the middle of the slab (i.e., a flat middle results).

- Level sprays on exit side only produce a distorted profile on the strip.

It can be added that in practice the spray pattern is unlikely to be that of exit side only because of the need for lubrication on the mill entry side to give some roll cooling effect.

7.5 RELATIONSHIP BETWEEN STRIP CROWN AND THERMAL CAMBER

If we keep in mind the objective of this study, we must constantly seek means of reducing the complex models for predicting roll thermal camber and strip profile to the most basic forms. A rapid method of predicting thermal cambers from a knowledge of the spray levels has been suggested in Chapter 6. A fast method of relating thermal cambers to strip profile will now be suggested.

Consider fig.7.5.1 below. We know that for any given change in roll thermal camber, such as the camber change from curve 1 to curve 2, there is a corresponding change in strip profile as, say, from that of curve 3 to curve 4.

Fig. 7.5.1. Diagrammatic representation of the effect of a change in roll camber on strip profile.

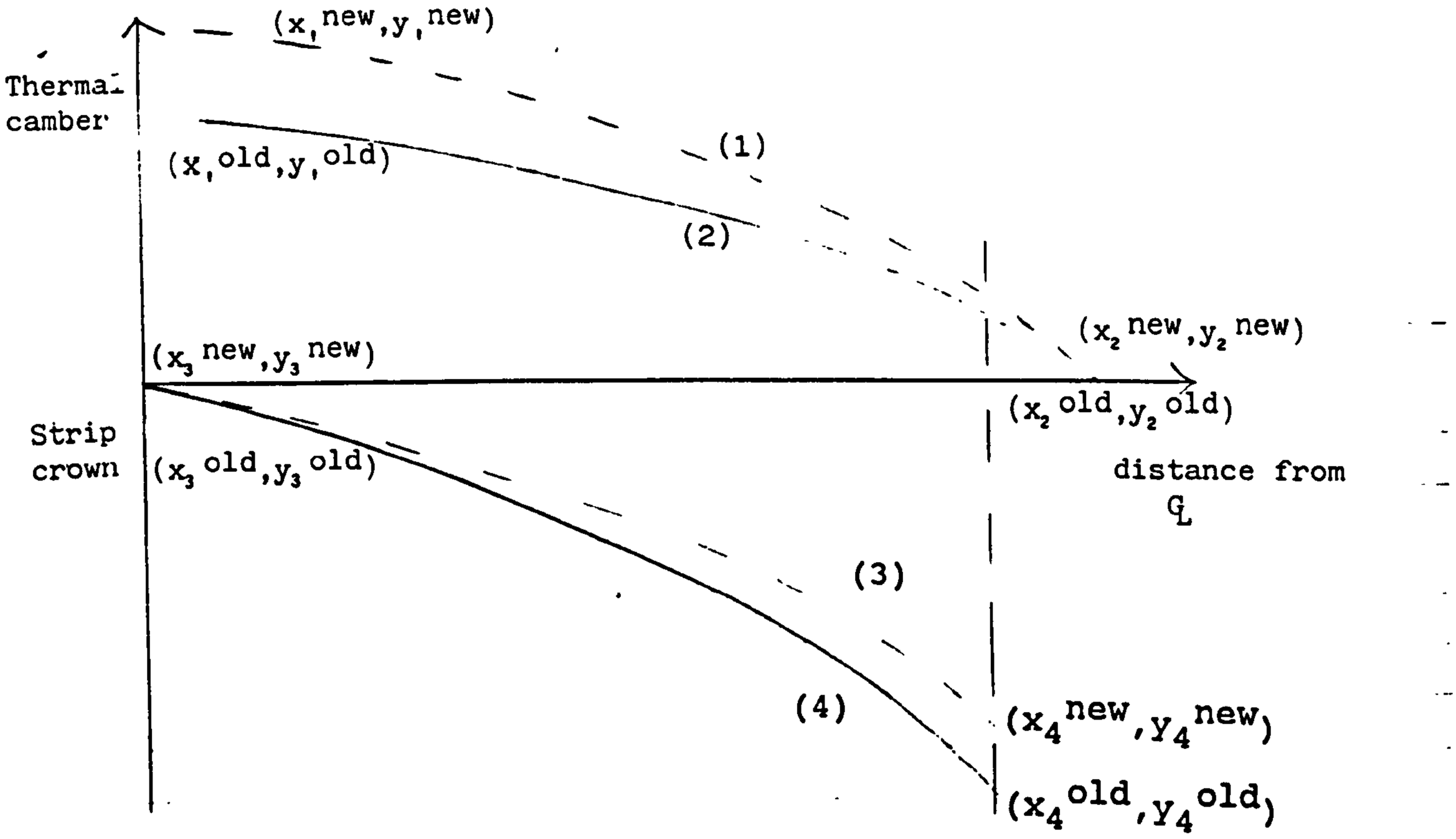

Consider that a point (x_1^{old}, y_1^{old}) changes to (x_1^{new}, y_1^{new}). The definition of thermal camber was with reference to the point (x_2^{old}, y_2^{old}) but is changed to (x_1^{new}, y_1^{new}), or (x_2^{new}, y_2^{new}). Since strip crown is fixed at the roll centre line (and is always equal to zero at this point from our definition of crown), then this camber change would result in a change in profile at the point (x_4^{old}, y_4^{old}) to (x_4^{new}, y_4^{new}). This suggests that a linear factor could relate these changes in thermal cambers to the change in strip profile if one curve maps on to the other.

For simplicity, consider that the change in thermal cambers, ΔC, and the change in strip profile, ΔP, are as described in fig. 7.5.2. Then ΔP could be mapped on to ΔC by a linear factor.

where (in fig. 7.5.2):

$$\Delta y_i = y_x^{new} - y_x^{old}$$

Fig. 7.5.2. A possible response of the strip profile to a change in roll thermal camber across the roll and strip.

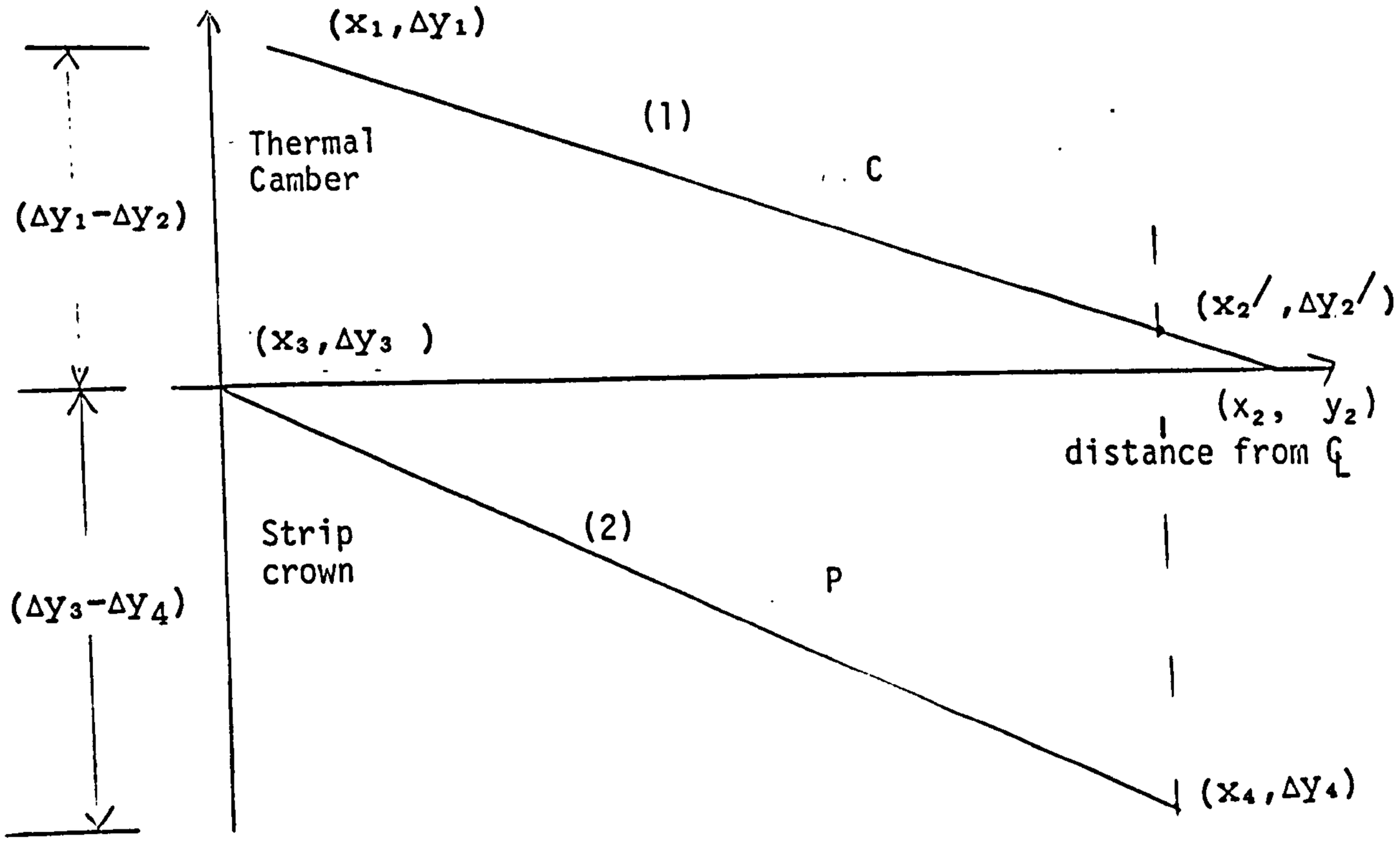

The point $(x_2', \Delta y_2')$ is included since the limiting value on the crown v distance from roll centre line graph does not generally coincide with the reference point on the thermal camber against distance from the roll centre line graphs. (This is due to the methods of dividing the roll in the two models). Hence to map ΔP to ΔC we must get

$$\Delta y_3 \;|\!\!\longrightarrow\; \Delta y_1$$

and

$$\Delta y_4 \;|\!\!\longrightarrow\; \Delta y_2$$

where $|\!\!\longrightarrow$ means maps onto

by changing the vertical axis for a change Δy on curve 2 of fig.7.5.2. Thus the ΔP's are related to changes in thermal cambers as in eqn. (7.5.1) below.

$$\frac{y_2' - \Delta y_1}{\Delta y_4 - \Delta y_3} (\Delta y - \Delta y_3) + \Delta y_1 \qquad (7.5.1)$$

The point (x_3, Δy_3) is always known since it is a reference point. The point (x_1,Δy_1) is also known since it would be specified. Hence, to map ΔP to ΔC, the scale factors for both the x and y axis are constants.

Hence, since

$$\Delta y_3 = 0 \text{ (always)}$$

eqn. (7.5.1) reduces to

$$\frac{\Delta y_1}{\Delta y_4}(\Delta y_x^p) + \Delta y_1 \quad |-----> \quad \Delta y_x^c \qquad (7.5.2)$$

where Δy_x^p is the desired change in strip profile at a point (x_x^p, Δy_x^p) from a change in thermal camber Δy_x^c at the point (x_x^c, Δy_x^c).

Suppose $\Delta y_1 // \Delta y_4$ is equal to k in all cases, then

$$\Delta y_1 = k\Delta y_4 \qquad (7.5.3)$$

and $-k\ \Delta y^p + k\ \Delta y_4 = \Delta yc$

At an axial position x,

$$\Delta y_x^c = k\ (\Delta y_4 - \Delta y_x^p) \qquad (7.5.4)$$

Fig. 7.5.3. shows how a selected change in spray pattern compares with a change in predicted profile using this technique.

The value of the constant k has been investigated for a multitude of changes from one spray pattern to another, and

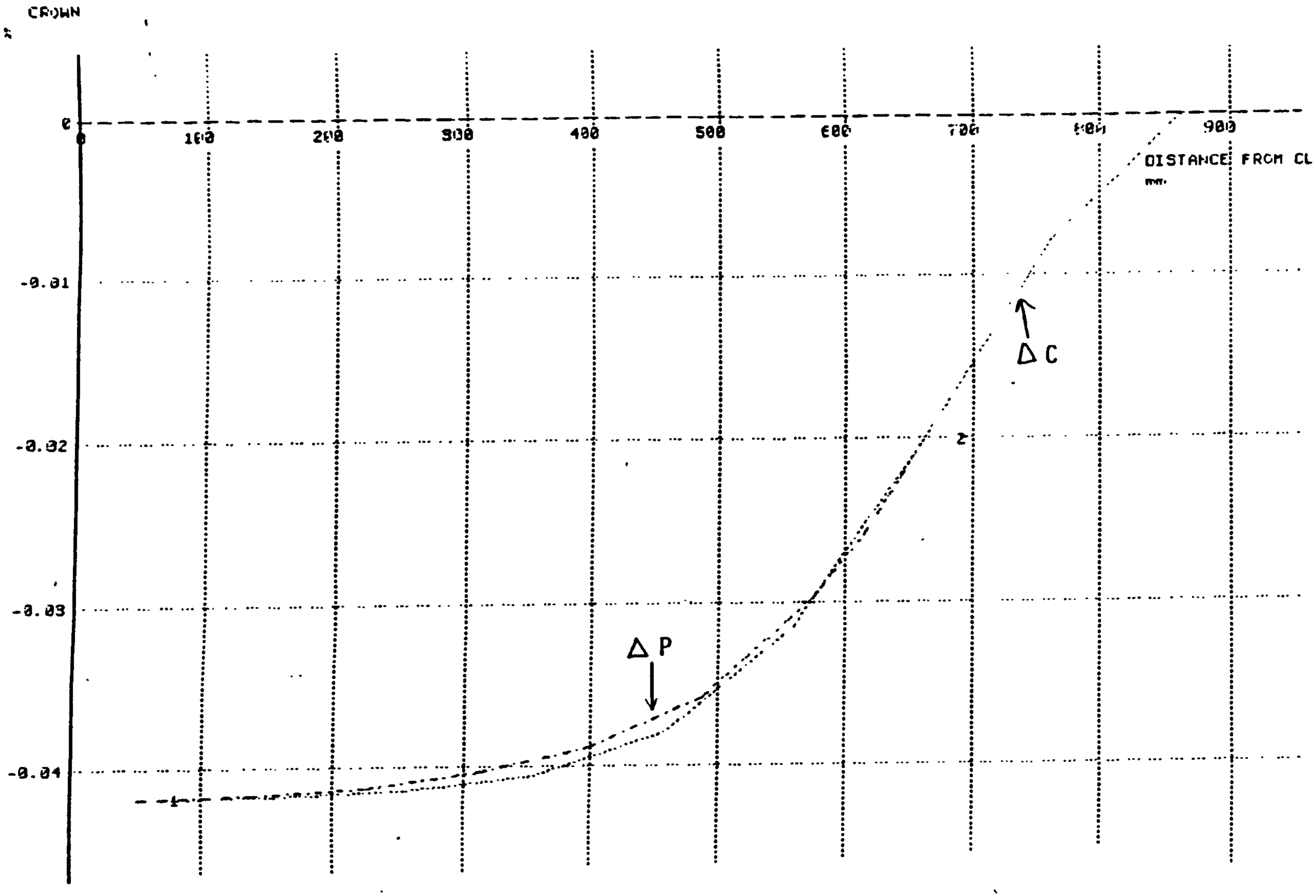

Fig. 7.5.3. Changes in strip profile mapped on to the changes in roll thermal camber which caused it.

U2.2 • 12-AUG-87

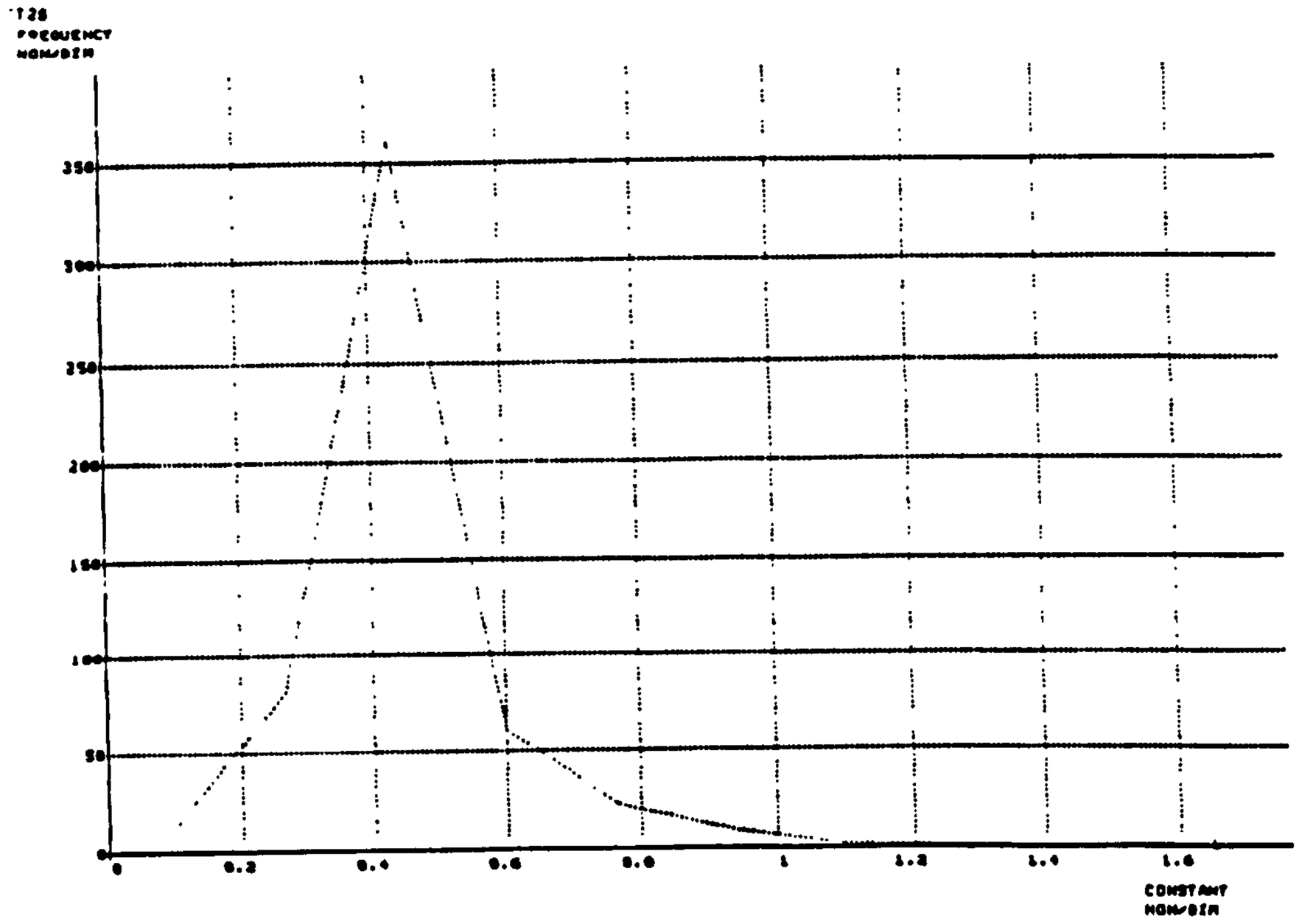

7.5.4. Values of k in eqn. (7.5.4). The variation in k is examined for the last seven passes of a 19 pass schedule, for 9 slabs and 9 simulated spray patterns in each case.

the resultant change in profile. The mean value of k is seen to be 0.42 in fig.7.5.4. The value of k will be mill and product dependent.

7.6 WORK ROLL BEND AND ROLLING LOAD EFFECTS

It is accepted rolling practice that increasing the work roll bending force (between the work roll chocks) has the effect of causing more negative crown in the strip. This is because applying more positive roll bending force results in the work roll necks being pushed apart, hence the roll centres are brought nearer to each other. The response of the strip to such changes in the roll gap profile is similar to that of over-cooling the roll ends or over-heating the roll centres.

The effect of changing the work roll bending force for fixed rolling loads and a single spray pattern at selected positions within the strip can be seen in figs. H19 and H20. In these figures the strip positions 1, 2, 3, etc., are defined as in fig. 7.6.1.

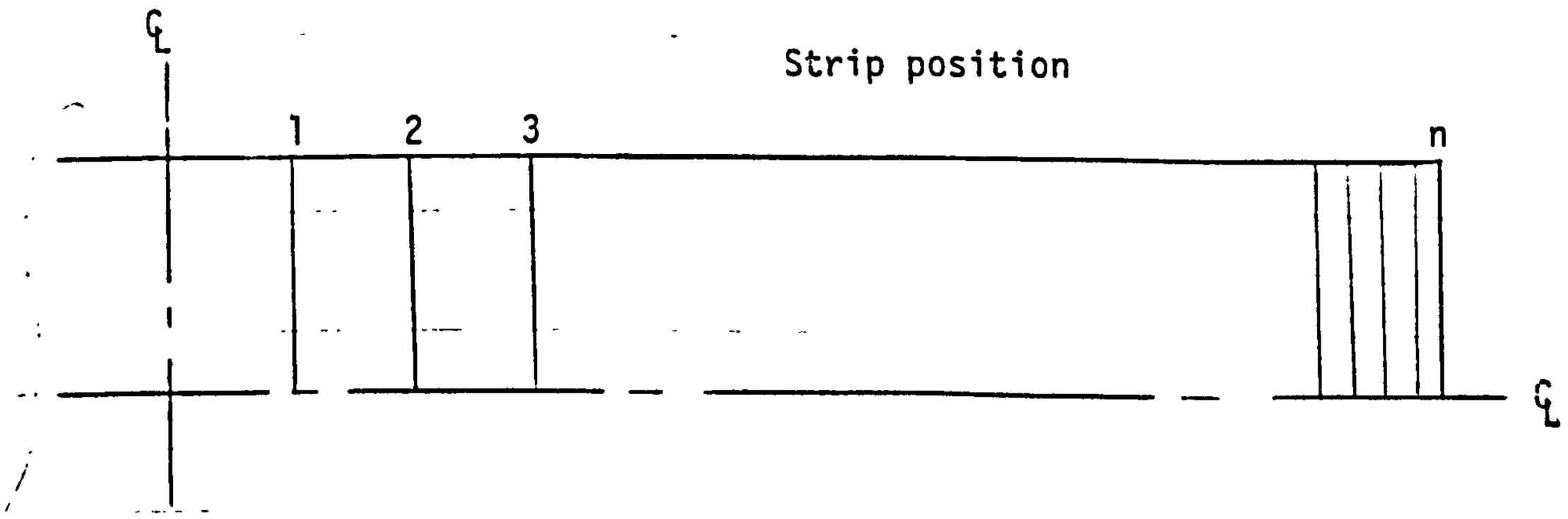

Fig. 7.6.1. Location of strip positions 1 to n for figs. H19 - H22.

Figures H19 and H20 show the relationship between work roll

Figures H19 and H20 show the relationship between work roll bending force and predicted strip crown at strip position 1 for simulated rolling sequences of 1 and 9 slabs, respectively. The sprays are set at level 3 within the strip width (exit side only). The rolling load is set at 10MN.

The curves clearly show that at each strip position at each rolling load and spray setting, the relationship between work roll bending force and strip profile is very nearly linear, irrespective of the number of slabs rolled, neglecting the first slab. It is interesting to note that only minor changes occur in the gradients of these curves for changes in rolling load. The intercepts, however, show greater differences for changes in rolling load.

The change in strip profile with variations in work roll bending force at comparative positions across the strip (for the first slab) is shown in figs. H23 and H24. Figure H23 reads, for example, that for the spray pattern shown, at a rolling load of 10MN, the maximum strip profile would be 0.3% at strip position 6. In this case, the work roll bending force is 1MN per side.

From the discussion above, it is evident that in general the relationship between work roll bending force and predicted strip profile takes a linear form. This behaviour is shown more clearly in fig. 7.6.2 for fixed rolling loads.

The general mathematical description is given by. eqn. (7.6.1).

$$y_i^p = m_j p x + c_j^p \qquad (7.6.1)$$

where

x = work roll bending force per side (MN)

m_j^p = gradient (strip location p and rolling load RL_j)

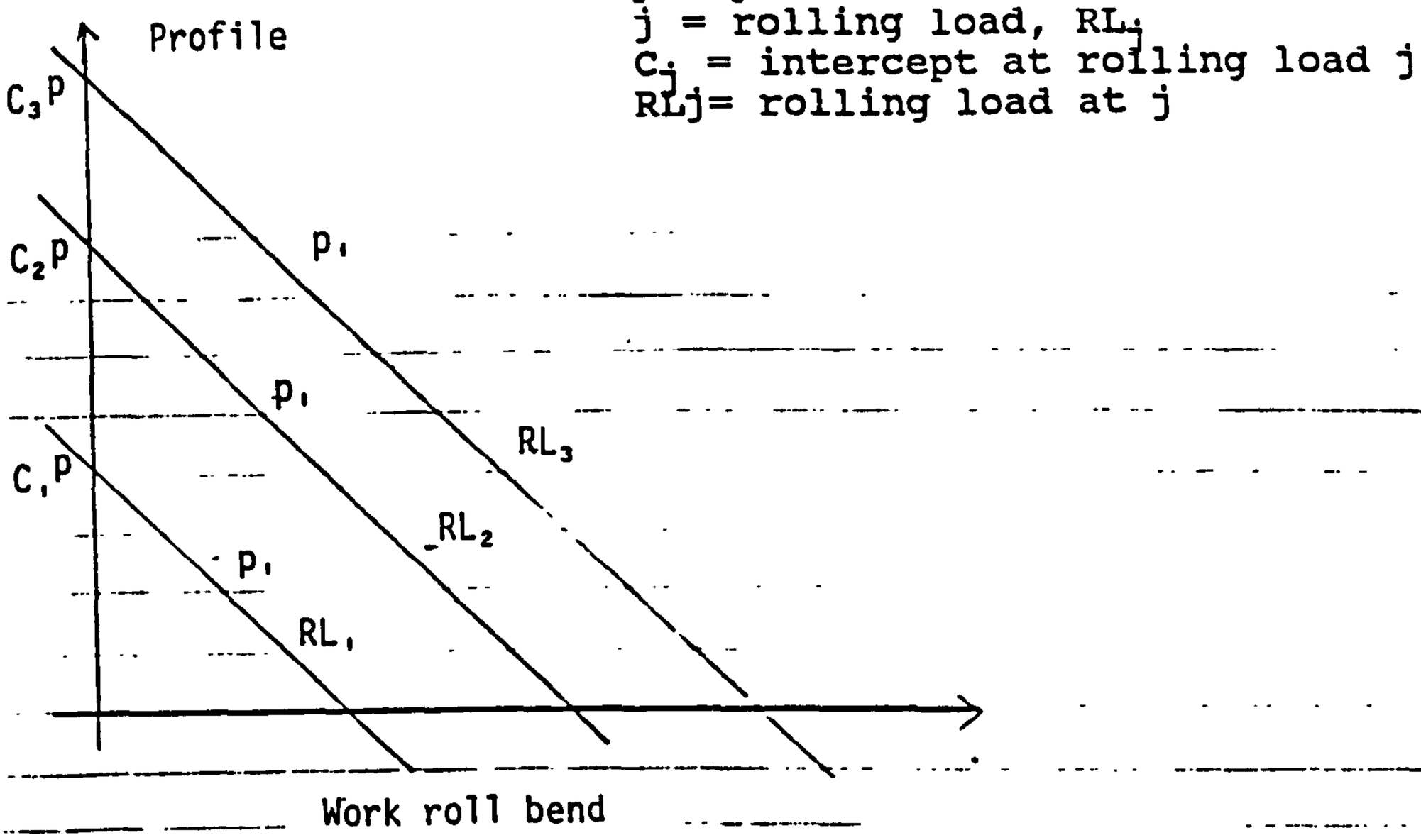

Fig. 7.6.2. General relationship between strip profile and work roll bending force at a given location in the strip and fixed rolling load.

Figures H19 to 22 show that there is only a small degree of variation in the values of the m_j^p's for changes in rolling loads, and number of slabs rolled. (Greater variation is exhibited with changes in spray pattern, but is not shown here). The values of the intercepts, c_j^p's, show a definite dependency on rolling load similar to that illustrated in fig.7.6.3.

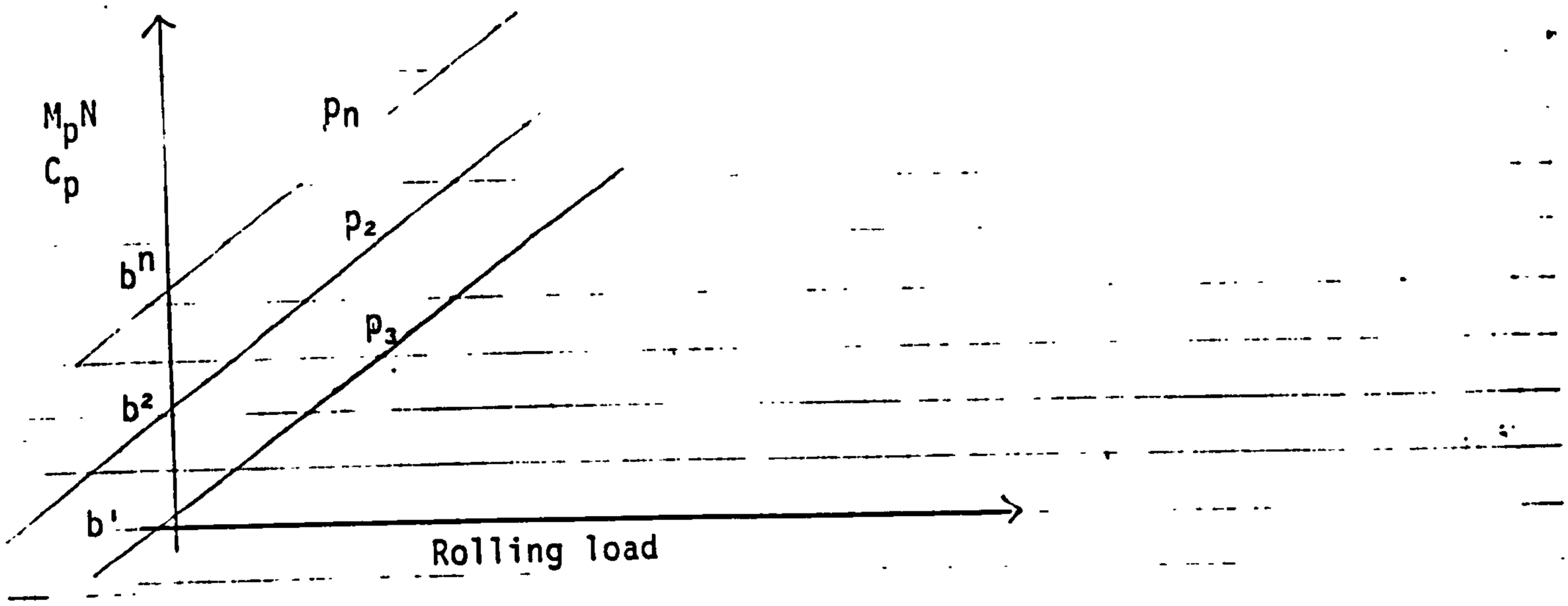

Fig. 7.6.3. Relationship between the gradient , m_j^p, or intercept, c_j^p, of eqn. (7.6.1).

Figure 7.6.3 can be translated in equation form as:

$$c_p = a_p{}^{c}RL + b_p{}^{c}$$

or

$$m_p = a_p{}^{m}RL + b_p{}^{m} \qquad (7.6.2)$$

Substituting eqn. (7.6.2) into eqn. (7.6.1) gives

$$y_j{}^{p} = (a_p{}^{m}RL + b_p{}^{m})x + (a_p{}^{c}RL + b_p{}^{c}) \qquad (7.6.3)$$

Equation (7.6.3) suggests that the work roll bending force required to achieve a desired strip profile, at any rolling load and a given spray pattern, can be predicted using a simple linear relationship.

CHAPTER 8

CONCLUSIONS

The successful development of a 2-dimensional roll temperature and thermal camber model has been presented in this thesis. The Fourier equations describing heat conduction in cylindrical coordinates in a work roll was solved using finite differences. The model takes account of the geometry of the work roll in a rolling mill. The model is capable of evaluating individual values for average heat transfer coefficients along the length of the roll. This accounts for the effectiveness of each nozzle in removing heat from the roll. The adoption of an average heat transfer coefficient to account for the various modes of heat removal from the roll, viz., radiation, convection and conductive heat transfer to the back-up roll, does not detract from the accuracy of the model in predicting roll thermal camber, if suitably calibrated. This calibration may be accomplished by matching predicted roll temperatures with measured data at known times during rolling. The relationship between spray levels and heat transfer coefficient can be determined from matching known spray levels for a given rolling schedule with values of heat transfer coefficient estimated using the methods discussed earlier. A complete set of values of heat transfer coefficient for all spray configurations can be determined

from any one of two methods. Firstly, an equation which describes the heat transfer characteristics of a coolant nozzle can be combined with a model of the roll angular temperature distribution[28] to give an "effective" or mean heat transfer coefficient at each spray level on each complete rotation of the work roll. Alternatively, by taking a few roll temperature measurements at known times during rolling, and at known spray levels, simple linear relationships between heat transfer coefficient, roll surface temperature and roll thermal cambers can be established.

The predicted values of thermal cambers from the models consistently compared well with actual plant measurements. The accuracy of the "fast" model based on the suggestion of Oshima[67] (to divide the roll into equal radial areas for finite difference integration) did not prove to be as accurate as the "large" model (with equal length radial elements).

It has been found that changing the spray pattern across the roll has a significant effect on strip profile. In addition, the following conclusions can be made about the effect of spray levels on strip profile:

- Generally, level spray patterns gave the best shape.

- Edge sprays sensitivity is important.

- Over-cooling outside the strip provides good parabolic shape.

- A change to exit side spray levels has a significant effect on strip profile.

- Exit side sprays only has a tendency of rolling out the middle of the slab (i.e. a flat middle).

- All level sprays on the exit side of the roll only produce a distorted profile on the strip.

It has been found that for any given change in roll thermal camber, there is a corresponding change in strip profile. The two changes can be related by a linear factor, (an "attenuation" factor), k. The value of the constant k has been investigated for a multitude of changes from one spray pattern to another, and the resultant change in profile. The mean value of k is seen to be 0.42 in fig.7.5.4 to move from a given strip profile change to the equivalent thermal camber change. It is product and mill dependent.

A linear relationship between work roll bending force and predicted strip profile can be established. However, further work needs to be done to establish the appropriate coefficients.

SUGGESTIONS FOR FURTHER WORK

Further experimental work and plant data gathering need to be performed in able to establish a more exact equation than presently available to predict heat transfer coefficients from the spray configuration alone. A series of trial simulations need to be performed to investigate roll thermal camber and strip profile behaviour:

- when rolling is started using cold rolls.

- when there is mixed product batches (eg. alloy and dimensional changes).

- when coolant is not switched off between passes or coil changes.

REFERENCES

(1) BARTON, M.V., & ITHACA, N.Y.,
"The Circular Cylinder with a Band of Uniform Pressure on a Finite Length of Surface", J.App. Mech., Sept.1941,pp.A-97-A104.

(2) DAVIES, C.E., & UNDERWOOD, L.R.
"Modern Metal Rolling Practice", Metal Ind., May 19,1944, pp.306-309.

(3) JAEGER, J.C.,
"Some Problems Involving Line Sources in Conduction of Heat", Philosophical Mag., Ser.7, vol.35, (1944), p169.

(4) JAEGER, J.C.,
"Note on a Problem in Radial Flow", Phys.Soc. 1944 60 (3), pp.197-203.

(5) MORT, J.M.
"Sheet and Tin Plate Mills,Roll Dressing Formulae", I.S.E., July 1947, pp.351-356.

(6) LUPPOV, A.N., OGLOBIN, B.G.,
"Approximate Solution to Non-linear Problems of Heat Conduction Theory", J.Eng. Physics (USA) vol.17,no.5 pp.915-917.

(7) MATHUR, S.L.
"On Heat Conduction - I", Ind. Journal Physics,vol. 45,no.1, pp.18-22, Jan 1971.

(8) TRIPATHI, G., SHUKLA, K.N., PANDEY, R.N.,
"General Solution to a Class of Unsteady Heat Conduction Problems in a Solid Cylinder with a Convective Type of Time Dependent Boundary Conditions", Period Polytechnic, Ech. Eng. vol.18, no.1, 1974, pp.71-85.

(9) KADINOVA, A.S. & KRIVIZHENKO, V.I.,
"Cooling Effect of Jets of Various Designs", UDC 121,783 748.4, trans. of Met. i. Termich, Obra, Met., no.3, pp.26-30. March,1968.

(10) CARSLAW, H.S. & JAEGER, J.C.,
"Conduction of Heat in Solids", 2nd ed. 1959, Oxford Uni.Press.

(11) ANDERSON, J.T. & SAUNDERS, D.A.,
"Convection from an Isolated Heated Horizontal Cylinder Rotating About its Axis", Proc. Roy. Soc. (London), Ser.A. vol.217, no.1131, May 21 1952, pp.555-562.

(12) PECK, C.F., BONETTI, J.M. & MAVIS, F.T.
"Temperature Stresses in Iron Work Rolls",I.S.E., June 1954, pp.45-58.

(13) BELANSKY, A.M. and PECK, C.F.,
"Roll Temperature Study on a Hot Strip Mill", I.S.E.Year Book,1956, pp.186-188.

(14) CERNI, S.,
"The Temperature and Thermal Stresses in the Rolling of Metal Strip", Thesis submitted to Carnegie Inst. of Tech., Sept. 15, 1961.

(15) WILLIAMS, W.J.,
"Banding in Hot Strip Mill Work Rolls", I.S. Eng., Aug.1962, pp.372-383.

(16) CERNI, S.,
"Temperatures & Thermal Stresses in the Rolling of Metal Strip", ISE Year Book, 1963, pp.717-725.

(17) CERNI, S., et al.,
I.S.E., Sept.1963, pp.165-173.

(18) EL-WAZIRI, A.H.,
"An Up-to-Date Examination of Rolling Theory"., AISE Yearly Proceedings, 1963, pp.53-760.

(19 FORSYTHE, G.E. and WASOW, W.R.,
"Finite Difference Methods for Partial Differential Equations", Willey and Sons,(1964).

(20) LARKE, E.C.,
"The Rolling of Strip,Sheet and Plate", Chapman and Hall, (1963).

(21) PEARSON, W.K.,
"Shape Measurement and Control", J.I.M., 1964-65, vol.93, pp.169-178.

(22) BARAKAT, H.Z. & CLARK, J.A.,
"On the Solution of the Differential Equation by Numerical Methods", Trans. A.M.E.J. Heat trans., Nov.1966.

(23) THOMPSON, P.C., et al.
"Strip Temperature Analysis in Hot Mills", I.S. Eng.,June 1966, pp.129-143.

(24) SHOHET, K.N. and TOWNSEND, N.A.,
"Roll Bending Methods of Crown Control in 4-High Plate Mills", BISRA Report, PE/C/11/68

(25) REIS, V.,
"Analysis of the Thermal Process in a Rectangula Parallel-piped and Solid Cylinder", J.Eng.Phys. (USA), vol.19,3, pp.1155-1158, Sept. 1970.

(26) KADINOVA, A.S.,& KHEIFETS, G.N.
"Factors Affecting Heat Exchange in Spray Cooling with Water", UDC 121, 783 748.4,trans. of Met i. Termich, Obra, Met.,No.3, Jan.1987, pp. 12 - 15.

(27) STEVENS, P.G., IVENS, K.P. & HARPER, P.,
"Improving Work Roll Life by Improved Roll Cooling Practice", J.I.S.I., June 1971, vol.209, pp.1-11.

(28) PARKE, D.M., & BAKER, J.L.L.,
"Temperature Effects of Cooling Work Rolls", I.S.Eng.,1972, pp.83-88.

(29) PAWELSKI, O.,
"Calculating the Temperature Field in the Work Rolls of Hot and Cold Rolling Mills", British I & S.Ind., trans.- Service, Nov.1972, Arch. Eisen., Oct.1971, pp.713-720.

(30) BEESTON, J.W. & EDWARDS, W.J.,
"Thermal Camber Analysis in Cold Rolling". Automation of Tandem Mills, ed. BRYANT, C.F., Iron & Steel Inst., London 1973.

(31) KING, W.D., & SILLS, R.M.,
"New Approaches to Cold Mill Gage Control", I.S.E, May 1973, pp.40-51.

(32) WILMOTTE, S., & MIGNON, J.,
"Thermal Variations of the Camber of the Working Rolls during Hot Rolling", C.R.M., no.34, March 1973, pp.7-34.

(33) KOOT, L.W.,
"Process Design Criteria for the Cooling of a Cold Strip Mill", ISI mech., Amsterdam, Feb.1973, pp.323-333.

(34) McPHERSON, D.J.,
"Contributions to the Theory and Practice of Cold Rolling", A.S.M., Met Trans,vol.5,Dec 1974.pp. 2479-2499.

(35) DIENER, A., et al,
"Heat Transfer When Cooling a Hot Steel Surface with Water", Hoesch-Estel Ber., 1975,(2), pp.78-86.

(36) ELGAWHARY, A.W.,
"Spray Cooling System Design", Chem.Eng.Progress, July 1975, vol.71,(7),pp.83-87.

(37) SMITH, D.J. et al,
"Preliminary Model of Hot Rolling", BNF Metals Tech.Centre, (Confidential Report), 1976.

(38) SMITH, D.J., et al.,
BNF METALS TECH., Research 307, Paper A.1899, Feb.1976.

(39) KOPINECK, H.J., & WLADIKA, H.,
"Rolling Technology - Present State and Tendencies", CEC Information Syp.; Measurement and Control Techniques in Rolling, Sept.2-3,1981,pp.4-33.

(40) POPLAWSKI, J.V.,
"Predicting Operating Temperatures in Rolling Element Bearings for Back-up Rolls", I.S. Eng.,March 1977, pp.41-48.

(41) WILMOTTE, S.,et al.,
"New Approach to Computers Set-up of the Hot Strip Mill", A.I.S.E. Year Book, 1977, p 291.

(42) HANICH, C., & WRIGHT, W.G.,
"Computer Simulation of Tandem Roughing Mill Rolling",ISE, Jan 1 1977, pp.39-44.

(43) BNF METALS TECH. CENTRE, (Confidential Report),
"An Appraisal of the Hot Rolling Model and the Aims of the Trials at CEGEDUR", Aug. 1977.

(44) FREDIANI, H.A. & SMITH, N.
"Mathematical Model for Spray Cooling Systems", J.Eng.for Power, April 1977, pp.279-283.

(45) IWAKI, et al.,
"Development of the Temperature Simulation Model for a Rolling Mill", IHI Eng. Review (English Ed.),1977, vol.10 no.4, pp.49-60.

(46) WILMOTTE, S., et al.,
"The Sigma-Roll Process: A New Approach to Hot Strip Mill Computer Control", C.R.M. no.52,May 1978,pp.7-15.

(47) WILMOTTE, S. et al.,
"A Study of the Cross-Profile of Hot-Rolled Strip", C.R.M. no.52, May. 1972,pp.11-28.

(48) IMBER, M.,
"Inverse Problem for the Solid Cylinder", Poly.Inst.of New York, A.A.A.J. vol.17, pp.91-94, Jan. 1979.

(49) MITOUTSUKA, M., & FAKUDA, K.
"Boiling Phenomena and Effects of Water Temperature on Heat Transfer in the Process of Immersion Cooling of a Heated Steel Plate", Trans. I.S.I.J., 1979, vol.19,pp.162-169.

(50) BOYARSHINOV, et al.,
"Prediction of Work Roll Wear during Hot Rolling", Stal, 1979, (61), pp.531-532.

(51) BOLLE, L. and MOUREAU, J.C.,
"Experimental Study of Heat Transfer by Spray Cooling", Int.Cent. Heat and Mass Transfer,1979, pp.528-534.

(52) PATULA, E.J.,
"Steady State Temperature Distribution in Rotating Roll Subject to Surface Heat Fluxes and Convective Cooling", A.S.M.E. no.79-HT-60, 1979 & Trans. ASME, vol. 103,Feb. 1981, pp.36-41

(53) WEBER, K.H. & UNGER, F.,
"Effect of the Barrel Length, Strip Width and Roll Gap Temperature on the Roll Temperature and Thermal Roll Camber During Cold Rolling", Neue Hutte, 1979 24 (9) pp.331-336.

(54) POPLAWSKI, J.V. & SECCOMBE, D.A.,
"Bethlehems Contribution to the Mathematical Modelling of Cold Rolling in Tandem Mills", I.S. ENG., SEPT.1980, pp.47-57.

(55) BNF METALS TECH. CENTRE,
"In Investigation of the Factors Controlling Flatness in the Rolling of Strip", Paper CN/193, Oct.1980.

(56) GRAY, L.E. and HILL, D.R.,
"Cooling of Work Rolls in Hot Rolling Mills", I.S.Eng.,vol.58, no.6, pp.57-62,June 1981.

(57) PAVLOSSOGLOU, J.,
A Mathematical Model of the Thermal Field in Continuous Hot Rolling of Strip and Simulation of the Process",Arch. Eisenhuttenwes,52 (4),pp.153-158, April 1981.

(58) PAVLOSSOGLOU, J.,
"Mathematical Modelling of The Thermal Field of Rolls and the Strip in Continuous Hot Rolling", Arch.Eisenhuttenwes, 52 (7),275-279,July 1981.

(59) HILL, D.R., & GRAY, L.E.,
"Cooling of Work Rolls in Hot Rolling Mills", Iron & Steel Eng., June 1981, pp.57-62.

(60) FLETCHER, J.D.,
"Modelling for Cold Strip Profile Prediction of Four-high Mills", Davy-Loewy Ltd., Aug.1981.

(61) ABDEL-WAHED, R.M. & HIFNI, M.A.,
"Measuring Thermal Diffusivity of Metals and Heat-transfer Coefficient by the Use of a Moving

Heat Source", Heat and Mass Transfer During Crystallization, Hemisphere Publ. Corp.,1981.

(62) BRYANT, G.F. and CHIU, T.S.L., "Simplified Roll-Cooling and Stress Effects, Met. Tech.,9 (12) 485-492, Dec 1982.

(63) BRYANT, G.F., and HESELTON, M.O., "Roll-gap Models for Hot Mills", Metals Tech.,Dec 1982,9,pp.469-477.

(64) BRYANT, G.F. and CHIU, T.S.L., "Simplified Roll Temperature Model:Convective Cooling",Metals Tech., Dec.1982,vol.9,pp.478-484.

(65) BOLLE, L. and MOUREAU, J.U., "Spray Cooling Multiphase Science and Technology", Ch.1,

(66) SPARTHMANN, R.P. & PAWELSKI, O., "Thermal Changes in the Shape of Work Rolls and Their Application to Influencing the Flatness of Cold Rolled Strip",Arch., Eisenhuttenwes, 1982 vol.53, pt.11, pp.427-434.

(67) OHSHIMA, et al., (Trans.Okazaki,H.),"Simulation of Flatness Control During Foil Rolling", R & D Kobe Steel,vol.33 no.2, 1983

(68) ATACK, P.A. & GORE, T.A. "Separated Cooling and Lubrication on Aluminium Cold Reducing Mills" Davy McKee (Poole) Library, Jan.1984

(69) PARKE, D.M. & BAKER, J.L.L., "Temperature Effects of Cooling Work Rolls", (final summary report), Ass.Iron & Steel Eng. Pittsburgh, 1972

(70) BRADLEY, B.F. et al., "Transient Temperature Behaviour of Aluminium During Rolling and Extrusion", Mathematical Models in Metallurgical Process Development, I & St. Inst., London,1970 pp.79-90

(71) TRAKHTENBERG, B.G., et al., "Temperature Field in a Solid Cylinder", Phys.& Chem. Mater Trent,(trans.of Fizika i Khimiya Obrabutki Materialov, USSR, vol.17., no.4, 1983, pp.22-4).

(72) PALLONE, G.T., "Transient Temperature Distribution in Work Rolls during Hot Rolling of Sheet and Strip", I.S. Eng., Dec.1983, pp.21-26.

(73) CARPENTER, R.R. and HANNAN, P.J., "Improving Efficiency of Work Roll Cooling Systems",

Mech. Working & Steel Processing, 25, pp.17-19, Oct.1984.

(74) SHEPPARD, T., & ROBERTS, J.M.,
"Shape Control and Correction in Strip and Sheet", Int.Met.Reviews, vol.18 (no.171).

(75) BAMBERGER, M. & PRINZ, B.,
"Heat Transfer to Water and its Importance for Metal Castings and Heat Treatment", 2nd Israel Materials Eng.Conf., Beer-shewe, 21-23 Feb.1984, pp.209-213.

(76) KAMATA, NKK.,
"Rolling Mill with Roll Bending Equipment", (Trans.Okazaki,H), from speeches at JISI, 1984.

(77) BENNON, W.D.,
"Evaluation of Effective Coolant Application for the Control of Work Roll Thermal Expansion", Trans.of the ASME., May 1985, vol.107, pp.146-152.

(78) YUEN, W.Y.D,
"On the Steady-state Temperature Distribution in a Rotating Cylinder Subject to Heating and Cooling Over its Surface", Trans.ASME Jou.of Heat Transfer, vol.106 pp.578-585.

(79) NAKAGAWA, trans. by OKAZAKI, H.,
"Thermal Crown in Aluminium Foil Rolling", (from Sumitomo Light Metals Tech.Report), July 1985.

(80) TANI, K., et al,
"Installation of 6-High Cold Rolling Mill with Roll Coolant Devices and their Performances", Inst.of Metals,Sept. 17-19, 1985., pp.66-71., London.

(81) YUEN, W.Y.D., et al.
"Thermal Effects in Cold Rolling", Advances in Cold Rolling Techniques, Inst.of Metals, Imperial Coll., London 17-19 Sept.,1985, pp.57-65.

(82) NAKAGAWA (Trans. OKAZAKI,H),
"Thermal Crown in Aluminium Foil Rolling",
Sumitomo Light Metals Technical Report, July 1985.

(83) HOLLANDER, F.,
"A Model to Calculate the Complete Temperature Distribution in Steel During Hot Rolling".
Mathematical Models in Metallurgical Process Development, I & St.Inst., London,1970 pp.46 - 74

(84) LIU, CHEN-YA., et al.,
"Natural Convection Heat Transfer in Long Horizontal

Cylindrical Annuli".

(85) HIRANO, et al.,(Trans.OKAZAKI,H.I.J.),
Japan Soc.for Tech.of Plasticity, Vol.25, no.282.

(86) DARBY, P.F.,
"Flat Rolling Calculations", ISE., Feb.1983,
pp.38-43.

(87) GIBSON, G.C., & SMITH, H.,
"The Principles of Aluminium Rolling", British Aluminium Co.Ltd., 1964.

(88) KONO, et al., (Trans. by Okazaki, H),
"Development of Mathematical Models in Crown Control in Cold Strip Rolling", Sumitomo Metals Tech.Report,vol.32, no.3.

(89) MATSUMOTO, NSC, (Trans. by Okazaki, H).,
"Theory of Sheet Profile and Shape in Sheet Rolling", JSI Conf. Sept.1983.

(90) SABATINI, B.,
"An Investigation into the Use of Tension and Roll Bending for the Control of Strip Shape", British I & S Research Assn., (confidential report), 1967.

(91) SHOHET, K.N., & TOWNSEND, N.A.,
"Roll Bending Methods of Crown Control in Four-high Plate Mills", JISI, Nov.1968, pp.1088-1098.

(92) WILLIAMS, W.J.,
"Banding in Hot Strip Mill Work Rolls", I & S Eng., Aug. 1962, pp.372-383.

(93) JORTNER, D.,et al.,
"An Analysis of the Mechanics of Cold Strip Rolling", ISE, May 1959, pp.127 - 135.

(91) LEE, P.W., et al.,
"Rolling Theory - A Method for Predicting Temperatures in Continuous Hot Strip Mills", Iron & Steel, 19 Dec.1962 pp.624 - 627.

(95) HODGSON, J.W., & SUNDERLAND, J.C.,
"Heat Transfer From a Spray-cooled Isothermal Cylinder",I & E C Fundamentals, Vol.7, No.4, Nov.1961, pp.567-571.

(96) DROPKIN, D., & CARMI, A.,
"Natural-Convection Heat Transfer from a Horizontal Cylinder Rotating in Air", Trans. of ASME, 1957, pp.741-749.

(97) BRYANT, C.F.,Ed.,
"Automation of Tandem Mills", ISI, London,1973

(98) TIMOSHENKO, S.P., & GOODIER, J.N.,
"Theory of Elasticity", McGraw-Hill Kogakusha, Ltd.,3rd ed.,1970.

(99) PAWELSKI, O,
Archiv fur das Eisenhutten - Wesen, Oct. 1968, pp.821 - 827.

(100) APACI, V.S.,
"Conduction Heat Transfer", Addison-Wesley, New York, 1966, pp.325 -328.

(101) UNGER, F, & WEBER, K.H.,
Neue Hutte, 1976, Vol. 21 (11) pp.653 - 657.

(102) IBID,
Neue Hutte, 1979, Vol. 24 (4), pp.138 - 140.

(103) JESCHAR, I.R., REINERS, U,
"Heat Transfer in Two-Phase Spray-Water Cooling",
Warme Gas Int., June/July 1984, pp.299 - 308.

(104) ALLEN, D.R., et al.,
"Future Development in Profile Thickness Gauging of Aluminium Hot-Rolled Strip", Aluminium Technology 1986, March 11 - 13, London, paper 41.

(105) BARTEN, E.A.,
"A New Generation of Foil Rolling Mills",
Aluminium Technology 1986, March 11 - 13, London, paper 40.

(106) BEAUDOIN, A.J., & WOODBURY, K.A..,
"Mathematical Modelling of Hot Rolling of Aluminium", Aluminium Technology 1986, March 11-13, London,paper 110.

(107) BROOKS, P.J.,
"Advances in Hot Rolling Technology", Aluminium Technology 1986, March 11 - 13, London, paper 108

(108) MIYAKE, Y, et al.,
"Development of Hot Rolling Technology for Improving Strip Profile and Flatness", Kawasaki Steel Tech. Report No.12, July 1985.

(109) LAMBERT, N., & ECONOMOPOULOS, M.,
"Measurements of the Heat-Transfer Coefficients in Metallurgical Processes", Math Models (as 70), pp.133 - 145.

(110) WANG, CHI-TEH,
"Applied Elasticity", McGraw-Hill, 1953.

(111) RYDER, G.H.,
"Strength of Materials", McMillan Press, 3rd Ed.1969.

(112) GERALD, C.E.,
"Applied Numerica Analysis", Addison-Wesley Pub.Co., 2nd Ed., 1980.

(113) MORT, J.M.,
"Sheet and Tinpate Mills.Measurement of Roll Camber" Iron & Steel, July 1947, pp. 416 -418

(114) LARKE, E.C.,
"The Rolling of Strip, Sheet and Plate", Chapman & Hall, 1963

(115) HINFORTH, R, et al.,
Neue Hutte, July 1972, pp. 412 - 416.

(116) SIBAKIN, J.G. et al.,
Proceed. Met. Soc. Conference, Chicago, Jan. 1959.

(117) POLUKHIN, P.I., et al,
Stal, 2, Feb. 1963, pp. 127 - 132.

(118) SOMERS, R.R. & KHEIFERS, G.N,
"The Predicted and Measured Expansion of Hot-strip mill Work Rolls"

(119) BAMBERGER, M. & PRINZ, B.,
"Determination of Heat Transfer Coefficients During Water Cooling of Metals", Material Science & Tech., April 1986, vol.2, pp. 410 - 415.

(120) YAMAMOT, et al.,(trans. OKAZAKI, H.),
"Simple equations of Roll Surface Temperature and Thermal Crown" 1986 Spring Conference for the Technology of Plasticity, Oct. 1986.

(121) GERALD, C.F.,
"Applied Numerical Analysis", 2nd Ed., Addison-Wesley Pub. Co., 1980.

(122) NECATI, M., ZISIK, O.,
"Heat Conduction". John Wiley, New York, 1980.

(123) WACHSPRESS, E.L.,
"Optimum Alternating-Direction-Implicit Iteration Parameters for a Model Problem", J.Soc.Indust.Appl Math., vol.10, No.2, June 1962,pp. 339-350.

(123) WACHSPRESS, E.L.,
"An Alternating-Direction-Implicit Iteration

Technique", J.Soc.Indust.Appl.Math.,vol 8, No.2, June 1960,pp. 403-424.

(125) PEACEMAN, D.W., & RACHFORD, H.H.,
"The Numerical Solution of Parabolic and Elliptic Differential Equations", Vol.3, No.1, March 1955, pp.28-41.

(126) ROBINSON, F.,
"An Initial Report on Heat Transfer Measurements of Kerosene Sprays", Davy McKee (Poole) Ltd.,Sept.1985.

(127) WATSON, J.,
"Preliminary Report on the Design and Selection of Coolant Spray Nozzles", Davy Mckee (Poole) Ltd., TD.137/R104, May 1986.

(128) ROBINSON, F.,
"An Initial Report on Heat Transfer Measurement of Kerosene Sprays", Davy McKee (Poole) Ltd., Sept. 1985

(129) BANWELL,S.,
"Strip Profile Prediction Model for Four-Hill Mills, TD/38/R074, Davy McKee (Poole) Ltd., Jan 1985.

(130) COLLINS, D.,
"Interim Report on Roll Thermal Camber Study". TD. 138/R106, Davy McKee (Poole) Ltd., July 1986.

APPENDIX A

THE ANALYTICAL SOLUTION TO THE UNSTEADY STATE HEAT CONDUCTION EQUATION

A1. INTRODUCTION

This section will examine the analytical solutions to the heat conduction equations of Chapter 3 for simple heat transfer situations; and uses the results as a means of checking the correctness of the computer program based on the finite difference method of solution.

In Chapter 3 it was shown that, subject to certain assumptions, the equation for heat conduction for a cylindrical work roll, when expressed in cylindrical coordinates, is given by:

$$\rho C \frac{\partial T}{\partial t} = k \left(\frac{\partial^2 T}{\partial r^2} + \frac{1}{r} \cdot \frac{\partial T}{\partial r} + \frac{\partial^2 T}{\partial x^2} \right) \qquad (A1)$$

A2. UNSTEADY TEMPERATURE, RADIAL HEAT FLOW

If a circular cylinder whose major axis is along the x-axis, and with symmetry along the axes, is heated, with the initial and boundary conditions independent of time, t, the temperature will be a function of r only. This reduces eqn. (A1) to:

$$\rho C \frac{\partial T}{\partial t} = k \left(\frac{\partial^2 T}{\partial r^2} + \frac{1}{r} \cdot \frac{\partial T}{\partial r} \right) \qquad (A2)$$

In the situation described by eqn. (A2), heat flows perpendicular to the x-axis with radial lines of flow only.

A3. UNSTEADY TEMPERATURE, RADIAL AND AXIAL HEAT FLOW

The following boundary and initial conditions apply to eqn. (A1).

for x:

$$T_{(0,\,r,\,t)} = f_1(r,t)\,(x=0) = T_s \tag{A3}$$

$$T_{(l,\,r,\,t)} = f_2(r,t)\,(x=L) \tag{A4}$$

$$\Rightarrow \left.\frac{\partial T}{\partial x}\right|_{L,\,r,\,t} = 0 \tag{A5}$$

for r :

$$Q_{(x,\,0,\,t)}(r) = 0\,, \qquad r=0 \tag{A6}$$

$$\Rightarrow \frac{\partial T}{\partial r} = 0 \tag{A7}$$

$$Q_{(x,\,R,\,t)}(r) = hA\left(T_{x,\,R,\,t} - T_0\right)\;;\; r = R \tag{A8}$$

$$-kA\frac{\partial T}{\partial r} = hA\left(T_{x,\,R,\,t} - T_0\right) \tag{A9}$$

for t

$$T_{x,\,r,\,0} = \phi_{x,\,r}, \qquad t=0 \tag{A10}$$

ANALYTICAL SOLUTIONS TO EQN. (A1)

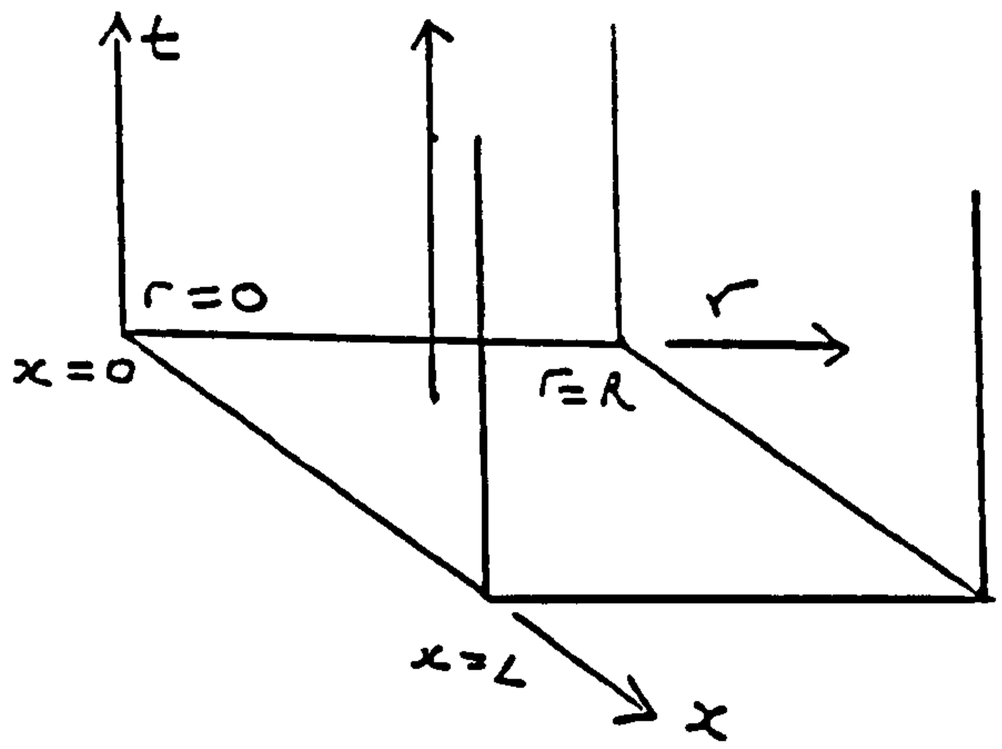

Fig. A3.1. 3-dimensional representation of eqn.(A1)- the marching problem

One method of solving eqn. (A1) is by separation of variables. This general method, based on the fact that a function $V(x,r,t) = X(x).R(r).T(t)$, where X, R, T are new functions leads to a sum of a series of such terms. Thus if we allow

$$T(x, r, t) = X(x).R(r).\theta(t) \tag{A11}$$

where X, R, and θ are, respectively, functions of x, r, and t only

eqn. (A11) becomes on substitution,

$$\frac{\alpha}{\theta}\frac{d\theta}{dt} = \frac{1}{R}\left(\frac{d^2R}{dr^2} + \frac{1}{r}.\frac{dR}{dr}\right) + \frac{1}{X}.\frac{d^2X}{dx^2} \tag{A12}$$

$$= \text{a constant} = -\omega^2 \tag{A12}$$

where

$$\alpha = \frac{\rho C}{k}$$

Therefore,

$$\frac{d\theta}{\theta} = -\frac{\omega^2}{\alpha}.dt$$

$$\therefore\ \theta = A\, e^{-\frac{\omega^2 t}{\alpha}} \qquad \text{(A13)}$$

where A is a constant to be determined from the initial conditions.

Also,

$$\frac{1}{R}\left(\frac{d^2R}{dr^2} + \frac{1}{r}.\frac{dR}{dr}\right) = -\omega^2 - \frac{1}{X}.\frac{d^2X}{dx^2}$$

$$= \text{a constant}$$

$$= -\lambda^2_{(say)} \qquad \text{(A14)}$$

$$\therefore\ \frac{d^2X}{dx^2} = -(\omega^2 - \lambda^2)X$$

$$X = B\cos\left(x\sqrt{\omega^2-\lambda^2}\right) + C\sin\left(x\sqrt{\omega^2-\lambda^2}\right) \qquad \text{(A15)}$$

where B and C are constants determined from the boundary conditions.

We also have

$$\frac{d^2R}{dr^2} + \frac{1}{r}.\frac{dR}{dr} + \lambda^2 R = 0 \qquad \text{(A16)}$$

or

$$r^2 \frac{d^2R}{dr^2} + r \frac{dR}{dr} + \lambda^2 r^2 R = 0 \qquad \text{(A17)}$$

Eqn. (A17) is a Bessel equation of order zero

$$\therefore R = D J_0(\lambda r) + E Y_0(\lambda r) \qquad \text{(A18)}$$

where J_0 and Y_0 are Bessel functions of the first and second kind, respectively, and of zero order. Thus,

$$\theta = \exp -\frac{\omega^2 t}{\alpha} . \left(B \cos x \sqrt{\omega^2 - \lambda^2} + C \sin x \sqrt{\omega^2 - \lambda^2} \right) \left(D J_0(\lambda r) + E Y_0(\lambda r) \right)$$

.... (A19)

Complete solutions to eqn. (A1) can also be found in ref. [10]

A4. INFINITELY LONG CYLINDER, RADIAL HEAT FLOW, VARIABLE TEMPERATURE.

Consider now the case where heat flows perpendicular to the x - axis with radial lines of flow, described by eqn. (A2) :

$$\rho C \frac{\partial T}{\partial t} = k \left(\frac{\partial^2 T}{\partial r^2} + \frac{1}{r} . \frac{\partial T}{\partial r} \right)$$

or re-writing :

$$\alpha \frac{\partial T}{\partial t} = \frac{\partial^2 T}{\partial r^2} + \frac{1}{r} . \frac{\partial T}{\partial r}; \quad 0 < r < R \qquad \text{(A20)}$$

Assume a solution of the form

$$T(x, r, t) = X(x).R(r).\theta(t)$$

$$= -\omega^2 = \text{a constant}$$

Let the initial condition be

at $t = 0$, $T = f(r)$

and the boundary condition

at $r = R$, $T = 0$ (or $T = T_0 + T_D$)

Put

$$T = R \exp\left(-\frac{\omega^2 t}{\alpha}\right)$$

where R is a function of R only

to get

$$\frac{d^2R}{dr^2} + \frac{1}{r}\frac{dR}{dr} + \omega^2 R = 0 \qquad \text{(A21)}$$

Eqn. (A21) is a Bessel equation of order zero.

Since the solution of the second kind is infinite at r = 0, the particular integral suitable for this problem is

$$T = A J_0(\omega r) \exp\left(-\frac{\omega^2 t}{\alpha}\right) \qquad \text{(A22)}$$

To satisfy the boundary conditions :

$$J_0(\omega r) = 0 \qquad \text{(A23)}$$

If $f(r)$ can be expanded in the series

$$f(r) = A_1 J_0(\omega_1 r) + A_2 J_0(\omega_2 r) + \ldots \qquad \text{(A24)}$$

the conditions of the problem can be satisfied by

$$T = \sum_{n=1}^{\infty} A_n J_0(\omega_n r) \exp\left(-\frac{\omega_n^2 t}{\alpha}\right) \tag{A25}$$

The values of the coefficient in eqn. (A25) can be obtained by following the method detailed in Carslaw and Jaeger[10] .

For the case of constant initial temperature $T(r) = T_0$, and zero surface temperature, the equation in T becomes

$$T = \frac{2T_0}{R} \cdot \sum_{n=1}^{\infty} \exp\left(-\frac{\omega_n^2 t}{\alpha}\right) \cdot \frac{J_0(r\omega_n)}{\omega_n J_1(R\omega_n)} \tag{A26}$$

where J_1 is a Bessel function of the first order.

If the cylinder has zero initial temperature and the surface is held at a constant temperature, T_0, for $t > 0$, a solution is found by subtracting eqn. (A26) from T_0 to give

$$T = T0 - \frac{2T_0}{R} \cdot \sum_{n=1}^{\infty} \exp\left(-\frac{\omega_n^2 t}{\alpha}\right) \cdot \frac{J_0(r\omega_n)}{\omega_n J_1(R\omega_n)} \tag{A27}$$

To transfer eqn. (A27) into dimensionless form put

$$R\omega_n = \beta_n \text{ and } \frac{t}{\alpha R^2} = \psi \tag{A28}$$

and eqn.(A27) becomes

$$\frac{T}{T_0} = 1 - 2\sum_{n=1}^{\infty} \exp\left(-\beta_n^2 \psi\right) \cdot \frac{J_0(r\beta_n/R)}{\beta_n J_1(\beta_n)} \tag{A29}$$

where now $\pm \beta$, n = 1, 2, ... are the roots of

$$J_0(\beta) = 0 \tag{A30}$$

The roots of this equation can be found in the literature[10].

A5. THE FINITE DIFFERENCE REPRESENTATION OF THE CLOSED FORM SOLUTION.

Consider again the situation of zero initial temperature and a fixed roll surface temperature,

when t = 0, T = 0

and

r = R, T = T_s

$$\frac{\partial T}{\partial x^*} = 0 \quad \text{when} \quad x^* = 0$$

$$\frac{\partial T}{\partial x^*} = 0 \quad \text{when} \quad x^* = x_0 \rightarrow \infty$$

$$\frac{\partial T}{\partial r^*} = 0 \quad \text{when} \quad r^* = 0$$

$$T = T_s \quad \text{when} \quad r^* = 1$$

The equations above can be used as a quick test on the correctness of the computer produced temperatures using the finite equations developed in Chapter 3 for simple heat

transfer situations. **Figs. A5.1 and A5.2** respectively show graphs of the temperature distribution at various times in a cylinder under the conditions described using eqn. (A27); and that of the finite difference equivalent.

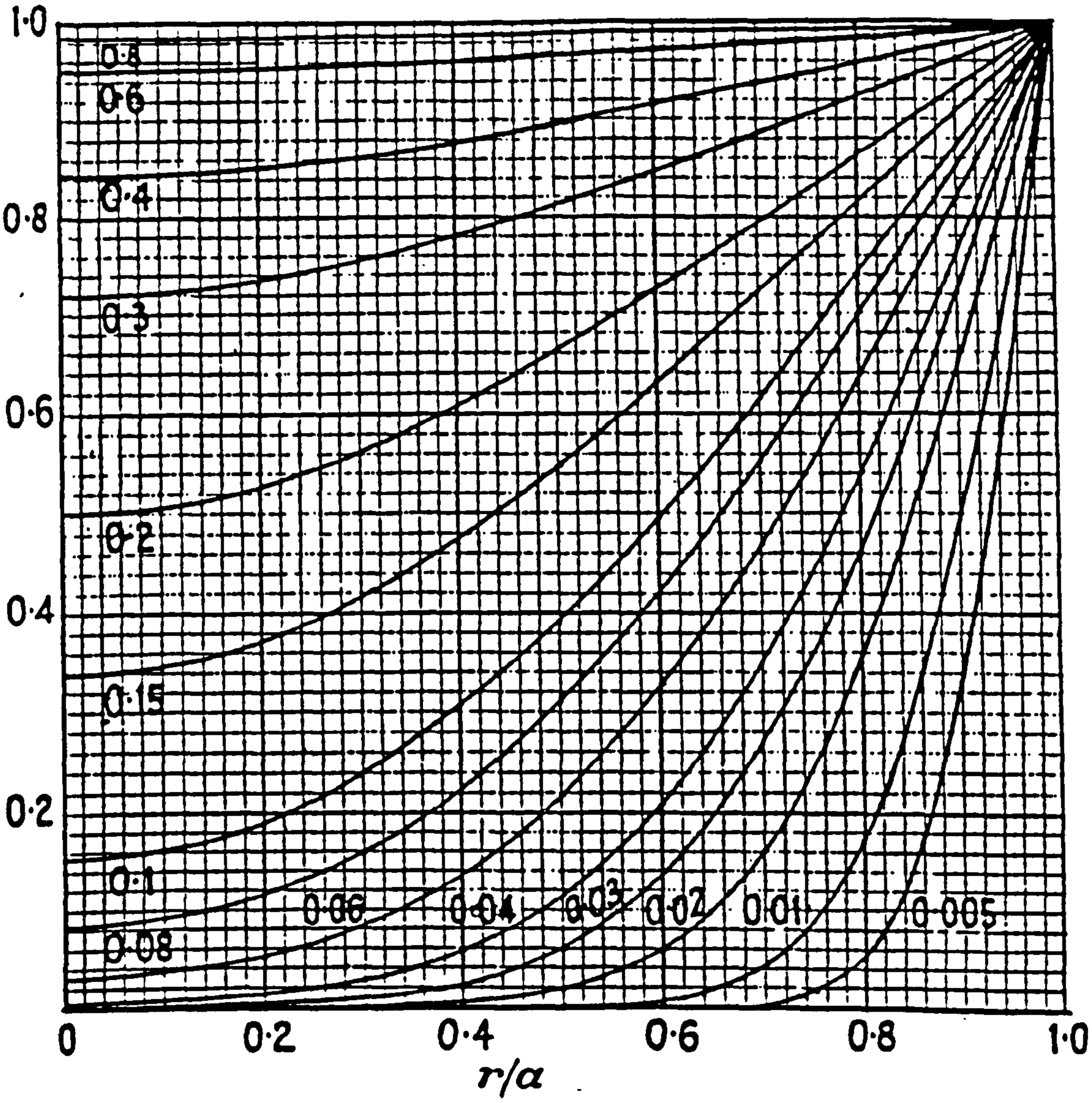

Fig. A5.1 Temperature distribution at various times in a cylinder of radius a with zero initial temperature and surface temperature V. The numbers on the curves are the values of $\kappa t/a^2$, where $\kappa = \dfrac{k}{\rho C_p}$

(ref. Carslaw and Jaeger[10]).

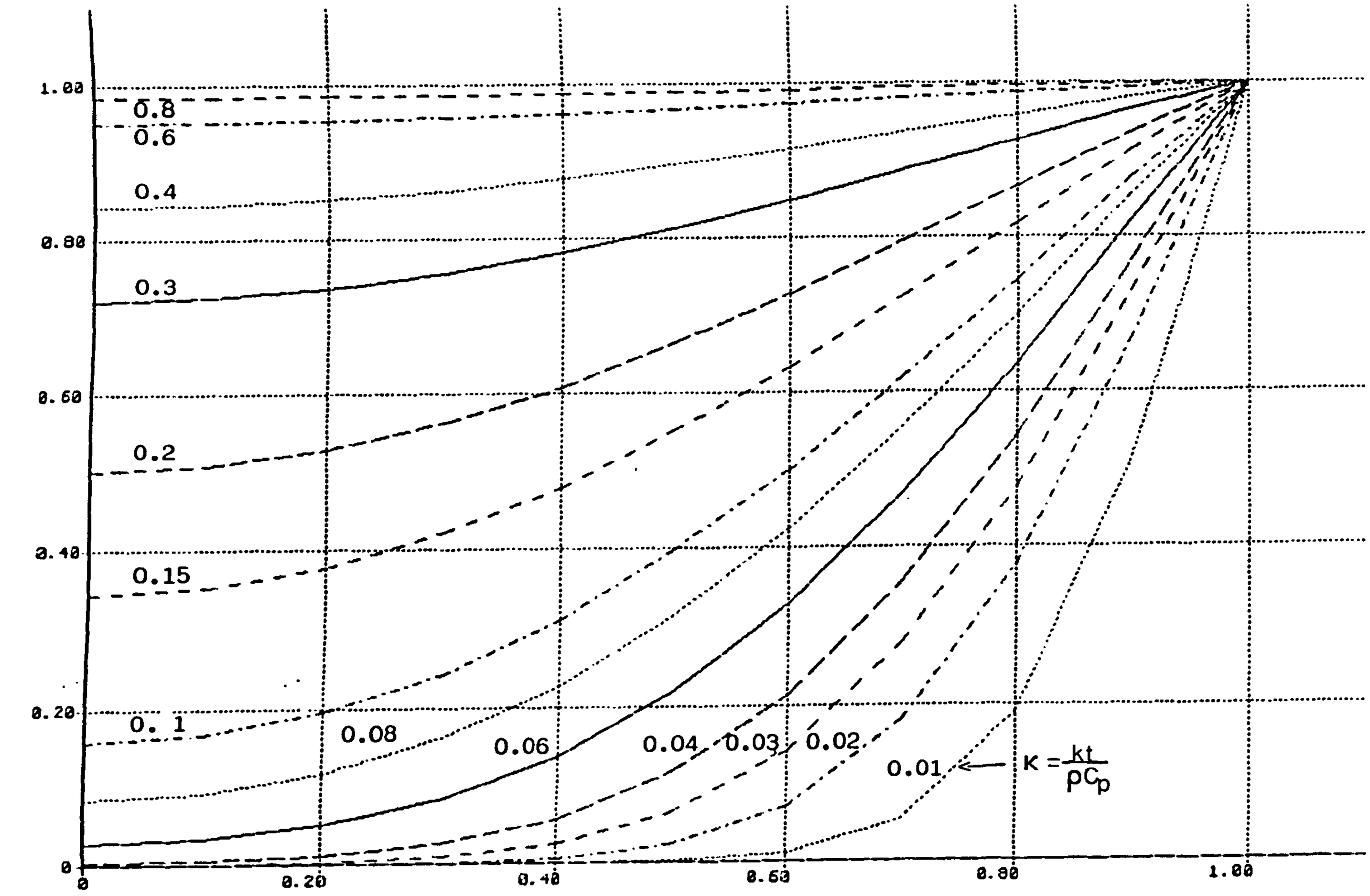

Fig. A5.2 Temp. map at various times in cylinder, radius=R

APPENDIX B

THERMAL CAMBER

B1. RADIAL EXPANSION IN A LONG CIRCULAR CYLINDER

An approximate model for the surface displacement of a circular cylinder is presented. It is assumed that there is radial temperature variation, no axial heat flow roll and an infinitely long cylinder. These are reasonable assumptions for a mill work roll except near the strip edge. The model will be modified to take into account the large axial temperature gradients occurring near the strip edge.

Consider the unrestrained elastic body at some uniform temperature. If this body is now heated to some temperature above the initial temperature, it will experience stresses for a non-equlibrium state. If this new temperature distribution is uneven throughout the body, then each element in the body will expand differentially in relation to the new temperature distribution. The strain of an element may be considered as consisting of two parts. One part of the expansion of an element is due to the bulk temperature rise and the other part is due to the stresses caused by the differential temperature gradients. If the temperature rise is T, the longitudinal strain would be αT, where α is the coefficient of linear expansion of the material, if no lateral constraint existed. Since our model assumes circumferential symmetry, no shearing strains will

be produced. If the element is able to expand freely, there is only the axial component of strain, and hence the element will not be stressed. If the expansion of the element is restrained, stresses will be produced. This is because the expansion of a body due to a temperature rise cannot generally proceed freely in a continuous body. The total strain of the element is therefore the sum of the part due to the stresses and the part due to the temperature.

Timoshenko and Goodier[98] gives an approximation for the roll surface displacement, u, for the situation described above, as:

$$u = 2\alpha R \int_0^1 T r^* . dr^* \qquad \text{(B1)}$$

where: $r^* = r/R$

r = radial distance

R = radius at the cylinder surface

B2. THE SMOOTHING FUNCTION

The error involved in predicting the thermal camber using eqn. (B1) will be greatest near the edge of the strip. This equation will predict a thermal camber smoother than the actual thermal camber. This is because eqn. (B1) does not take into account that differential expansion in adjacent roll sections tends to oppose changes in thermal camber. The predicted camber will also be in error near the roll end because the infinite roll length assumption is no longer valid.

Beeston and Edwards[30] have suggested using a smoothing

function to the displacement function $u(x')$ to reduce the calculation error near the strip edge. The suggested method is to filter the displacement $u(x')$ by using a Green's function description to give the thermal camber, $y_\theta(x^*)$. Thus,

$$y_\theta(x^*) = \int_{-x_0}^{x_0} g(x^*, x').u(x').dx' \qquad \text{(B2)}$$

where: $x^* = x/R$

x = axial position

l = characteristic length

$g(x^*, x')$ = influence function

Due to axial symmetry

$$u(x') = u(-x')$$

and

$$g(x^*, x') = g(-x^*, -x')$$

It can be seen that $y_\theta(x^*)$ need only be solved for $0 \leq x^* \leq 1/R$ and not for the entire roll (i.e., half the roll length).

An even function

$$\frac{\beta}{\sqrt{2\pi}}.\exp -\frac{1}{2}\left[\beta(x^* - x^*)\right]^2$$

was assumed for $g(x^*, x')$. The constant β can be adjusted to give the required results (see next section, B2.1). Compensation for end effects can be obtained by normalizing the influence function to have unit area, i.e.,

$$g(x^*, x') = \frac{\exp\left(-\frac{1}{2}\left[\beta(x^* - x')\right]^2\right)}{\int_{-x_0}^{x_0} \exp\left(-\frac{1}{2}\left[\beta(x^* - x')\right]^2\right) .dx'} \qquad \text{(B3)}$$

B2.1 INVESTIGATION OF THE EFFECT OF THE CONSTANT β (IN EQN. (B3)).

If a continuous function can be defined as

$$f(x) = \frac{\beta}{\sqrt{2\pi}} \exp\left(-\frac{\beta}{2}(x - \mu)^2\right) \qquad \text{(B4)}$$

then its integral cannot be evaluated analytically unless the limits of integration are $\pm\infty$, in which case we get a total area equal to unity; (the denominator $\sqrt{(2\pi)}$ is that to make it unity).

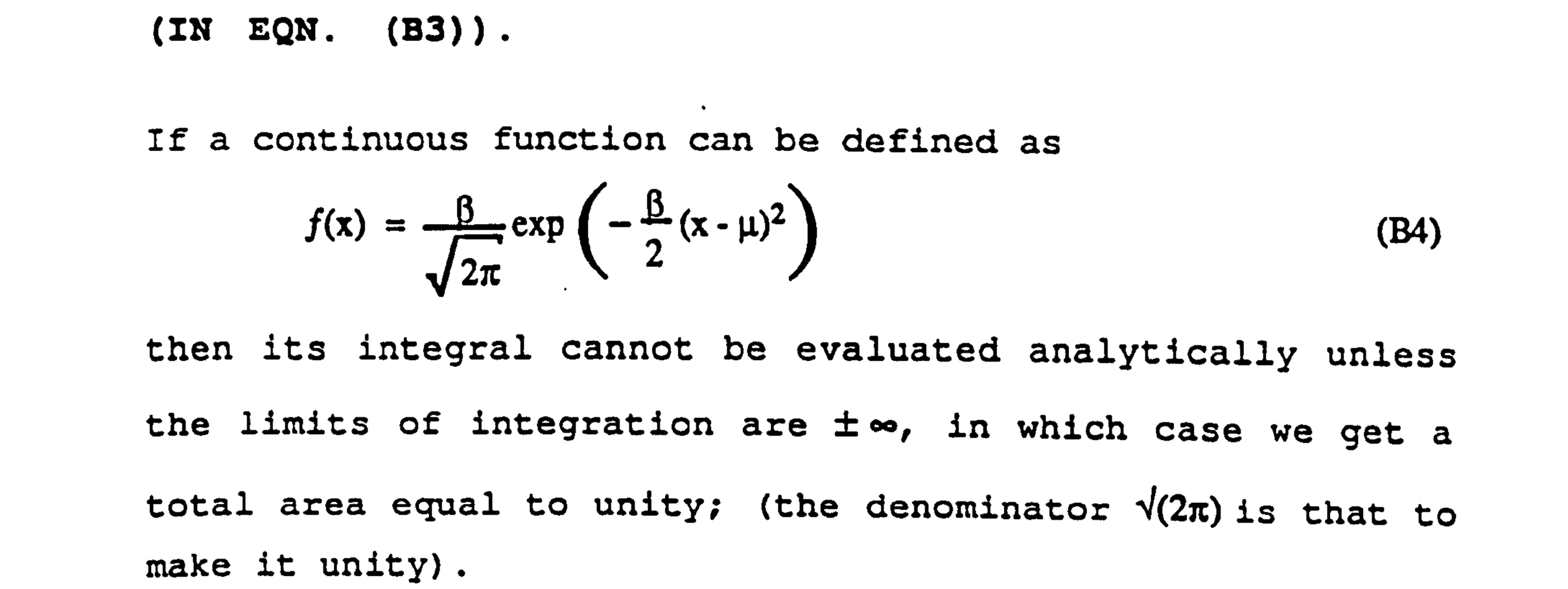

Fig. B2.1. Graphical representation of eqn. (B4).

Let

$$F(x_1) = \int_{x_1}^{x_2} f(x).dx$$

$$= P(x_1 < X < x_2) \qquad \text{(B5)}$$

and defining

$$P(\bar{X} > x_1) = \int_{x_1}^{\infty} \frac{\beta}{\sqrt{2\pi}} \exp\left(-\frac{\beta}{2}(x-\mu)^2\right).dx \qquad \text{(B6)}$$

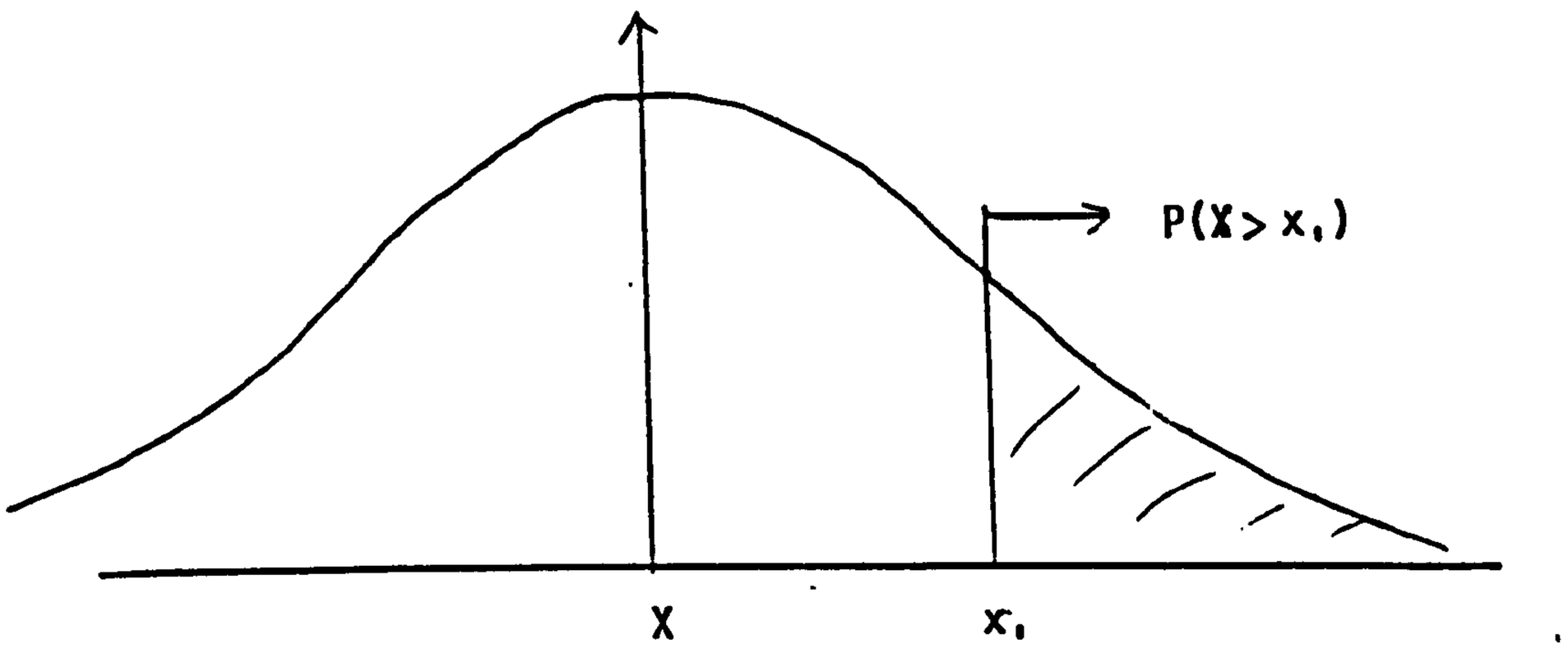

Fig. B2.2. Graphical representation of eqn. (B6).

The integral can be simplified by a change of variable.

Let $z = \beta.(x - \mu)$ so that

$dz = \beta.dx$ and $z_1 = \beta(x_1 - \mu)$

then

$$P(X > x_1) = \int_{z_1}^{\infty} \frac{1}{\sqrt{2\pi}} \exp\left(-\frac{z^2}{2}\right).dz \qquad \text{(B7)}$$

The new integrand is in the form of a normal probability function with $\mu = 0$ and $\beta = 1$. It amounts to changing the origin (subtracting μ), and changing scale (multiply by β).

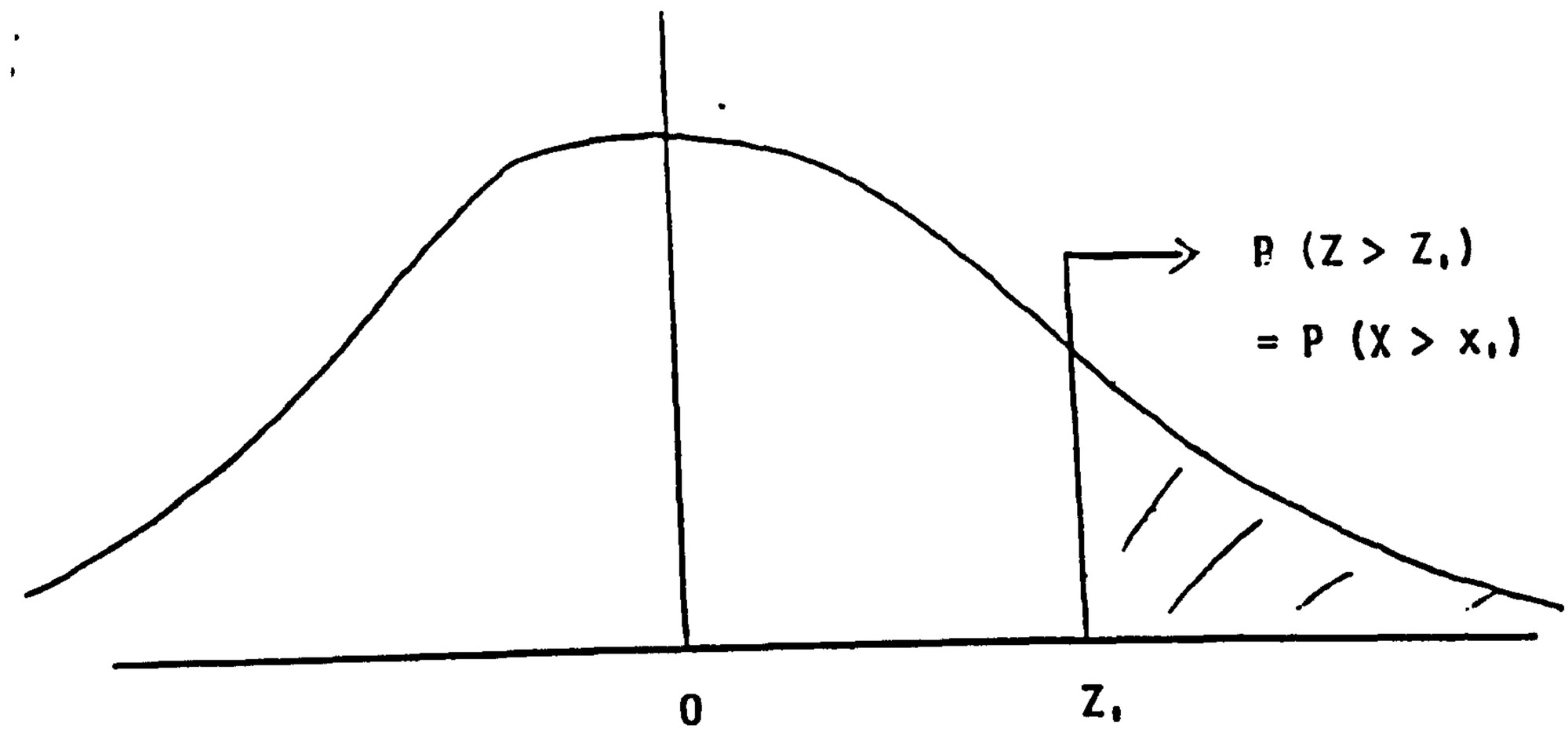

Fig. B2.3 . Normal probabilty distribution with mean μ equal zero.

Hence as β gets larger F(x) tends to unity.

Fig.B2.4 shows the effect of varying the value of β when eqn. (B 2) is solved numerically. The graphs show that for $\beta = 0$, the function $y_\theta(x^*)$ would be smoothed out to produce a uniform thermal camber across the width of the roll. An

appropriate value of β is taken to be 4.

If $\beta = 0$, eqn. (B3) becomes

$$g(x^*, x') = \frac{1}{x_0} = \frac{1}{2x_0}$$

$$\int_{-x_0} dx'$$

and

$$y_\theta(x^*) = \int_{-x_0}^{x_0} g(x^*, x').u(x').dx'$$

$$= \int_{-x_0}^{x_0} \left\{ \frac{1}{2x_0} . 2\alpha R \int_0^1 \theta(x', r^*) r^* . dr^* \right\} .dx'$$

$$= \frac{\alpha R}{x_0} \int_{-x_0}^{x_0} \int_0^1 \theta(x', r^*) r^* . dr^* . dx'$$

$$= 2\alpha R \int_0^1 \theta(x', r^*) r^* . dr^* \qquad \text{(B8)}$$

Thus eqn. (B2) reverts to eqn. (B1) when $\beta = 0$, i.e., the unsmoothed displacement function $u(x')$.

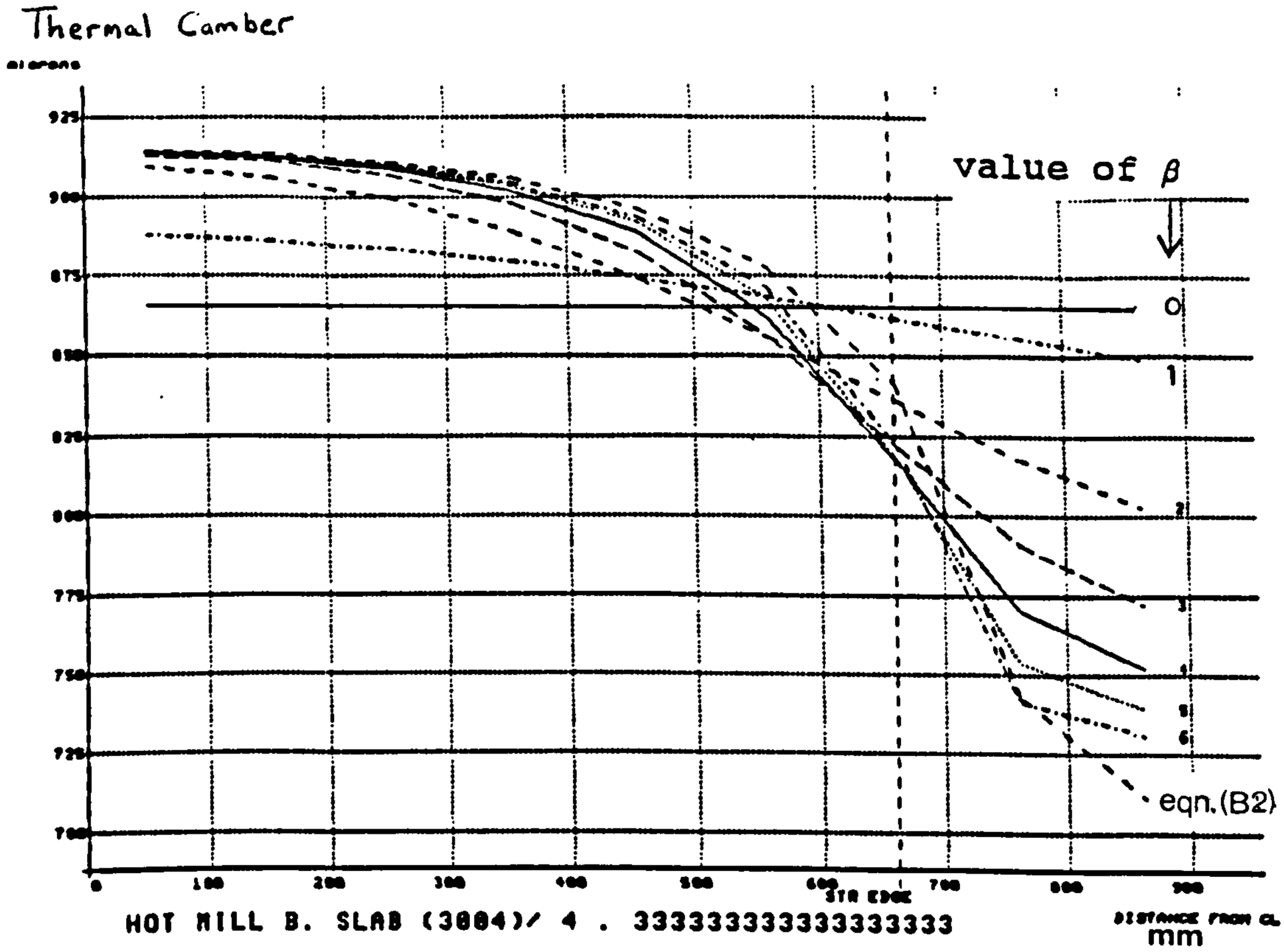

Fig. B2.4. Effect of changing the value of β, in eqn.(B2), on the displacement function $u(x')$.

APPENDIX C

THE ROLL BITE HEAT TRANSFER MODEL

C1 INTRODUCTION

The roll bite temperature model used to determine the heat input into the work roll when in contact with a hot slab is developed from the work of Bradley et al.[70] The heat conduction equations are solved using the finite difference method. The assumptions used in the solution are:

(1)The strip and roll are at uniform, though different temperatures before being brought into contact.

(2)There is no resistance to heat transfer at the roll-strip interface.

(3)There is negligible slip between strip and rolls so that frictional heat generation is neglected.

(4)Symmetry about the strip centre line.

(5)Plane sections remain plain.

(6)The roll radius is negligibly deformed.

C2 ROLL BITE HEAT TRANSFER MODEL

Consider figs. C2.1 and C2.2 below. Figure C2.1 depicts a strip passing between two work rolls. Consider that the roll and strip can be divided into elements as shown in fig. C2.2

Fig. C2.1. Strip in roll bite.

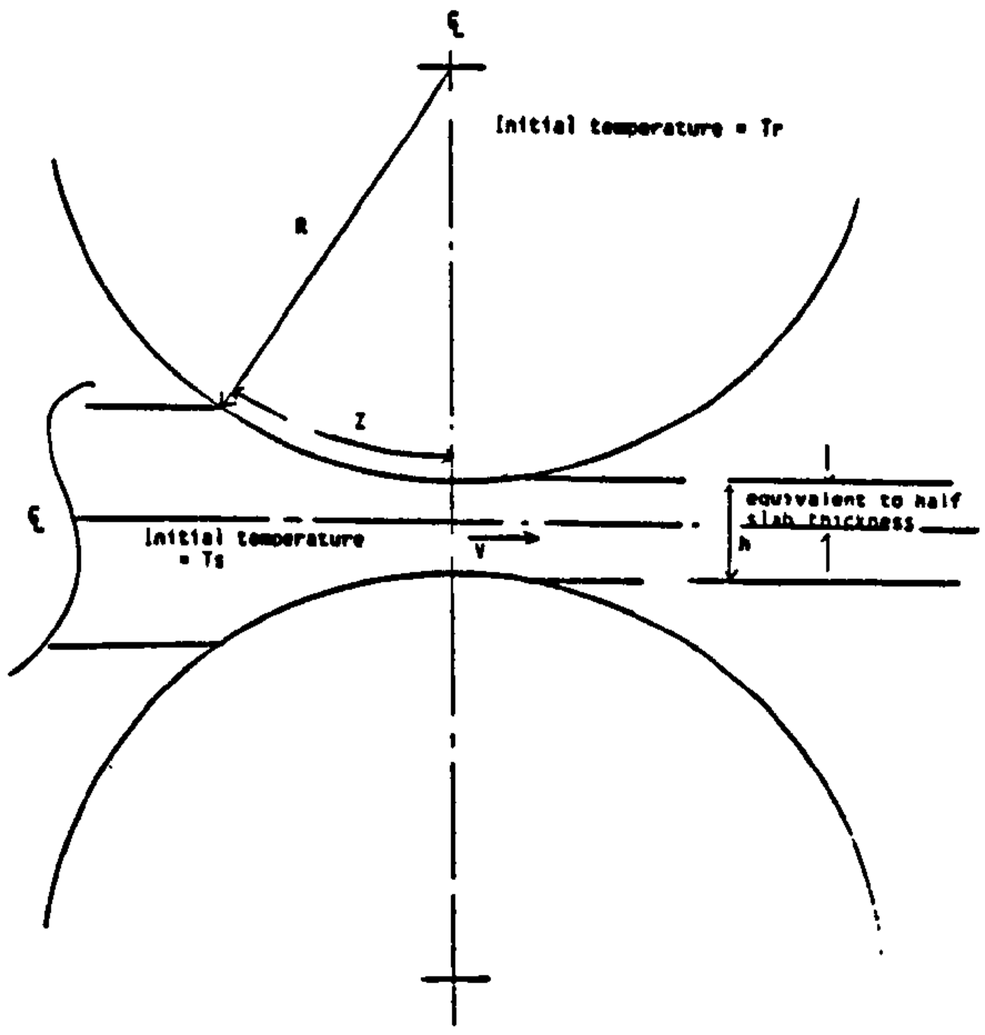

Fig. C2.2. Diagram showing division of strip and roll into elements.

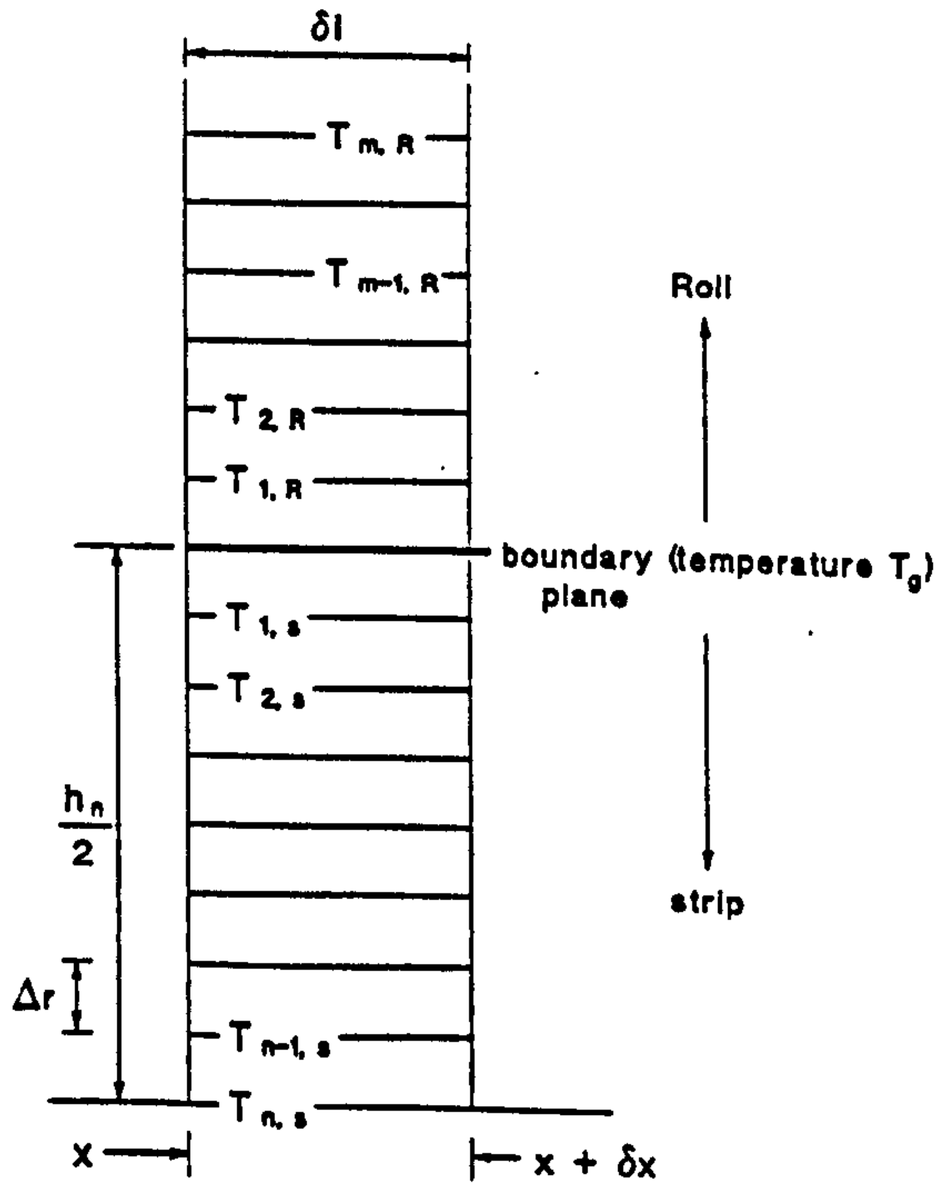

Consider now the heat transport characteristic of the situation depicted above.

Imagine a non-surface element of the strip as shown in fig. C2.3. Assume that the observer is moving with the element.

Fig. C2.3. An element within the strip.

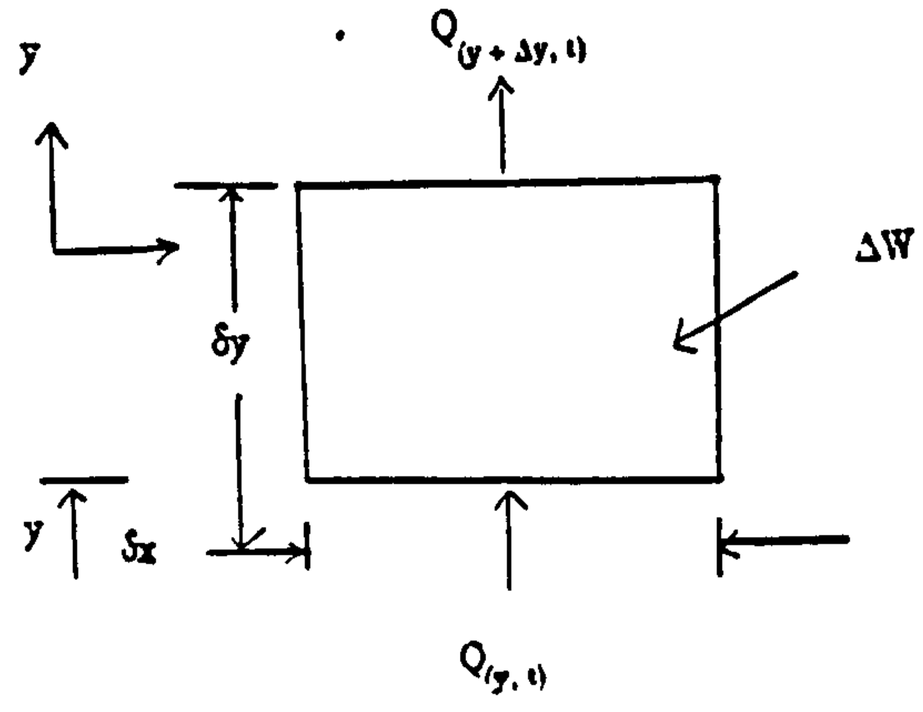

Let:

ΔA = area through which heat transfer occurs

$Q_{(x,t)}$ = heat flow rate into element at vertical position y and time t.

ΔW = elemental energy input.

F(t) = heat flow rate into element at time t.

An energy balance on the element gives,

$$Q_{(y,\,t)} - Q_{(y+\,\delta y,\,t)} + \Delta W = F(t) \qquad \text{(C2.1)}$$

and

$$Q_{(y,\,t)} = -k_s \Delta A \left.\frac{\partial T}{\partial y}\right|_{y,\,t} \qquad \text{(C2.2)}$$

Using a truncated Taylor series for the terms $Q_{(y\,+\,\delta y,\,t)}$, eqn. (C2.1) becomes:

$$Q_{(y,\,t)} - Q_{(y,\,t)} - \left.\frac{\partial Q}{\partial y}\right|_{y,\,t} .\delta y + \Delta W = F(t)$$

$$-\frac{\partial}{\partial y}\left(-k\,\Delta A\frac{\partial T}{\partial y}\right).\delta y + \Delta W = F(t) \qquad \text{(C2.3)}$$

Consider the term F(t). This is given by

$$F(t) = \frac{\partial}{\partial t}\left(\Delta A\,\delta y\,\rho\,C_{p_s} T\right) \qquad \text{(C2.4)}$$

where $T = T_s$ = temperature function for the strip

C_{ps} = specific heat capacity of strip

If we pause before we develop the term ΔW, and making the substitution of eqn. (C2.4) into eqn. (C2.3), we get:

$$k\,\Delta A\,\delta y\,\frac{\partial^2 T}{\partial y^2} + \Delta W = \Delta A\,\delta y\,\rho\,C_{p_s}\frac{\partial T}{\partial t}$$

$$\frac{k}{\rho C_{p_s}}\frac{\partial^2 T}{\partial y^2} + \frac{\Delta W}{\Delta A\,\rho\,C_{p_s}.\delta y} = \frac{\partial T}{\partial t} \qquad \text{(C2.5)}$$

Let $\alpha = \dfrac{k}{\rho\,C_{p_s}}$

so that eqn. (C2.5) gives

$$\frac{\partial T}{\partial t} = \alpha\frac{\partial^2 T}{\partial y^2} + \frac{\Delta W}{\Delta A\,\rho\,C_{p_s}\,\delta y} \qquad \text{(C2.6)}$$

Let us now consider the finite difference representation of the terms

$$\frac{\partial^2 T}{\partial x^2} \text{ and } \frac{\partial T}{\partial t}$$

The region of interest in the space domain is bounded, i.e., $0 \le y \le h$, and in the time domain extends from $t = 0$ to infinity. We can construct a finite difference net in the y-domain with constant mesh size Δy.

Then, the space and time domain coordinates x and t are denoted by

$$y = j\Delta y \ , \quad j = 1, 2, 3, \ldots N \text{ with } h = N\Delta x$$
$$t = k\Delta t \ , \quad k = 0, 1, 2, 3, \ldots \qquad \text{(C2.7)}$$

and the temperature $T_{(y,\ t)}$ is represented by:

$$T(y, t) = T(j\Delta y, k\Delta t) = T_j^k \qquad \text{(C2.8)}$$

Hence, using this notation and employing the finite difference formula

$$\left.\frac{\partial^2 T}{\partial y^2}\right|_{j,k} = \frac{T_{j-1}^k - 2T_j^k + T_{j+1}^k}{(\Delta y)^2} + O_{(\Delta y)^2} \qquad \text{(C2.9)}$$

The finite derivative with respect to the time variable, $\partial T/\partial t$, is represented in the finite difference formula[121,122] as

$$\left.\frac{\partial T}{\partial t}\right|_{j,k} = \frac{T_j^{k+1} - T_j^k}{\Delta t} + O_{(\Delta t)} \qquad \text{(C2.10)}$$

with a truncation error of $O(\Delta t) + O(\Delta y)^2$

On substitution into eqn. (C2.6) we get

$$T_j^{k+1} = fT_{j-1}^k + (1 - 2f)T_j^k + fT_{j+1}^k + \frac{\Delta W \Delta t}{\Delta A\, \rho\, C_{p_s}\, \delta y}, \quad \begin{matrix} j = 1, 2, 3, \ldots N-1 \\ n = 0, 1, 2, \ldots \end{matrix} \qquad \text{(C2.11)}$$

$$\text{where } f = \text{Fourier number} = \frac{\alpha \Delta t}{(\Delta y)^2} \qquad \text{(C2.12)}$$

The restriction on the parameter f in the finite difference method is is governed by

$$0 < f = \frac{\alpha \Delta t}{(\Delta y)^2} \leq \frac{1}{2} \qquad \text{(C2.13)}$$

Consult Chapter 3 and references 121 - 125 for further details on the derivation of error limits.

Consider now the heat flow at the strip - roll interface (fig. C2.4).

Fig. C2.4. An element at the strip-roll interface

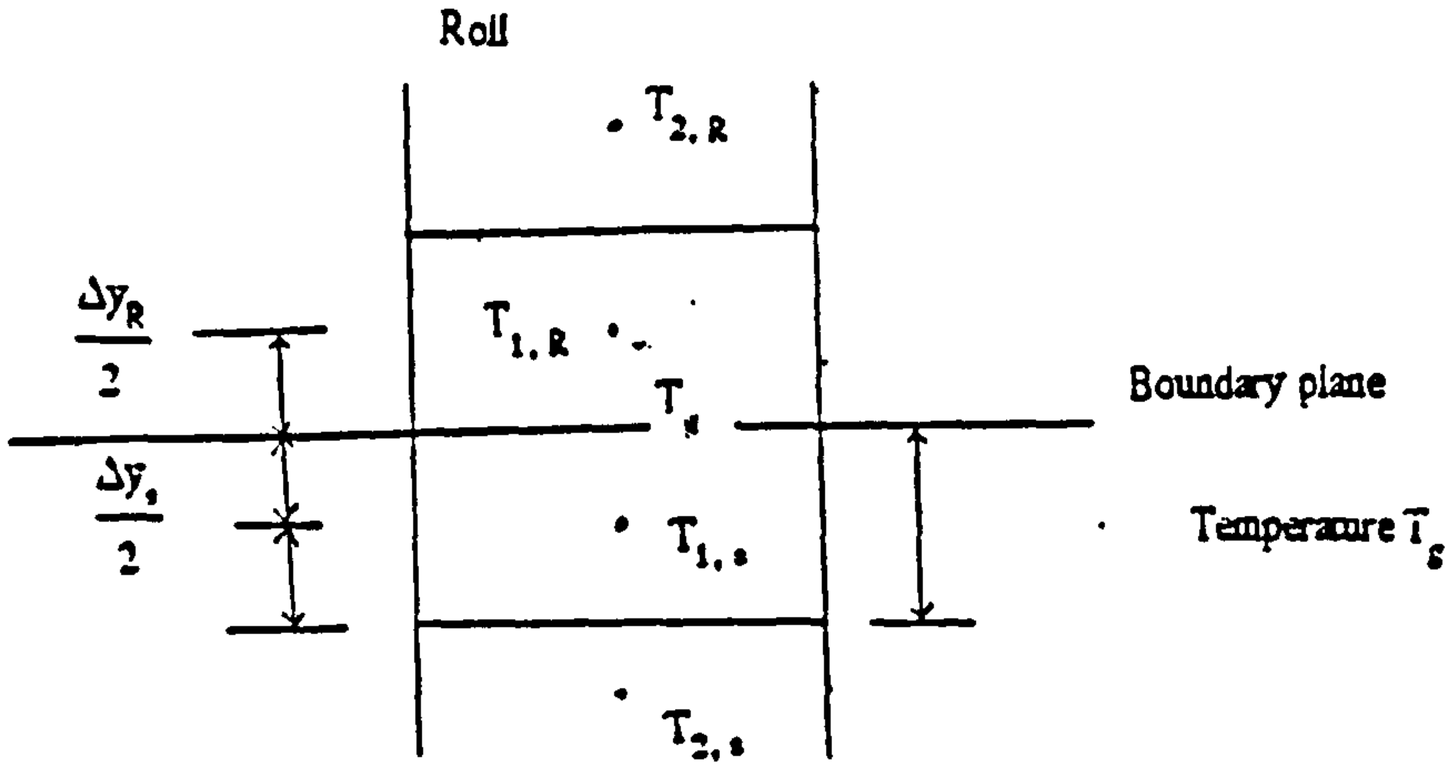

The heat flow equations at the boundary are:

$$q_R = -\Delta A.\, k_R \frac{\partial T_R}{\partial y_R}.\, \delta t \qquad \text{(C2.14)}$$

$$q_s = -\Delta A\,.\, k_s \frac{\partial T_s}{\partial y_s}.\, \delta t \qquad \text{(C2.15)}$$

$$\frac{\partial T_R}{\partial y_R} = \frac{T_{1,R} - T_s}{\Delta y_R/2} = \frac{2(T_{1,R} - T_s)}{\Delta y_R} \qquad \text{(C2.16)}$$

$$\frac{\partial T_s}{\partial y_s} = \frac{2(T_{1,s} - T_{1,s})}{\Delta y_s} \qquad \text{(C2.17)}$$

Since the heat flow out of the strip is equal to that entering the roll, then eqn. (C2.16) and eqn. (C2.17) reveal, when the relevant substitutions are made using eqns. (C2.18) and eqn. (C2.19), that

$$\Delta A\, k_R \frac{2(T_{1,R} - T_s)}{\Delta y_R}.\, \delta t = \Delta A\, k_s \frac{2(T_{1,s} - T_s)}{\Delta y_s}.\, \delta t$$

Hence,

$$T_g = \left[\frac{T_{1,R} + \frac{\Delta y_R}{\Delta y_s} \cdot \frac{k_s}{k_R} \cdot T_{1,s}}{1 + \frac{\Delta y_R}{\Delta y_s} \cdot \frac{k_s}{k_R}} \right] \qquad \text{(C2.18)}$$

Consider the first strip element. Since we have omitted, for the moment, from the present analysis, the effect of work roll power input into the strip, for simplicity we only consider (from eqn. (C2.8) the term

$$\frac{\partial T_s}{\partial t} = \alpha_s \frac{\partial^2 T_s}{\partial y^2} \qquad \text{(C2.19)}$$

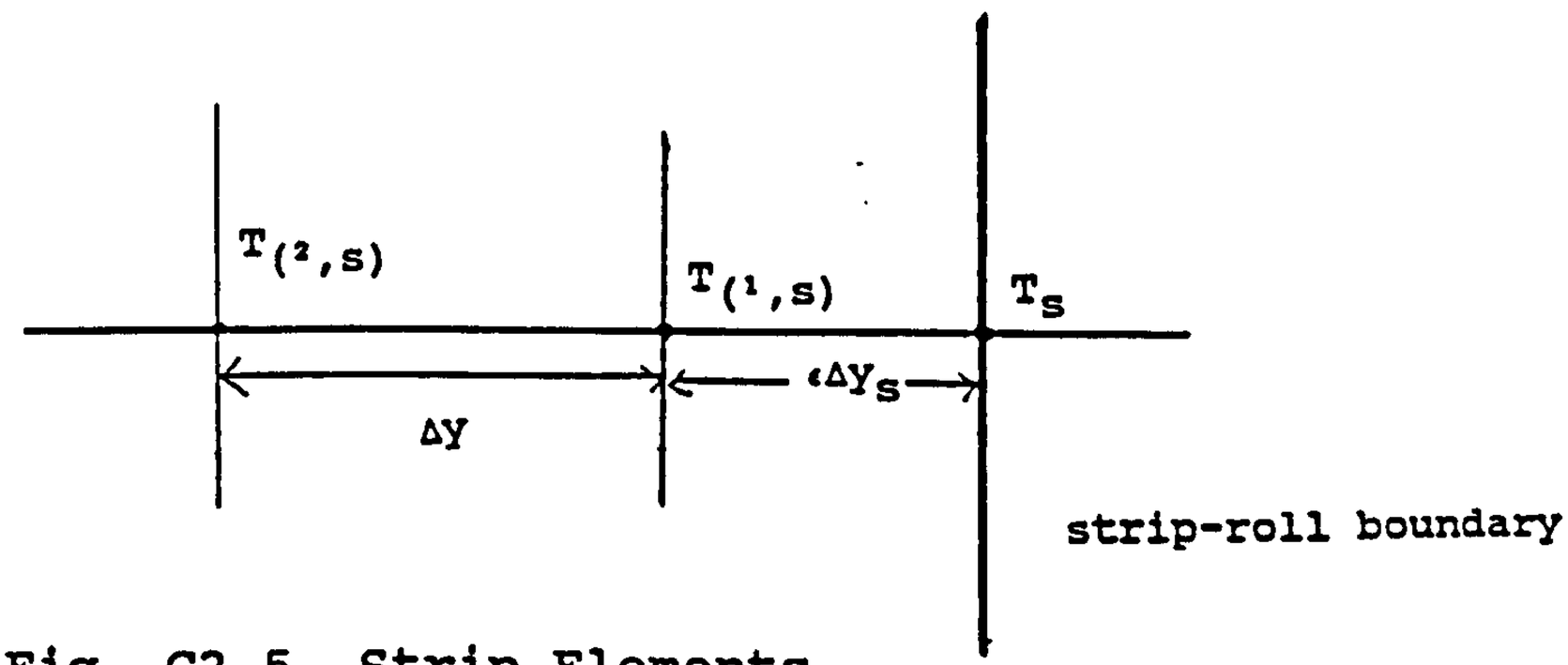

Fig. C2.5. Strip Elements

Consider fig. C2.5 above. The distance ($\epsilon \Delta y_s$) between the nodes (1,s) and g, where $\epsilon \leq 1$ is less than the mesh size Δy_s. By a Taylor series expansion in powers of ($\epsilon \Delta y_s$) and Δy_s), respectively, we get

$$T_g = T_{1,s} + (\epsilon \Delta y_s) \cdot \left.\frac{\partial T_s}{\partial y}\right|_{1,s} + \frac{(\epsilon \Delta y_s)^2}{2!} \cdot \left.\frac{\partial^2 T_s}{\partial y^2}\right|_{1,s} + O(\Delta y_s)^3 \ldots \qquad \text{(C2.20)}$$

$$T_{2,s} = T_{1,s} - \Delta y_s \cdot \left.\frac{\partial T_s}{\partial y}\right|_{1,s} + \frac{(\Delta y_s)^2}{2!} \cdot \left.\frac{\partial^2 T_s}{\partial y^2}\right|_{1,s} + O(\Delta y_s)^3 \qquad \text{(C2.21)}$$

Elimination of $\left.\frac{\partial T}{\partial y}\right|_{1,s}$ between eqn. (C2.20) and eqn. (C2.21) reveal that

$$\left.\frac{\partial^2 T}{\partial y^2}\right|_{1,s} = \frac{2}{\Delta y_s^2} \left\{ \frac{T_g}{\epsilon(1+\epsilon)} + \frac{T_{2,s}}{1+\epsilon} - \frac{T_{1,s}}{\epsilon} \right\} \qquad \text{(C2.22)}$$

For $\epsilon = 1/2$, eqn. (C2.22) becomes

$$\left.\frac{\partial^2 T}{\partial y^2}\right|_{1,s} = \frac{2}{\Delta y_s^2} \left\{ \frac{4 T_g}{3} + \frac{2 T_{2,s}}{3} - 2 T_{1,s} \right\}$$

$$= \frac{4}{3\,(\Delta y_s)^2}\left\{ 2T_s + T_{2,s} - 3T_{1,s} \right\} \qquad \text{(C2.23)}$$

Hence, eqn. (C2.19)

$$\frac{\partial T_s}{\partial t} = \frac{4\alpha_s}{3\,(\Delta y_s)^2}\left\{ 2T_s + T_{2,s} - 3T_{1,s} \right\} \qquad \text{(C2.24)}$$

A similar treatment would represent the roll temperature behaviour at the surface.

The assumption of a constant number of strip elements (n) implies that h_n decreases as the strip passes through the roll-gap, hence reducing (Δy_s) as well to satisfy the error criterion of eqn. (C2.13).

The average strip temperature is taken to be

$$T_{av,s} = \frac{\sum_{1}^{n} T_{n,s}}{n} \qquad \text{(C2.25)}$$

C3. ROLL BITE LENGTH ESTIMATION

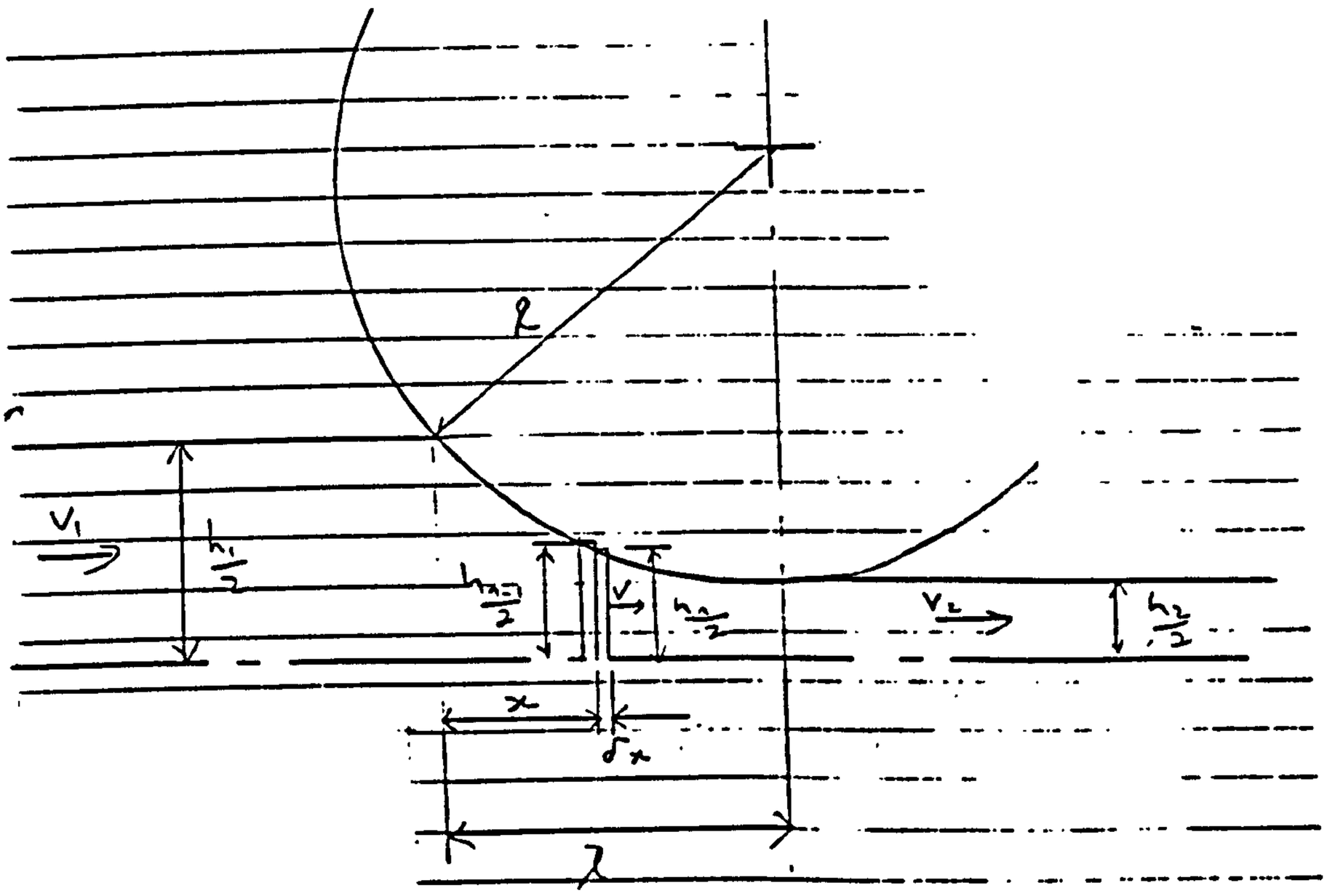

Fig. C3.1. Elements in the roll-strip contact region

If the reduction is small compared to the undeformed roll radius the length of arc of contact is approximately equal to the roll bite length, l, (fig. C3.1). Hence,

$$l = R \sin\left[\cos^{-1}\left\{1 - \left(\frac{h_1 - h_2}{2R}\right)\right\}\right] \qquad (C3.1)$$

$\simeq$ length of arc of contact.

From the assumption of the conservation of mass,

$$v = \frac{v_1 h_1}{h_n} \qquad (C3.2)$$

and

$$h_n = h_2 + 2R\left[1 - \cos\left\{\sin^{-1}\left(\frac{l - x}{R}\right)\right\}\right] \qquad (C3.3)$$

C4. ESTIMATION OF THE ENERGY INPUT DUE TO ROLLING WORK INTO THE ELEMENT AT POINT x

It is assumed that all the energy required to deform the strip is converted into heat. Then,

work energy input α elemental reduction.

The reduction in elemental height from strip element n-1 to n (fig. C2.2) is $h_{n-1} - h_n$.

The ratio of elemental decrement to total strip reduction is

$$\frac{h_{n-1} - h_n}{h_1 - h_2}$$

Hence, if the total rolling power is W, then, elemental power,

$$\Delta W = W\left(\frac{h_{n-1} - h_n}{h_1 - h_2}\right) \qquad (C4.1)$$

Therefore, an energy balance on the element n, results in

$$\rho_s \delta l\, w\, h_n . C_{p_s} \Delta T_w = W \left(\frac{h_{n-1} - h_n}{h_1 - h_2} \right) \delta t \qquad \text{(C4.2)}$$

where

ρ_s = strip density

w = strip width

C_{ps} = volumetric specific heat capacity of the strip

ΔTw = temperature rise of element due to rolling work

δt = elemental time increment

$$\delta l = v\, \delta t = \frac{v_1 h_1}{h_n} . \delta t \qquad \text{(C4.3)}$$

Hence, if eqn. (C4.3) is substituted in eqn. (C4.2), we get

$$\Delta T_w = \frac{W}{w \rho_s C_{p_s} v_1 h_1} \left(\frac{h_{n-1} - h_n}{h_1 - h_2} \right) \qquad \text{(C4.4)}$$

$$\text{Let } a_s = \frac{A_s}{\rho_s C_{p_s}}$$

where

a_s = thermal diffusivity of the strip

A_s = thermal conductivity of strip

so that on substitution into eqn. (C4.4), we get

$$\Delta T_w = \frac{W}{w} . \frac{a_s}{A_s v_1 h_1} \left(\frac{h_{n-1} - h_n}{h_1 - h_2} \right) \qquad \text{(C4.5)}$$

APPENDIX D

DETAILS OF COMPUTER ALGORITHMS

D1.1 INTRODUCTION

Several methods of evaluating thermal cambers have been examined in this work. Thermal cambers are required as input to the strip profile model described below. This appendix details the computer program for the "large" model, based on the theories of Chapter 3, and appendices A, B and C. The method suggested by Oshima et al.[67] has been used to examine a "fast" model. In addition, computation can be speeded-up considerably by the method suggested by the author in Chapter 7.

The validity of the models have been demonstrated by comparing the results of measurements taken at two hot rolling mills with the results of the calculations.

D1.2 THE PROFILE MODEL

The prediction of strip profile, (or strip transverse gauge distribution) is solved in the strip profile model. The final strip profile is essentially due to the shape of the input strip, the deflection and deformation of the rolls, in particular, that caused by uneven thermal crowns across

the rolls. A computer program which evaluated strip profile, located at Davy McKee (Poole) Ltd.[129] has been modified and upgraded by the author to assist in the task of predicting strip profile. The model predicts the roll deflections by taking into account the incoming strip profile and other physical and mechanical properties, roll stack geometry, rolling loads, bending forces, ground crowns or inflated crowns and thermal crowns. The effects of roll bending and shear. Poisson strain and flattening between strip and work roll are also included. Work roll and back-up roll interface are treated as a beam on elastic foundation. The resultant roll gap crown is then imposed on the strip. The rolling pressure is then recalculated across the strip using strip flow stress and redistributed tensions, iterating until the roll and strip displacements are equal at each element position.

D1.3 THE MODELLING NETWORK

A complete simulation and control system involves complex interactions between recorded data on favourable operating mill settings, mathematical modelling of the rolling process, and corrective action in a control sequence. Fig. D1.3.1 depicts one possible control process. The block marked "recorded data" represents a data base of normal operating modes, flow stress data from previous experiments and calculation, and desired strip profile. The modelling section could include scheduling, roll camber and roll bend models. The models could initially be calibrated using previously recorded data. The control block in fig. D1.3.1 shows that strip profile can be influenced and controlled with corrective actions from the mechanical, thermal or metallurgical (i.e, changes in slab dimensions and alloy types) actuators.

Fig. D1.3.1

COMPUTER MODULES

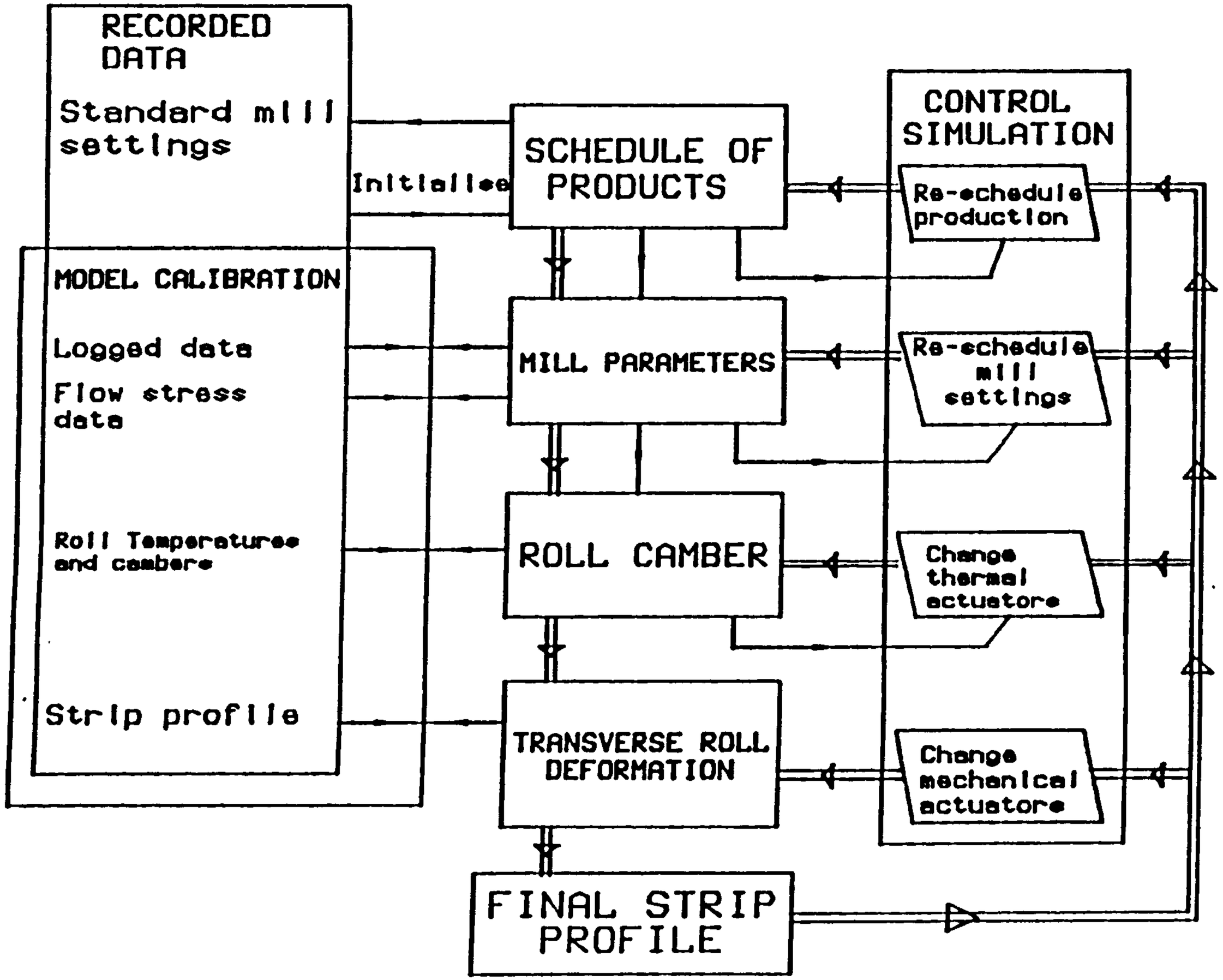

D1.4 "LARGE" THERMAL CAMBER MODEL, "SPRAY"

The "large" thermal camber model evaluates the heat balance in the roll gap between sensible heat in the strip and the energy generated by rolling, and the roll temperature and expansion at the time of re-entry to the roll bite. The influence of coolant sprays, ambient cooling and other heat losses during rotation of the roll are taken into account. Suitable heat transfer coefficients are estimated or calculated for spray cooling, ambient cooling and heat transferred to the roll bearings, and roll ends. These heat transfer coefficients do not explicitly include heat transfer by radiation and heat conduction to the back-up rolls but are "lumped" in with that of the coolant. Heat transfer coefficients are also estimated for heat losses due to coolant flowing through a hole drilled centrally along the major axis of the roll.

D2.1 PROGRAM MAIN (Fig. D1)

The main program segment of the computer program "SPRAY" controls the calculation sequence when the roll thermal displacement is evaluated. The structure of this program module is illustrated by fig. D1. The figure shows that error flags are set and external file units are open immediately on execution of the program. Next, data on the geometry of the roll, nozzle pitch, external temperatures, an output control flag, and the physical properties of the roll and strip are read on the first call to the subroutine INPUT. On return from this call, program MAIN then activates the sub-program EMENT where the division of the roll into the necessary axial and radial elements is performed. Reference to the subroutine NDPROG converts the ambient, bearing and roll end heat transfer coefficients to the non-dimensional forms. If no error has occurred in the data input and calculation sequence up to this stage, all data read in so far will be printed to the screen by calls to the relevant output subroutines. The variable T

containing the roll temperature array is next initialized by a call to the subroutine INITZ, followed by a call to GRAPH which sets up an external file to allow a graphical display of the thermal expansion of the roll at a desired stage in the rolling sequence. Since the "influence" coefficients of eqn. B34 need only be evaluated once, the subroutine NIF is next activated and the coefficients are stored in an array for later use.

The simulation of the rolling schedule can now begin in earnest by starting a counter equating to the number of slabs rolled. Data for each pass, corresponding to the strip input and output thicknesses, power input to the mill, strip entry, strip entry temperature, rolling times and the time interval between passes is now read in by another call to INPUT. If rolling temperatures are required after a given time following the end of rolling, this time is also read in. The spray settings and conditions (i.e whether the sprays are left on and off between passes) are also noted here. The data read in is shown to the user when a call to the subroutine OUT3 is made.

Next, the heat input to the roll is evaluated by a call to the subroutine LCHR.

The number of iterations that will be performed in the temperature calculation routine, TEMCAL, at each stage of the rolling sequence is determined by subroutine TIMIT.

A call to the subroutine READ will determine the state of the sprays, followed by the activation of the subroutine RADMOD to set the heat transfer coefficient values for sections of the roll not undergoing spray cooling. For areas of the roll covered by sprays, a call to subroutine SPRAY_SETTINGS determines the heat transfer coefficient values based on the spray settings.

The temperature iteration routine based on the equations of Chapter 3 can now be activated for each pass. The roll thermal displacement is now calculated by a call to the subroutine THMCAM.

This simulated sequence is repeated until the rolling schedule is completed

D2.2 SUBROUTINE INPUT (Fig. D2)

This subroutine allows input of data needed to carry out the simulation sequence. Subroutine INPUT is activated from the master module, PROGRAM MAIN. On being referenced for the first time, data for the roll geometry (roll radius, roll neck radius, barrel length, total roll length, nozzle pitch, etc.), external temperatures, roll initial temperature, ambient, bearing area and roll end area heat transfer coefficients are read in. A flag to control the output of calculated data is also read at this stage, as well as the roll and strip physical properties, before a return is made to the calling program.

The next call to INPUT results in the reading of data for the rolling schedule (strip input and output thicknesses) power to roll, strip ingoing speed, rolling and rest times between passes) for each pass.

The spray settings are read and if the coolant is switched on between passes or before the end of each pass, a flag should be set. Control is then returned to the calling program.

D2.3 SUBROUTINE EMENT (FIG.D3)

This subroutine whose flow diagram is shown by fig. D3, divides the roll into radial and axial nodes in each

section of the roll, given the roll geometry and nozzle pitch. The number of radial nodes is set by the user. If the number of radial nodes exceeds the array size for the roll temperature array an error condition is generated. The user is then requested to modify the number of nodes to within the acceptable limit. This subroutine is initiated by PROGRAM MAIN, the master module.

D2.4 SUBROUTINE NDPROG (FIG. D4)

The flow diagram for subroutine NDPROG is given by fig. D4. NDPROG is responsible for converting heat transfer coefficients to the non-dimensional forms. Control is returned to the coolant PROGRAM MAIN.

D2.5 SUBROUTINE NIF (FIG. D5)

This subroutine (fig. D5) computes the normalised influence coefficients of eqn. B3. These coefficients are used to predict the thermal displacements of eqn. B2. The integration of eqn. B3 is performed using the trapezoidal rule. On completion, control is returned to PROGRAM MAIN.

D2.6 SUBROUTINE INITZ (FIG. D6)

This subroutine is responsible for initialising the roll temperature array.

D2.7 SUBROUTINE SPRAY_SETTINGS (Fig. D7)

This subroutine accepts a given spray setting in the form of a character variable and converts it to integer values corresponding to each spray level. The spray levels can be modified if too high or too low for the spray system being considered. The program then calls the subroutines LES_EFF to return heat transfer coefficients based on the spray

levels. The conversion of levels to values of heat transfer coefficient can be obtained from a data base or from an equation converting a given spray configuration to heat transfer coefficient.

D2.8 SUBROUTINE LCHR (FIG. D8)

The rate of heat input into the roll for each pass is calculated in this subroutine. The rate of heat flow is calculated by considering the difference between the strip entry temperature and roll background temperature. The rate of heat flow into the roll is determined from an initial temperature difference between the strip and roll. A new heat flow at a temperature 50^{o}C above this initial temperature is found by interpolation from a linear curve between these two values.

D2.9 SUBROUTINE TIMIT (FIG. D9)

The number of iterations that will be performed in subroutine TEMCAL is computed in subroutine TIMIT. The time interval for each iteration is usually determined from the minimum rolling or rest time between slabs, although this can be modified.

D2.10 SUBROUTINE READ (FIG. D10)

This subroutine reads data, to identify in which pass sprays are switched off before the end of the pass, in the form of a character variable, SWITCH. The pass numbers must be read on a single line of input in a format of nA3 (no commas are allowed). This data is checked for errors, and if detected will print an error message before stopping.

D2.11 SUBROUTINE TEMCAL (FIG. D11)

The integration of eqn. (3.2.14) is carried out in this subroutine using the finite difference formulae developed in Chapter 3. Relevant boundary conditions are set before the temperature in the next time step is evaluated at each node throughout the roll. The heat transfer coefficients are set at appropriate points at the surface to that of the prevailing environmental conditions, such as for areas of coolant flow. The iteration is repeated for the number of time steps determined in subroutine TIMIT.

D2.12 SUBROUTINE THMCAM (FIG. D12)

This subroutine calculates thermal cambers based on eqn. B32. The smoothing function of eqn. B34 is applied to eqn. B32 to form eqn. B33. Thermal cambers are evaluated only at intervals determined by an input flag.

D2.13 SUBROUTINE BITE (FIG. D13)

This sub-program calculates the heat exchange by conduction between the roll and strip using the equations of appendix C. A simple finite difference technique is employed to solve these equations. From the difference between inlet and outlet temperatures and the power to roll for the pass, the net heat transfer into the roll is computed. intervals determined by an input flag.

FIG. D 1 FLOW DIAGRAM OF MAIN PROGRAM OF ROLL THERMAL CAMBER PREDICTION MODEL

PROGRAM MAIN

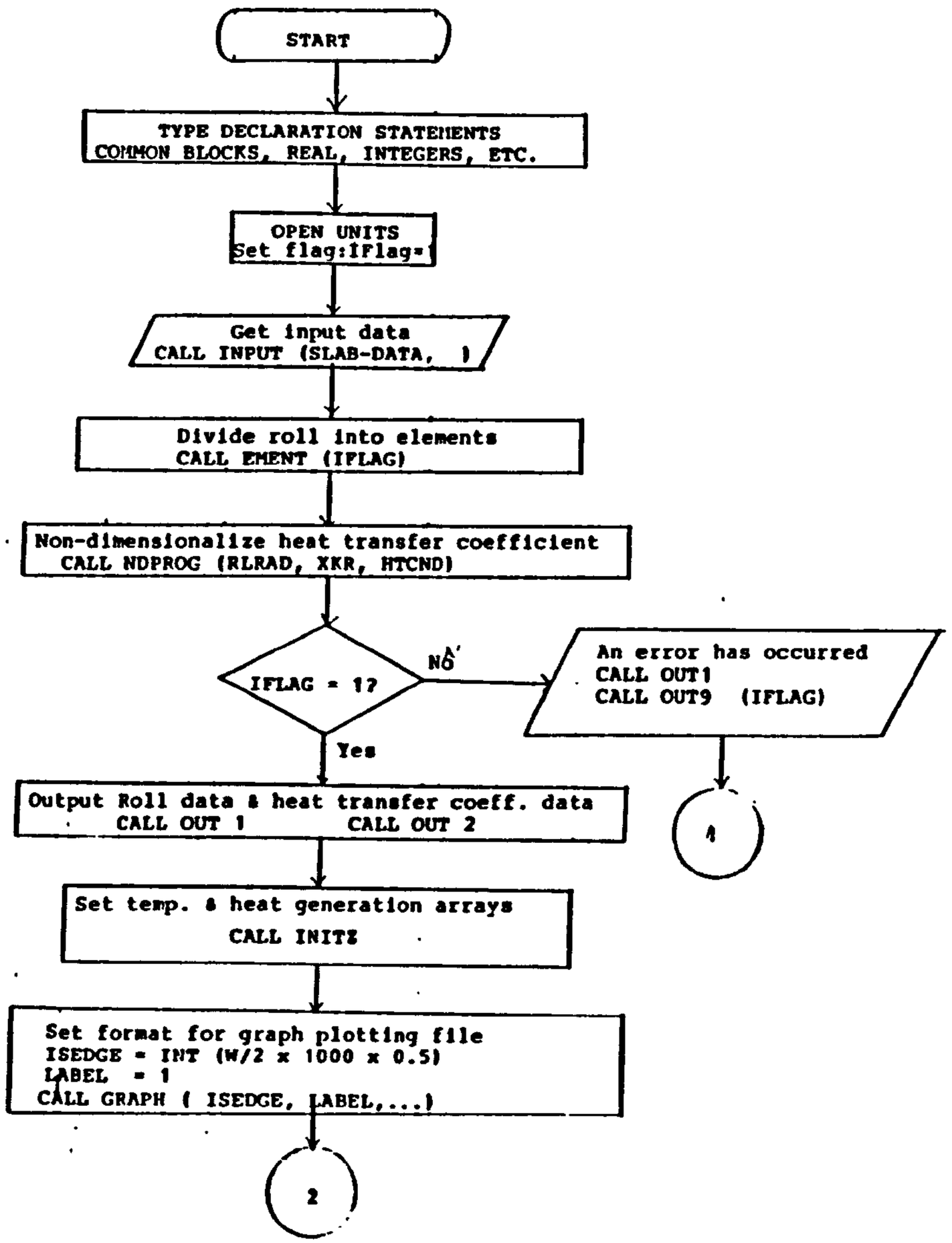

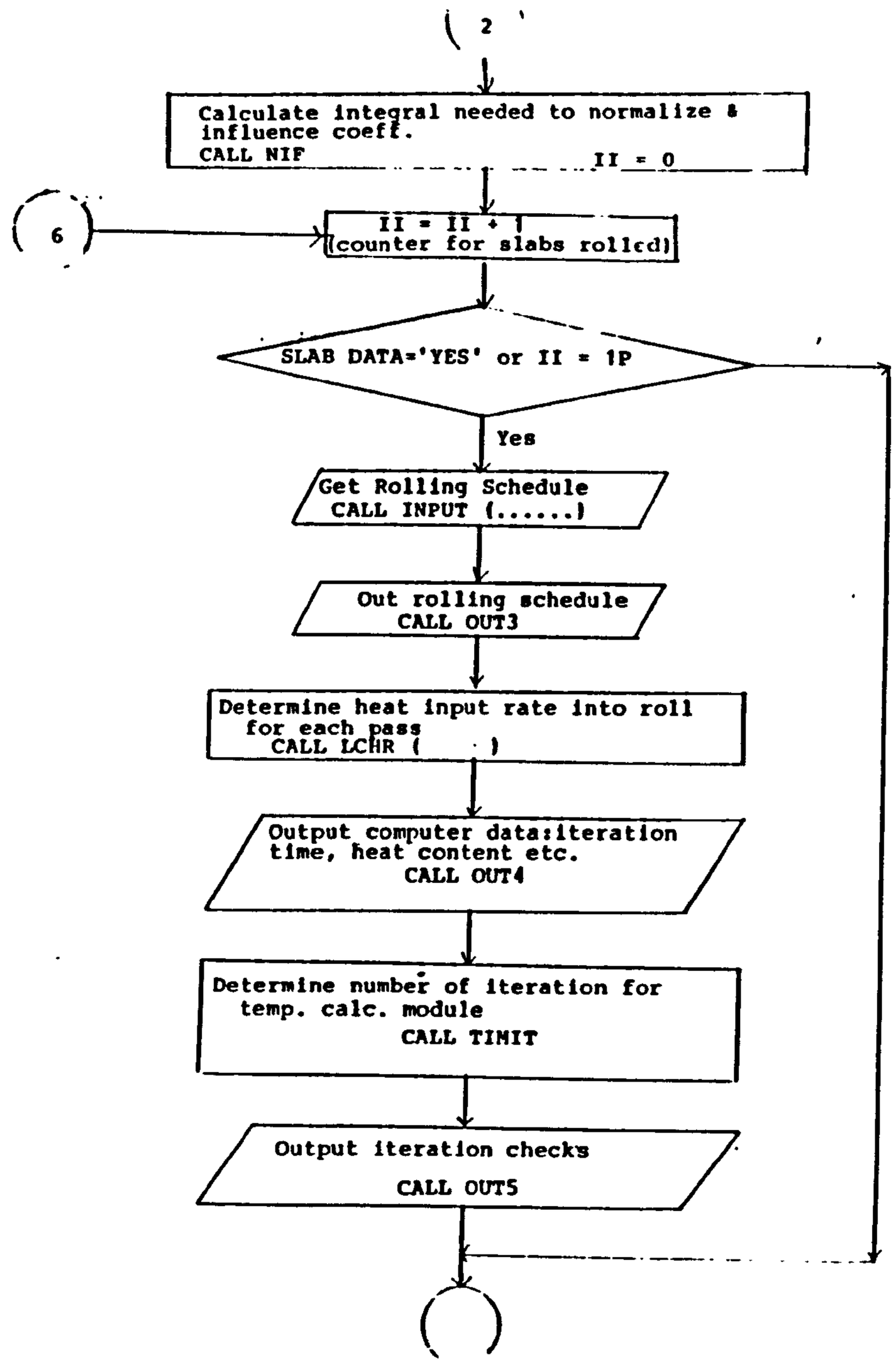
2
Calculate integral needed to normalize & influence coeff.
CALL NIF
II = 0
6
II = II + 1
(counter for slabs rolled)
SLAB DATA='YES' or II = 1P
Yes
Get Rolling Schedule
CALL INPUT (.....)
Out rolling schedule
CALL OUT3
Determine heat input rate into roll for each pass
CALL LCHR ( )
Output computer data:iteration time, heat content etc.
CALL OUT4
Determine number of iteration for temp. calc. module
CALL TIMIT
Output iteration checks
CALL OUT5

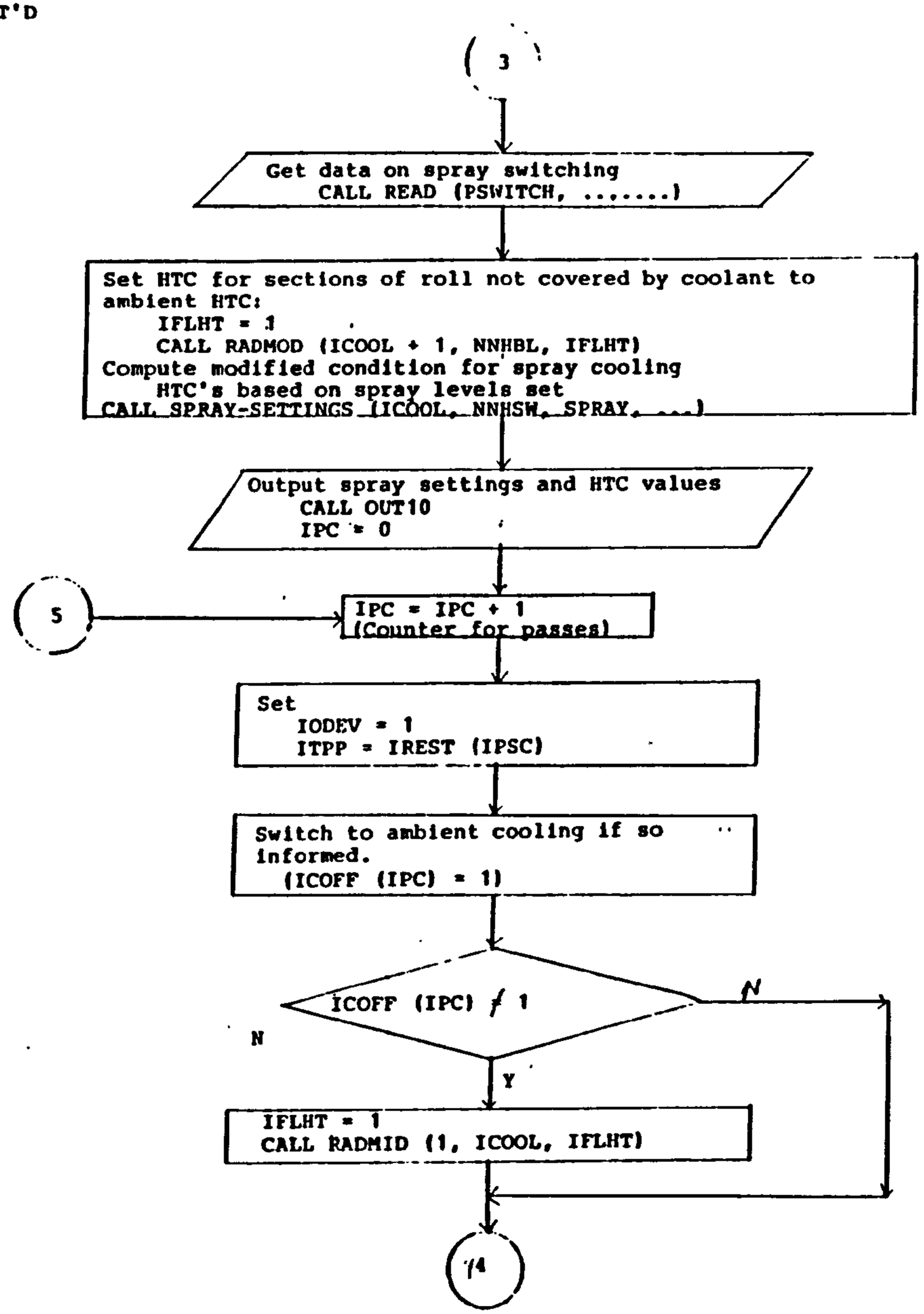
3
Get data on spray switching
CALL READ (PSWITCH, ...)
Set HTC for sections of roll not covered by coolant to ambient HTC:
IFLHT = 1
CALL RADMOD (ICOOL + 1, NNHBL, IFLHT)
Compute modified condition for spray cooling
HTC's based on spray levels set
CALL SPRAY-SETTINGS (ICOOL, NNHSW, SPRAY, ...)
Output spray settings and HTC values
CALL OUT10
IPC = 0
5
IPC = IPC + 1
(Counter for passes)
Set
IODEV = 1
ITPP = IREST (IPSC)
Switch to ambient cooling if so informed.
(ICOFF (IPC) = 1)
ICOFF (IPC) ≠ 1
N
Y
N
IFLHT = 1
CALL RADMID (1, ICOOL, IFLHT)
14

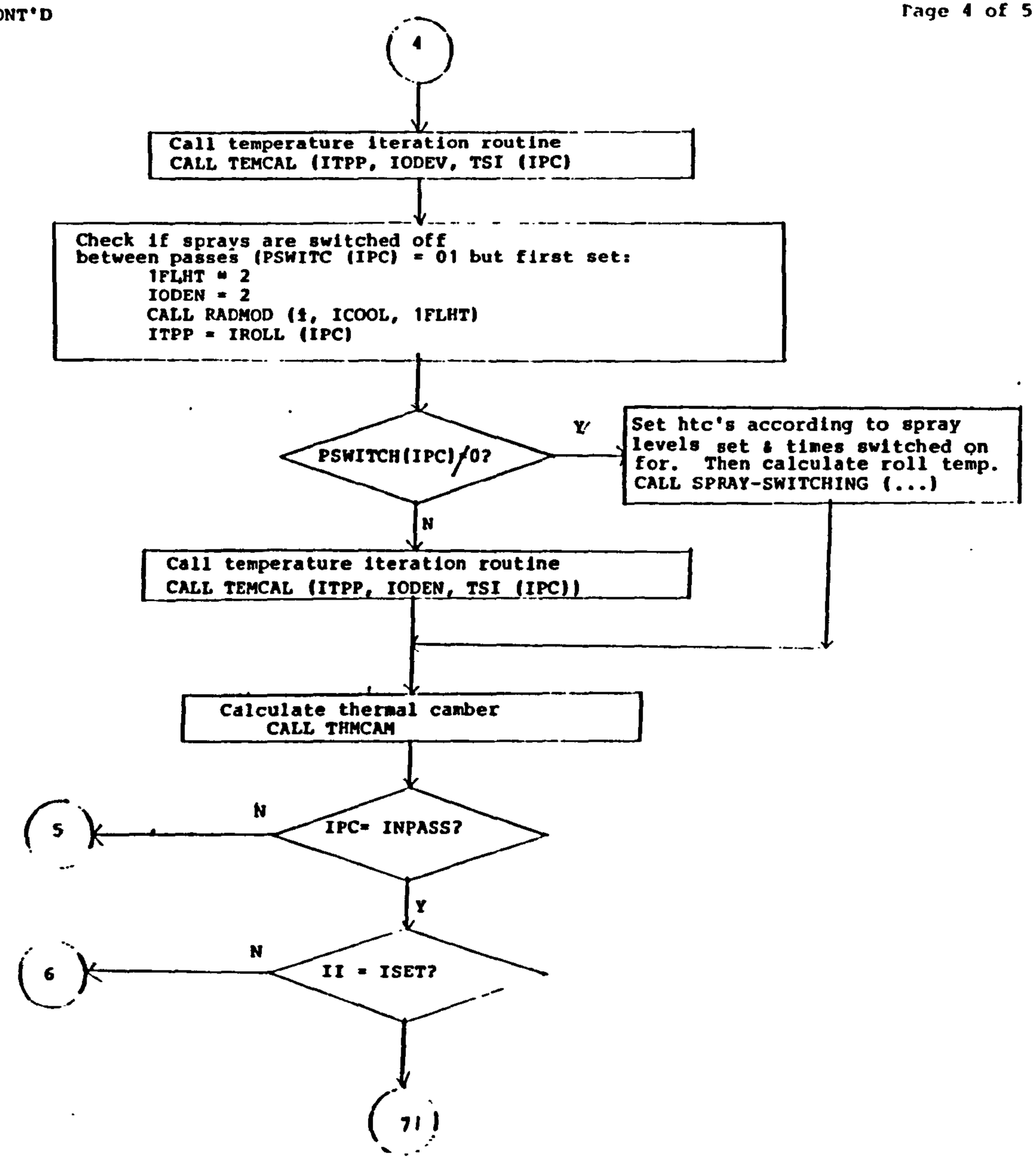
4
Call temperature iteration routine
CALL TEMCAL (ITPP, IODEV, TSI (IPC)
Check if sprays are switched off
between passes (PSWITC (IPC) = 01 but first set:
1FLHT = 2
IODEN = 2
CALL RADMOD (1, ICOOL, 1FLHT)
ITPP = IROLL (IPC)
PSWITCH(IPC)/0?
Y
Set htc's according to spray levels set & times switched on for. Then calculate roll temp.
CALL SPRAY-SWITCHING (...)
N
Call temperature iteration routine
CALL TEMCAL (ITPP, IODEN, TSI (IPC))
Calculate thermal camber
CALL THMCAM
IPC= INPASS?
N
5
Y
II = ISET?
N
6
71

FIG. D 1 CONT'D

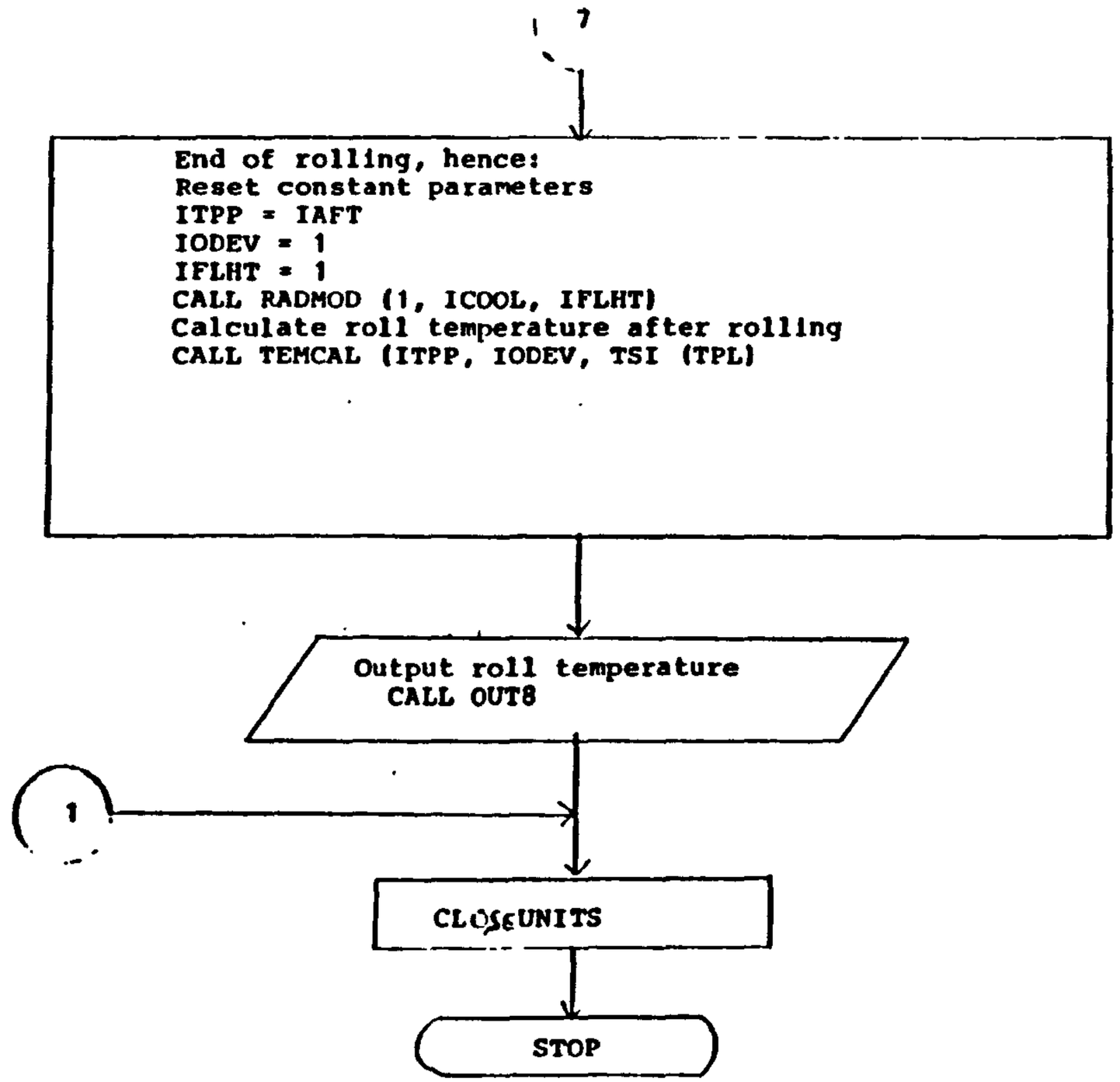
7
End of rolling, hence:
Reset constant parameters
ITPP = IAFT
IODEV = 1
IFLHT = 1
CALL RADMOD (1, ICOOL, IFLHT)
Calculate roll temperature after rolling
CALL TEMCAL (ITPP, IODEV, TSI (TPL)
Output roll temperature
CALL OUT8
1
CLOSEUNITS
STOP

FIG. D 2 FLOW DIAGRAM OF SUBROUTINE INPUT

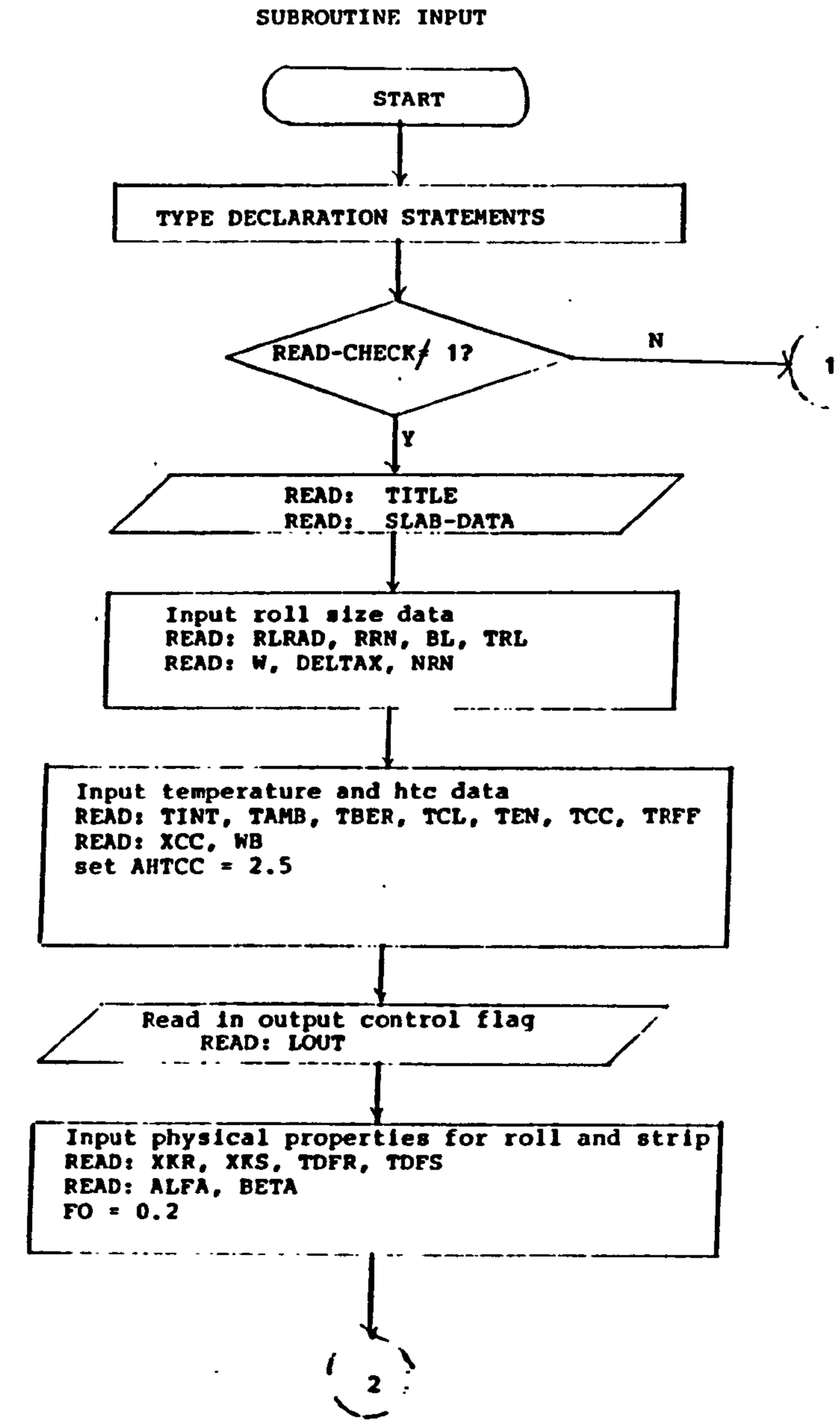

FIG. D2 cont'd

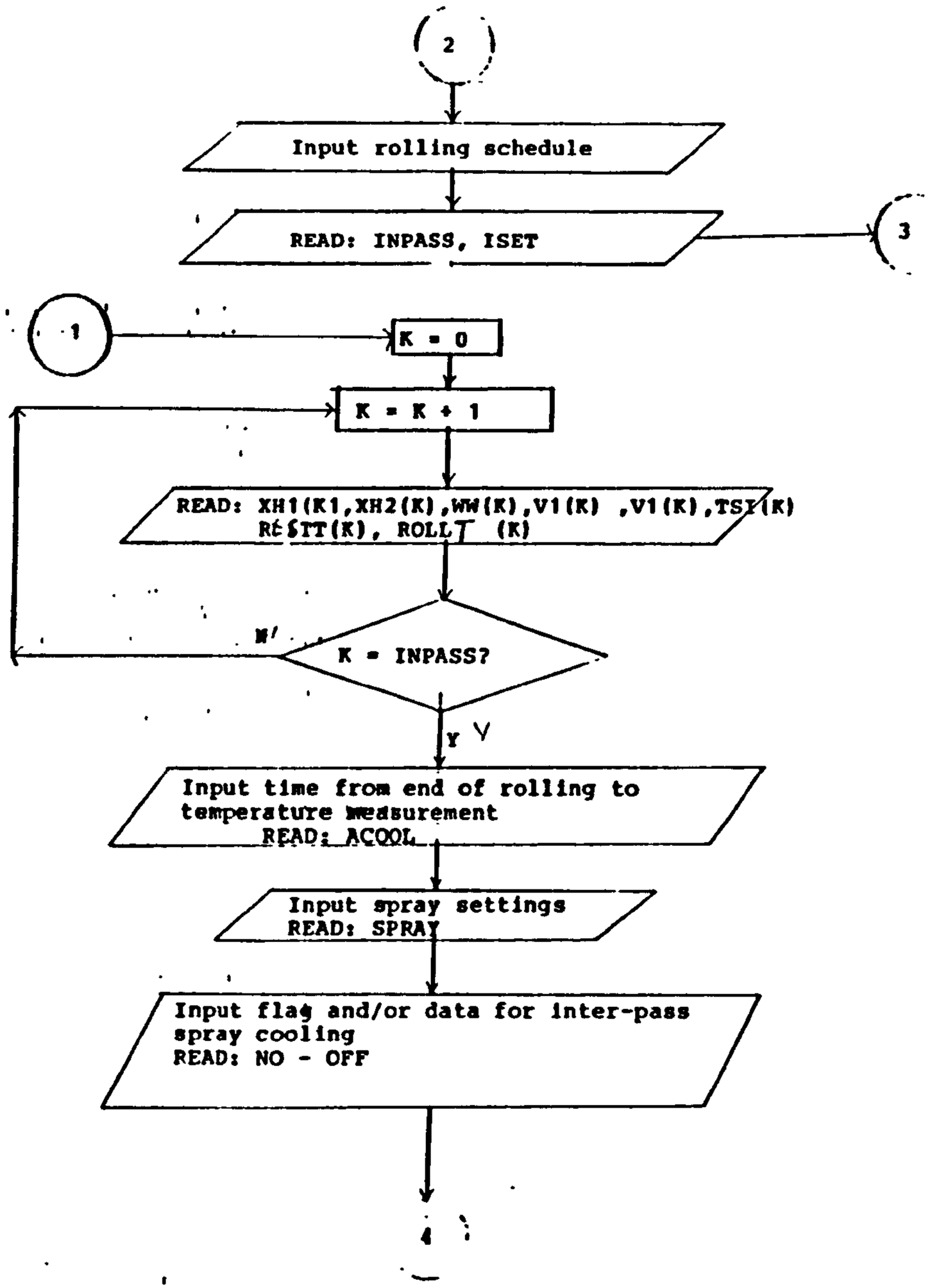
2
Input rolling schedule
READ: INPASS, ISET
3
1
K = 0
K = K + 1
READ: XH1(K1,XH2(K),WW(K),V1(K) ,V1(K),TSI(K)
RESTT(K), ROLLT (K)
N
K = INPASS?
Y
Input time from end of rolling to temperature measurement
READ: ACOOL
Input spray settings
READ: SPRAY
Input flag and/or data for inter-pass spray cooling
READ: NO - OFF
4

FIG. D2 cont'd

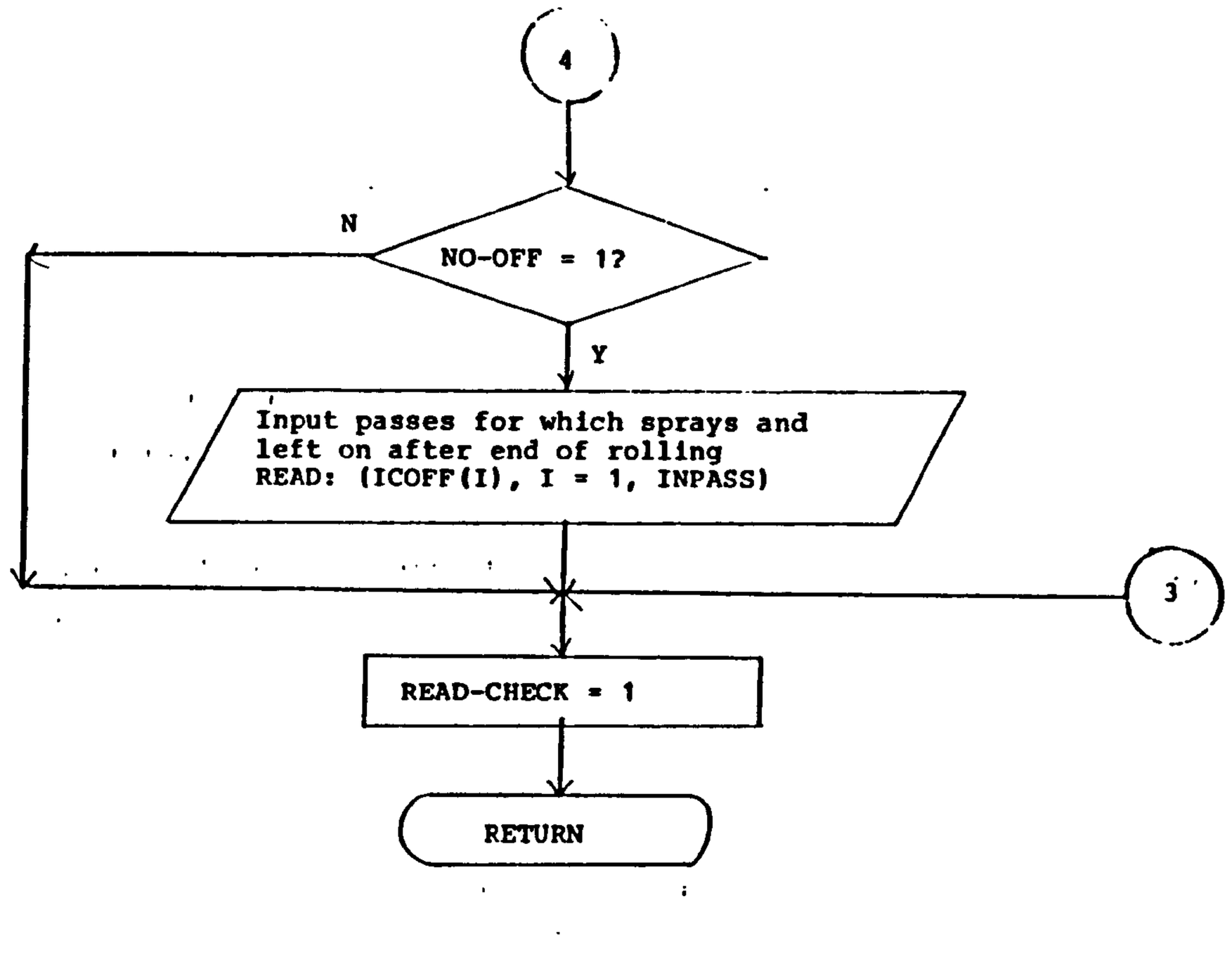
4
N
NO-OFF = 1?
Y
Input passes for which sprays and
left on after end of rolling
READ: (ICOFF(I), I = 1, INPASS)
3
READ-CHECK = 1
RETURN

Fig. D2 cont'd

```
      SUBROUTINE INPUT(TITLE,SLAB_DATA,TREF,SPRAY)

C READS DATA NEEDED TO COMPUTE TEMPERATURE DISTRIBUTION AND
C THERMAL CAMBER FOR A ROLL SUBJECT TO A FIXED ROLLING SCHEDULE

C VARIABLES
C ---------
C AAHT      AMBIENT HEAT TRANSFER COEFF       kW/(m**2.C)
C ABHT      BEARING HEAT TRANSFER COEFF       kW/(m**2.C)
C ACHT      COOLANT HEAT TRANSFER COEFF       kW/(m**2.C)
C ACOOL     TIME AFTER ROLLING                S
C AEHT      ENDPLATE HEAT TRANSFER COEFF      kW/(m**2.C)
C AHTCC     CENTRE PIPE COOLANT HTC           kW/(m**2.C)
C ALFA      THERMAL EXPANSION COEFF ROLL      /DEG C
C BETA      FUDGE FACTOR IN ROLL EXP EQ
C BL        BARREL LENGTH                     m
C DELTAX    NOZZLE PITCH
C FO        FOURIER NUMBER-ROLL BITE CALC
C FOFF      FRACTION OF PASS WHEN OFF
C FONA      FRACTION OF PASS WHEN ON
C HTC()     HTC PRODUCT
C INPASS    NUMBER OF PASSES PER SLAB
C ISET      NUMBER OF SLABS ROLLED
C ISOFF     SLAB NUMBER WHEN SPRAY OFF
C ICOFF     PASS NUMBER WHEN SPRAY OFF
C ICOOL     NUMBER OF NODES COOLED (NOZZLES)
C INPASS    NUMBER OF PASSES PER SLAB
C ISET      NUMBER OF SLABS ROLLED
C LOUT      INTEGER CONTROLLING OUTPUT
C NNHSW     NUMBER OF NODES IN HALF STRIP
C NRN       NUMBER OF RADIAL NODES
C QB        HEAT GENERATED IN BEARING                 N.D.
C READ_CHECK  INPUT CONTROL FOR CHTFR()
C RESTT()   REST TIME BEFORE ROLLING                  SEC
C RLRAD     ROLL RADIUS                               M
C ROLLT()   ROLLING TIME                              SEC
C RRN       RADIUS OF ROLL NECK                       M
C SLAB_DATA INPUT CONTROL FOR INDIVIDUAL SLAB DATA
C TAMB      TEMP OF AMBIENT                           DEG C
C TBER      TEMP OF BEARING                           DEG C
C TCC       TEMP OF CENTRE HOLE COOLANT               DEG C
C TCL       TEMP OF COOLANT                           DEG C
C TREF      REFERENCE TEMPERATURE                     DEG C
C TDFR      THERMAL DIFFUSIVITY ROLL                  M/SEC**2
C TDFS      THERMAL DIFFUSIVITY STRIP                 M/SEC**2
C TEN       TEMP OF ENDPLATE COOLANT                  DEG C
C TINT      INITIAL TEMP OF ROLL                      DEG C
C TITLE     PROGRAM RUN IDENTIFICATION
C TRL       TOTAL ROLL LENGTH                         M
C TS1()     ENTRY PLATE TEMPERATURE                   DEG C
C V1()      INGOING PLATE SPEED                       M/SEC
C W         STRIP WIDTH                               M
C WW()      POWER TO ROLL PASS                        W
C XCC       BARREL LENGTH COVERED BY COOLANT    M
C XKR       THERMAL CONDUCTIVITY ROLL                 kW/(M.C)
C XKS       THERMAL CONDUCTIVITY STRIP                kW/(M.C)
C XH1()     INGOING PLATE THICKNESS                   M
C XH2()     EXIT PLATE THICKNES                       M
```

FIG. D.3 Flow diagram of subroutine EMENT

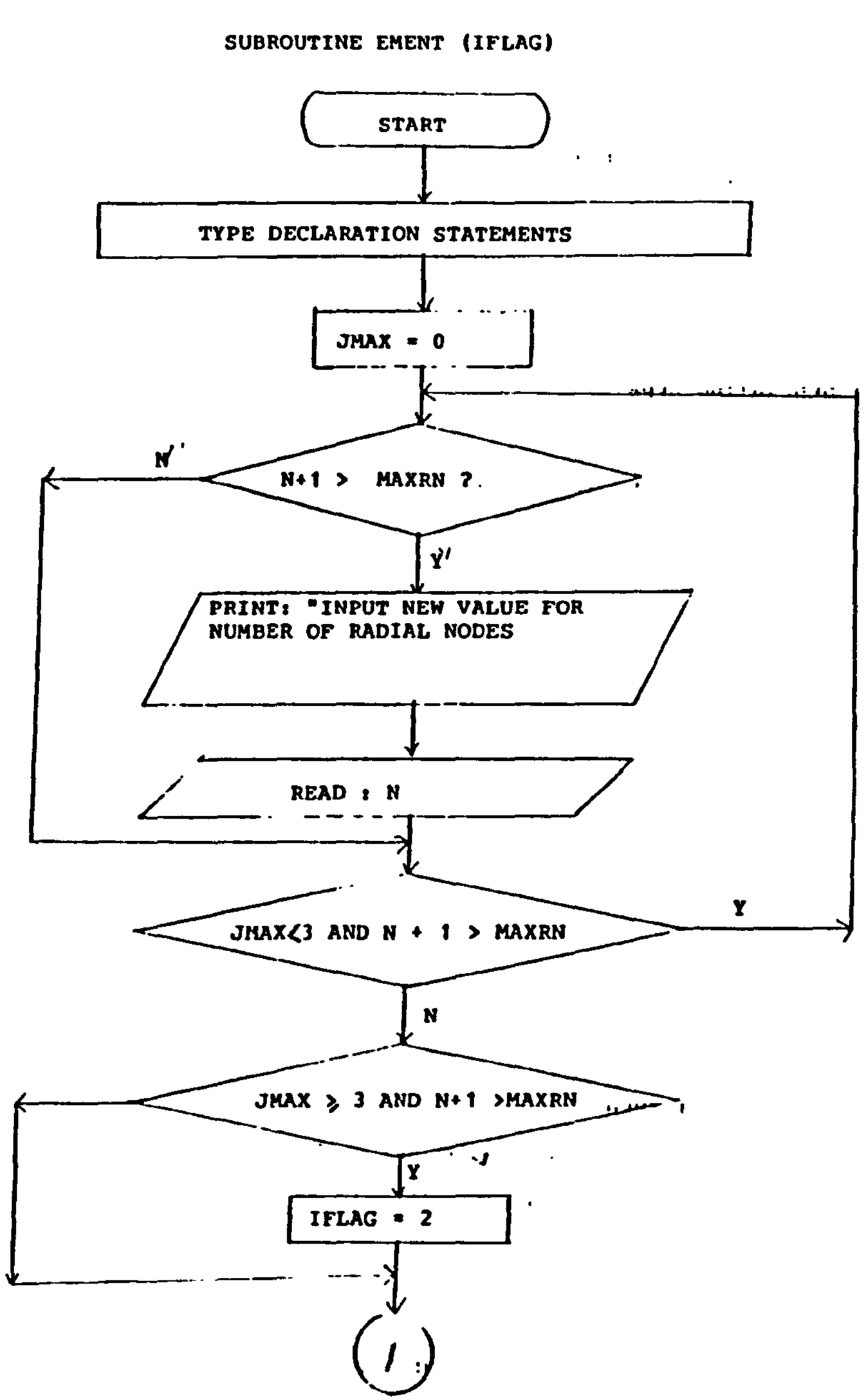

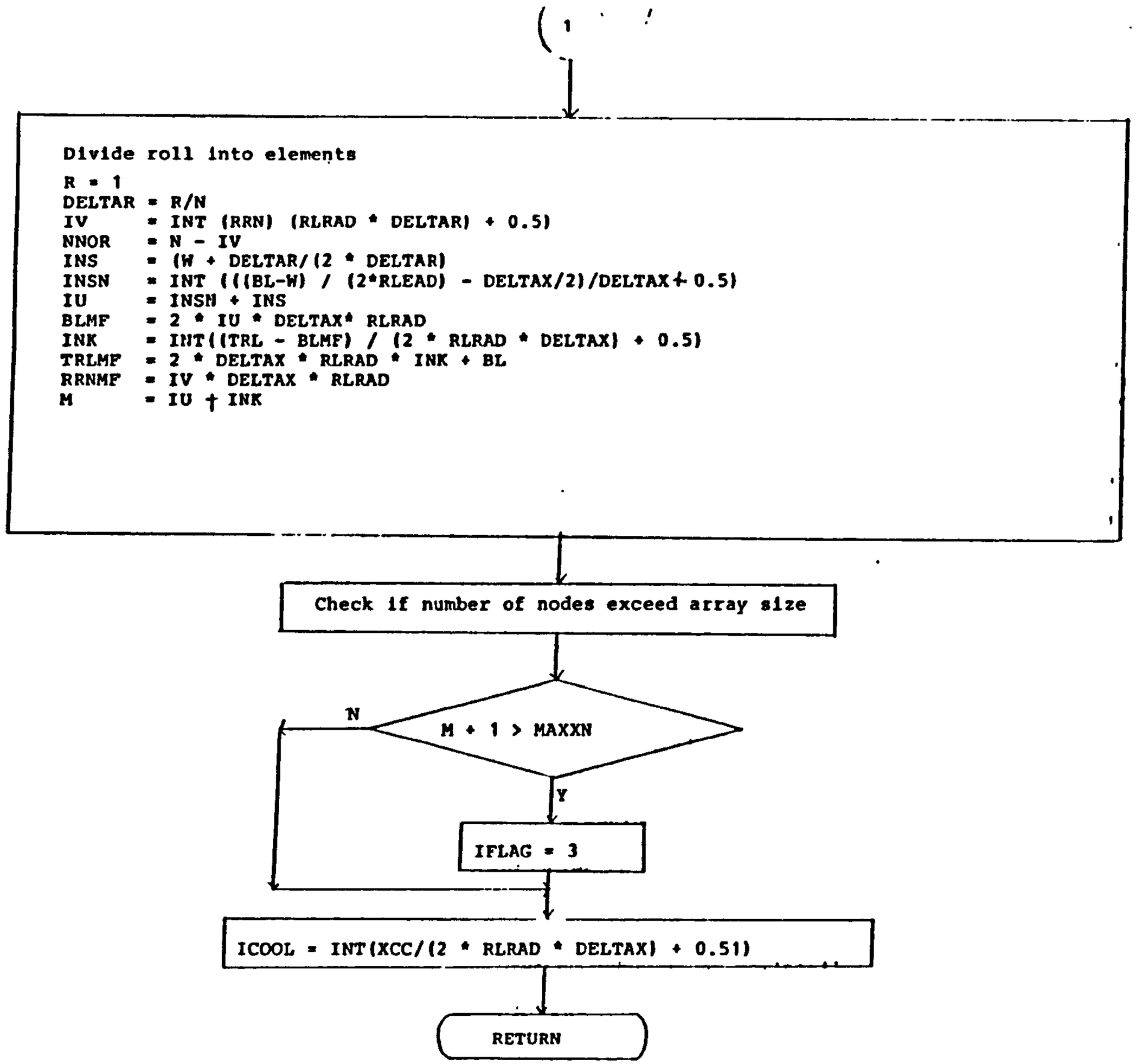
1
Divide roll into elements
R = 1
DELTAR = R/N
IV = INT (RRN) (RLRAD * DELTAR) + 0.5)
NNOR = N - IV
INS = (W + DELTAR/(2 * DELTAR)
INSN = INT (((BL-W) / (2*RLEAD) - DELTAX/2)/DELTAX + 0.5)
IU = INSN + INS
BLMF = 2 * IU * DELTAX* RLRAD
INK = INT((TRL - BLMF) / (2 * RLRAD * DELTAX) + 0.5)
TRLMF = 2 * DELTAX * RLRAD * INK + BL
RRNMF = IV * DELTAX * RLRAD
M = IU + INK
Check if number of nodes exceed array size
N
M + 1 > MAXXN
Y
IFLAG = 3
ICOOL = INT(XCC/(2 * RLRAD * DELTAX) + 0.51)
RETURN

```
*****************************************************************
*                                                               *
* PROGRAM NAME        SUBROUTINE EMENT                          *
* PROGRAM AUTHOR      D.COLLINS                                 *
* DATE                4th NOVEMBER,1985                         *
*                                                               *
*****************************************************************

                    SUBROUTINE EMENT(IFLAG)

C SUBROUTINE DIVIDES ROLL INTO ELEMENTS GIVEN THE ROLL SIZE AND
C THE NUMBER OF ELEMENTS IN HALF THE STRIP WIDTH

C INPUT
C -----
C BL          BARREL LENGTH                              M
C NNHSW       NUMBER OF ELEMENTS IN HALF STRIP
C N=NRN       NUMBER OF RADIAL NODES
C MAXXN       MAXIMUM NUMBER AXIAL ELEMENTS
C MAXRN       MAXIMUM NUMBER RADIAL ELEMENTS
C TRL         TOTAL ROLL LENGTH                          M
C RLRAD       ROLL RADIUS                                M
C RRN         RADIUS OF ROLL NECK                        M
C W           STRIP WIDTH                                M
C XCC       BARREL LENGTH COVERED BY COOLANT             M

C OUTPUT
C ------
C BLMF        BARREL LENGTH FOR SIMPLE MESH FIT          M
C DELTAR      NON-DIMENSIONAL SIZE RADIAL ELEMENT
C DRELEM      RADIAL SIZE OF SINGLE ELEMENT              M
C DXELEM      AXIAL LENGTH OF SINGLE ELEMENT             M
C DELTAX      NON-DIMENSIONAL SIZE AXIAL ELEMENT
C IFLAG       FLAG INDICATING FAILURE
C IU=NNHBL    NUMBER NODES HALF BARREL LENGTH
C M=NNHRL     NUMBER NODES HALF ROLL LENGTH
C IV=NNRN     NUMBER NODES IN ROLL NECK
C NNOR        NUMBER NODES IN OUTER ROLL
C RRNMF       RADIUS ROLL NECK FOR SIMPLE MESH FIT       M
C TRLMF       TOTAL ROLL LENGTH FOR MESH FIT             M
```

FIG. D.4 Flow diagram of subroutine NDPROG

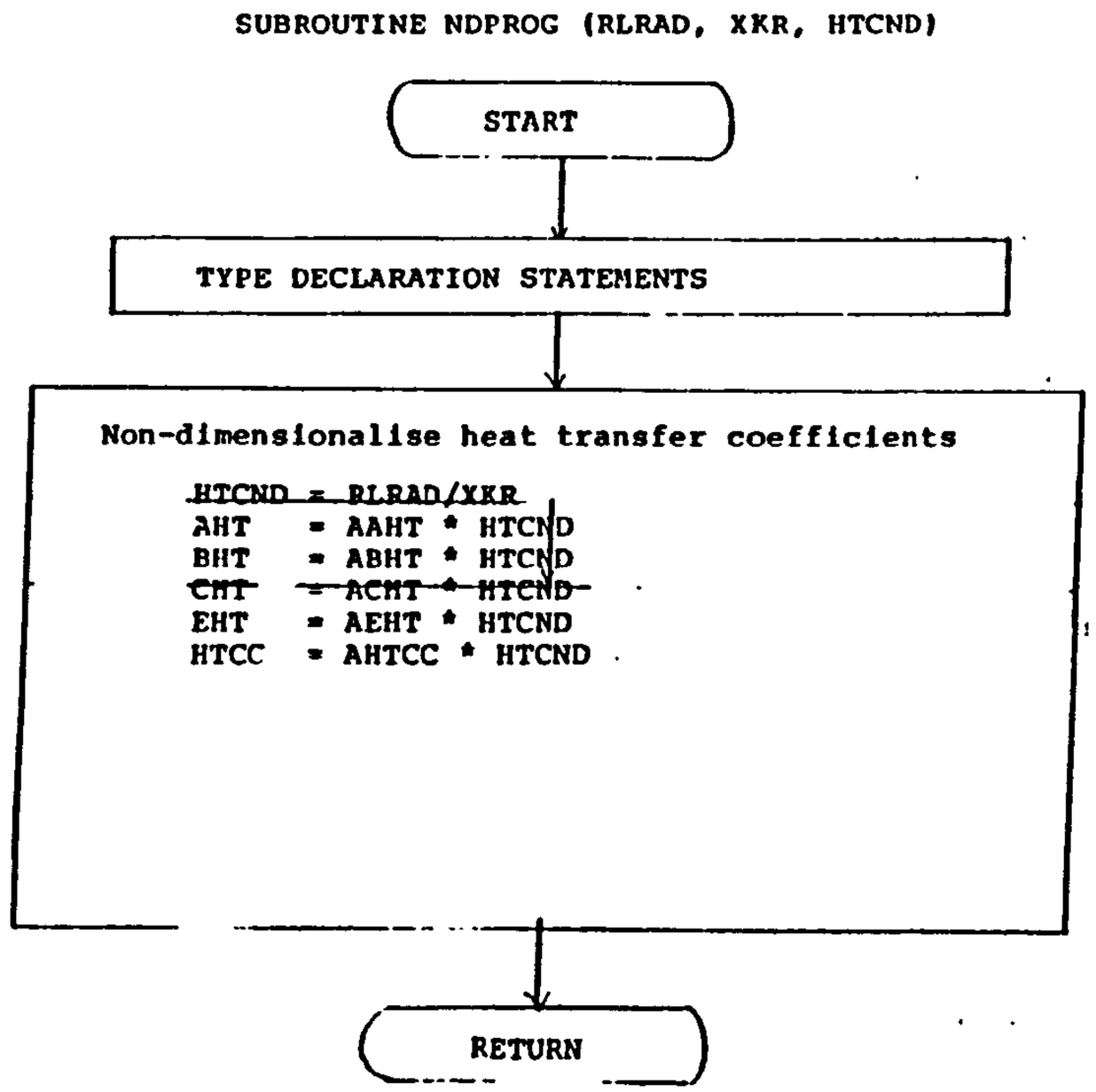

```
**************************************************************
*                                                            *
* PROGRAM NAME    SUBROUTINE NDPROG                          *
**************************************************************

      SUBROUTINE NDPROG(RLRAD,XKR,HTCND)

C INPUT
C -----
C AAHT   HEAT TRANSFER COEFFICIENT IN AIR COOLING   W/(M**2.C)
C ABHT   HEAT TRANSFER COEFFICIENT IN BEARING       W/(M**2.C)
C ACHT   HEAT TRANSFER COEFFICIENT IN FOR COOLANT   W/(M**2.C)
C AEHT   HEAT TRANSFER COEFFICIENT FOR ROLL END     W/(M**2.C)
C AHTCC  HEAT TRANSFER COEFFICIENT FOR PIPE COOLANT W/(M**2.C)

C OUTPUT
C ------

C AHT    HEAT TRANSFER COEFFICIENT IN AIR COOLING   N.D
C BHT    HEAT TRANSFER COEFFICIENT IN BEARING       N.D
C CHT    HEAT TRANSFER COEFFICIENT IN FOR COOLANT   N.D
C EHT    HEAT TRANSFER COEFFICIENT FOR ROLL END     N.D
C HTCC   HEAT TRANSFER COEFFICIENT FOR PIPE COOLANT N.D
```

Fig. D.5 Flow diagram of subroutine NIF

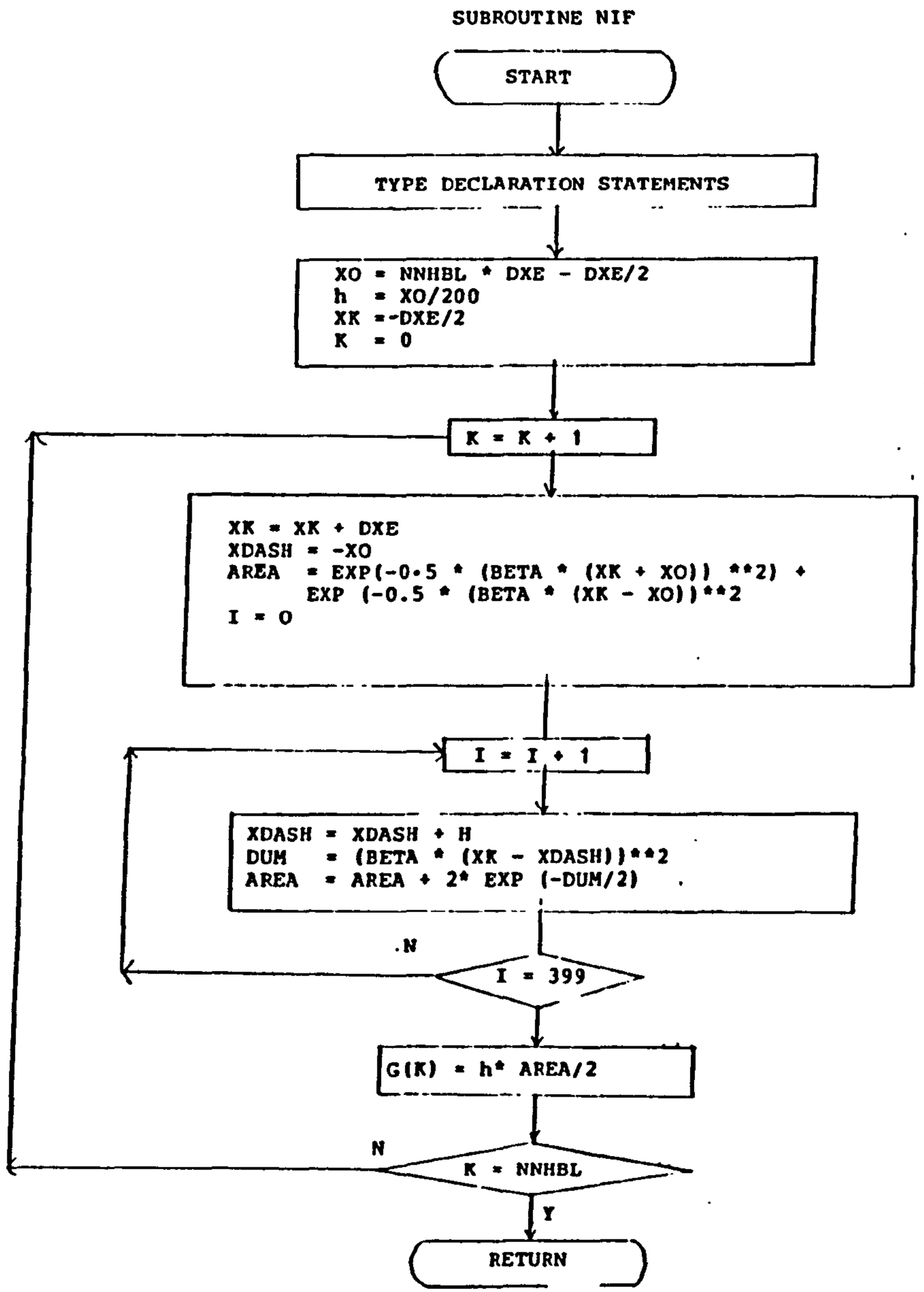

```
**********************************************************************
*                                                                    *
* PROGRAM NAME      SUBROUTINE NIF                                   *
* PROGRAM AUTHOR    D.COLLINS                                        *
*                                                                    *
**********************************************************************
                      SUBROUTINE NIF
C COMPUTES NORMALIZED INFLUENCE COEFFICIENT FOR USE IN
C COMPUTING THERMAL GROWTH OF ROLL AS DESCRIBED BY BEESTON
C AND EDWARDS IN "AUTOMATION OF A TANDEM MILL"

! VARIABLES
! ---------
C AREA      Area under curve from trapezoidal rule
C BETA        FUDGE FACTOR IN ROLL EXP EQ
C BLMF        BARREL LENGTH FOR SIMPLE MESH FIT      M
C DRE=DELTAR  NON-DIMENSIONAL SIZE RADIAL ELEMENT
C DXE=DELTAX  NON-DIMENSIONAL SIZE AXIAL ELEMENT
C G ()      NORMALISED INFLUENCE COEFFICIENT
C H      INTEGRAL STEP
C NNHBL       NUMBER NODES HALF BARREL LENGTH
C NNHSW       NUMBER OF ELEMENTS IN HALF STRIP
C NRN         NUMBER OF RADIAL NODES
C Xo          N.D LENGTH OF BARREL
C X*          N.D AXIAL POSITION
C Xdash       NORMALISED X- COORDINATE
```

FIG. D.6 Flow diagram of subroutine INITZ

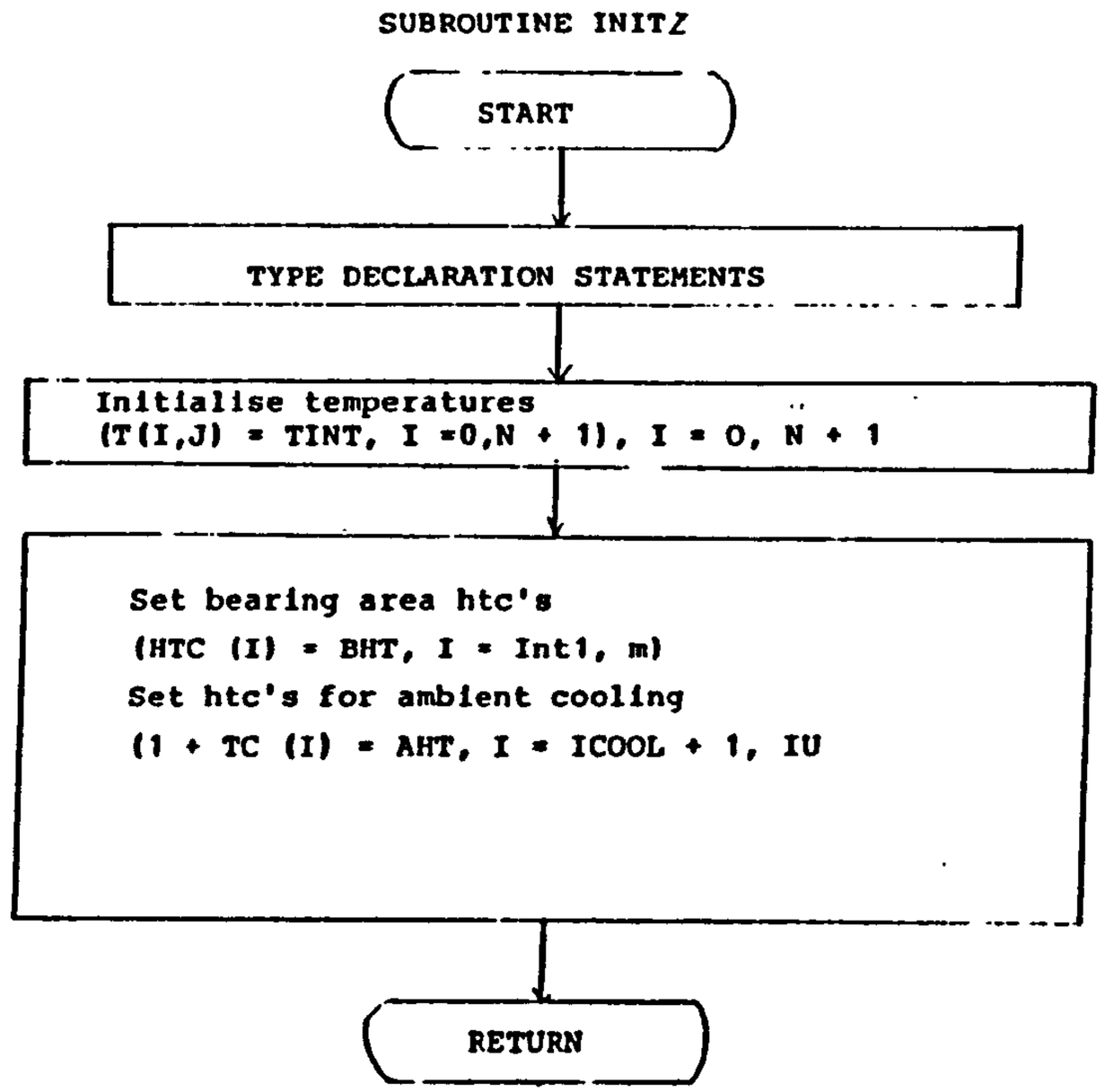

FIG. D7 SUBROUTINE SPRAY_SETTINGS

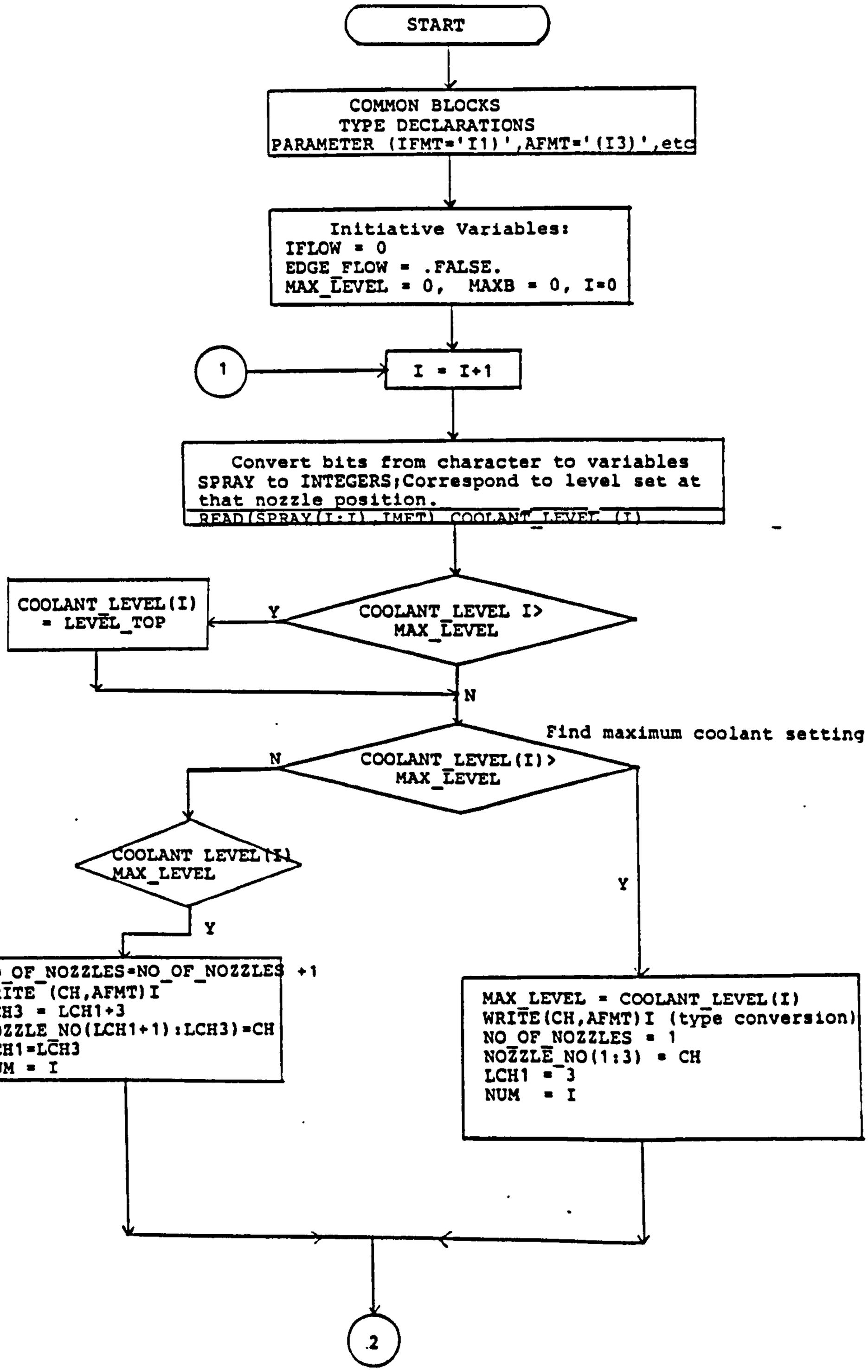

Fig. D7 cont'd

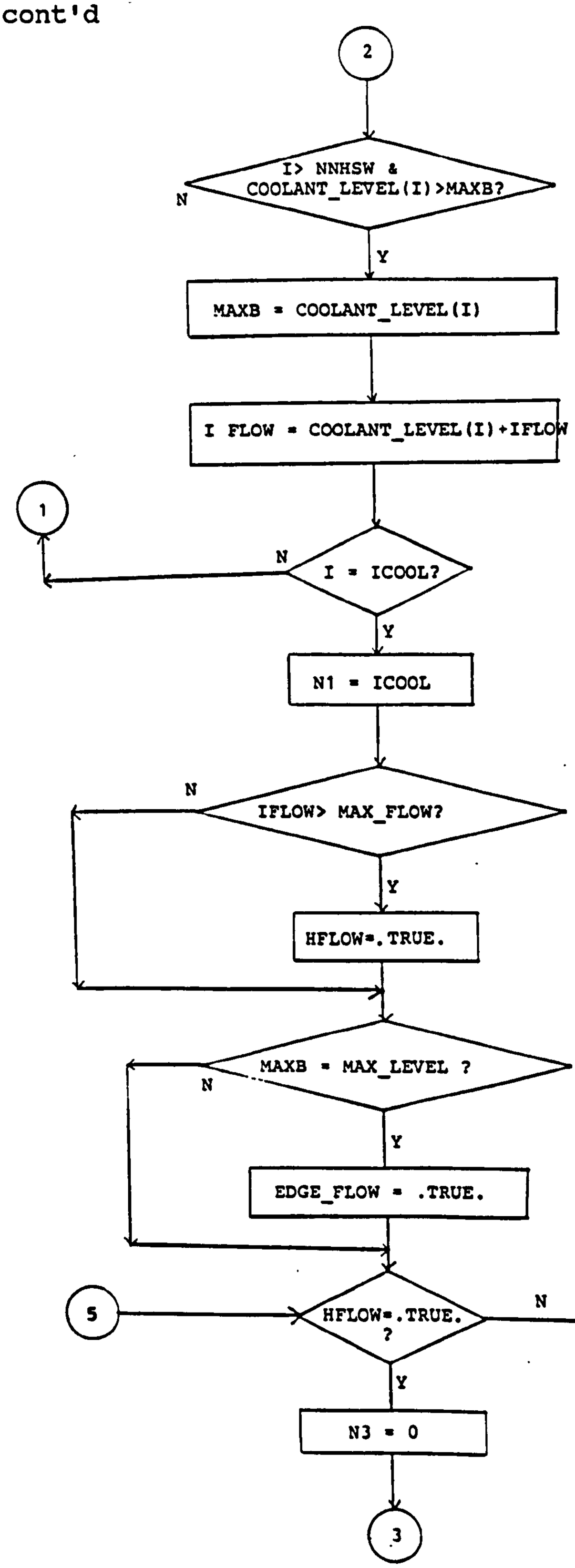
2
I> NNHSW &
COOLANT_LEVEL(I)>MAXB?
N
Y
MAXB = COOLANT_LEVEL(I)
I FLOW = COOLANT_LEVEL(I)+IFLOW
1
N
I = ICOOL?
Y
N1 = ICOOL
N
IFLOW> MAX_FLOW?
Y
HFLOW=.TRUE.
MAXB = MAX_LEVEL ?
N
Y
EDGE_FLOW = .TRUE.
5
HFLOW=.TRUE.
?
N
2
Y
N3 = 0
3

Fig. D7 cont'd

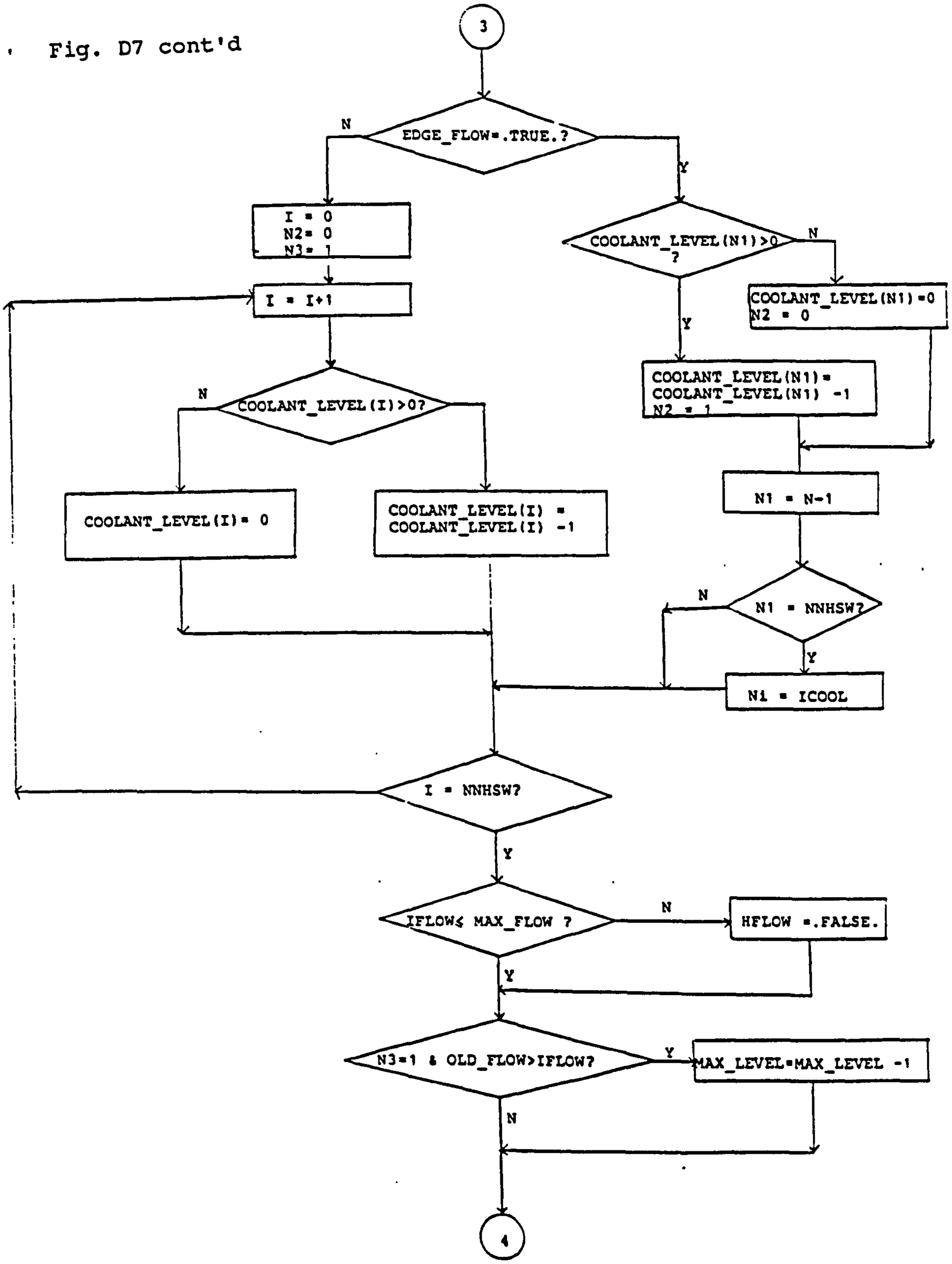
3
EDGE_FLOW=.TRUE.?
N
Y
I = 0
N2= 0
N3= 1
COOLANT_LEVEL(N1)>0 ?
N
Y
COOLANT_LEVEL(N1)=0
N2 = 0
I = I+1
COOLANT_LEVEL(N1)=
COOLANT_LEVEL(N1) -1
N2 = 1
N
COOLANT_LEVEL(I)>0?
N1 = N-1
COOLANT_LEVEL(I)= 0
COOLANT_LEVEL(I) =
COOLANT_LEVEL(I) -1
N
N1 = NNHSW?
Y
N1 = ICOOL
I = NNHSW?
Y
IFLOW≤ MAX_FLOW ?
N
HFLOW =.FALSE.
Y
N3=1 & OLD_FLOW>IFLOW?
Y
MAX_LEVEL=MAX_LEVEL -1
N
4

Fig. D7 cont'd

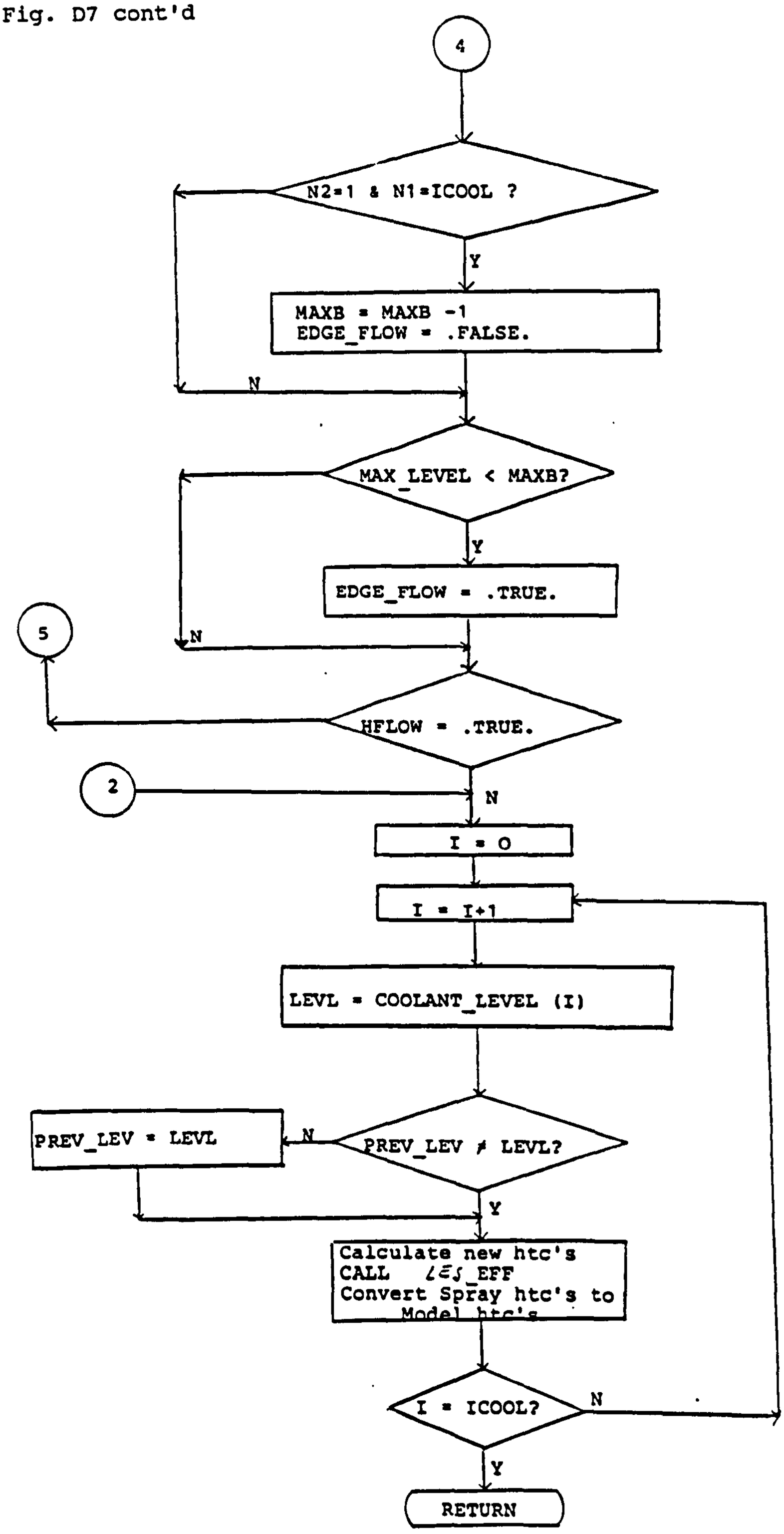
4
N2=1 & N1=ICOOL ?
Y
MAXB = MAXB -1
EDGE_FLOW = .FALSE.
N
MAX_LEVEL < MAXB?
Y
EDGE_FLOW = .TRUE.
5
N
HFLOW = .TRUE.
2
N
I = 0
I = I+1
LEVL = COOLANT_LEVEL (I)
PREV_LEV = LEVL
N
PREV_LEV ≠ LEVL?
Y
Calculate new htc's
CALL ∠∈ʃ_EFF
Convert Spray htc's to
Model htc's
I = ICOOL?
N
Y
RETURN

```
**************************************************************
*                                                            *
* PROGRAM NAME       SUBROUTINE SPRAY_SETTINGS               *
* PROGRAM AUTHOR     D.COLLINS                               *
* DATE               AUGUST,1986                             *
*                                                            *
**************************************************************

      SUBROUTINE SPRAY_SETTINGS(ICOOL,NNHSW,SPRAY,V)

C THIS SUBROUTINE TAKES A GIVEN SPRAY SETTING IN THE FORM OF A CHARACTER
! VARIABLE OF CHARACTER LENGTH EQUAL TO NUMBER OF SPRAYS ON HALF ROLL BARREL,
! CONVERTS IT TO INTEGER VALUES CORRESPONDING TO EACH SPRAY LEVEL, AND
! MODIFY SPRAY LEVELS IF TOO HIGH OR TOO LOW. PROGRAM THEN EVALUATES HTC'S BASED
! ON THESE SETTINGS BEFORE CONVERTING THEM TO EQUIVALENT HTC'S FOR USE BY THE
! CALLING PROGRAM

!-------------------------------------------------------------
!  VARIABLES
!  ---------

C  CHTFR ()         Fractional htc based on spray configuration
C  COOLANT_LEVEL()  Integer form of spray configuration
C  EDGE_FLOW        Log. var.. Test if highest settings outside strip width
C  HFLOW            Log. var.. Test if flow too high
C  HT_COEFF    Current value of htc depending on spray level set
C  ICOOL            Number of nodes cool. Passed as argument
C  IFLOW            Total coolant flow
C  IFMT             Format for an internal READ statement
C  IPSC   Current pass value on s/r call. Passed by argument
C  IV   Holds last pass value at s/r call. Passed by argument
C  LEVEL_TOP        Maximum level of any nozzle or valve
C  MAX_FLOW         Maximum possible coolant flow. Fixed by actual sprays
C  MAX_LEVEL        Max. spray level set
C  MIN_FLOW         Minimum possible coolant flow. Fixed by sprays
C  MODEL_FN         Presently unknown function to cal. spray htc
                                        !based on spray settings
C  NNHSW            Number of nodes inside strip width
C  NOZZLE_NO        The number of the nozzle with higest coolant flow
C  NO_OF_NOZZLES    The number of nozzles at higest setting
C  SPRAY_HTC ()     HTC's based on spray settings
C  STRIP_OUT_HIGH   Highest value of htc in strip width area
```

SUBROUTINE LCHR (TINT, XKR)

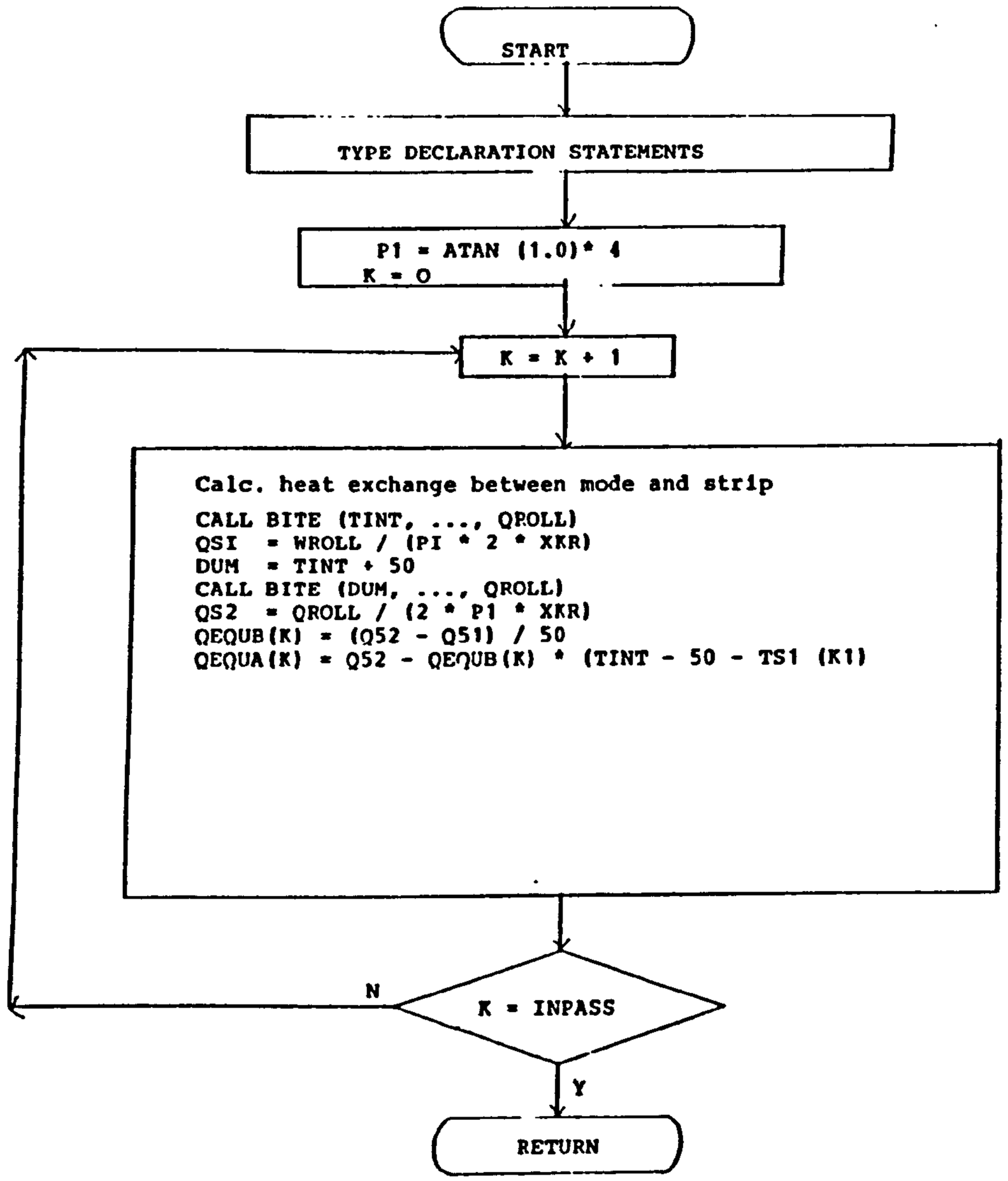

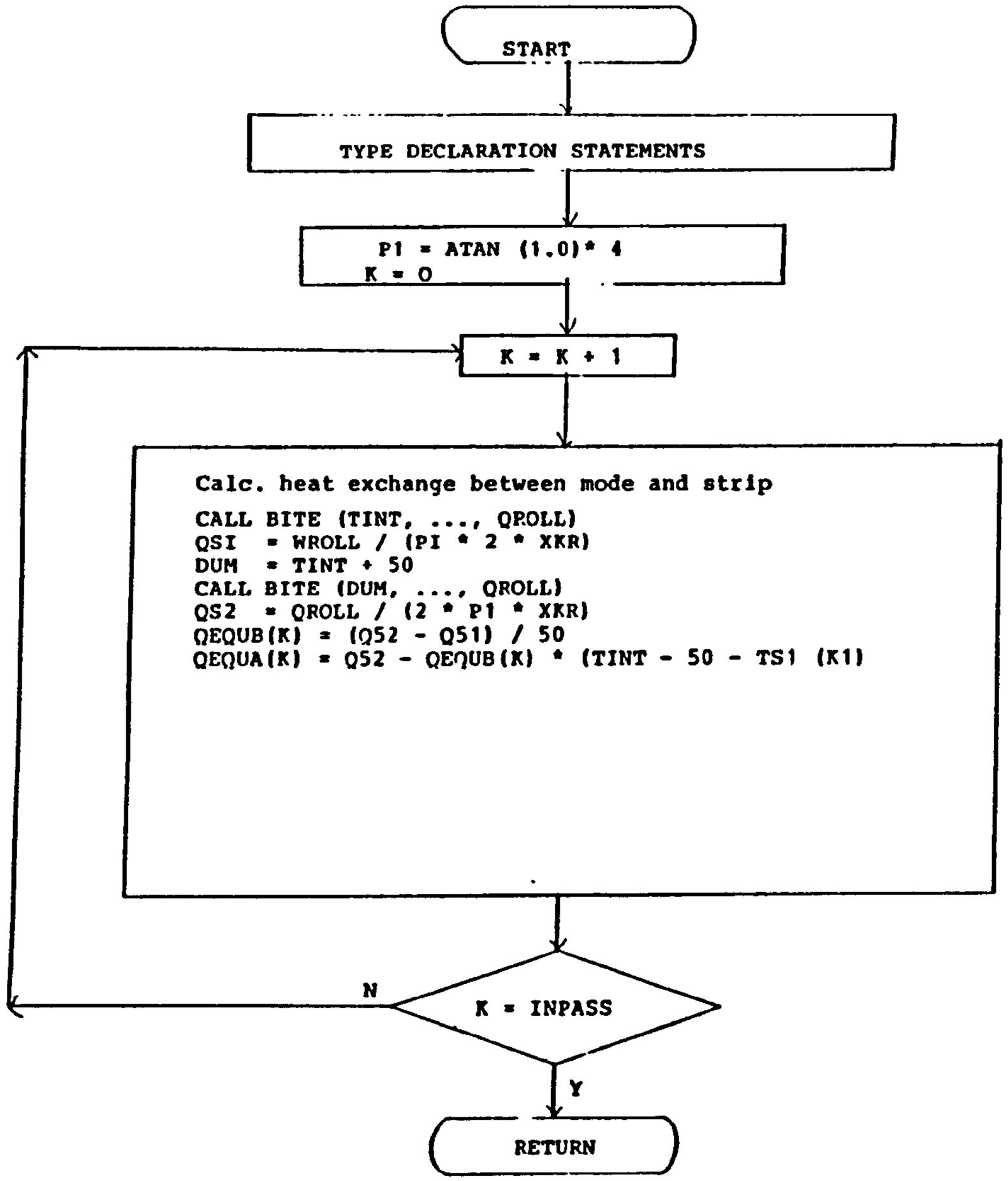
SUBROUTINE LCHR (TINT, XKR)
START
TYPE DECLARATION STATEMENTS
P1 = ATAN (1.0)* 4
K = 0
K = K + 1
Calc. heat exchange between mode and strip
CALL BITE (TINT, ..., QROLL)
QSI = WROLL / (PI * 2 * XKR)
DUM = TINT + 50
CALL BITE (DUM, ..., QROLL)
QS2 = QROLL / (2 * P1 * XKR)
QEQUB(K) = (Q52 - Q51) / 50
QEQUA(K) = Q52 - QEQUB(K) * (TINT - 50 - TS1 (K1)
N
K = INPASS
Y
RETURN

```
*****************************************************************
*                                                               *
* PROGRAM NAME     SUBROUTINE LCHR                              *
* PROGRAM AUTHOR   D. COLLINS                                   *
* DATE             1985                                         *
*****************************************************************

      SUBROUTINE LCHR(TINT,XKR)

C DETERMINES THE RATE OF HEAT INPUT INTO THE ROLL FOR EACH
C PASS.AN INITIAL ROLL TEMP IS ASSUMED.THE RATE OF HEAT FLOW
C IS DETERMINED.A NEW ROLL TEMP,50 DEG C ABOVE FIRST IS
C ASSUMED AND NEW HEAT FLOW DETERMINED.USING THESE VALUES
C A LINEAR CURVE IS DETERMINED FOR HEAT FLOW BASED ON
C THE DIFFERENCE BETWEEN STRIP ENTRY TEMP AND ROLL BACK-
C GROUND TEMP

C INPUT
C -----
C INPASS    NUMBER OF PASSES PER SLAB
C TINT      INITIAL ROLL TEMP                    DEG C
C XKR       THERMAL CONDUCTIVITY OF ROLL         W/(M**2.C)

C OUTPUT
C ------
C QEQUA()   CONSTANT IN Q DOT EQUATION           N.D.
C QEQUB()   LINEAR TERM IN Q DOT EQUATION        N.D.

C LOCAL
C -----
C QROLL     HEAT TRANSFER INTO ROLL              W
C QS1       NON DIMENSIONAL HEAT FLOW            N.D.
C QS2        "    "       "    "      "
C DV        DUMMY VARIABLE=TINT+50
```

FIG. D.9. FLOW DIAGRAM OF SUBROUTINE TIMIT

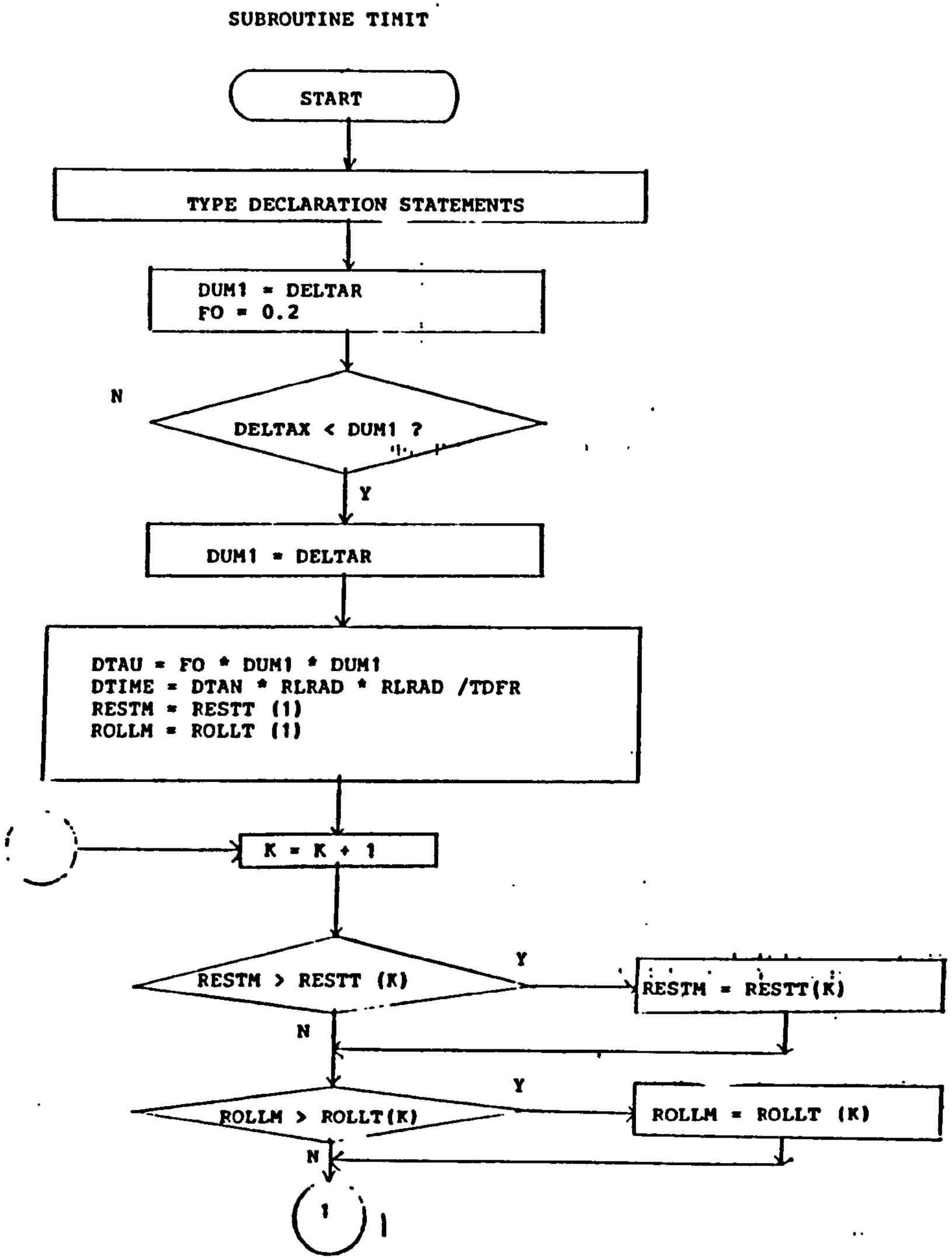

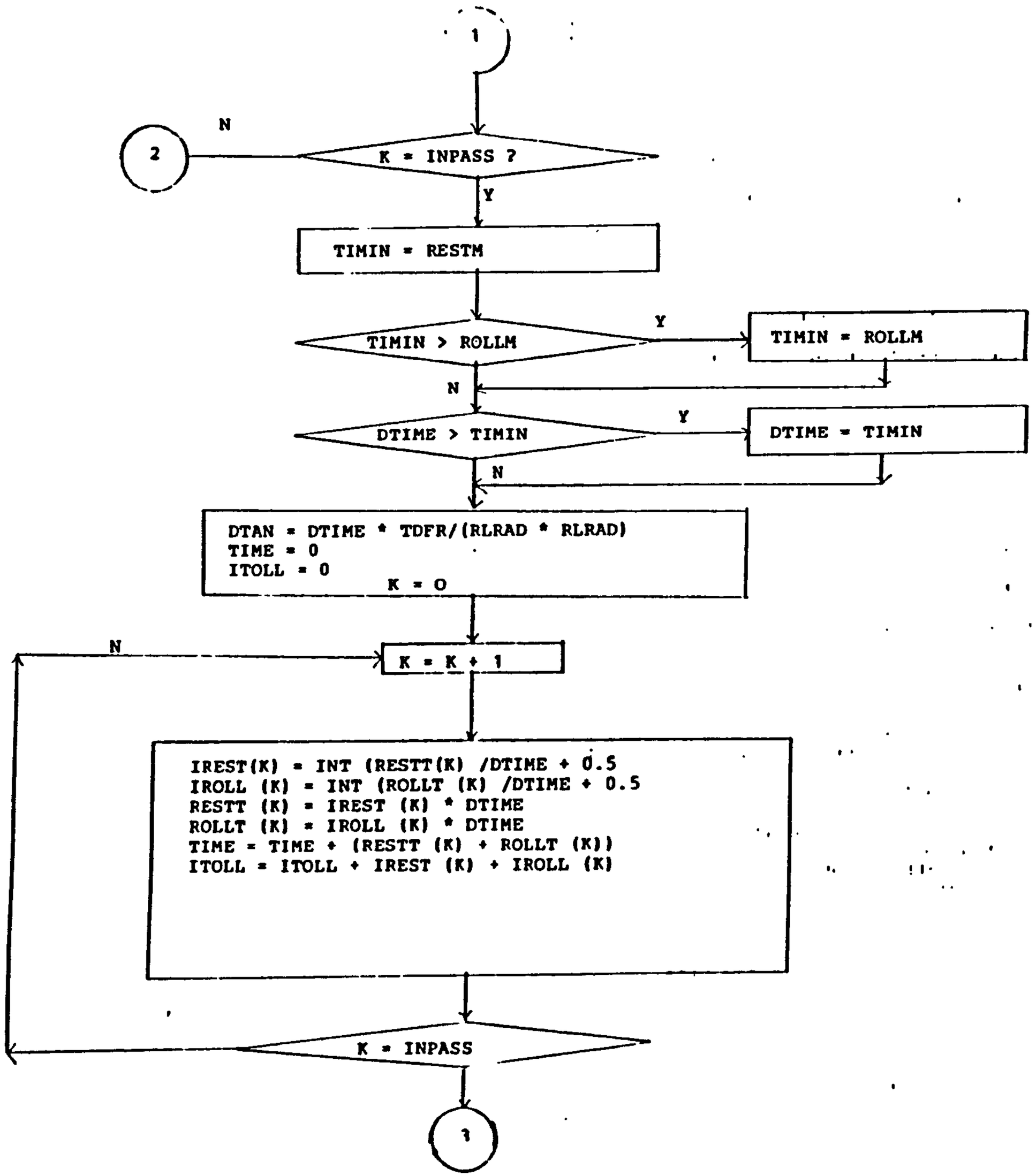
1
N
2
K = INPASS ?
Y
TIMIN = RESTM
Y
TIMIN > ROLLM
TIMIN = ROLLM
N
Y
DTIME > TIMIN
DTIME = TIMIN
N
DTAN = DTIME * TDFR/(RLRAD * RLRAD)
TIME = 0
ITOLL = 0
K = O
N
K = K + 1
IREST(K) = INT (RESTT(K) /DTIME + 0.5
IROLL (K) = INT (ROLLT (K) /DTIME + 0.5
RESTT (K) = IREST (K) * DTIME
ROLLT (K) = IROLL (K) * DTIME
TIME = TIME + (RESTT (K) + ROLLT (K))
ITOLL = ITOLL + IREST (K) + IROLL (K)
K = INPASS
1

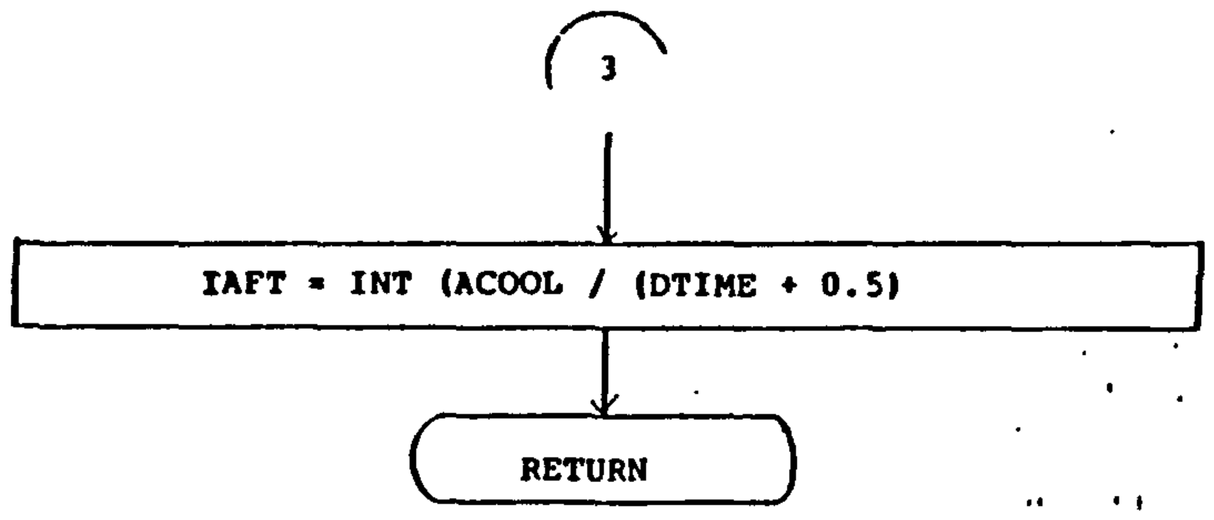
3
IAFT = INT (ACOOL / (DTIME + 0.5)
RETURN

```
*****************************************************************
*                                                               *
* PROGRAM NAME      SUBROUTINE TIMIT                            *
* PROGRAM AUTHOR    D. COLLINS                                  *
*                                                               *
*****************************************************************

                    SUBROUTINE TIMIT

C COMPUTES TIME REPRESENTED BY ONE ITERATION AND CHECKS AGAINST
C MINIMUM ROLLING OR HANDLING TIME.MIN IS THEN USED IN ITERATION

C INPUT
C -----
C ACOOL       COOLING TIME AFTER ROLLING              SEC
C DELTAR      RADIAL ELEMENT SIZE                     N.D.
C DELTA       AXIAL ELEMENT SIZE                      N.D.
C FO          FOURIER NUMBER
C FOFF        FRACTION OF PASS TIME WHEN TURNED OFF
C FONA        FRACTION OF PASS TIME WHEN TURNED ON
C ICOFF       PASS WHERE SPRAYS SWITCHED
C INPASS      NUMBER OF PASSES PER SLAB               SEC
C RESTT()     REST TIME BEFORE ROLLING PASS           SEC
C RLRAD       ROLL RADIUS                             M
C ROLLT()     ROLLING TIME FOR PASS                   SEC
C TDFR        THERMAL DIFFUSIVITY OF ROLL             M/SEC**2

C OUTPUT
C ------
C DTAU        TIME INCREMENT                          N.D.
C DTIME       TIME INCREMENT                          SEC
C IAFT        NUMBER OF ITERATIONS AFTER ROLLING
C INOFF       NUMBER ITER BEFORE SPRAY SWITCHED OFF
C INON        NUMBER ITER BETWEEN WHEN BACK ON
C IREST()     NUMBER OF ITERATION IN REST PERIOD
C IROLL()     NUMBER OF ITERATIONS IN ROLL PERIOD
C ITTOL       TOTAL NUMBER OF ITERATION PER SLAB
C TIME        TIME TO ROLL ONE SLAB                   SEC
C
C LOCAL
C -----
C DUM1        DUMMY VARIABLE
C RESTM       MINIMUM REST TIME                       S
C ROLLM       MINIMUM ROLL TIME                       S
C TIMIN       MINIMUM TIME                            S
C
```

FIG. D.10 FLOW DIAGRAM OF SUBROUTINE READ

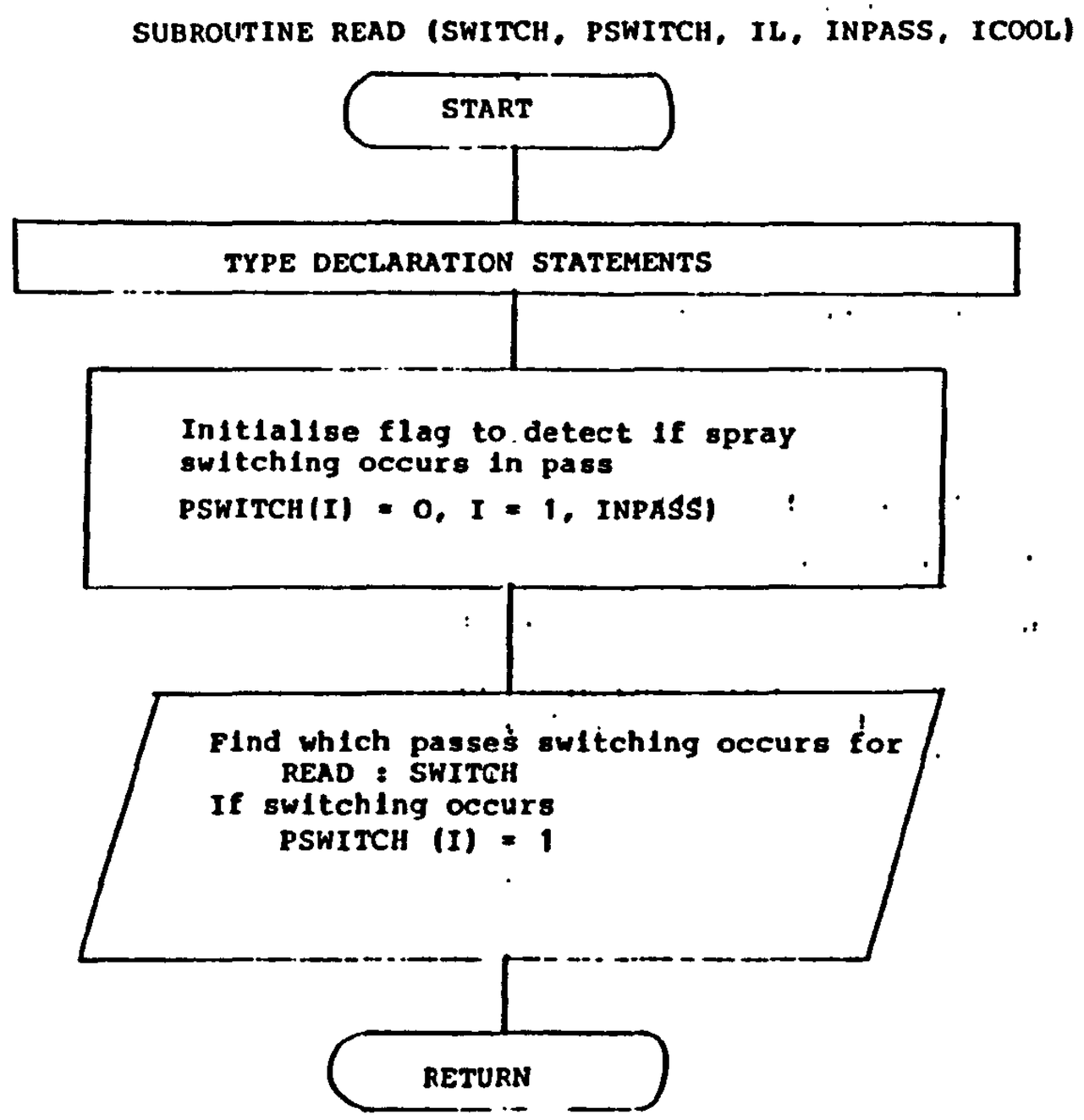

```
*****************************************************************
*                                                               *
* PROGRAM NAME        SUBROUTINE READ                           *
* PROGRAM AUTHOR      D.COLLINS                                 *
* DATE                AUGUST,1986                               *
*                                                               *
*****************************************************************

      SUBROUTINE READ(SWITCH,PSWITCH,IL,INPASS,ICOOL)

C   This subroutine reads data, to identify in which pass sprays
* are switched off before the end of the pass, in the form of a
* character variable, SWITCH, of length 80 characters. The pass
* numbers must be read on a single line of input in a format of nA3
* (no commas are allowed). This data is checked for errors, and if
* detected will print an error message before stopping.

!  VARIABLES
*  ---------

* AFMT  Character format spec. Parameter
* NP  Detects if error in input format
* ICOOL             Number of nodes cooled.Passed as argument
* IFMT  Integer format spec. Parameter
* IL  Detects length of SWITCH occupied
* INPASS            Number of passes per slab. Passed as argument
* IPS  Used in type conversion from SWITCH
* LCH  PARAMETER: equals 3
* PSWITCH ()        Flag to detect if spray switching occurs in pass
* SWITCH ()         Records passes in which switching occur. Character variable,
!                    up to 80 characters in batches of A3
```

FIG. D.11 FLOW DIAGRAM OF SUBROUTINE TEMCAL

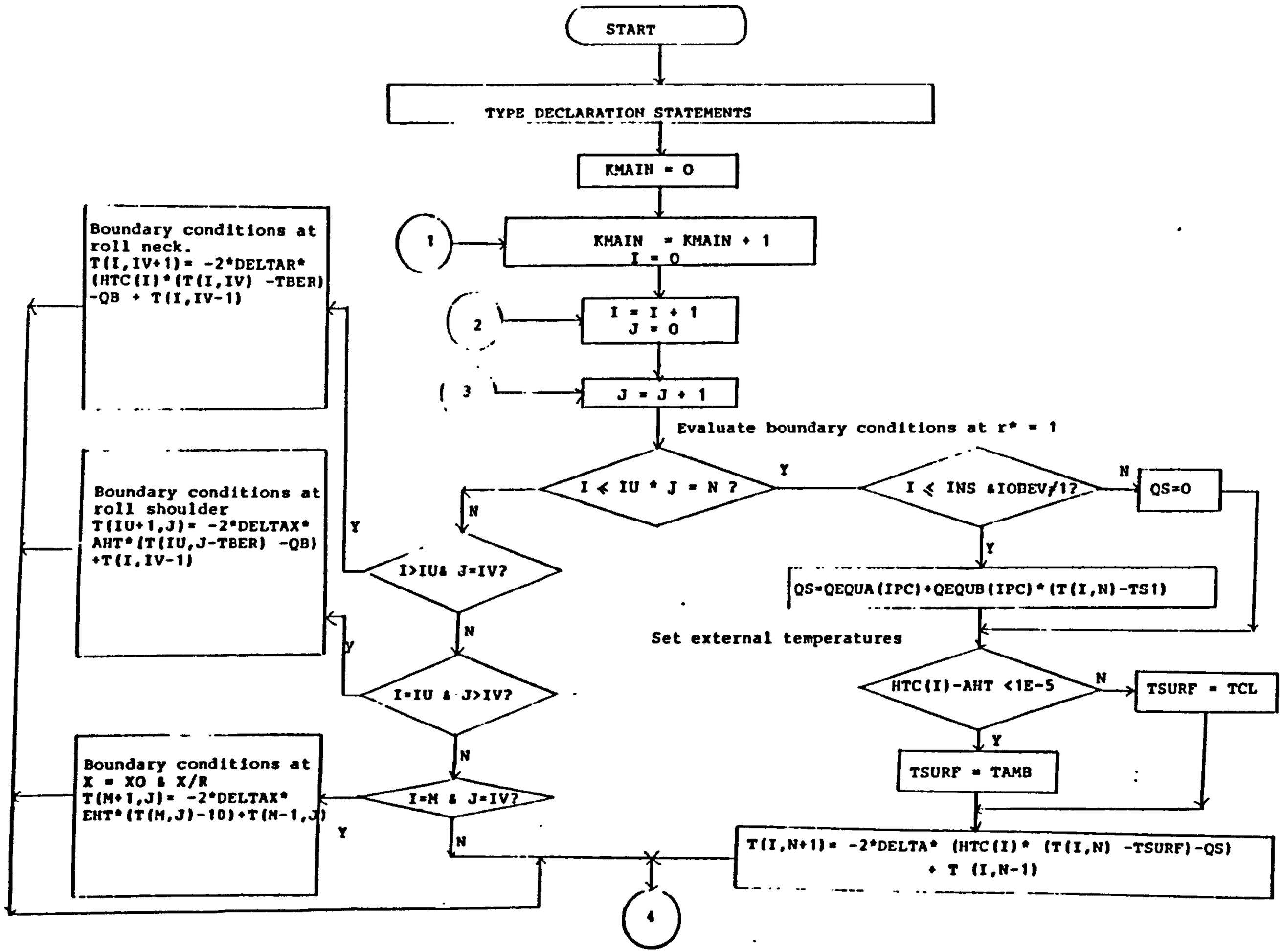

FIG.D11 CONT'D

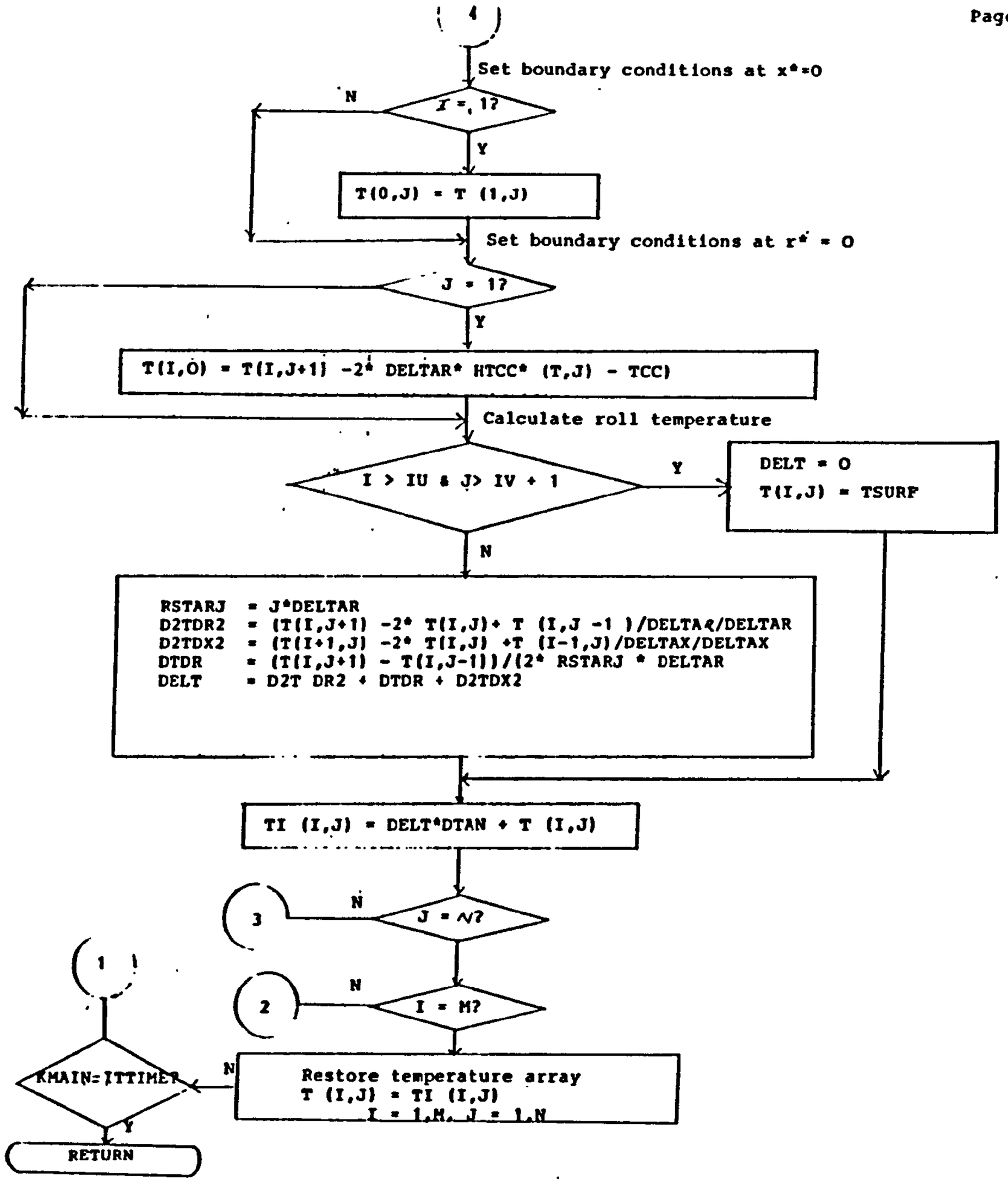

FIG. D.12

FLOW DIAGRAM OF SUBROUTINE THMCAM

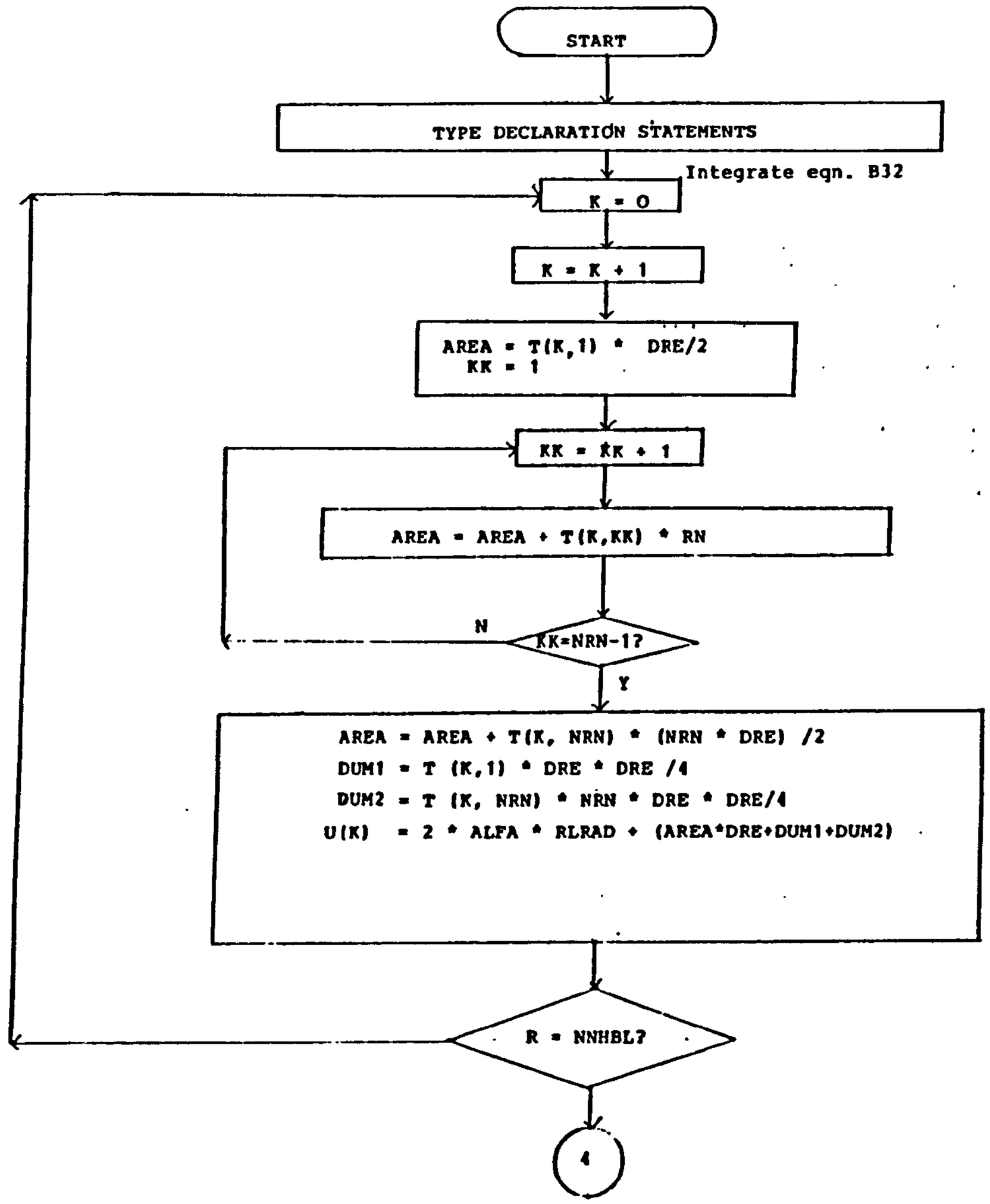

FIG. D.12

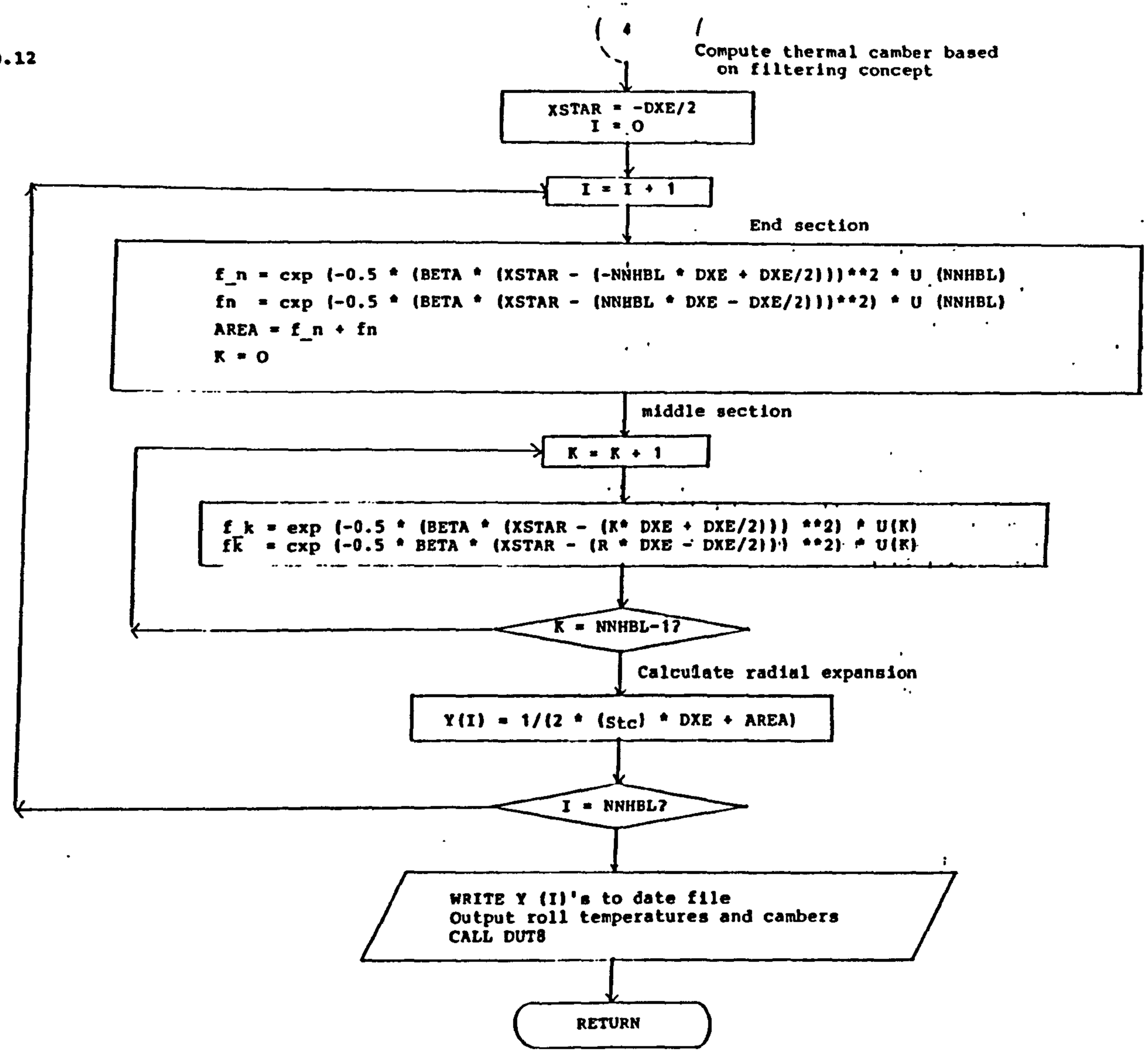
4
Compute thermal camber based on filtering concept
XSTAR = -DXE/2
I = O
I = I + 1
End section
f_n = cxp (-0.5 * (BETA * (XSTAR - (-NNHBL * DXE + DXE/2)))**2 * U (NNHBL)
fn = cxp (-0.5 * (BETA * (XSTAR - (NNHBL * DXE - DXE/2)))**2) * U (NNHBL)
AREA = f_n + fn
K = O
middle section
K = K + 1
f_k = exp (-0.5 * (BETA * (XSTAR - (K* DXE + DXE/2))) **2) * U(K)
fK = cxp (-0.5 * BETA * (XSTAR - (R * DXE - DXE/2))) **2) * U(K)
K = NNHBL-1?
Calculate radial expansion
Y(I) = 1/(2 * (Stc) * DXE + AREA)
I = NNHBL?
WRITE Y (I)'s to date file
Output roll temperatures and cambers
CALL DUT8
RETURN

```
*****************************************************************
*                                                               *
* PROGRAM NAME      SUBROUTINE THMCAM                           *
* PROGRAM AUTHOR    D.COLLINS                                   *
*                                                               *
*****************************************************************
                    SUBROUTINE THMCAM

C SUBPROGRAM TO CALCULATE THERMAL CAMBER OF ROLLS USING METHOD DETAILED IN
C APPENDIX B

! VARIABLES
! ---------

C ALFA        THERMAL EXPANSION COEFF ROLL     /DEG C
C AREA      Area under curve from trapezoidal rule
C BETA        FUDGE FACTOR IN ROLL EXP EQ
C BLMF        BARREL LENGTH FOR SIMPLE MESH FIT     M
C DRE=DELTAR  NON-DIMENSIONAL SIZE RADIAL ELEMENT
C DXE=DELTAX  NON-DIMENSIONAL SIZE AXIAL ELEMENT
C fn      POSITIVE END SECTION OF CURVE
C f_n      NEGATIVE END SECTION OF CURVE
C G ()      NORMALISED INFLUENCE COEFFICIENT
C H       INTEGRAL STEP
C ICOOL         NUMBER OF NODES COOLED (NOZZLES)
C NNHBL         NUMBER NODES HALF BARREL LENGTH
C NNHSW         NUMBER OF ELEMENTS IN HALF STRIP
C NRN           NUMBER OF RADIAL NODES
C U ()          THERMAL EXPANSION
C Xstar         N.D AXIAL POSITION
C Y ()          NORMALISED THERMAL EXPANSION
```

FIG. D.13 FLOW DIAGRAM OF SUBROUTINE BITE

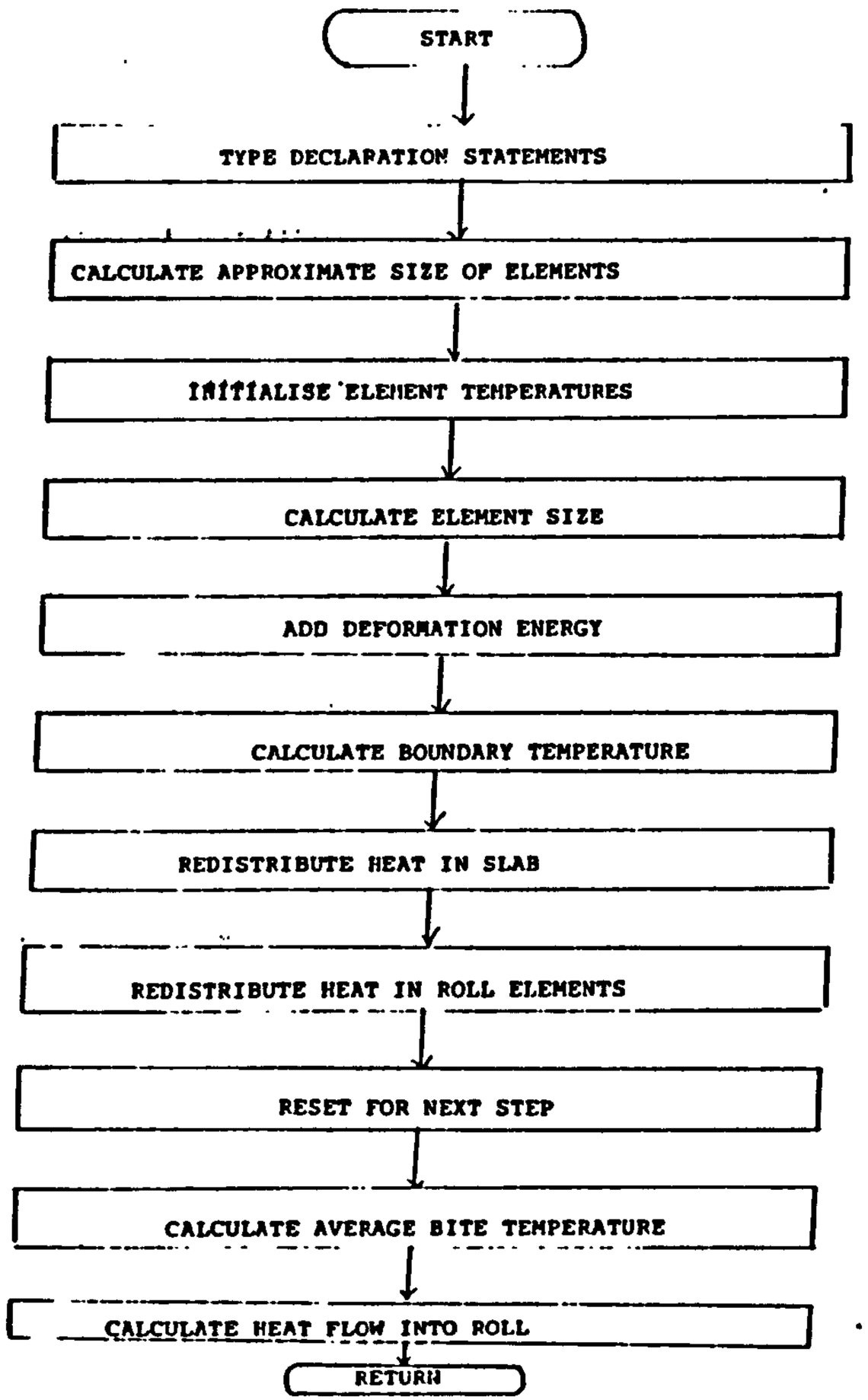

APPENDIX E

MEASURED DATA

Fig. E1 Examples of chart recordings taken at Mill A

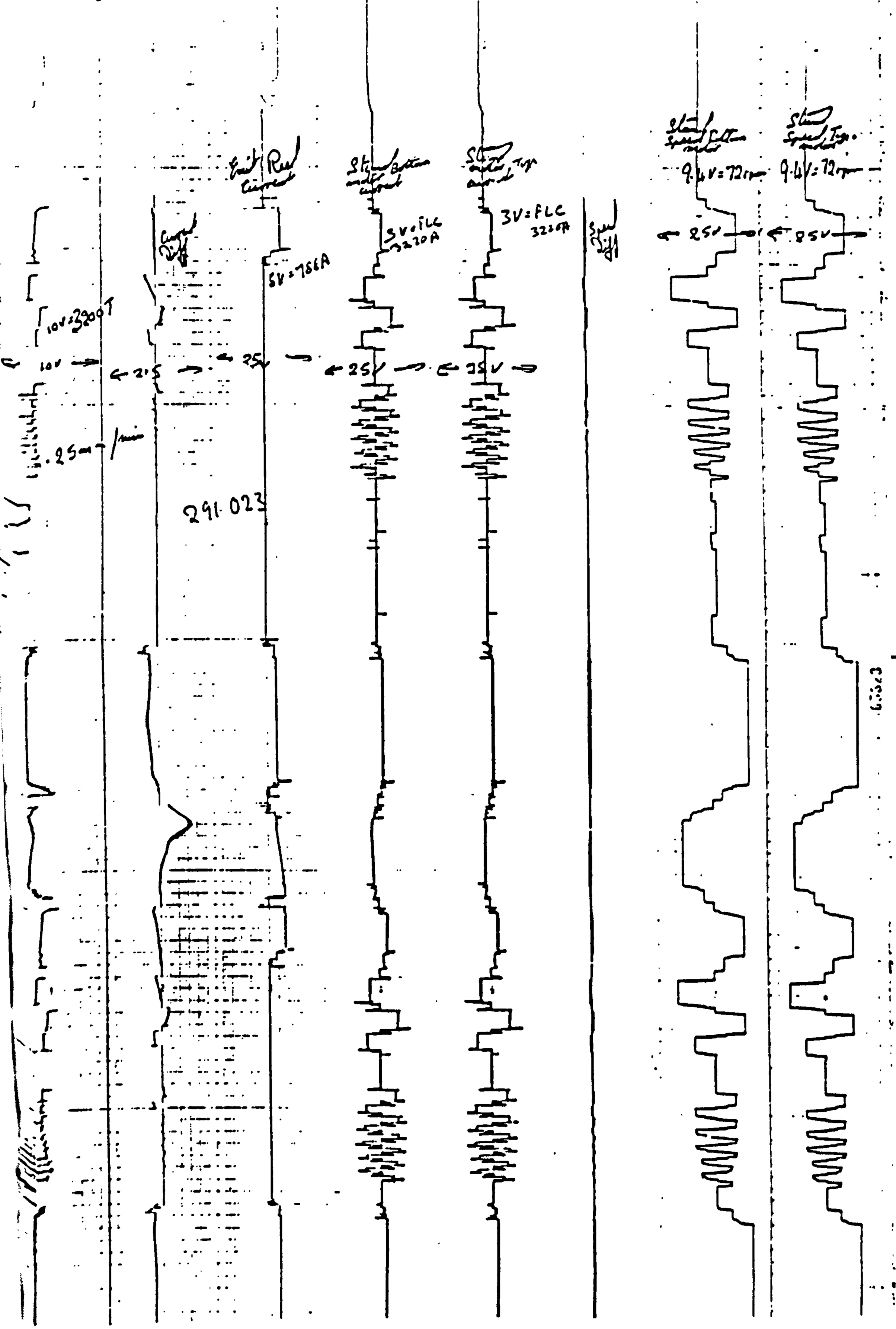

Fig.E2. HOT ALUMINIUM REVERSING MILL A - File of recorded data

Key:

PASS Pass number
ENT Entry Gauge (m)
EXT Exit Gauge (m)
PWR Motor Power (kW)
SPD Mill Speed ($m\ s^{-1}$)
TEMP Slab temperature (°C)
LT Location of temperature readings:
RST Rolling time (s)
RLT Rest time between rolling (s)

First digit	Second digit
0 calculated	0 unkown location
1 at mill entry	1 slab nose
2 at mill exit	2 slab centre
3 after handling	3 slab tail
4 on coiler	

All slab locations based on first pass orientation

Mill A -
Wednesday,16th Oct, 1985
Roll diameter 884 mm
Barrel length 2160 mm
Total roll length 5188 mm
Initial roll temp. 55 °C
Roll end temp. 40 °C
Ambient temperature 40 °C
Coolant temperature 60 °C
Spray width 1650 mm
7 schedules
All slabs characterised as:
Alloy 5182
Size (mm) 456 x 1100 x 5350

Slab 1 Time 14:25

PASS	ENT m	EXT m	PWR kW	SPD m/s	TEMP °C	LT	RST s	RLT s
1	0.4560	0.4400	6440.0	1.285	479.0	11	1.00	4.40
2	0.4400	0.4130	6976.0	1.285	480.0	00	7.20	4.60
3	0.4130	0.3820	8050.0	1.285	478.0	11	34.00	5.60
4	0.3820	0.3510	7782.0	1.285	479.0	00	6.00	6.00
5	0.3510	0.3200	9660.0	1.750	472.0	11	32.60	5.20
6	0.3200	0.2890	9124.0	1.795	472.0	00	6.20	5.20
7	0.2890	0.2580	8854.0	1.750	485.0	11	30.80	5.80
8	0.2580	0.2270	8586.0	1.795	486.0	00	6.00	6.40
9	0.2270	0.1960	8318.0	1.750	492.0	11	29.60	7.40
10	0.1960	0.1650	7782.0	1.795	494.0	00	5.80	8.80
11	0.1650	0.1340	7648.0	1.750	496.0	11	22.60	10.40
12	0.1340	0.1030	7648.0	1.795	499.0	00	7.00	13.00
13	0.1030	0.0720	7648.0	1.750	504.0	11	24.20	18.40
14	0.0720	0.0420	11002.0	2.260	507.0	00	66.80	23.60
15	0.0420	0.0250	10734.0	3.235	508.0	11	25.80	28.00
16	0.0250	0.0162	6440.0	3.257	513.0	00	14.20	43.00
17	0.0162	0.0098	4830.0	2.659	496.0	11	36.20	98.20
18	0.0098	0.0055	3756.0	2.703	443.0	00	13.20	163.00
19	0.0055	0.0030	2952.0	3.279	380.0	42	20.80	263.40

Slab 2 Time 14:59

PASS	ENT mm	EXT mm	PWR kW	SPD m/s	TEMP oC	LT	RST s	RLT s
1	0.4560	0.4400	6172.0	0.864	487.0	11	930.00	5.60
2	0.4400	0.4130	7110.0	1.352	488.0	00	6.40	5.20
3	0.4130	0.3820	7244.0	1.263	488.0	11	5.80	5.00
4	0.3820	0.3510	7514.0	1.352	489.0	00	6.20	5.60
5	0.3510	0.3200	8854.0	1.750	490.0	11	8.00	5.00
6	0.3200	0.2890	8854.0	1.795	491.0	00	6.20	4.80
7	0.2890	0.2580	8318.0	1.750	489.0	11	32.20	5.40
8	0.2580	0.2270	8184.0	1.795	490.0	00	7.00	6.20
9	0.2270	0.1960	7782.0	1.773	492.0	11	9.60	7.00
10	0.1960	0.1650	7514.0	1.773	494.0	00	5.60	8.80
11	0.1650	0.1340	7514.0	1.773	502.0	11	15.80	10.60
12	0.1340	0.1030	7110.0	1.795	503.0	00	6.80	13.40
13	0.1030	0.0720	7514.0	1.773	508.0	11	14.80	18.80
14	0.0720	0.0420	10600.0	2.238	510.0	00	58.20	23.60
15	0.0420	0.0250	10734.0	3.235	511.0	11	18.00	28.60
16	0.0250	0.0162	6306.0	3.257	517.0	00	8.80	44.00
17	0.0162	0.0098	4830.0	2.659	504.0	11	24.00	98.80
18	0.0098	0.0055	3756.0	2.703	452.0	00	14.00	161.40
19	0.0055	0.0030	2952.0	3.279	384.0	42	36.40	253.40

Slab 3 Time 15:19

PASS	ENT mm	EXT mm	PWR kW	SPD m/s	TEMP oC	LT	RST s	RLT s
1	0.4560	0.4400	6440.0	1.352	466.0	11	205.00	4.60
2	0.4400	0.4130	7514.0	1.285	466.0	00	40.00	5.20
3	0.4130	0.3820	7782.0	1.329	467.0	11	5.80	5.40
4	0.3820	0.3510	8050.0	1.263	468.0	00	7.00	5.80
5	0.3510	0.3200	9124.0	1.795	472.0	11	28.60	5.00
6	0.3200	0.2890	9124.0	1.773	473.0	00	6.80	5.00
7	0.2890	0.2580	8854.0	1.795	476.0	11	29.20	6.00
8	0.2580	0.2270	8586.0	1.773	477.0	00	5.60	6.20
9	0.2270	0.1960	8050.0	1.795	487.0	11	23.00	7.20
10	0.1960	0.1650	8050.0	1.773	489.0	00	6.40	9.00
11	0.1650	0.1340	7514.0	1.795	493.0	11	22.00	10.40
12	0.1340	0.1030	7514.0	1.773	496.0	00	6.00	13.60
13	0.1030	0.0720	7648.0	1.795	502.0	11	16.80	18.40
14	0.0720	0.0420	10734.0	2.216	504.0	00	60.80	23.80
15	0.0420	0.0250	11002.0	3.279	513.0	11	18.00	28.20
16	0.0250	0.0162	6172.0	3.213	519.0	00	8.60	43.60
17	0.0162	0.0102	4562.0	2.725	499.0	11	25.60	98.80
18	0.0102	0.0057	4024.0	2.681	468.0	00	14.40	157.20
19	0.0057	0.0030	2684.0	3.324	383.0	42	37.60	250.80

Slab 4 Time 16:03

PASS	ENT mm	EXT mm	PWR kW	SPD m/s	TEMP oC	LT	RST s	RLT s
1	0.4560	0.4400	6172.0	1.352	469.0	11	1574.00	4.60
2	0.4400	0.4130	7244.0	1.285	469.0	00	6.60	5.20
3	0.4130	0.3820	7514.0	1.329	478.0	11	30.00	5.20
4	0.3820	0.3510	7514.0	1.285	479.0	00	6.20	5.60
5	0.3510	0.3200	8990.0	1.795	479.0	11	31.40	5.20
6	0.3200	0.2890	8854.0	1.795	480.0	00	6.00	5.00
7	0.2890	0.2580	8452.0	1.795	484.0	11	27.00	5.80
8	0.2580	0.2270	8050.0	1.795	485.0	00	6.00	6.20
9	0.2270	0.1960	7916.0	1.795	487.0	11	26.00	7.40
10	0.1960	0.1650	7514.0	1.795	489.0	00	6.60	8.40
11	0.1650	0.1340	7380.0	1.795	498.0	11	27.60	10.20
12	0.1340	0.1030	6976.0	1.795	501.0	00	6.80	13.00
13	0.1030	0.0720	7514.0	1.795	503.0	11	19.40	18.20
14	0.0720	0.0420	10196.0	2.216	504.0	00	62.00	23.80
15	0.0420	0.0250	10196.0	3.257	509.0	11	21.40	27.80
16	0.0250	0.0162	5904.0	3.235	512.0	00	11.00	42.40
17	0.0162	0.0102	4024.0	2.703	501.0	11	24.40	94.40
18	0.0102	0.0057	4294.0	2.659	464.0	00	12.80	151.20
19	0.0057	0.0030	3220.0	3.324	370.0	42	37.00	248.60

Slab 5 Time 16:23

PASS	ENT mm	EXT mm	PWR kW	SPD m/s	TEMP oC	LT	RST s	RLT s
1	0.4560	0.4400	6976.0	1.329	470.0	11	144.00	4.80
2	0.4400	0.4130	8586.0	1.285	471.0	00	6.60	5.20
3	0.4130	0.3820	8854.0	1.329	457.0	11	39.20	5.60
4	0.3820	0.3510	8586.0	1.285	457.0	00	6.00	5.80
5	0.3510	0.3200	10464.0	1.817	453.0	11	40.60	5.20
6	0.3200	0.2890	10464.0	1.773	454.0	00	7.00	5.60
7	0.2890	0.2580	9660.0	1.817	461.0	11	31.60	5.80
8	0.2580	0.2270	9124.0	1.773	462.0	00	6.40	6.20
9	0.2270	0.1960	9124.0	1.817	470.0	11	28.00	7.60
10	0.1960	0.1650	8452.0	1.773	473.0	00	6.40	8.40
11	0.1650	0.1340	8318.0	1.817	476.0	11	25.00	10.40
12	0.1340	0.1030	7782.0	1.773	480.0	00	6.40	13.40
13	0.1030	0.0720	7648.0	1.817	489.0	11	21.40	18.20
14	0.0720	0.0420	11270.0	2.216	492.0	00	60.60	23.80
15	0.0420	0.0250	11002.0	3.257	498.0	11	20.00	27.80
16	0.0250	0.0162	6038.0	3.235	505.0	00	12.40	42.80
17	0.0162	0.0102	4024.0	2.725	489.0	11	26.20	103.00
18	0.0102	0.0057	3086.0	2.681	454.0	00	15.60	164.40
19	0.0057	0.0030	2684.0	3.324	384.0	42	38.80	270.00

Slab 6 Time 17:14

PASS	ENT mm	EXT mm	PWR kW	SPD m/s	TEMP oC	LT	RST s	RLT s
1	0.4560	0.4400	6440.0	1.329	468.0	11	2208.00	4.60
2	0.4400	0.4130	6976.0	1.285	468.0	00	5.00	4.60
3	0.4130	0.3820	7648.0	1.329	470.0	11	35.20	4.80
4	0.3820	0.3510	7514.0	1.285	470.0	00	5.20	5.80
5	0.3510	0.3200	9124.0	1.817	474.0	11	36.40	4.60
6	0.3200	0.2890	8854.0	1.773	474.0	00	5.80	5.60
7	0.2890	0.2580	8452.0	1.817	485.0	11	30.20	5.30
8	0.2580	0.2270	8318.0	1.773	486.0	00	6.20	6.40
9	0.2270	0.1960	7782.0	1.817	491.0	11	21.80	7.20
10	0.1960	0.1650	7514.0	1.773	493.0	00	5.80	8.80
11	0.1650	0.1340	7514.0	1.817	497.0	11	21.00	10.40
12	0.1340	0.1030	6976.0	1.773	500.0	00	6.20	12.60
13	0.1030	0.0720	7380.0	1.817	506.0	11	20.00	18.20
14	0.0720	0.0420	10464.0	2.216	508.0	00	57.40	22.80
15	0.0420	0.0250	10464.0	3.279	516.0	11	8.00	27.60
16	0.0250	0.0162	6038.0	3.257	521.0	00	9.00	42.00
17	0.0162	0.0102	4294.0	2.681	506.0	11	22.40	83.80
18	0.0102	0.0057	3622.0	2.748	471.0	00	28.20	160.20
19	0.0057	0.0030	3488.0	3.324	386.0	42	19.40	251.40

Slab 7 Time 17:32

PASS	ENT mm	EXT mm	PWR kW	SPD m/s	TEMP oC	LT	RST s	RLT s
1	0.4560	0.4400	7244.0	1.285	453.0	11	50.00	4.40
2	0.4400	0.4130	8318.0	1.329	454.0	00	7.20	4.60
3	0.4130	0.3820	8854.0	1.285	454.0	11	41.60	5.40
4	0.3820	0.3510	8586.0	1.329	456.0	00	5.00	5.60
5	0.3510	0.3200	10464.0	1.773	460.0	11	32.40	5.20
6	0.3200	0.2890	9928.0	1.773	462.0	00	6.40	5.60
7	0.2890	0.2580	9660.0	1.773	469.0	11	26.40	6.00
8	0.2580	0.2270	9124.0	1.773	471.0	00	6.40	6.80
9	0.2270	0.1960	8854.0	1.773	476.0	11	26.80	6.60
10	0.1960	0.1650	8586.0	1.773	479.0	00	6.80	8.60
11	0.1650	0.1340	8050.0	1.773	481.0	11	27.60	10.20
12	0.1340	0.1030	7648.0	1.773	485.0	00	6.40	12.60
13	0.1030	0.0720	7782.0	1.773	492.0	11	20.00	18.40
14	0.0720	0.0420	11002.0	2.216	495.0	00	60.00	23.20
15	0.0420	0.0250	11136.0	3.235	503.0	11	23.00	27.00
16	0.0250	0.0162	6172.0	3.257	510.0	00	11.60	42.00
17	0.0162	0.0098	4562.0	2.858	493.0	11	29.40	104.00
18	0.0098	0.0056	3622.0	2.703	436.0	00	14.00	138.40
19	0.0056	0.0030	3086.0	3.545	384.0	42	47.00	247.00

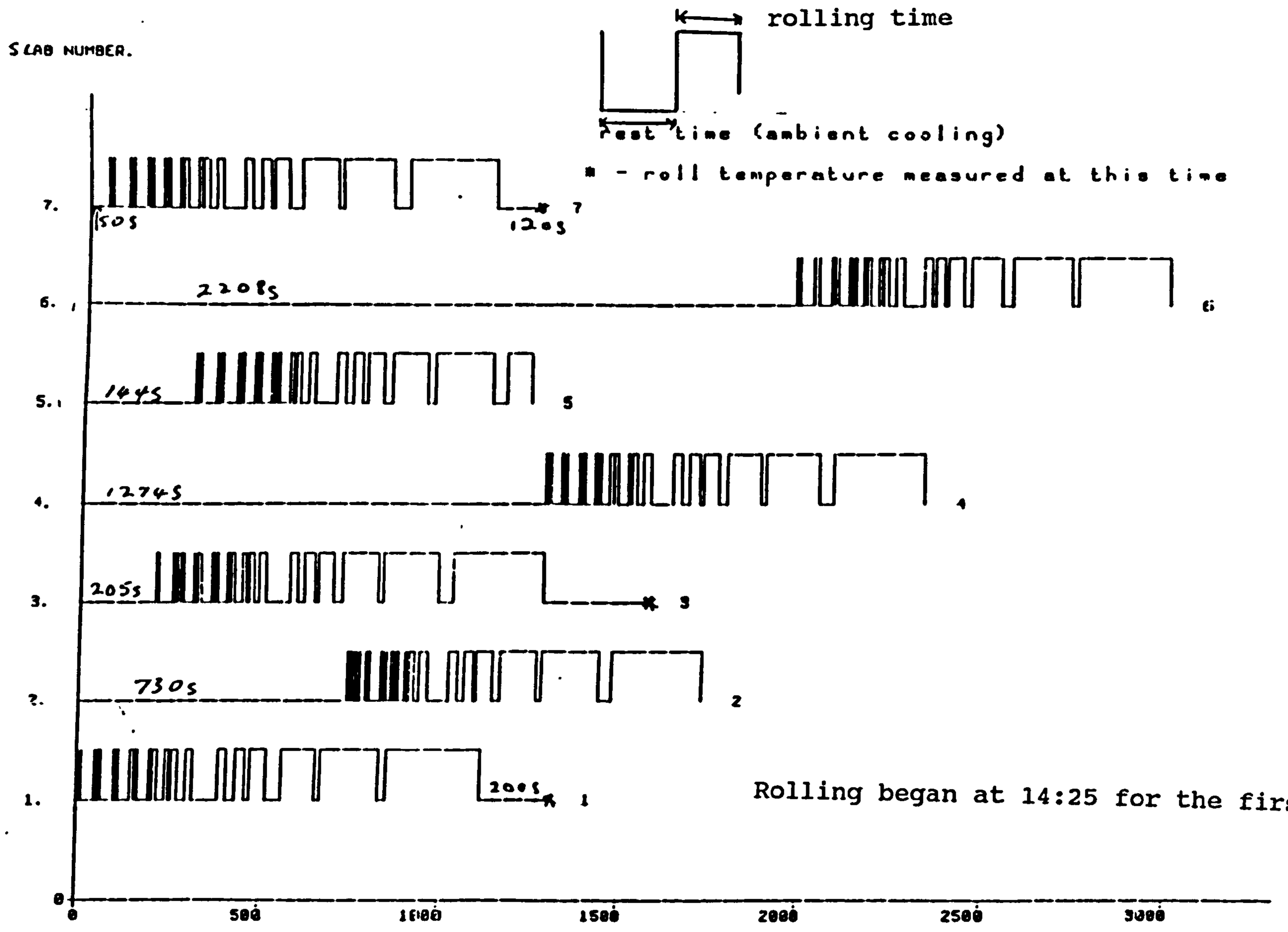

Rolling began at 14:25 for the first slab.

FIG. E3 GRAPH SHOWS MOVEMENT OF SLABS THROUGH THE MILL

Fig 4. ROLL COOLANT DISTRIBUTION FOR MILL A

SCALE 1 CM : 5 CM

1080 mm

℄

825 mm

ZONE 1 | ZONE 2 | ZONE 3 | ZONE 4 | ZONE 5

1 2 3 4 5 6 7 8 9 10 11 12 13 14 15 16 17 NOZZLE POSITIONS

Strip edge

WORK ROLL

2594 mm

ROLL END

℄

CENTRE HOLE

FIG. E5 GRAPH SHOWING DEVELOPMENT OF THERMAL CAMBER ON THE ALCOA SWANSEA WORK ROLL (MILL A)

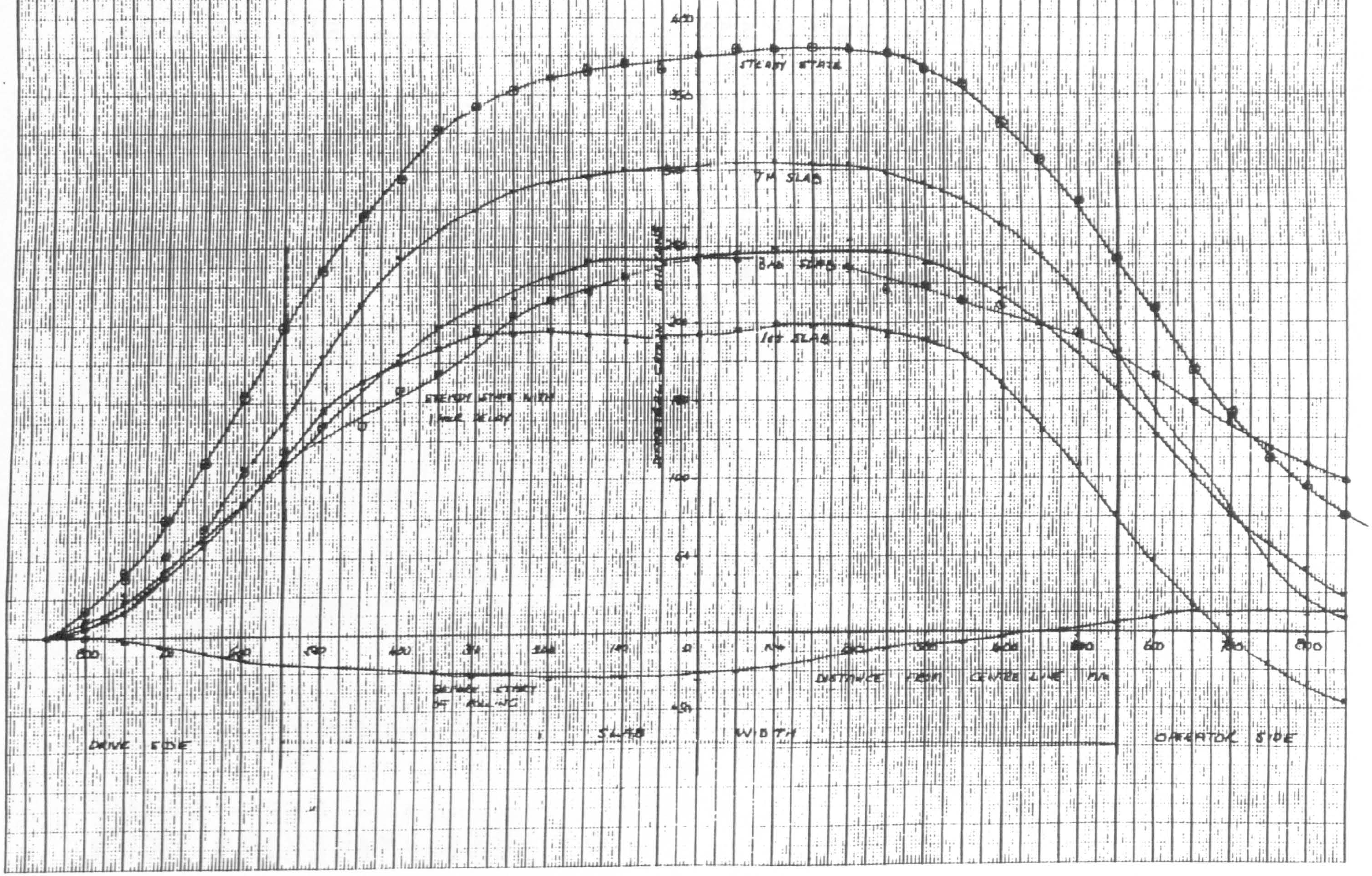

Fig.E6. Hot Aluminium Reversing Mill B - File of recorded data

Key:

PASS Pass number
ENT Entry Gauge (m)
EXT Exit Gauge (m)
PWR Motor Power (kW)
SPD Mill Speed ($m\ s^{-1}$)
TEMP Slab temperature (°C)
RST Rolling time (s)
RLT Rest time between rolling (s)

Mill B
Friday, 7th November, 1986

Roll diameter	965 mm
Barrel length	1880 mm
Total roll length	5436 mm
Initial roll temp.	20 °C
Roll end temp.	50 °C
Ambient temperature	40 °C
Coolant temperature	55 °C
Spray width	1727 mm

9 schedules
All slabs characterised as:
Alloy 3004
Size (mm) 559 x 1321 x 8179

Coil 1

PASS	ENT m	EXT m	PWR kW	SPD $m\ s^{-1}$	TEMP °C	RST s	RLT s
1	0.5588	0.5334	4229.1	1.817	535.580	134.000	5.000
2	0.5334	0.5080	4776.1	1.766	534.240	22.000	6.000
3	0.5080	0.4826	4876.1	1.807	533.230	22.000	6.000
4	0.4826	0.4572	4557.5	1.772	532.190	23.000	7.000
5	0.4572	0.4128	7538.1	1.797	531.020	22.000	7.000
6	0.4128	0.3683	7474.6	1.772	530.490	20.000	8.000
7	0.3683	0.3239	7291.8	1.812	529.930	21.000	9.000
8	0.3239	0.2794	6945.5	1.782	529.170	22.000	11.000
9	0.2794	0.2349	6663.4	1.807	528.240	19.000	12.000
10	0.2349	0.1905	6544.8	1.777	526.910	20.000	14.000
11	0.1905	0.1460	6408.2	1.812	525.220	19.000	18.000
12	0.1460	0.1041	6097.8	1.777	522.630	21.000	24.000
13	0.1041	0.0635	6709.0	1.807	517.460	36.000	37.000
14	0.0635	0.0432	3509.0	1.787	507.220	67.000	53.000
15	0.0432	0.0259	4092.5	1.807	488.300	18.000	88.000
16	0.0259	0.0160	3062.7	1.838	470.970	53.000	135.000
17	0.0160	0.0108	2050.7	2.000	425.560	61.000	192.000
18	0.0108	0.0081	1285.1	1.980	375.030	25.000	256.000
19	0.0081	0.0055	1667.9	2.472	312.300	58.000	305.000

Coil 2

PASS	ENT m	EXT m	PWR kW	SPD m/s	TEMP oC	RST s	RLT s
1	0.5588	0.5334	2944.0	1.584	535.470	139.000	4.000
2	0.5334	0.5080	4803.7	1.741	533.910	23.000	4.000
3	0.5080	0.4826	4739.6	1.817	532.910	22.000	4.000
4	0.4826	0.4572	4739.6	1.772	531.880	20.000	4.000
5	0.4572	0.4128	7838.8	1.802	530.770	22.000	5.000
6	0.4128	0.3683	7474.6	1.777	530.280	24.000	5.000
7	0.3683	0.3239	7373.9	1.812	529.550	30.000	6.000
8	0.3239	0.2794	7046.3	1.766	528.850	21.000	7.000
9	0.2794	0.2349	6772.4	1.802	527.940	21.000	9.000
10	0.2349	0.1905	6535.8	1.772	526.680	20.000	10.000
11	0.1905	0.1460	6216.4	1.807	525.000	19.000	13.000
12	0.1460	0.1041	6198.5	1.777	522.300	20.000	17.000
13	0.1041	0.0635	6709.0	1.812	517.230	37.000	26.000
14	0.0635	0.0432	3509.0	1.787	507.270	64.000	38.000
15	0.0432	0.0259	4019.4	1.817	488.420	18.000	62.000
16	0.0259	0.0160	2816.4	1.756	470.790	36.000	99.000
17	0.0160	0.0108	1932.1	1.954	423.190	67.000	137.000
18	0.0108	0.0081	1239.6	1.964	372.010	29.000	180.000
19	0.0081	0.0055	1704.5	2.442	309.580	66.000	215.000

Coil 3

PASS	ENT m	EXT m	PWR kW	SPD m/s	TEMP oC	RST s	RLT s
1	0.5588	0.5334	3910.4	1.772	535.320	152.000	4.000
2	0.5334	0.5080	4575.4	1.675	534.030	22.000	5.000
3	0.5080	0.4826	4748.5	1.802	532.970	24.000	4.000
4	0.4826	0.4572	4730.6	1.756	531.780	31.000	5.000
5	0.4572	0.4128	8185.1	1.807	530.620	26.000	5.000
6	0.4128	0.3683	7520.1	1.761	530.270	23.000	6.000
7	0.3683	0.3239	7483.6	1.807	529.730	23.000	6.000
8	0.3239	0.2794	7018.7	1.761	529.100	21.000	7.000
9	0.2794	0.2349	6891.0	1.812	528.140	24.000	8.000
10	0.2349	0.1905	6763.4	1.782	526.940	21.000	10.000
11	0.1905	0.1460	6462.7	1.807	525.450	19.000	13.000
12	0.1460	0.1041	6143.3	1.777	523.020	20.000	17.000
13	0.1041	0.0635	6745.5	1.817	517.720	41.000	26.000
14	0.0635	0.0432	3527.6	1.782	506.450	81.000	37.000
15	0.0432	0.0259	3973.9	1.751	487.060	22.000	64.000
16	0.0259	0.0160	2834.3	1.751	469.240	51.000	100.000
17	0.0160	0.0108	1941.0	1.929	421.520	74.000	139.000
18	0.0108	0.0076	1594.8	1.929	369.780	69.000	193.000
19	0.0076	0.0055	1230.6	2.437	306.990	77.000	219.000

Coil 4

PASS	ENT m	EXT m	PWR kW	SPD m/s	TEMP oC	RST s	RLT s
1	0.5588	0.5334	1841.0	1.817	517.010	1474.000	6.000
2	0.5334	0.5080	4858.2	1.782	515.330	21.000	5.000
3	0.5080	0.4826	4529.9	1.807	514.330	31.000	6.000
4	0.4826	0.4572	4475.4	1.766	513.390	18.000	7.000
5	0.4572	0.4128	7602.2	1.812	511.840	54.000	7.000
6	0.4128	0.3683	7337.3	1.777	511.480	20.000	8.000
7	0.3683	0.3239	6991.0	1.797	510.940	27.000	9.000
8	0.3239	0.2794	6918.7	1.772	510.240	23.000	9.000
9	0.2794	0.2349	6690.3	1.822	509.340	28.000	11.000
10	0.2349	0.1905	6499.3	1.782	508.270	20.000	13.000
11	0.1905	0.1460	6417.2	1.812	506.870	19.000	17.000
12	0.1460	0.1041	6106.7	1.782	504.410	29.000	23.000
13	0.1041	0.0635	6817.9	1.807	499.450	45.000	36.000
14	0.0635	0.0432	3536.6	1.782	490.360	71.000	53.000
15	0.0432	0.0259	4192.5	1.817	472.500	23.000	85.000
16	0.0259	0.0165	2816.4	1.822	457.410	37.000	129.000
17	0.0165	0.0108	2379.1	2.000	415.030	48.000	184.000
18	0.0108	0.0076	1659.0	2.000	369.590	40.000	259.000
19	0.0076	0.0055	1203.0	2.452	309.290	64.000	304.000

Coil 5

PASS	ENT m	EXT m	PWR kW	SPD m/s	TEMP oC	RST s	RLT s
1	0.5588	0.5334	2779.9	1.807	535.170	163.000	6.000
2	0.5334	0.5080	5095.5	1.766	533.530	28.000	5.000
3	0.5080	0.4826	4958.2	1.812	532.610	23.000	5.000
4	0.4826	0.4572	4785.1	1.772	531.680	19.000	7.000
5	0.4572	0.4128	7976.1	1.797	530.580	23.000	7.000
6	0.4128	0.3683	7620.1	1.777	530.210	21.000	8.000
7	0.3683	0.3239	7438.1	1.807	529.750	20.000	9.000
8	0.3239	0.2794	6863.4	1.772	529.110	21.000	11.000
9	0.2794	0.2349	7018.7	1.812	528.090	23.000	11.000
10	0.2349	0.1905	6709.0	1.782	527.000	20.000	13.000
11	0.1905	0.1460	6653.7	1.817	525.310	24.000	17.000
12	0.1460	0.1041	6335.1	1.782	522.800	26.000	23.000
13	0.1041	0.0635	7000.7	1.812	518.120	34.000	36.000
14	0.0635	0.0432	3627.6	1.782	509.110	60.000	54.000
15	0.0432	0.0259	4220.1	1.817	489.670	26.000	86.000
16	0.0259	0.0165	2853.0	1.858	473.100	43.000	129.000
17	0.0165	0.0108	2351.5	1.975	428.370	47.000	190.000
18	0.0108	0.0076	1667.9	1.985	380.070	37.000	265.000
19	0.0076	0.0055	1211.9	2.431	317.040	44.000	310.000

Coil 6

PASS	ENT m	EXT m	PWR kW	SPD m/s	TEMP oC	RST s	RLT s
1	0.5588	0.5334	1850.0	1.853	530.100	521.000	6.000
2	0.5334	0.5080	5204.5	1.726	528.350	22.000	5.000
3	0.5080	0.4826	4812.7	1.766	527.580	20.000	6.000
4	0.4826	0.4572	4758.2	1.741	526.680	19.000	6.000
5	0.4572	0.4128	7793.3	1.756	525.640	24.000	7.000
6	0.4128	0.3683	7501.5	1.766	525.340	20.000	8.000
7	0.3683	0.3239	7520.1	1.812	524.810	28.000	8.000
8	0.3239	0.2794	7291.8	1.782	524.280	23.000	9.000
9	0.2794	0.2349	7027.6	1.817	523.630	22.000	11.000
10	0.2349	0.1905	6626.9	1.777	522.650	22.000	14.000
11	0.1905	0.1460	6699.3	1.807	520.060	57.000	17.000
12	0.1460	0.1041	6316.4	1.782	516.990	48.000	23.000
13	0.1041	0.0635	7046.3	1.812	510.830	69.000	35.000
14	0.0635	0.0432	3026.1	1.497	494.980	144.000	62.000
15	0.0432	0.0259	4520.9	1.817	465.960	111.000	84.000
16	0.0259	0.0165	2889.6	1.736	453.350	44.000	133.000
17	0.0165	0.0108	2442.5	1.959	412.180	54.000	186.000
18	0.0108	0.0076	1694.8	1.990	368.410	34.000	260.000
19	0.0076	0.0055	1056.7	2.401	309.440	54.000	305.000

Coil 7

PASS	ENT m	EXT m	PWR kW	SPD m/s	TEMP oC	RST s	RLT s
1	0.5588	0.5334	218.7	1.721	535.670	127.000	4.000
2	0.5334	0.5080	5113.4	1.772	533.440	23.000	5.000
3	0.5080	0.4826	4830.6	1.817	532.600	20.000	6.000
4	0.4826	0.4572	4940.3	1.777	531.620	22.000	5.000
5	0.4572	0.4128	8258.2	1.817	530.620	23.000	6.000
6	0.4128	0.3683	7911.9	1.777	530.350	23.000	7.000
7	0.3683	0.3239	7492.5	1.812	529.980	25.000	8.000
8	0.3239	0.2794	7200.7	1.772	529.460	20.000	10.000
9	0.2794	0.2349	7082.1	1.812	528.720	22.000	10.000
10	0.2349	0.1905	6936.6	1.777	527.600	26.000	12.000
11	0.1905	0.1460	6644.8	1.807	526.370	19.000	17.000
12	0.1460	0.1041	6389.6	1.782	524.210	21.000	22.000
13	0.1041	0.0635	7000.7	1.797	517.680	72.000	36.000
14	0.0635	0.0432	3062.7	1.482	498.370	178.000	63.000
15	0.0432	0.0259	4648.5	1.792	464.090	157.000	84.000
16	0.0259	0.0165	3344.8	1.949	452.300	35.000	120.000
17	0.0165	0.0108	2533.6	1.949	415.270	40.000	189.000
18	0.0108	0.0076	1722.4	1.980	371.510	28.000	264.000
19	0.0076	0.0055	947.8	2.091	311.410	181.000	354.000

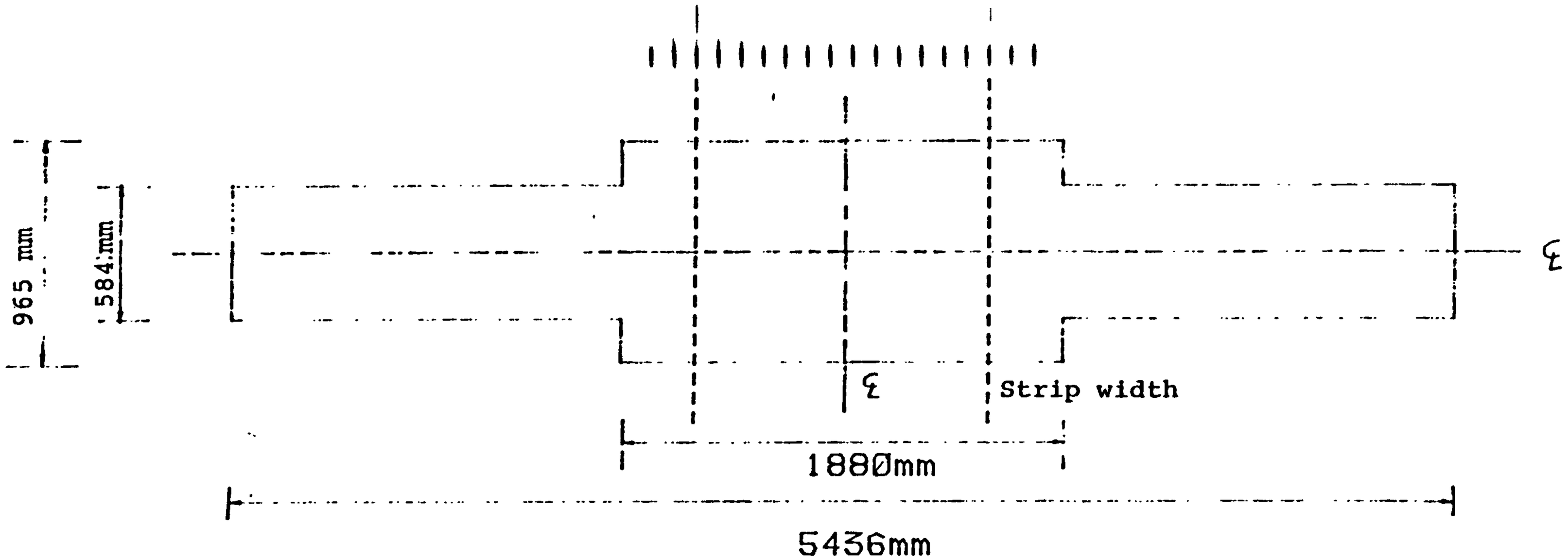
965 mm
584 mm
℄
Strip width
1880mm
5436mm

S

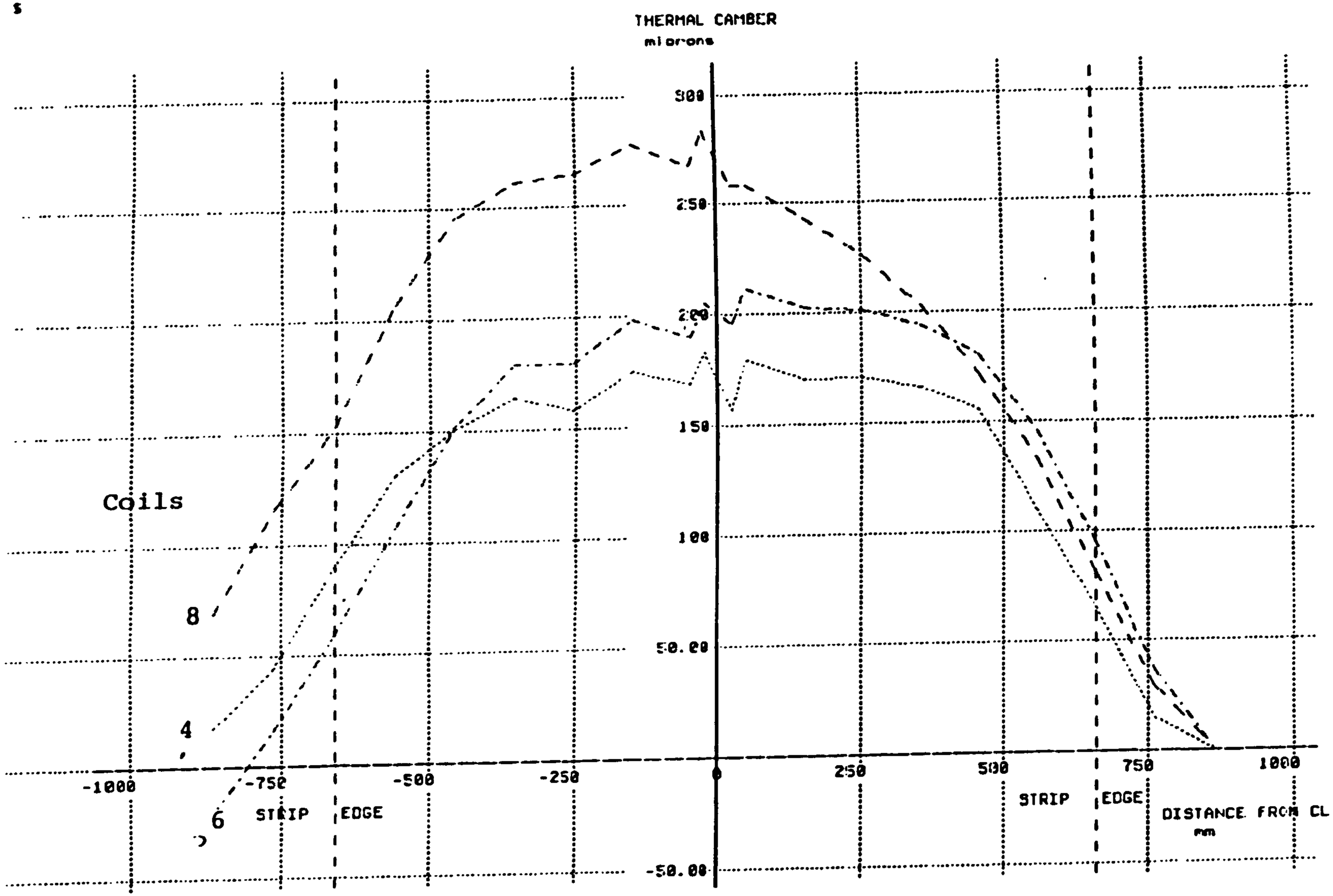

HOT MILL B .7/11/86. SLAB (3004)/ 4,6,8

APPENDIX F

GRAPHS COMPARING MEASURED TEMPERATURES AND THERMAL CAMBERS TO CALCULATED VALUES

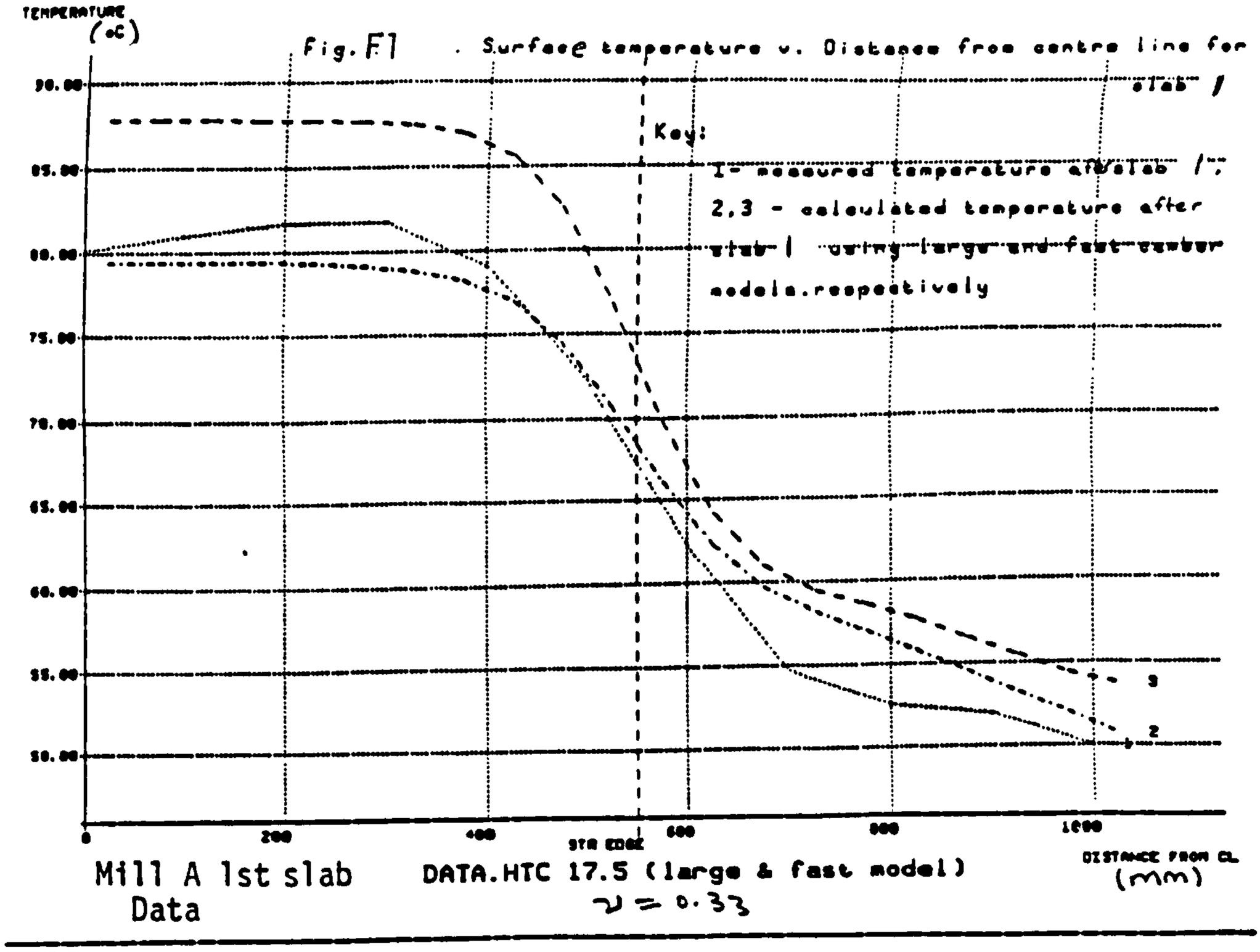

Fig. F1 . Surface temperature v. Distance from centre line for slab 1

Mill A 1st slab Data

DATA.HTC 17.5 (large & fast model) $\nu = 0.33$

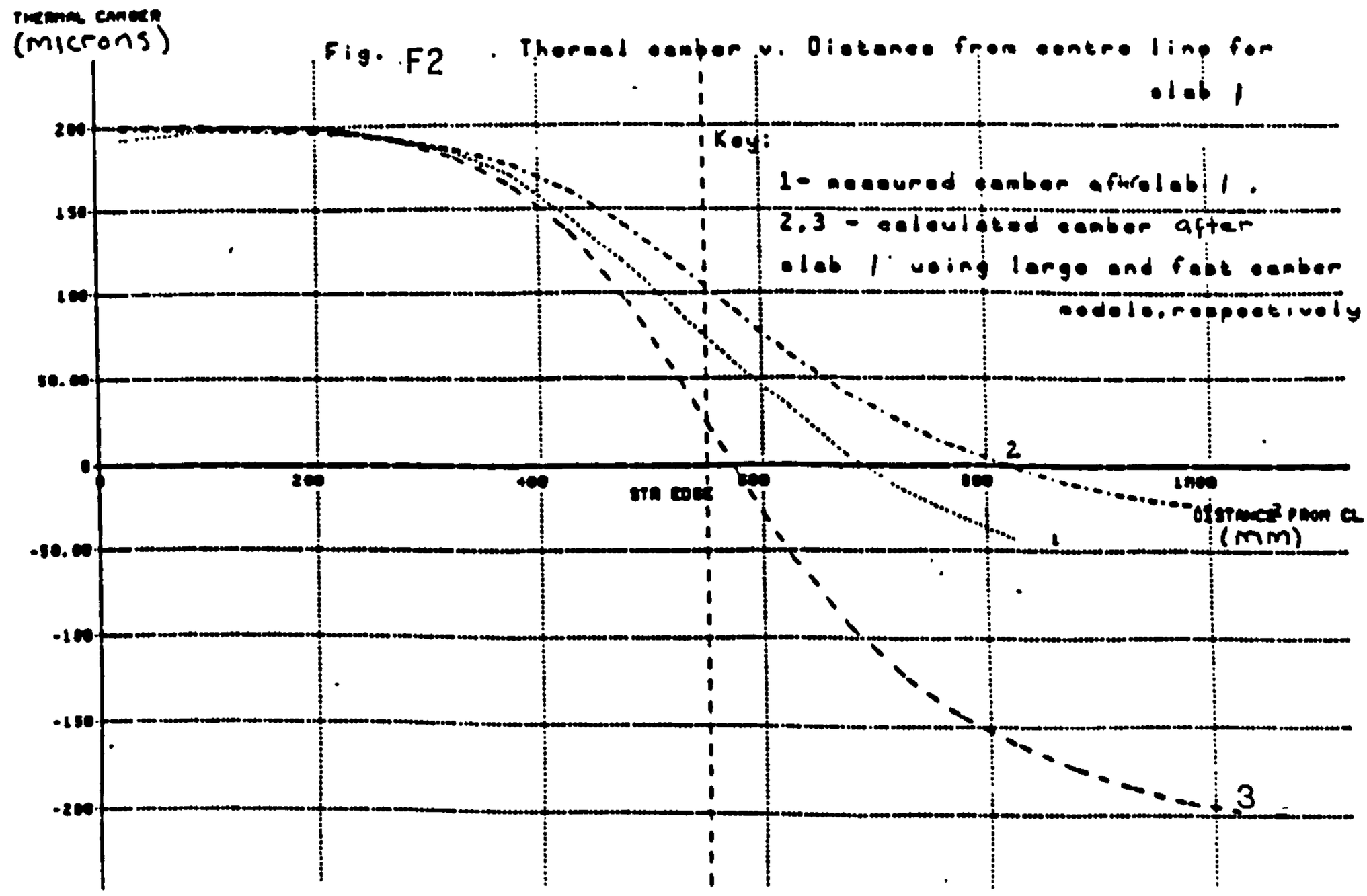

Fig. F2 . Thermal camber v. Distance from centre line for slab 1

Mill A 1st slab Data

DATA.HTC 17.5 (large & fast model) $\nu = 0.33$

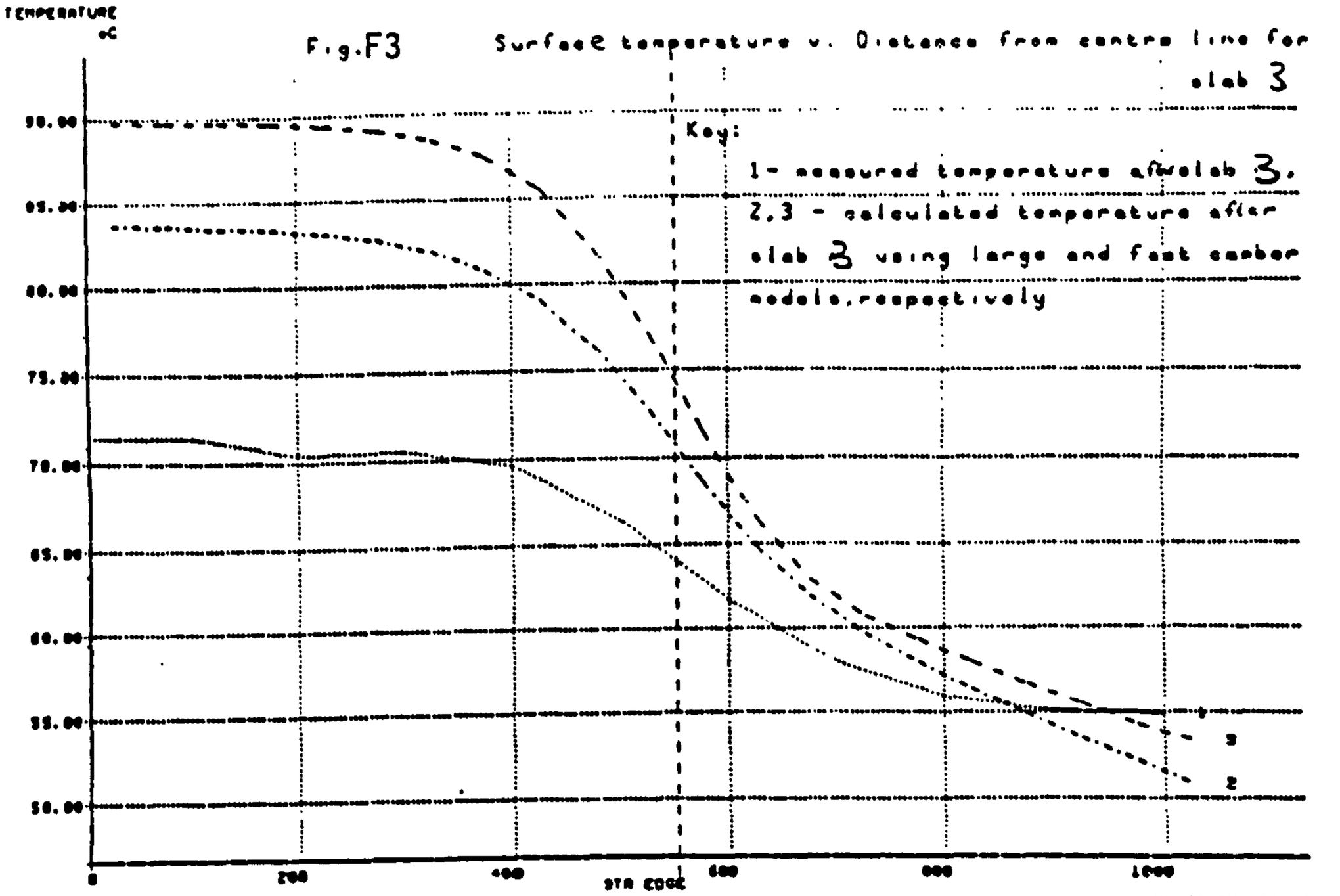

Fig.F3 Surface temperature v. Distance from centre line for slab 3

Mill A slab 1-3 data DATA.HTC 17.5 (large & fast model) $\nu = 0.33$

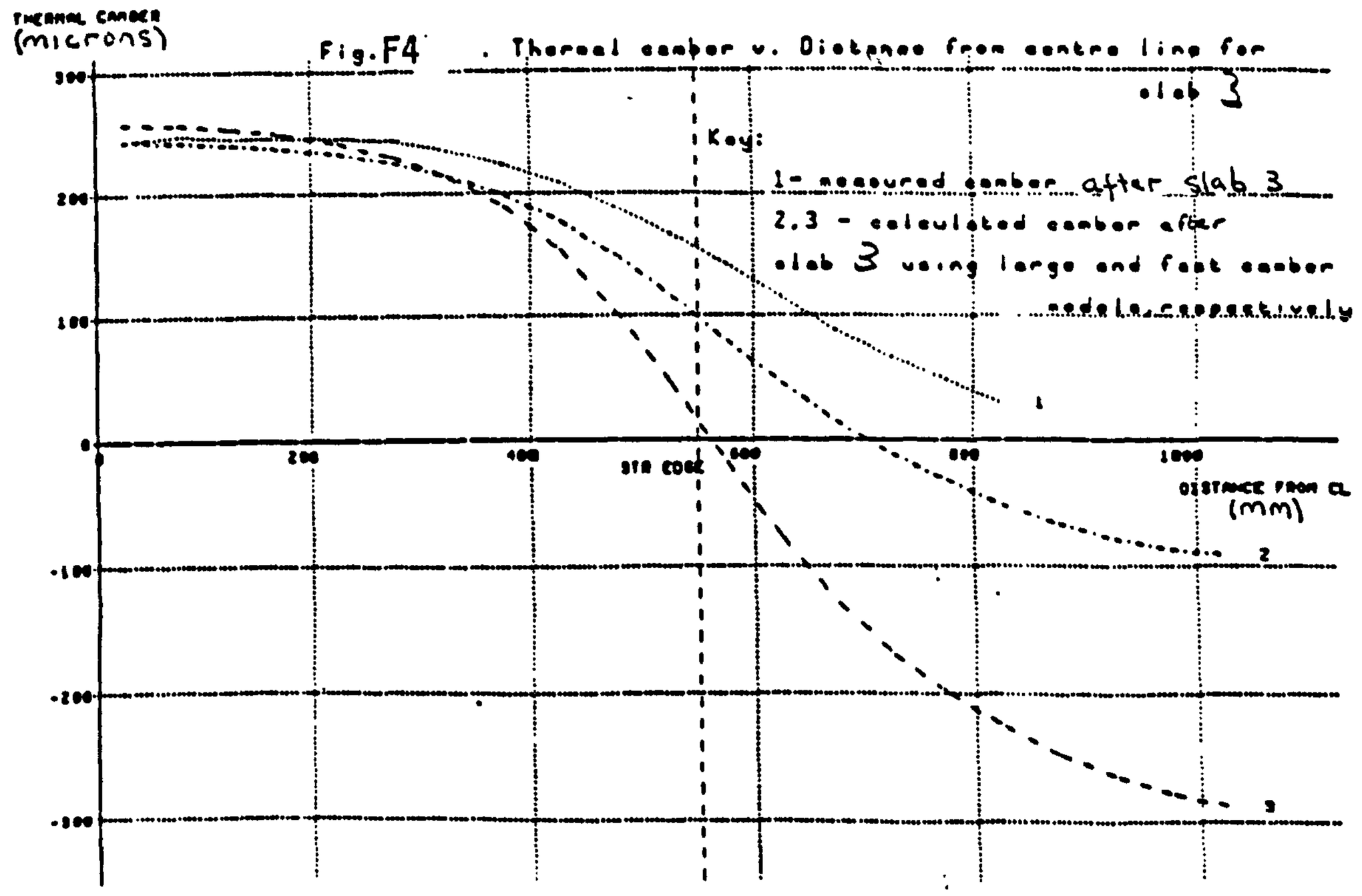

Fig.F4 . Thermal camber v. Distance from centre line for slab 3

Mill A slab 1-3 Data DATA.HTC 17.5 (large & fast model) $\nu = 0.33$

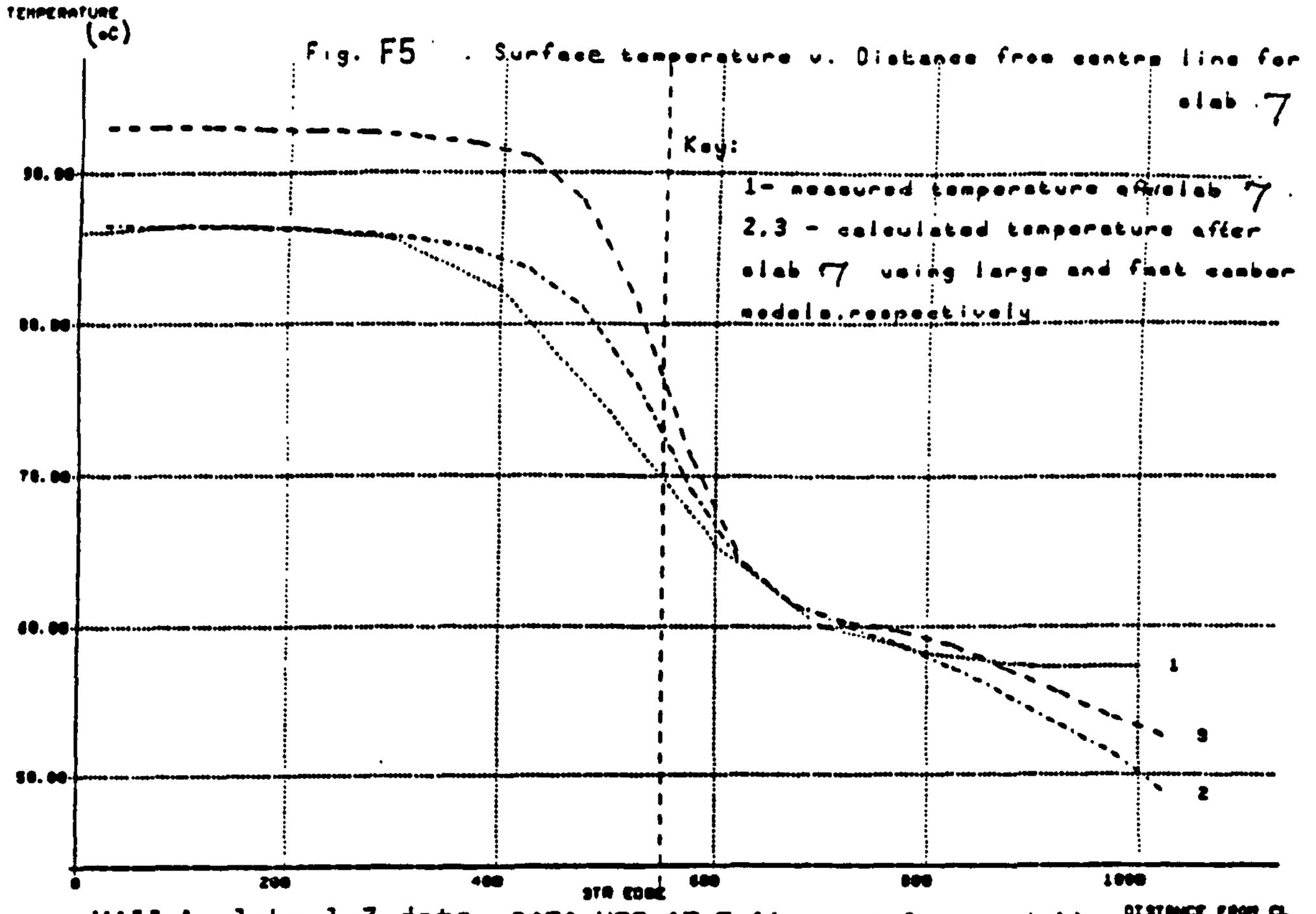

Fig. F5 . Surface temperature v. Distance from centre line for slab 7

Key:
1- measured temperature after slab 7.
2,3 - calculated temperature after slab 7 using large and fast camber models, respectively

Mill A slabs 1-7 data DATA.HTC 17.5 (large & fast model)
$\nu = 0.33$

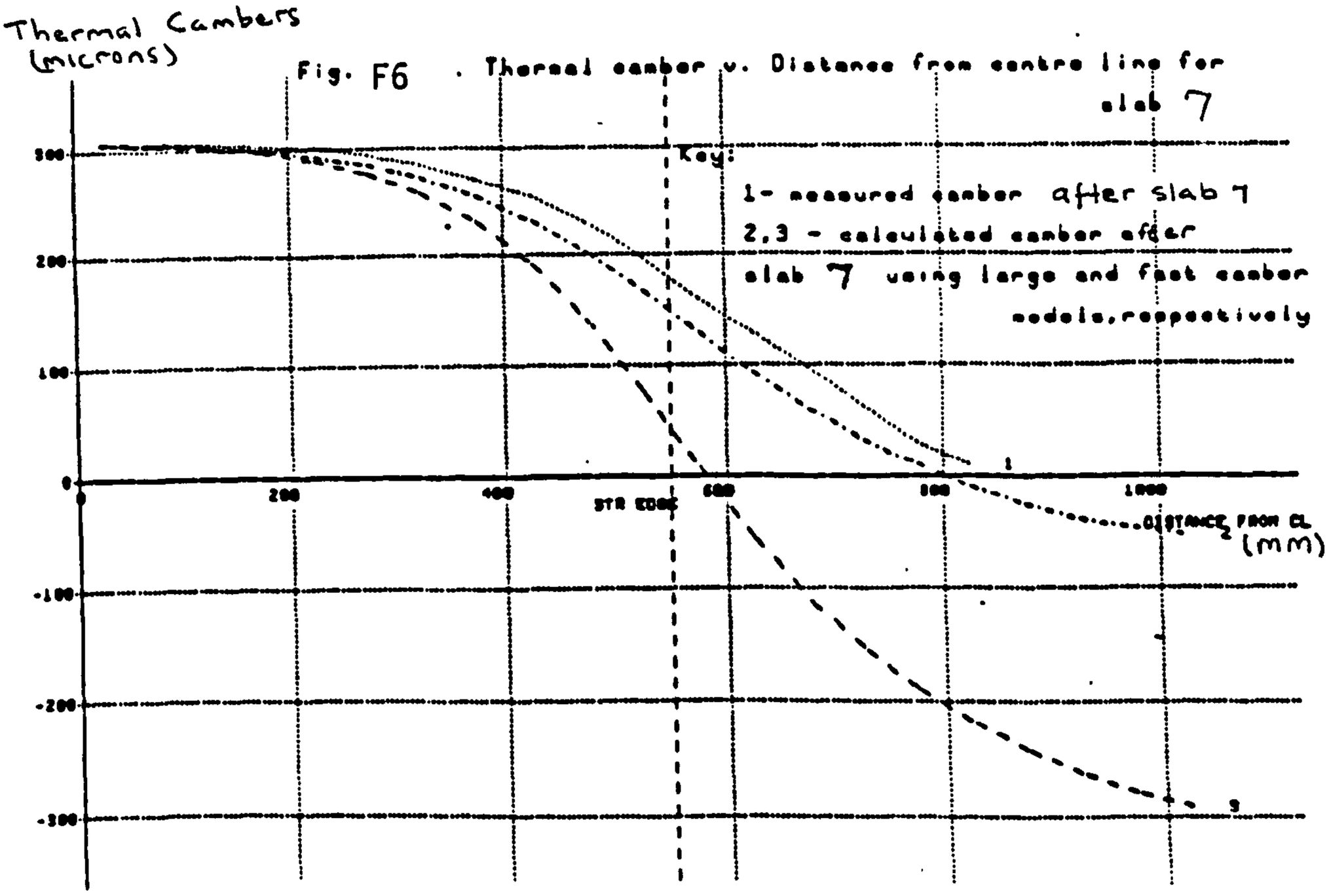

Fig. F6 . Thermal camber v. Distance from centre line for slab 7

Key:
1- measured camber after slab 7
2,3 - calculated camber after slab 7 using large and fast camber models, respectively

Mill A slabs 1-7 data .HTC 17.5 (large & fast model)
$\nu = 0.33$

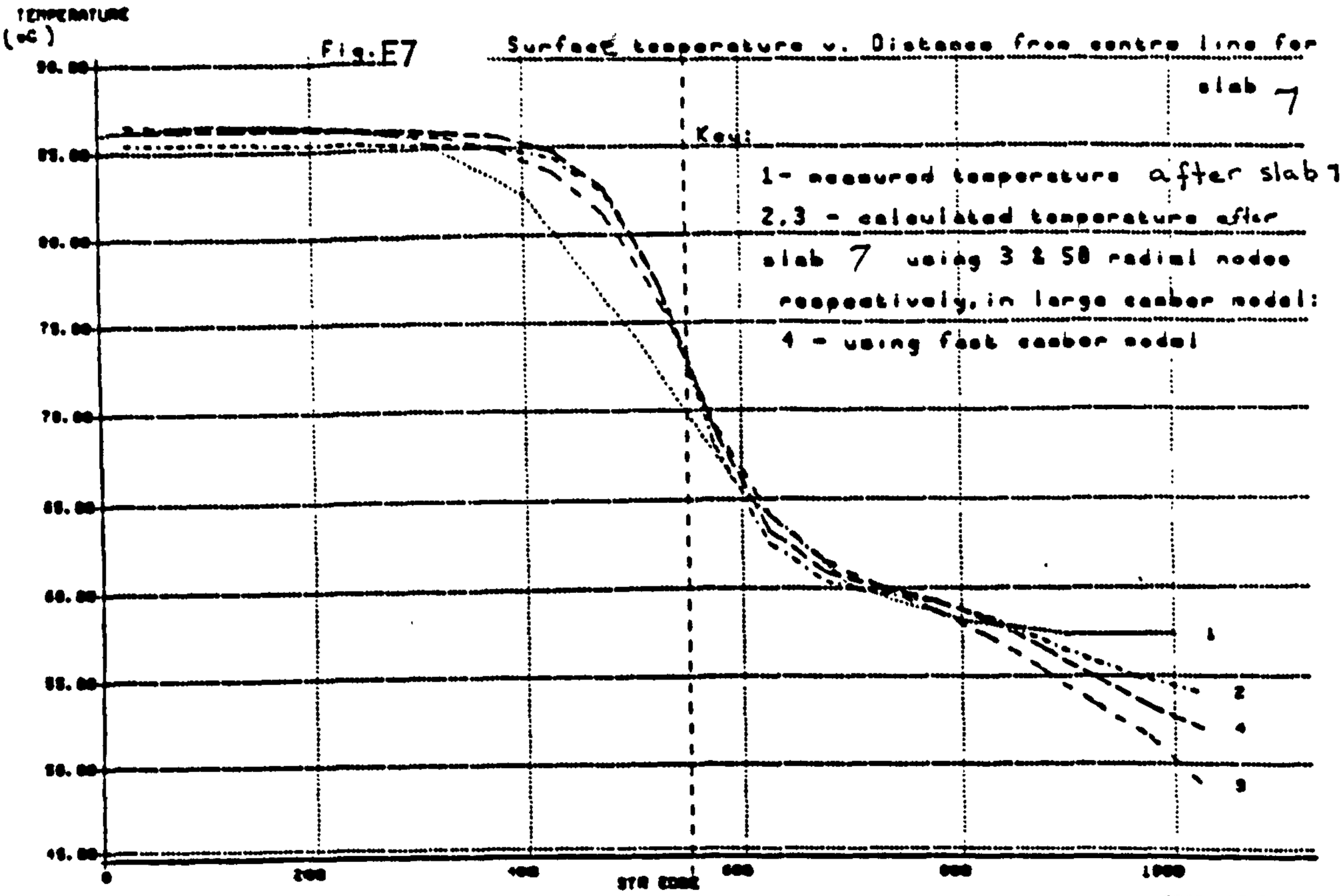

Mill A :slabs HTC=17.5 (large) and 22.0 (fast) model 1-7 data

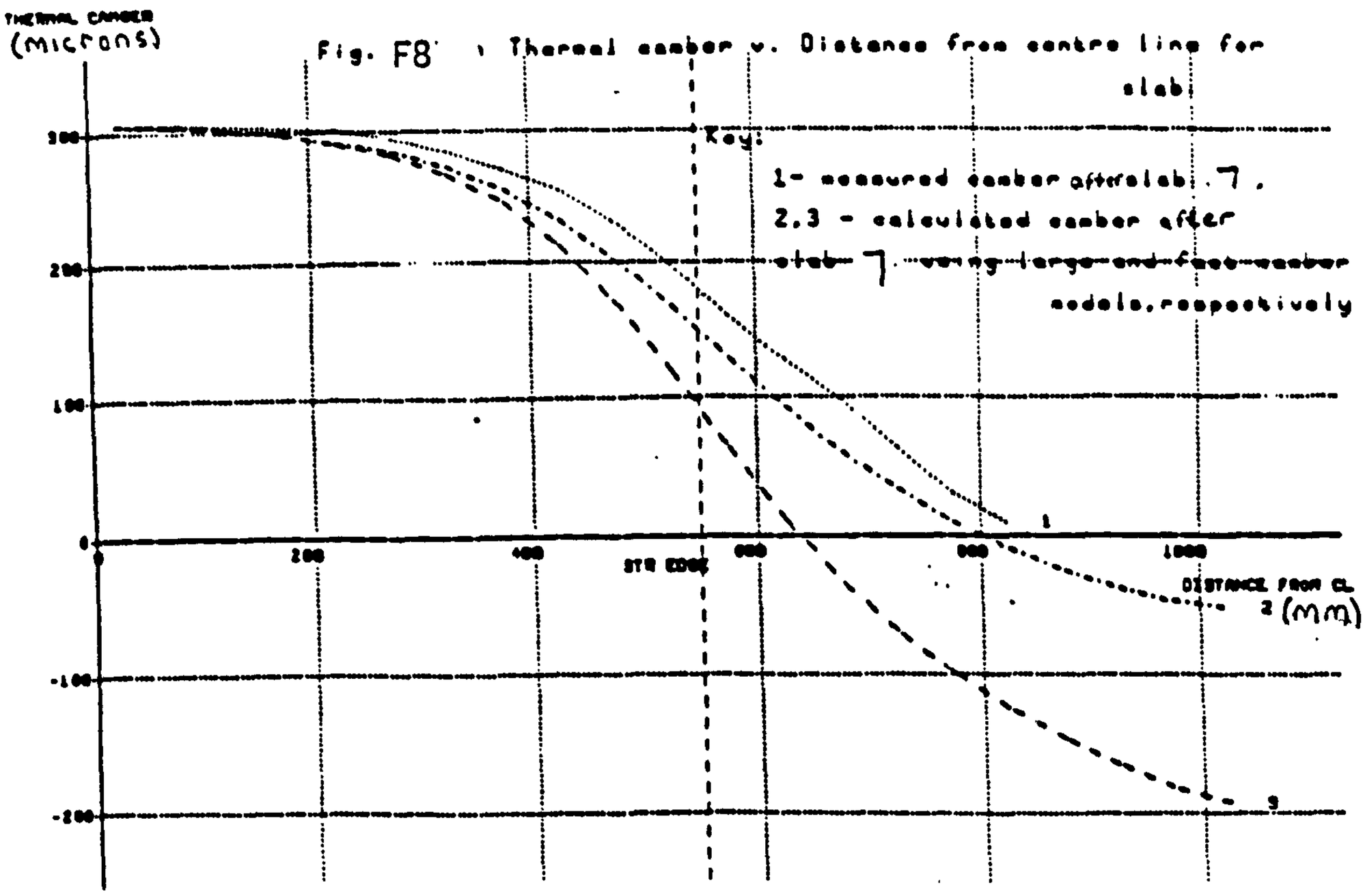

Mill-A slabs 1-7 data : DATA.HTC 17.5 (large) & 22. (fast model) $\nu = 0.3$

Thermal Cambers (microns)

Fig. F9 Thereal camber v. Distance from centre line for seventh slab rolled

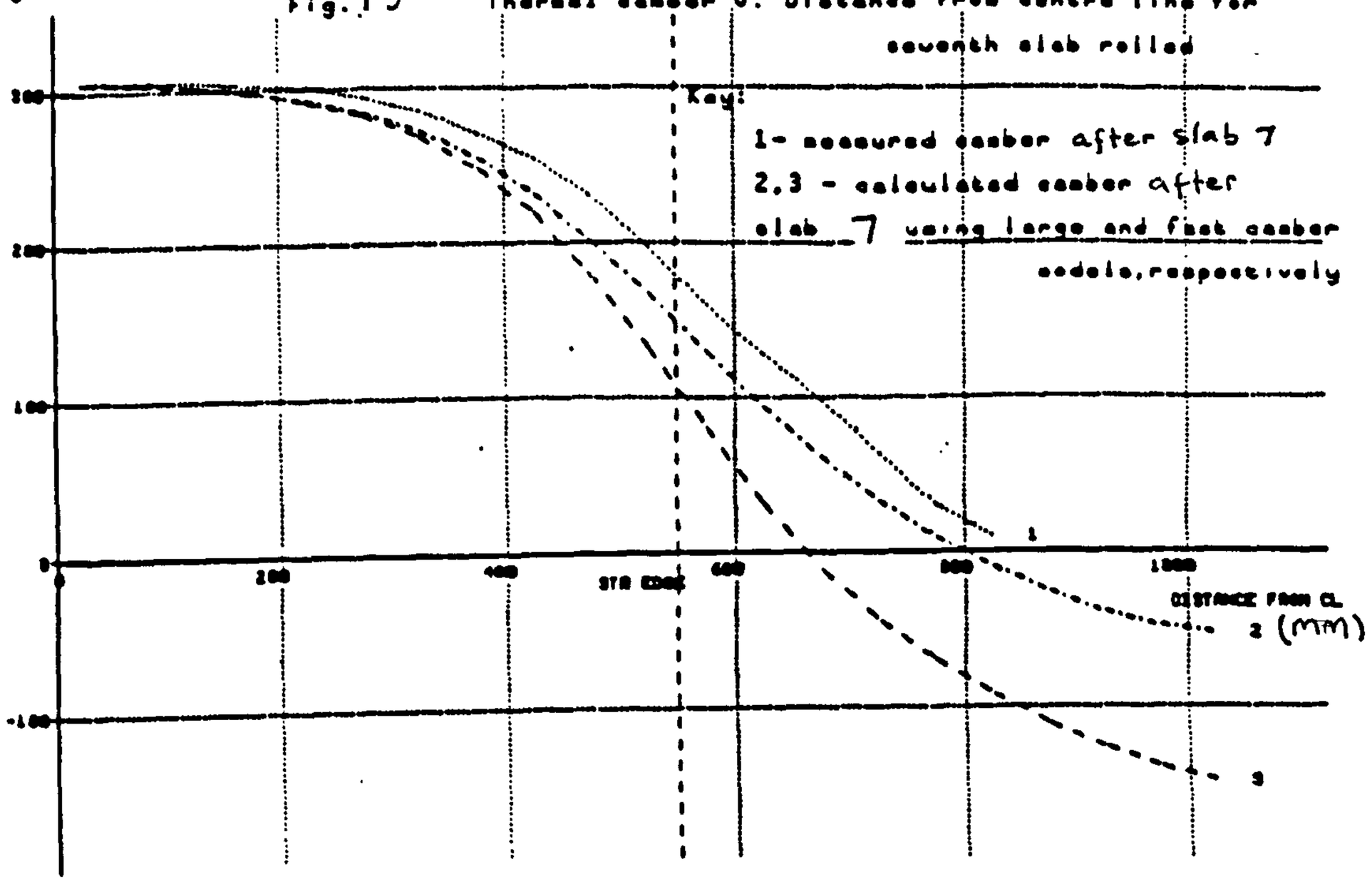

Mill A slabs 1-7 data

DATA HTC=17.5 (large and fast model[μ=0])

Fig. F10 Thereal camber v. Distance from centre line for seventh slab rolled

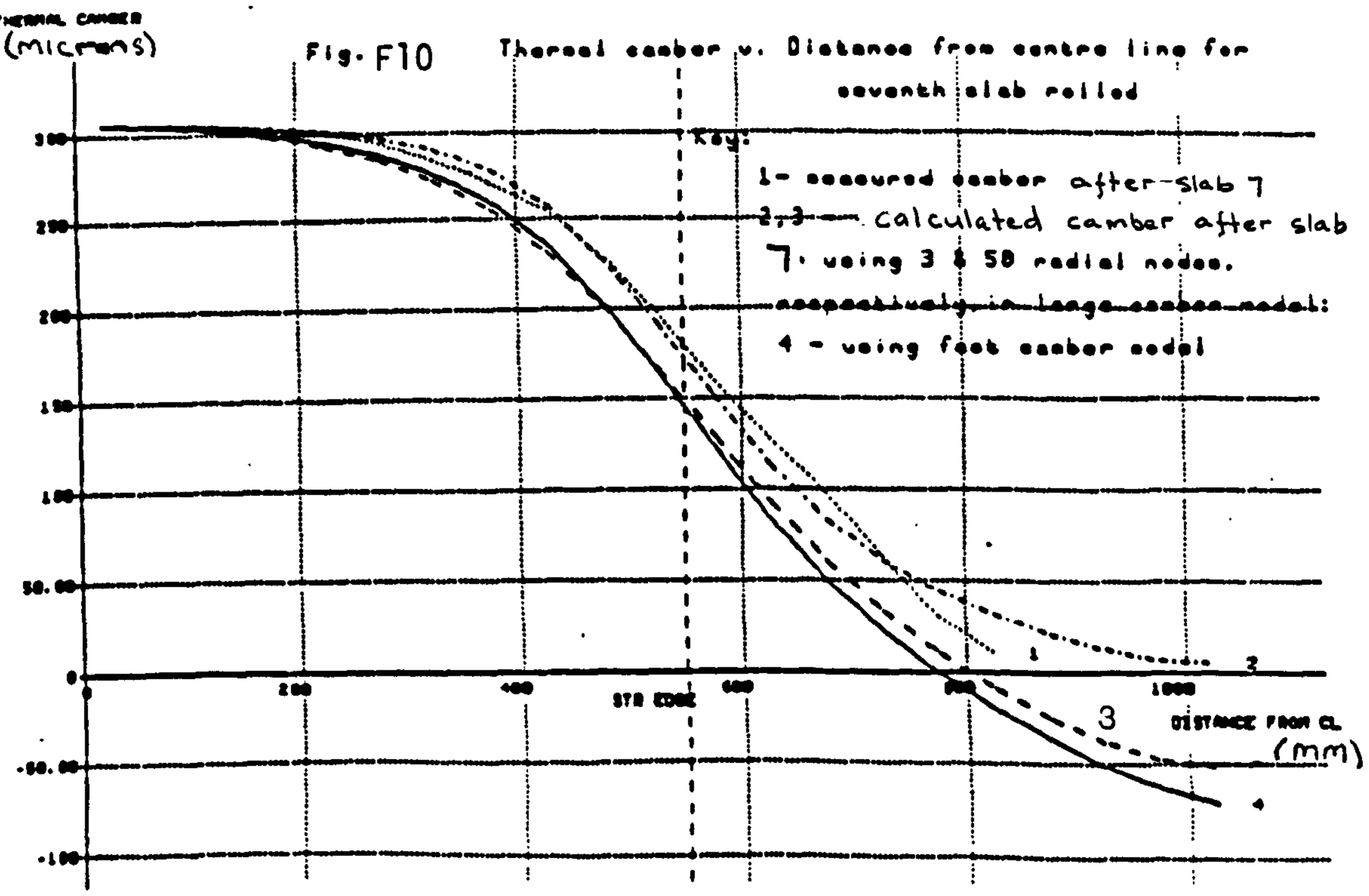

Mill A slabs 1-7 data

HTC=17.5 (large) and 22.0 (fast) model (μ=0)

Fig. F11 Thermal camber v. distance from roll centre line after 4 coils were rolled

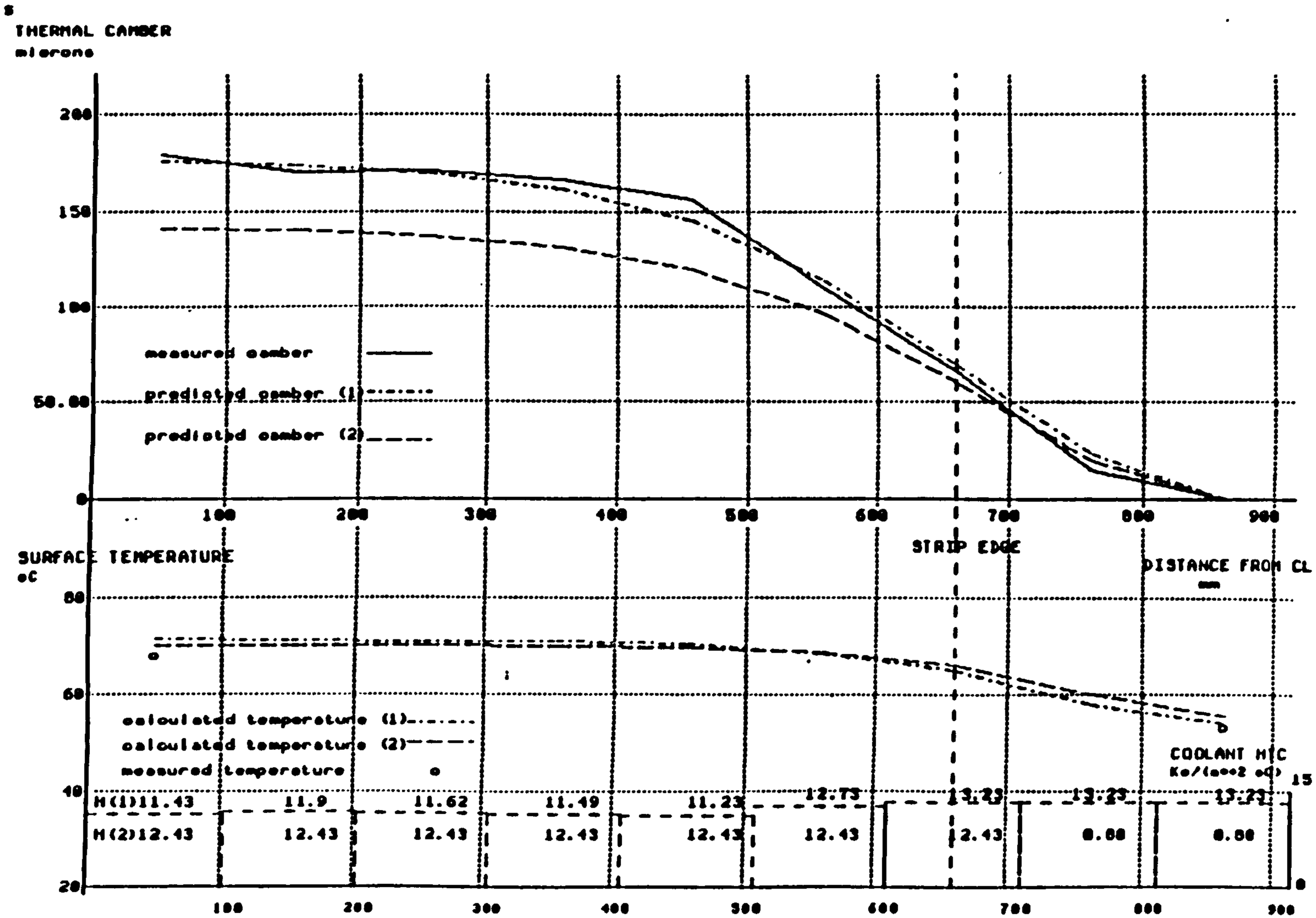

Mill B HOT MILL.7/11/86. SLAB (3004)/ 4

Fig. F12 Thermal camber v. distance from roll centre line after 6 coils were rolled.
Cambers calculated as normal.

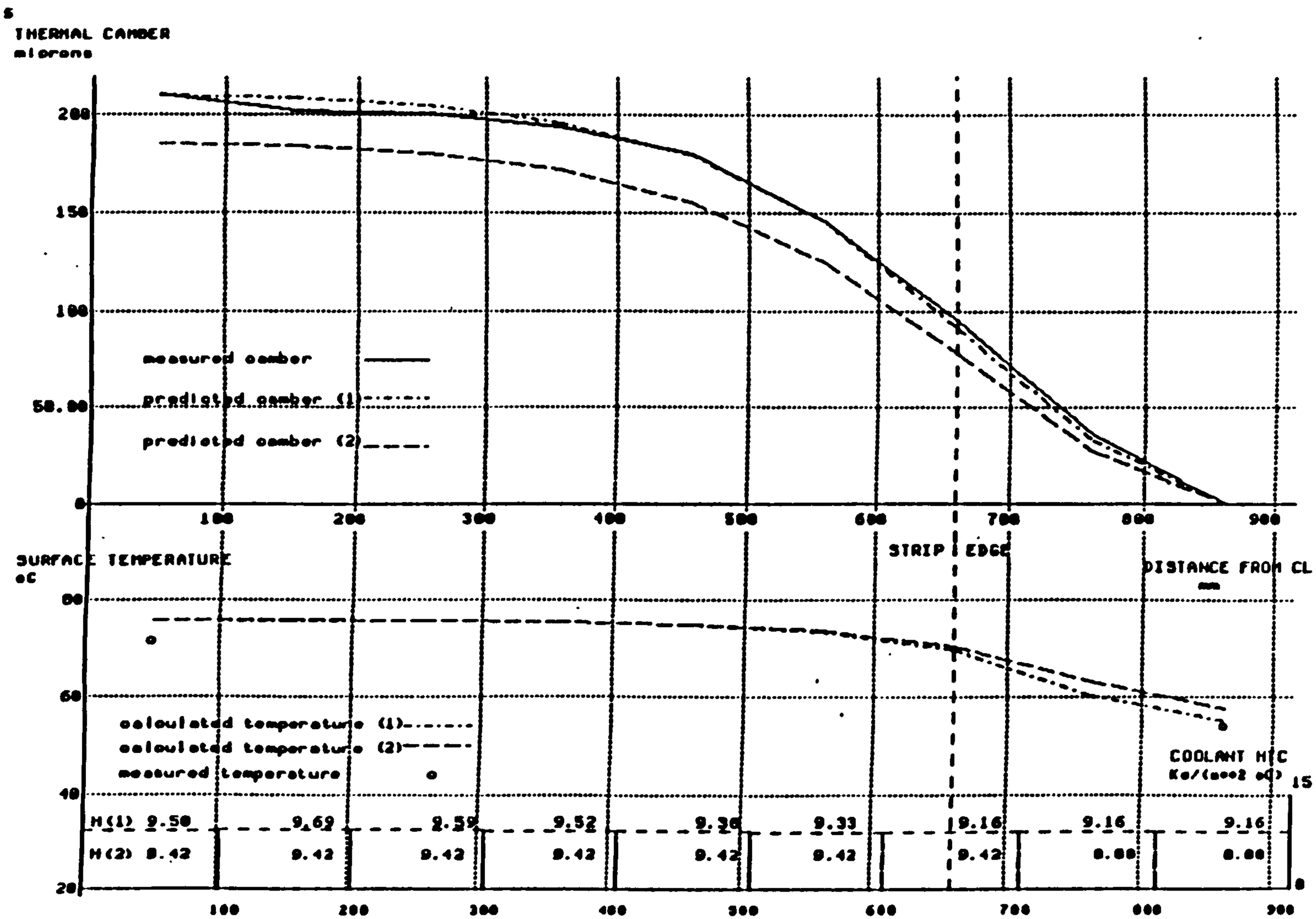

Mill B HOT MILL.7/11/86. SLAB (3004)/ 6

distance from roll centre line after 8 coils were rolled.

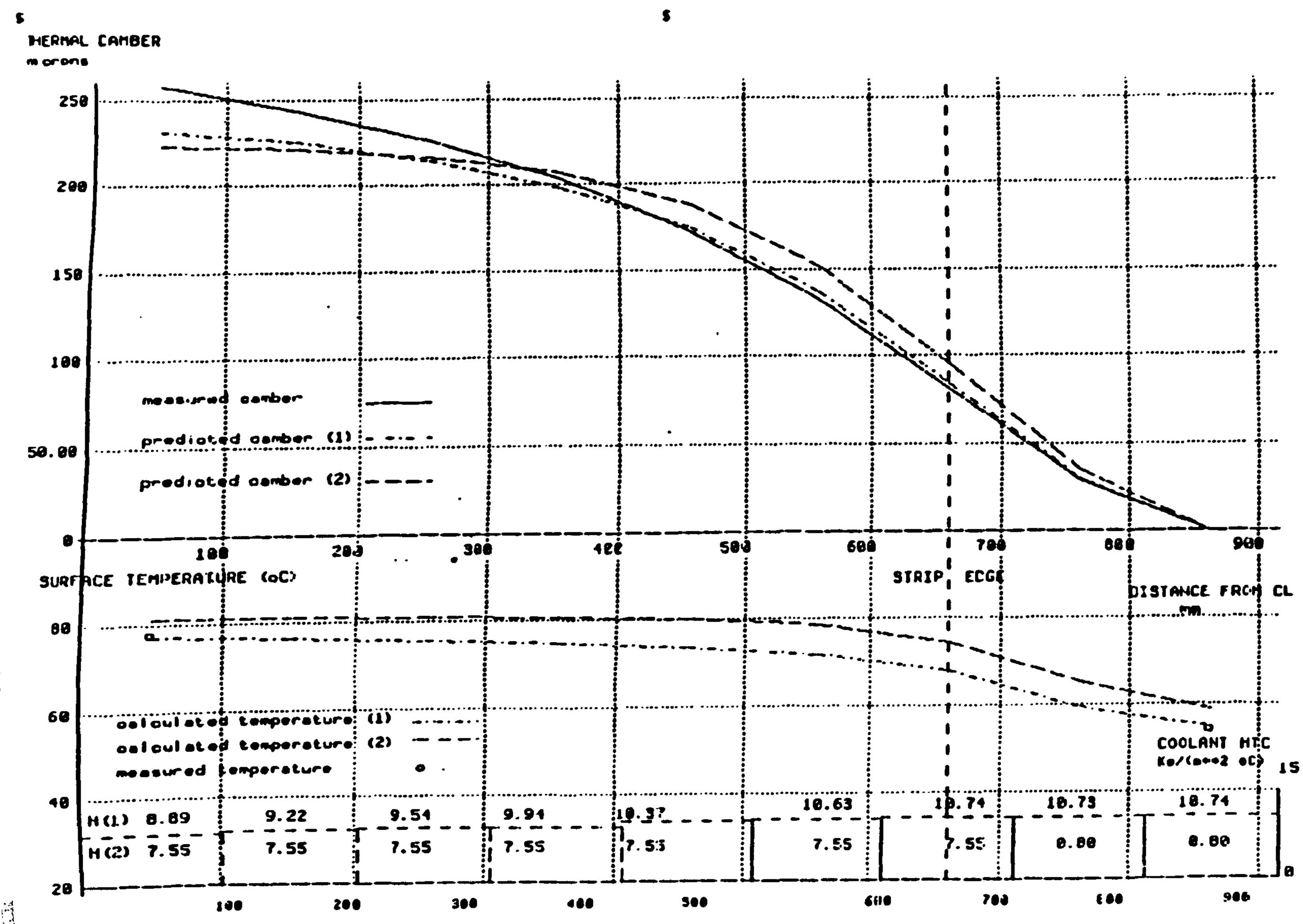

Mill B

HOT MILL. 7/11/86. SLAB (3004)/ 8

APPENDIX G

GRAPHS SHOWING VARIATION OF ROLL SURFACE TEMPERATURE AND ROLL DIAMETRAL EXPANSION WITH HEAT TRANSFER COEFFICIENT

Fig. G1

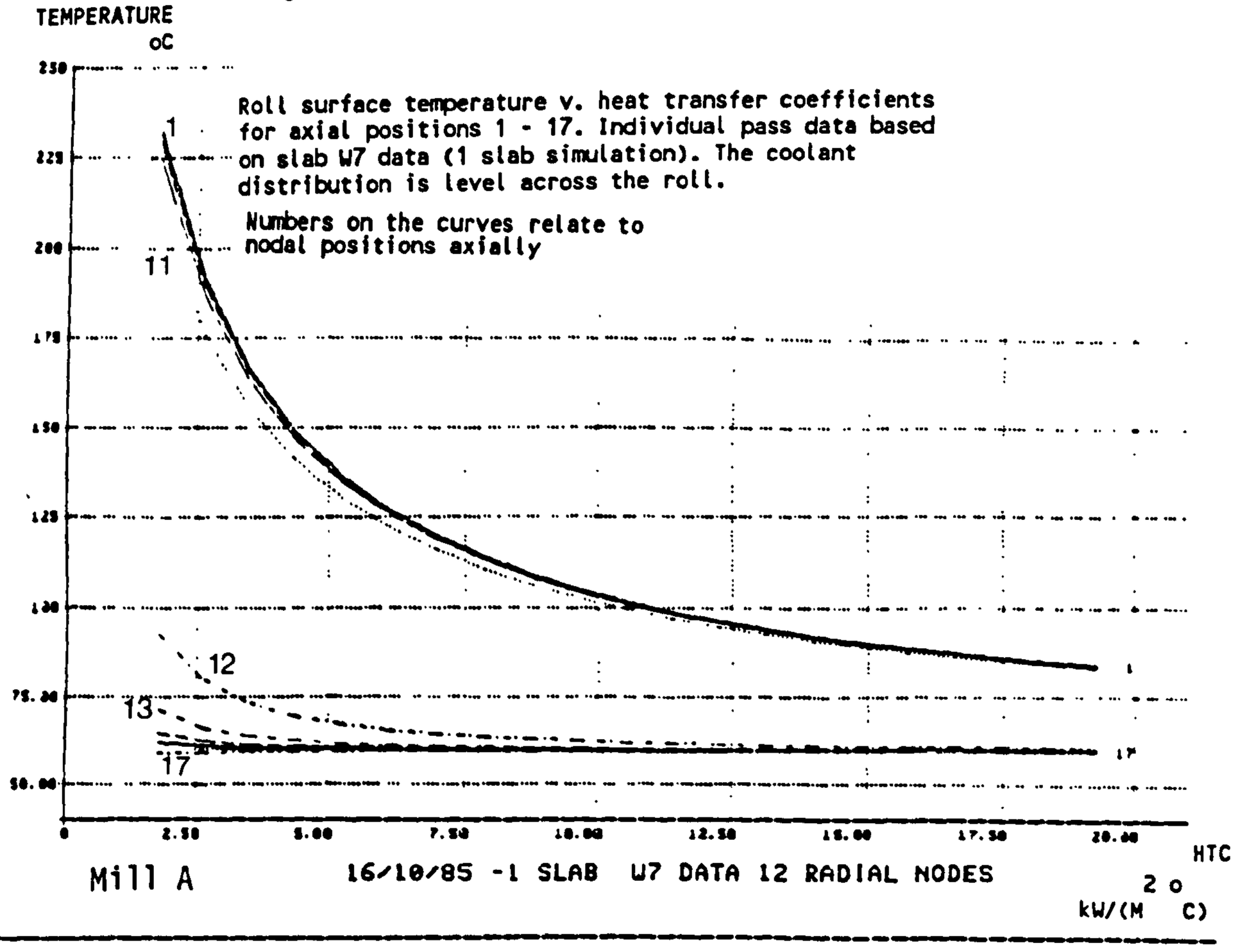
TEMPERATURE
oC
250
225
200
175
150
125
100
75.00
50.00
1
11
12
13
17
Roll surface temperature v. heat transfer coefficients for axial positions 1 - 17. Individual pass data based on slab W7 data (1 slab simulation). The coolant distribution is level across the roll.
Numbers on the curves relate to nodal positions axially
0
2.50
5.00
7.50
10.00
12.50
15.00
17.50
20.00
HTC
2 o
kW/(M C)
Mill A
16/10/85 -1 SLAB W7 DATA 12 RADIAL NODES

Fig. G2

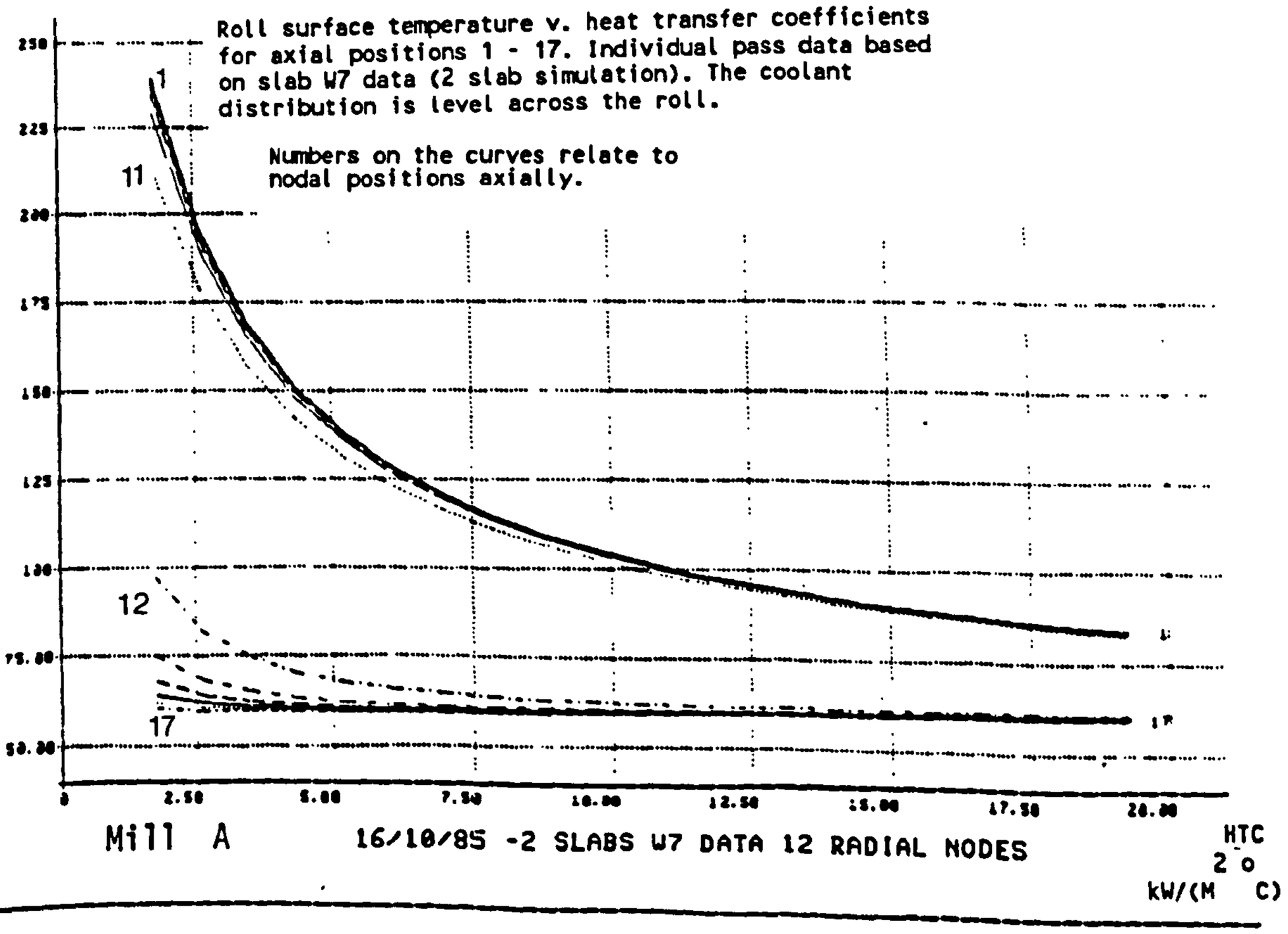
TEMPERATURE
oC
250
225
200
175
150
125
100
75.00
50.00
1
11
12
17
Roll surface temperature v. heat transfer coefficients for axial positions 1 - 17. Individual pass data based on slab W7 data (2 slab simulation). The coolant distribution is level across the roll.
Numbers on the curves relate to nodal positions axially.
0
2.50
5.00
7.50
10.00
12.50
15.00
17.50
20.00
HTC
2 o
kW/(M C)
Mill A
16/10/85 -2 SLABS W7 DATA 12 RADIAL NODES

Fig. G3

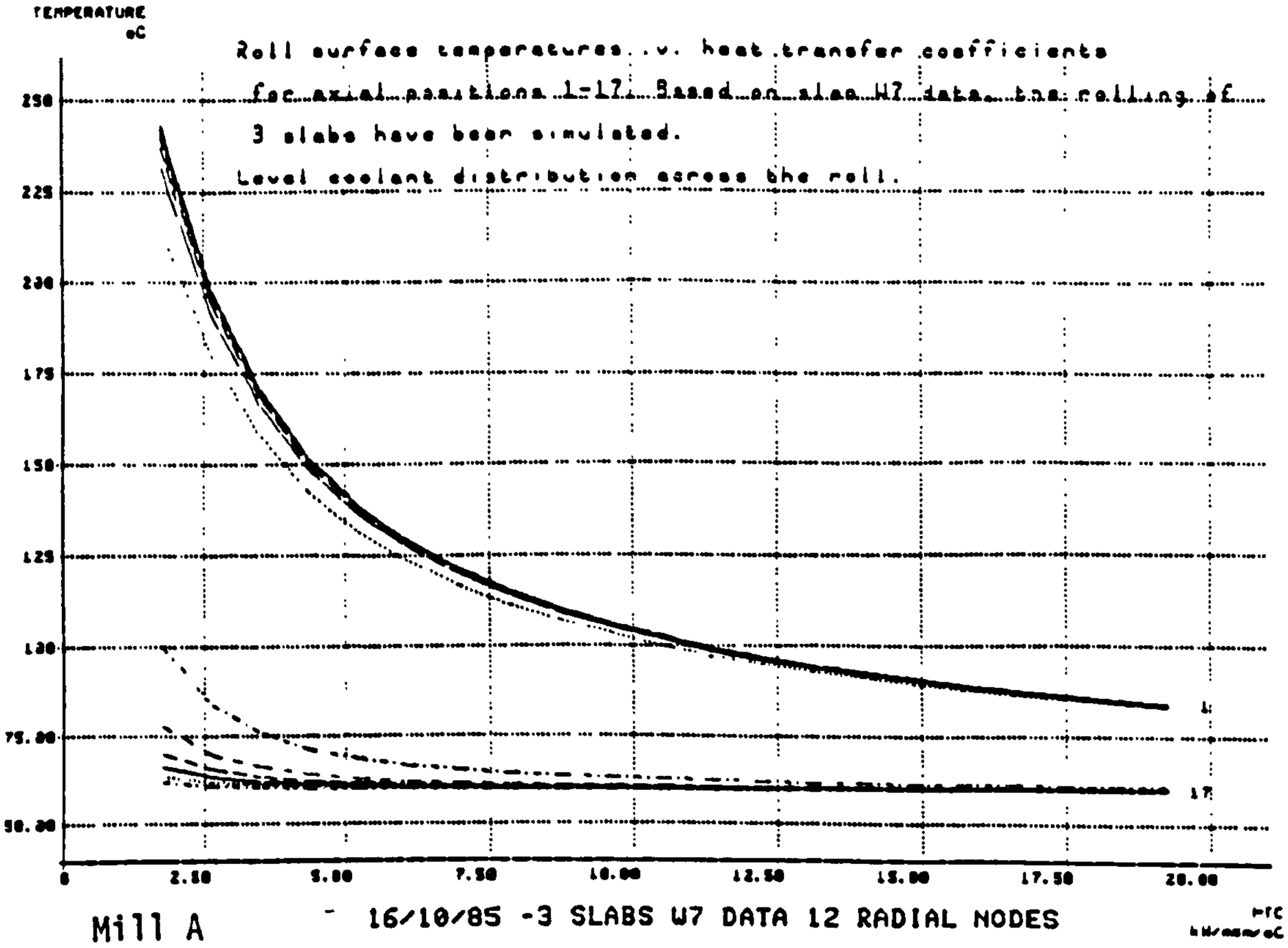
TEMPERATURE
oC
Roll surface temperatures .v. heat transfer coefficients
for axial positions 1-17. Based on slab W7 data. the rolling of
3 slabs have been simulated.
Level coolant distribution across the roll.
250
225
200
175
150
125
100
75.00
50.00
0
2.50
5.00
7.50
10.00
12.50
15.00
17.50
20.00
Mill A
16/10/85 -3 SLABS W7 DATA 12 RADIAL NODES
HTC

Fig. G4

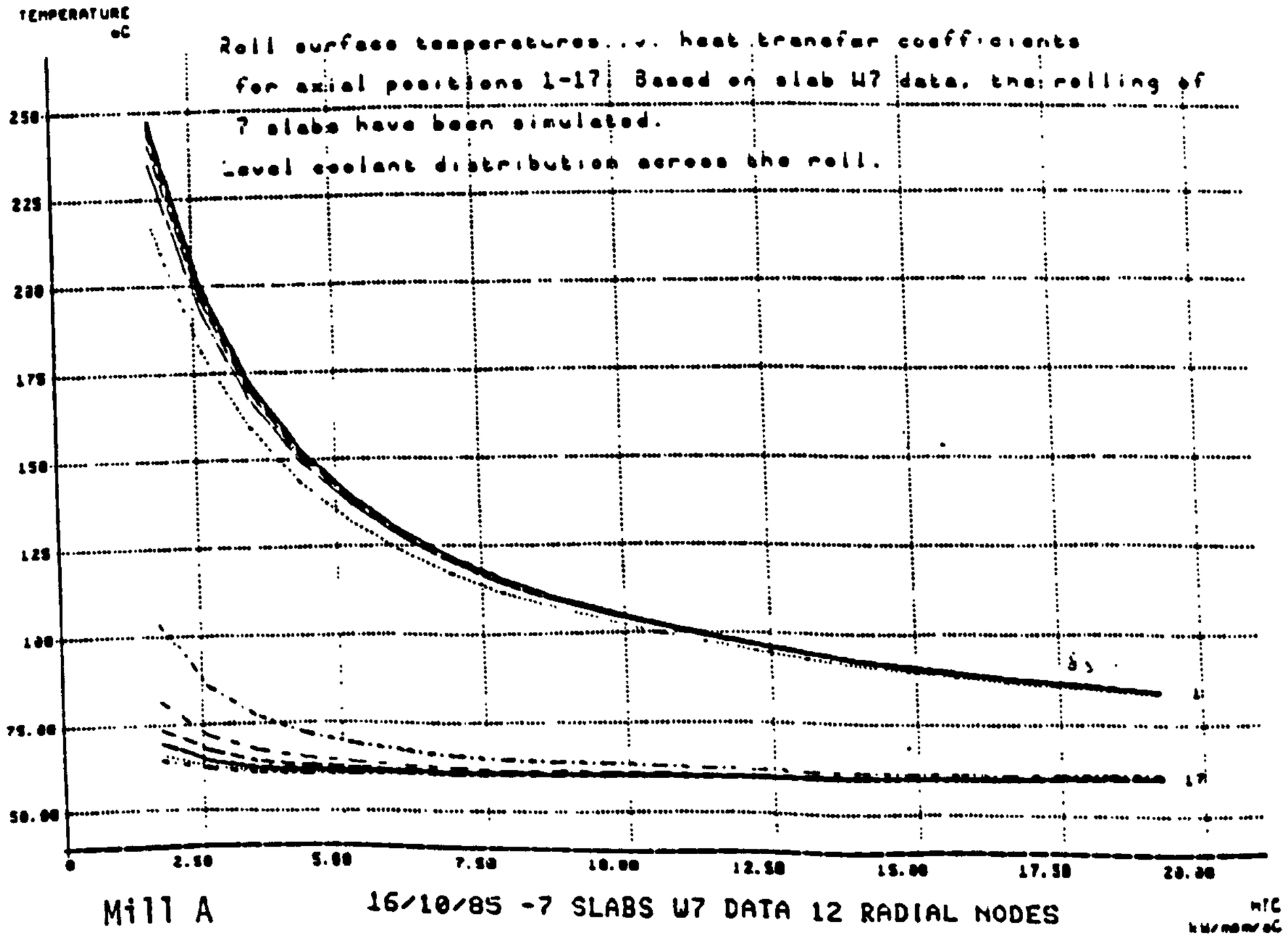
TEMPERATURE
oC
Roll surface temperatures .v. heat transfer coefficients
for axial positions 1-17. Based on slab W7 data. the rolling of
7 slabs have been simulated.
Level coolant distribution across the roll.
250
225
200
175
150
125
100
75.00
50.00
0
2.50
5.00
7.50
10.00
12.50
15.00
17.50
20.00
Mill A
16/10/85 -7 SLABS W7 DATA 12 RADIAL NODES
HTC

Fig. G5

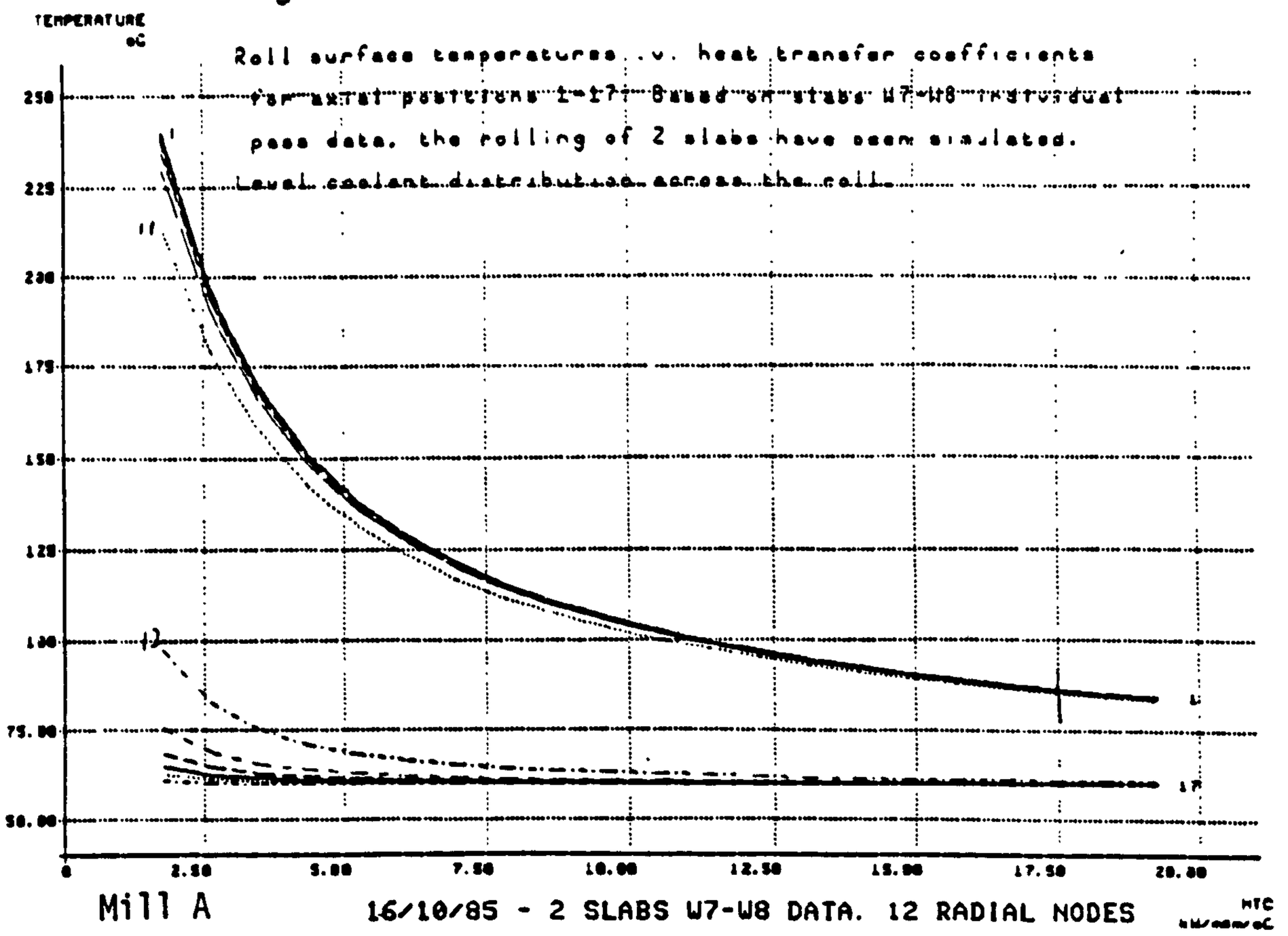
TEMPERATURE
oC
Roll surface temperatures .v. heat transfer coefficients
for extra positions 1-17. Based on stabs W7-W8 transducer
pass data. the rolling of 2 slabs have been simulated.
Level coolant distribution across the roll
250
225
200
175
150
125
100
75.00
50.00
0
2.50
5.00
7.50
10.00
12.50
15.00
17.50
20.00
I
II
12
1
17
Mill A
16/10/85 - 2 SLABS W7-W8 DATA. 12 RADIAL NODES
HTC

Fig. G6

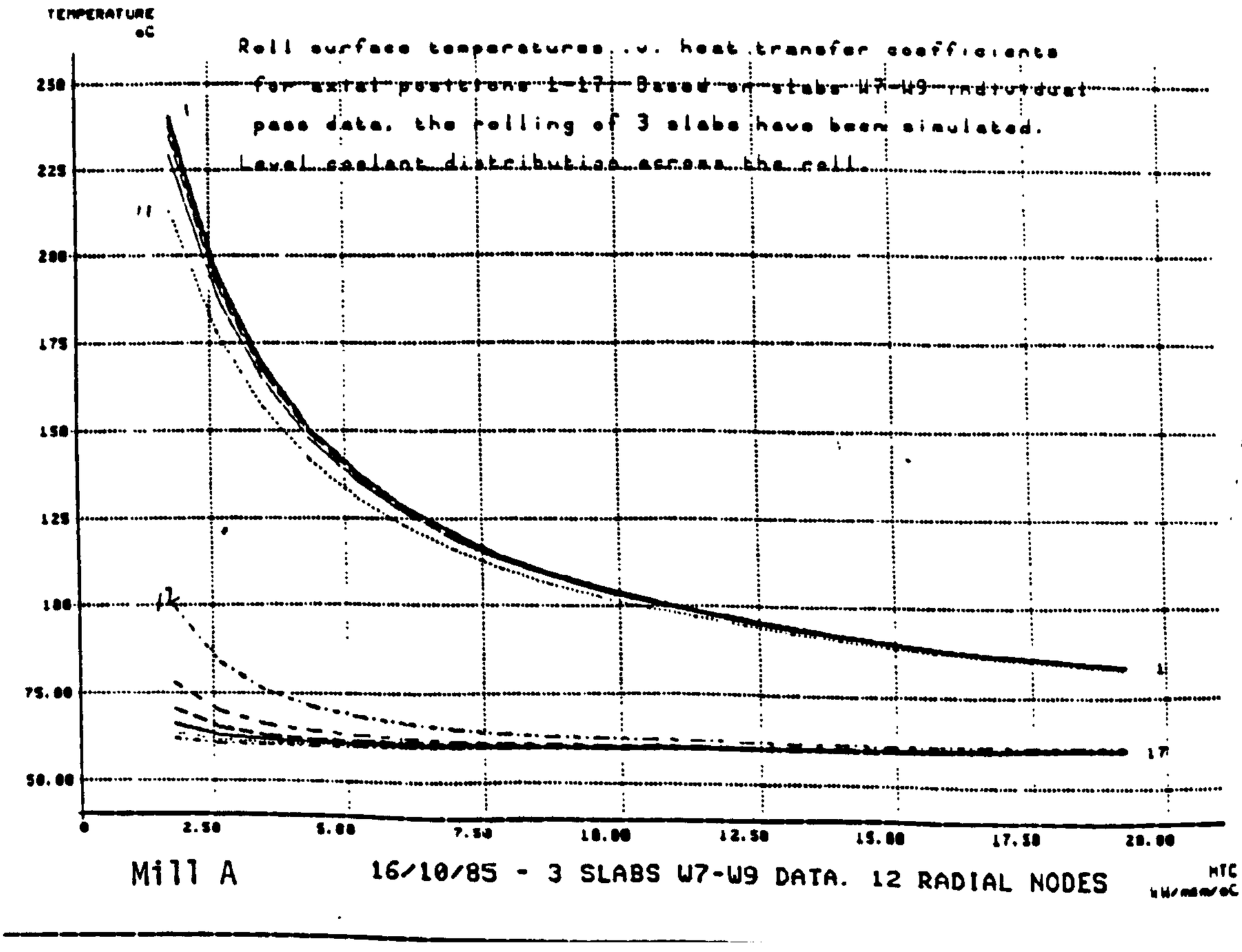
TEMPERATURE
oC
Roll surface temperatures .v. heat transfer coefficients
for extra positions 1-17. Based on stabs W7-W9 transducer
pass data. the rolling of 3 slabs have been simulated.
Level coolant distribution across the roll
250
225
200
175
150
125
100
75.00
50.00
0
2.50
5.00
7.50
10.00
12.50
15.00
17.50
20.00
I
II
12
1
17
Mill A
16/10/85 - 3 SLABS W7-W9 DATA. 12 RADIAL NODES
HTC

Fig. G7

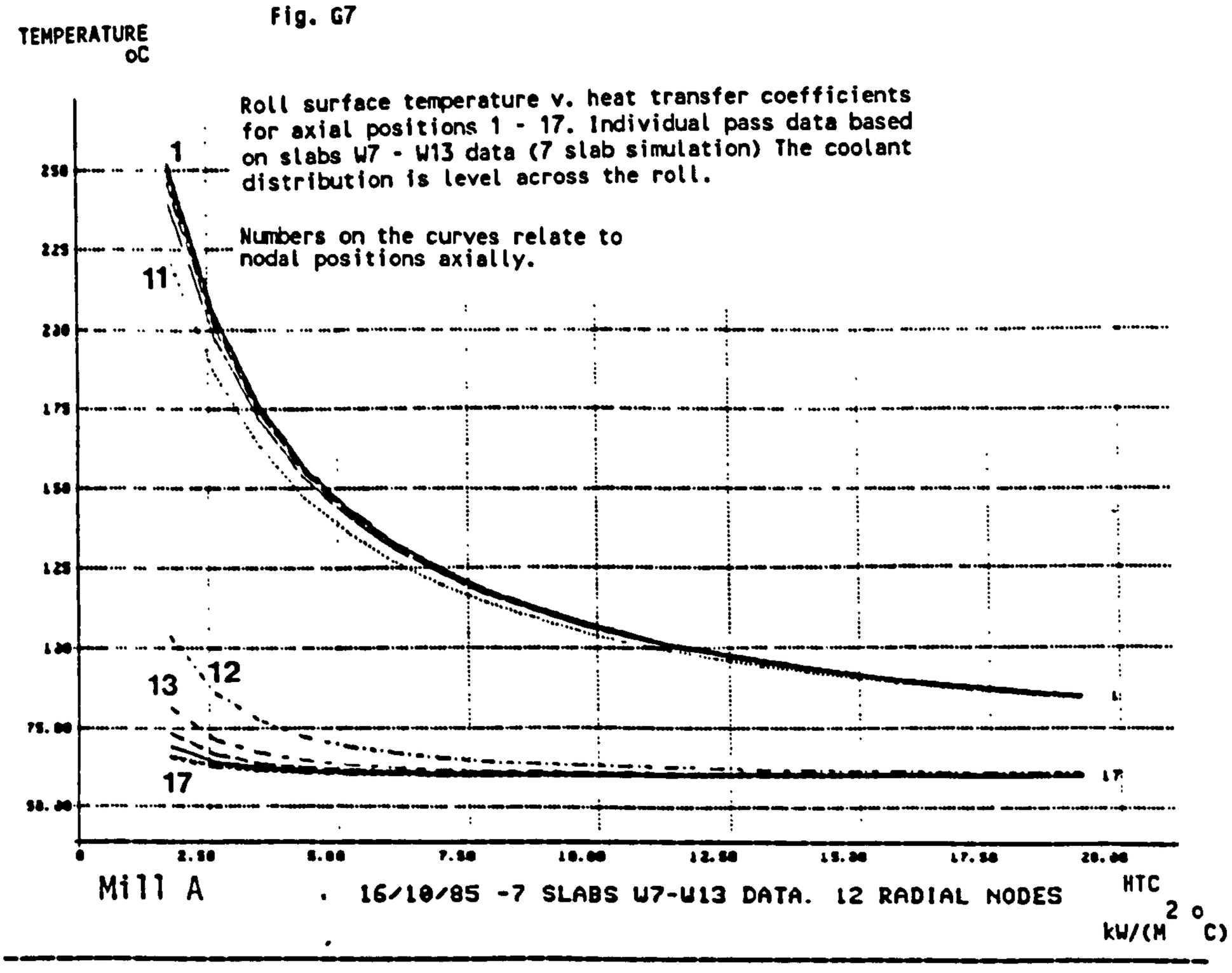
TEMPERATURE oC
Roll surface temperature v. heat transfer coefficients for axial positions 1 - 17. Individual pass data based on slabs W7 - W13 data (7 slab simulation) The coolant distribution is level across the roll.
Numbers on the curves relate to nodal positions axially.
1
11
12
13
17
250
225
200
175
150
125
100
75.00
50.00
0
2.50
5.00
7.50
10.00
12.50
15.00
17.50
20.00
Mill A
16/10/85 -7 SLABS W7-W13 DATA. 12 RADIAL NODES
HTC
kW/(M2 oC)

Fig. G8

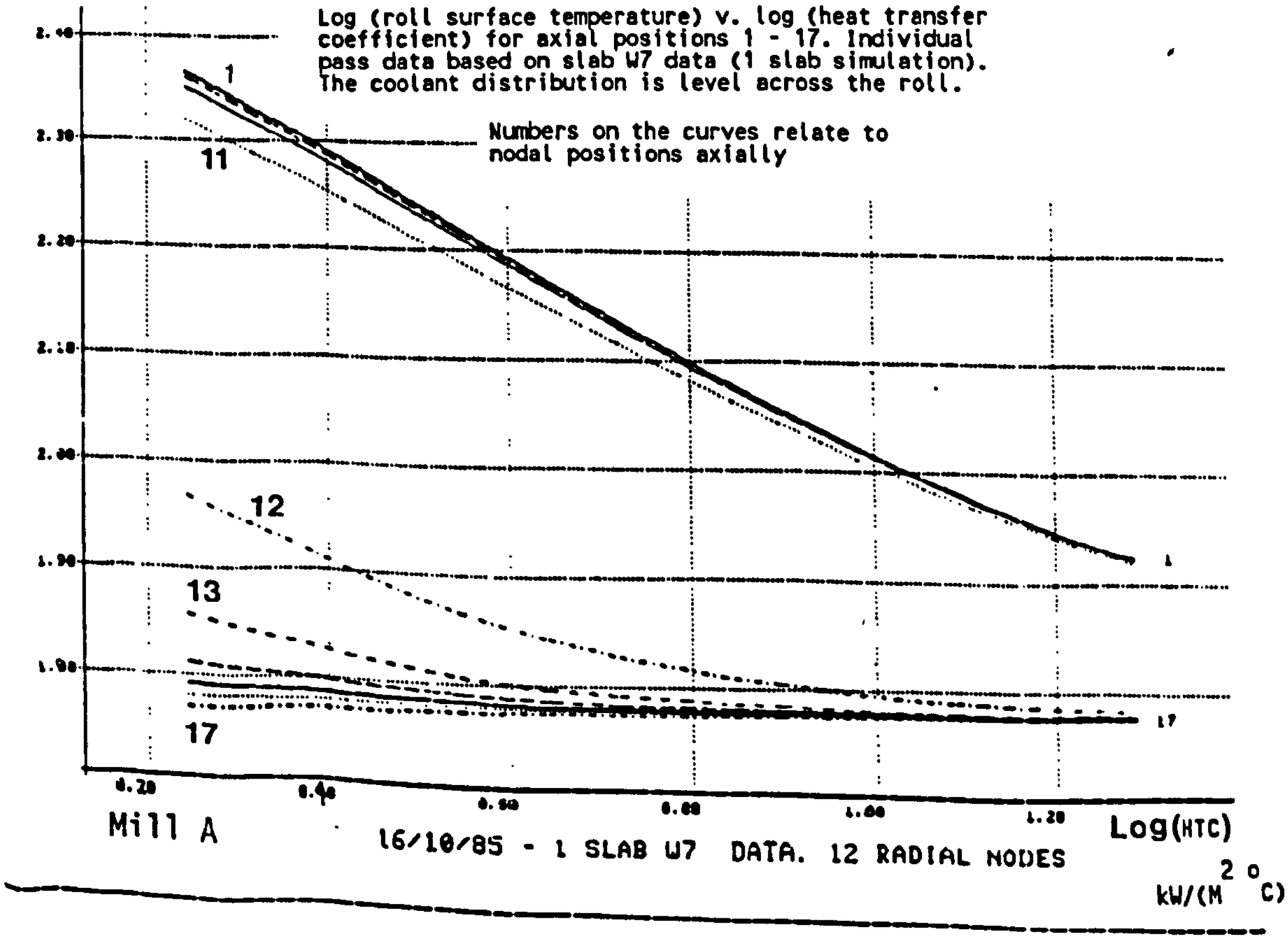
Log(TEMPERATURE) oC
Log (roll surface temperature) v. log (heat transfer coefficient) for axial positions 1 - 17. Individual pass data based on slab W7 data (1 slab simulation). The coolant distribution is level across the roll.
Numbers on the curves relate to nodal positions axially
1
11
12
13
17
2.40
2.30
2.20
2.10
2.00
1.90
1.80
0.20
0.40
0.60
0.80
1.00
1.20
Mill A
16/10/85 - 1 SLAB W7 DATA. 12 RADIAL NODES
Log(HTC)
kW/(M2 oC)

Fig. G9

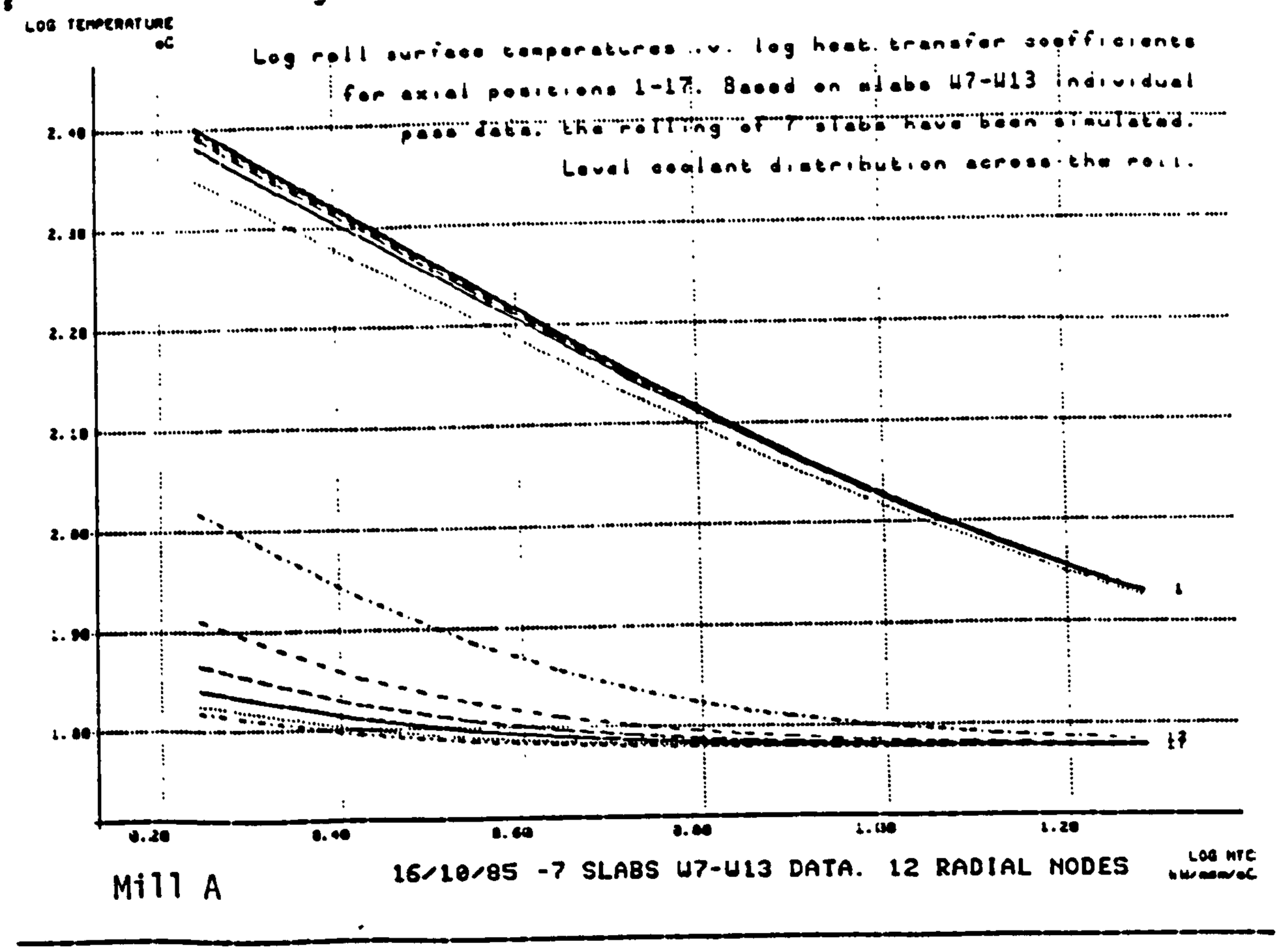

Fig. G10

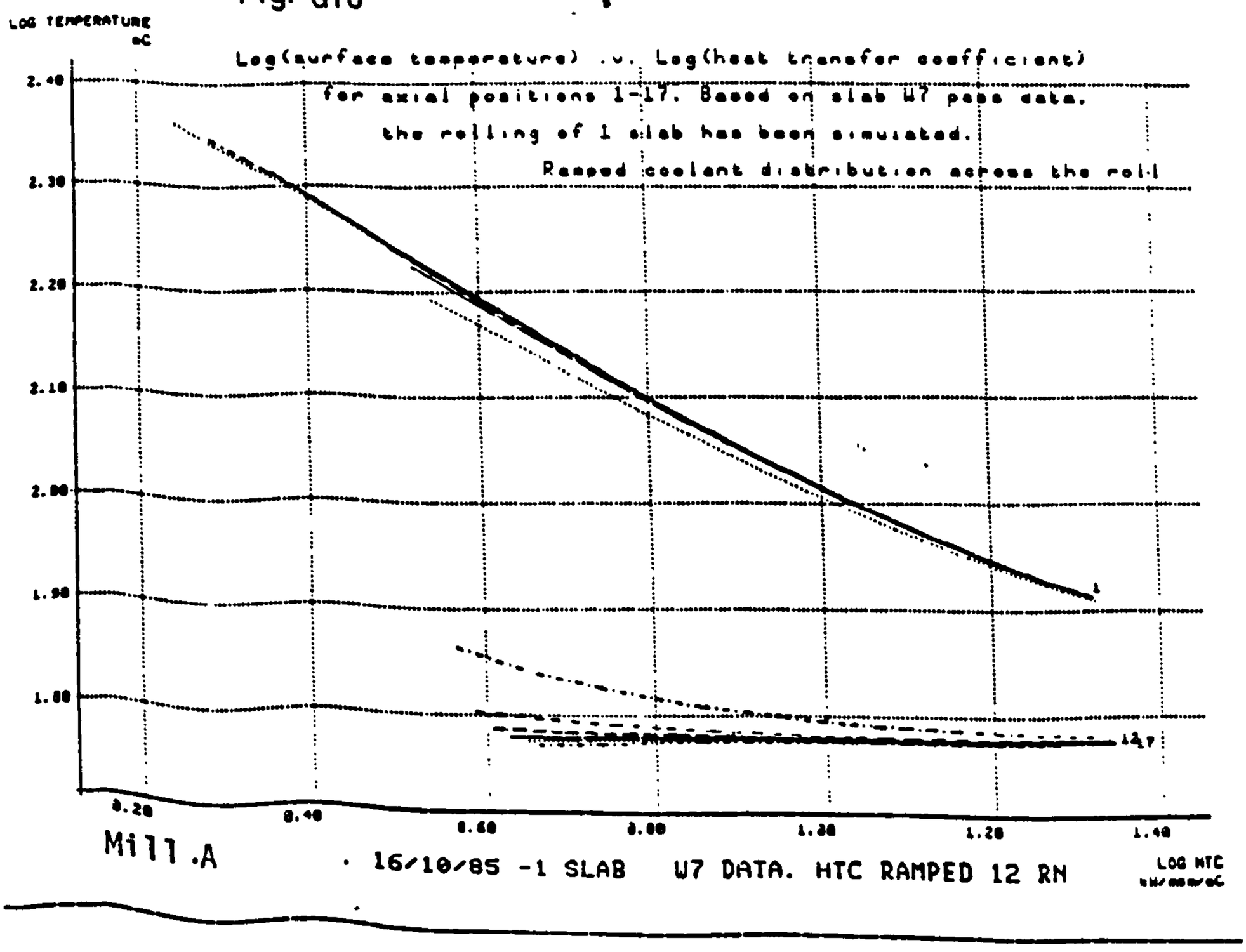

Fig. G11

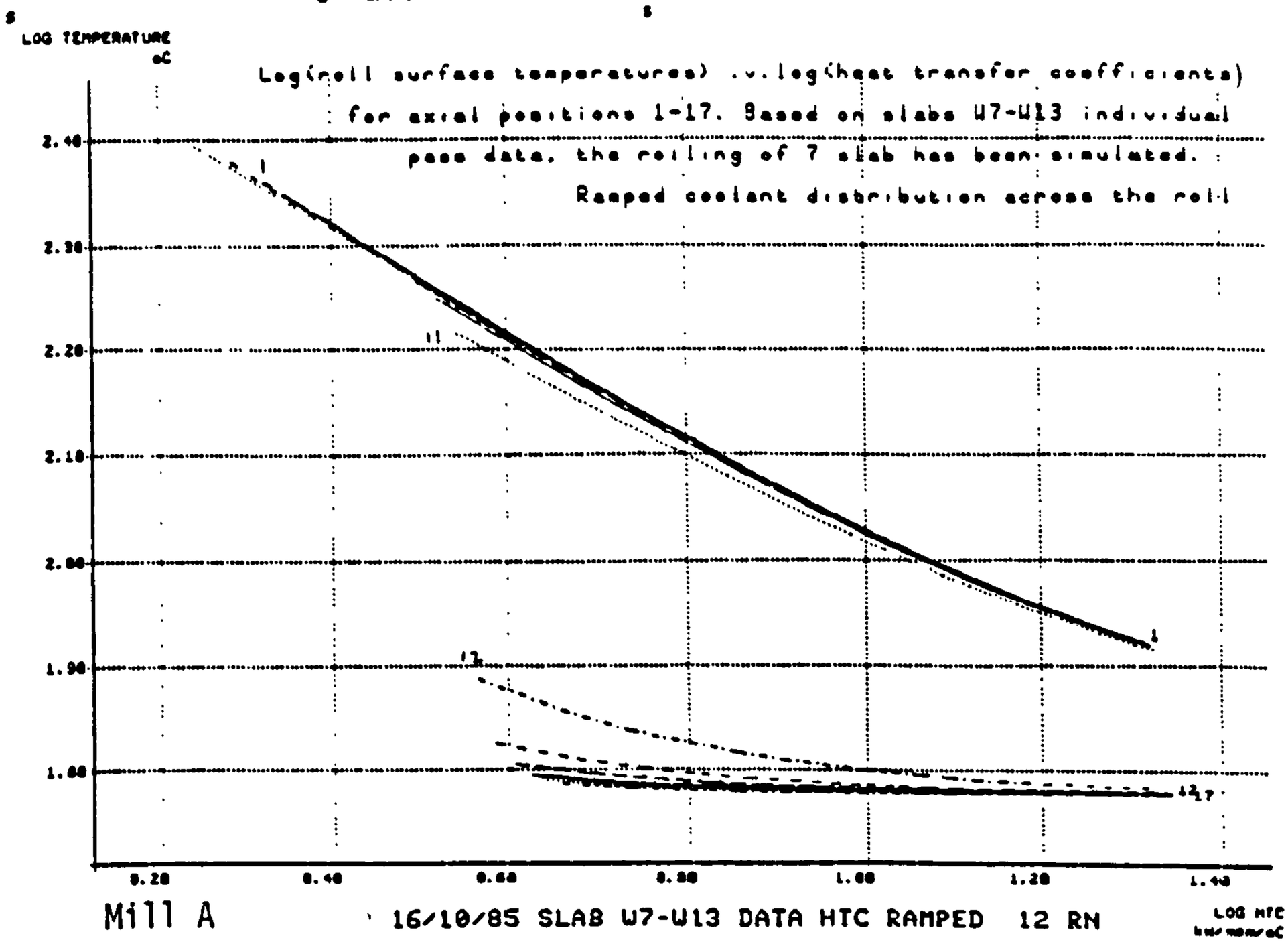

Mill A 16/10/85 SLAB W7-W13 DATA HTC RAMPED 12 RN

Fig. G12

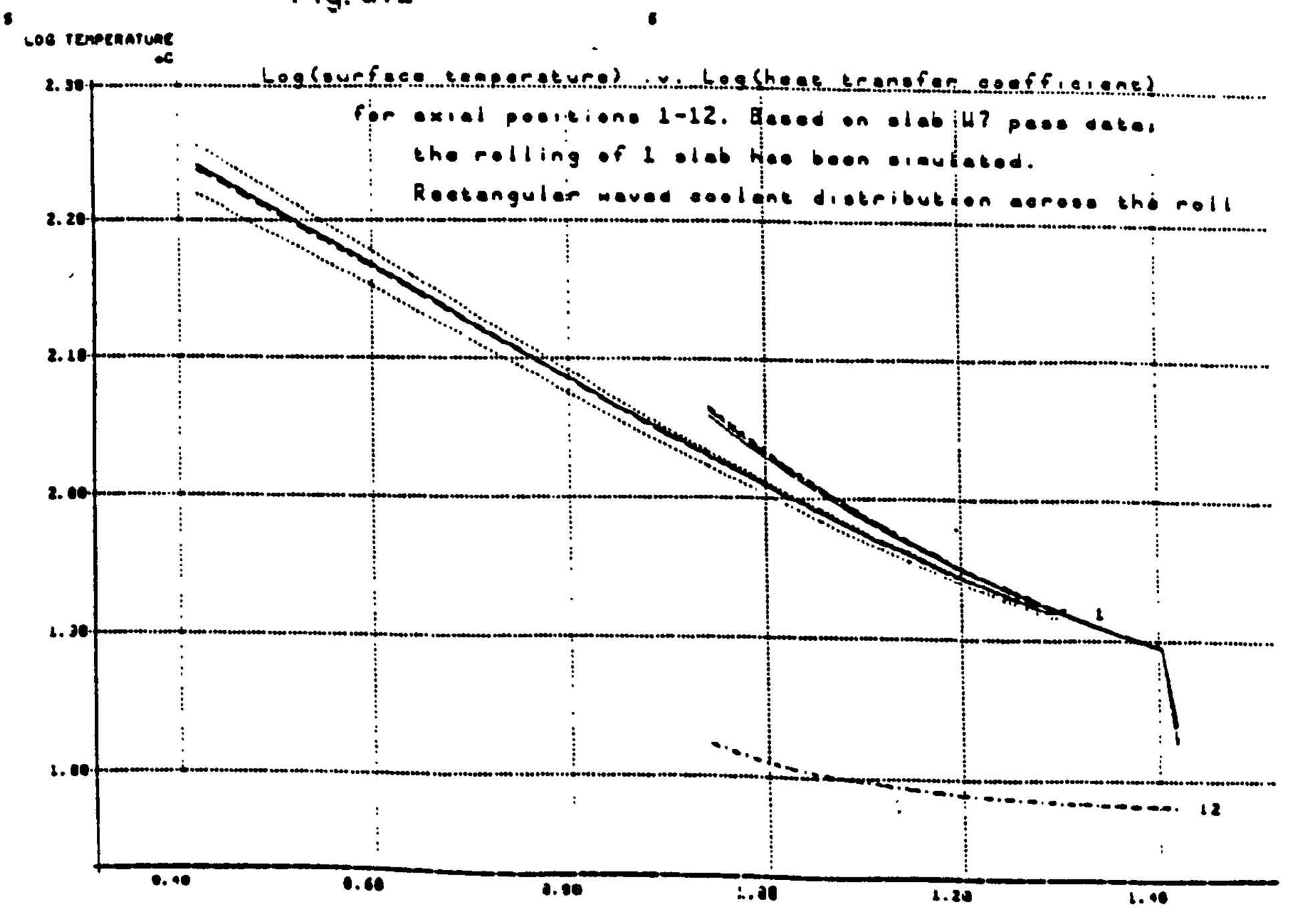

Mill A 16/10/85 -1 SLAB W7 DATA.(Rectglar waves) 12 RN

Fig. G13

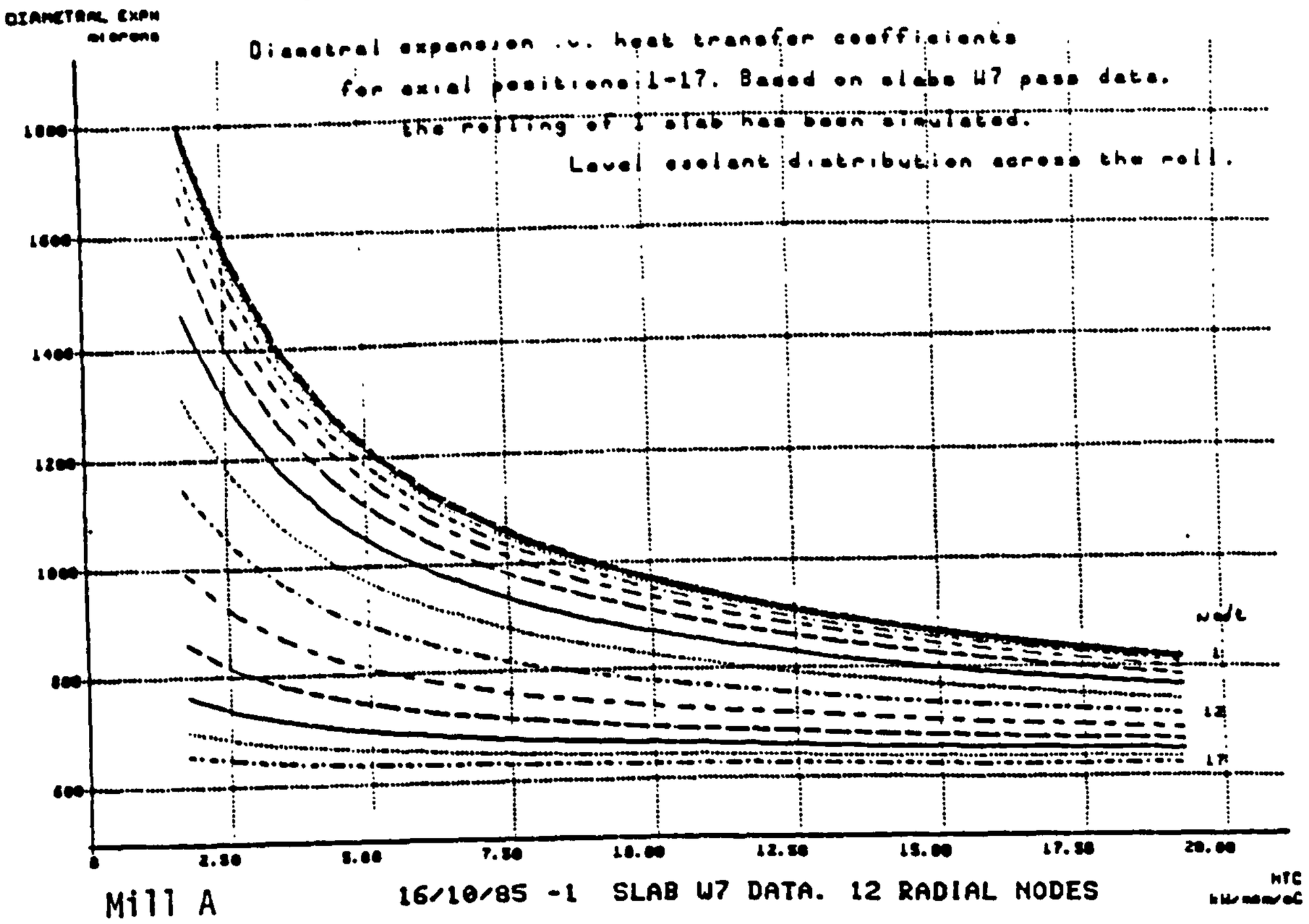

Fig. G14

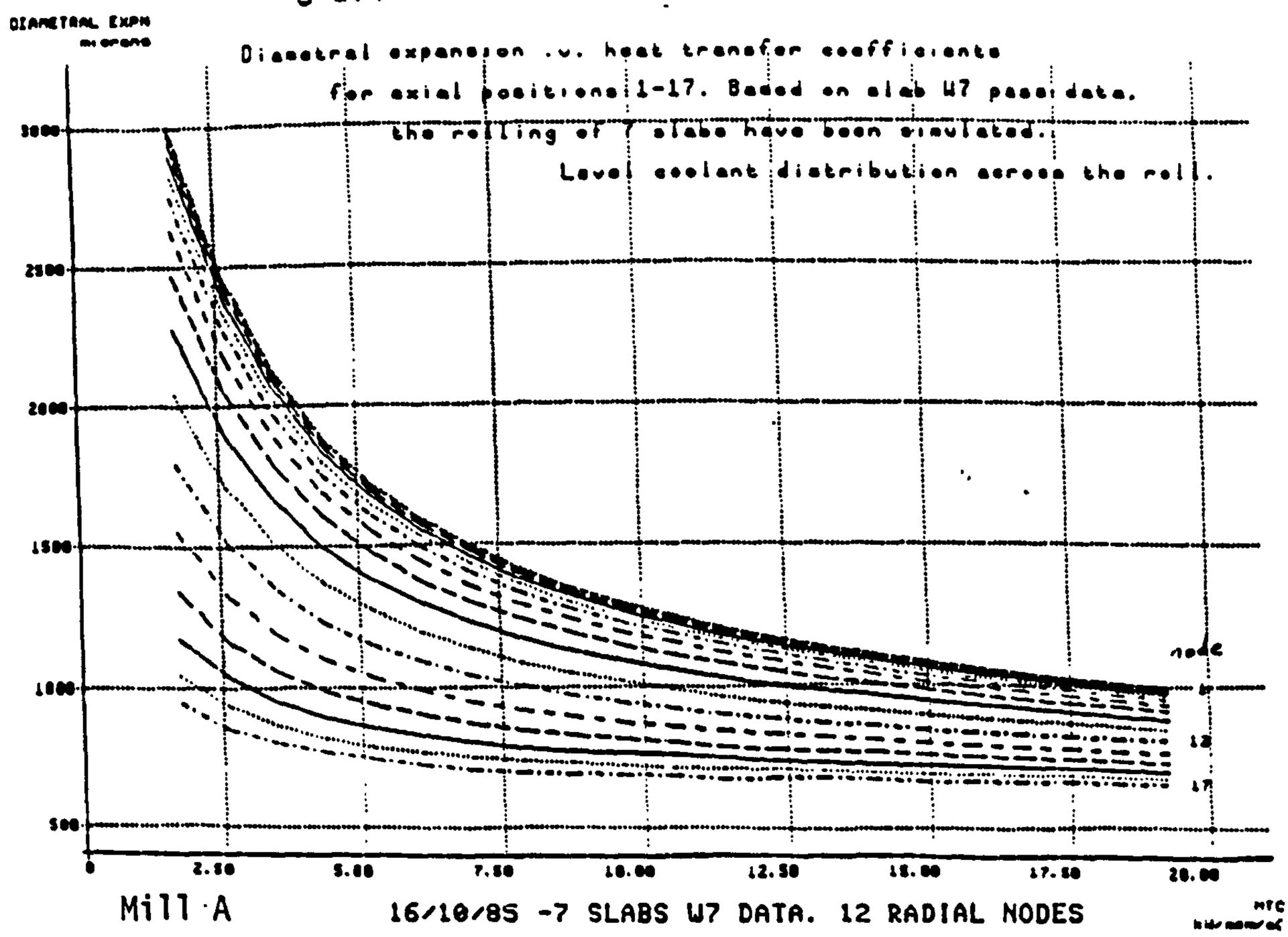

Fig. G15

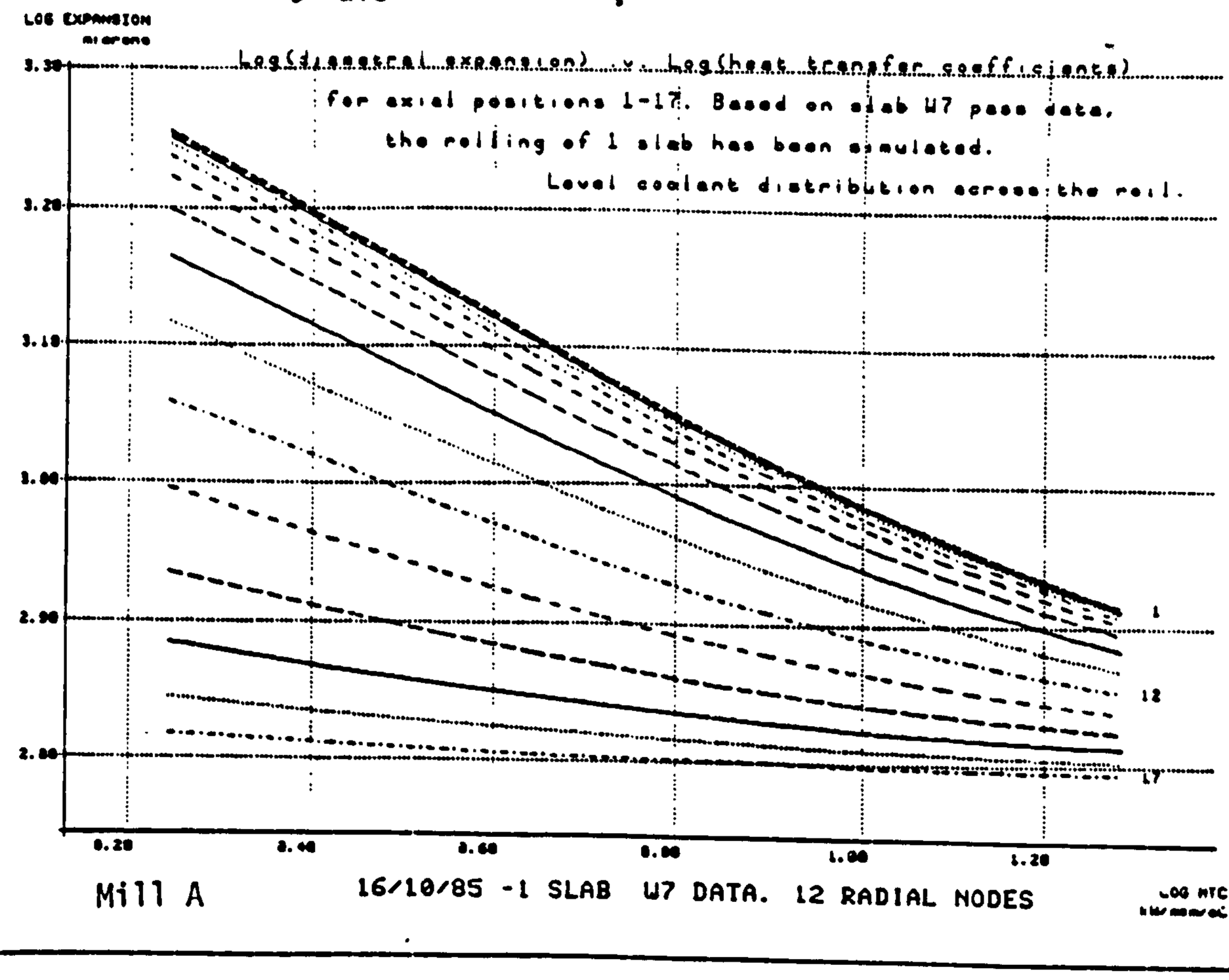

Fig. G16

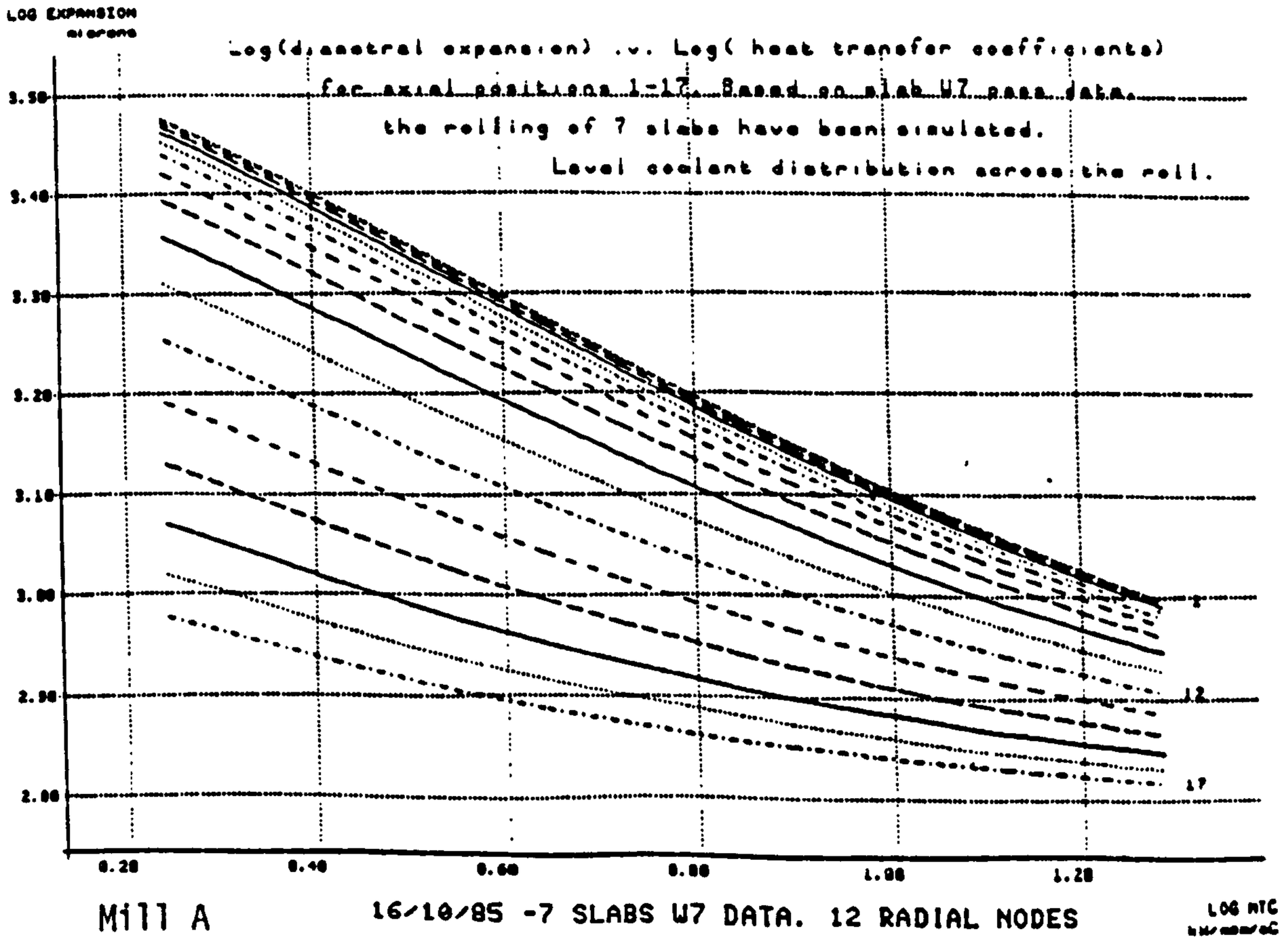

Fig. G17 Roll surface temperature v roll diametral expansion after 7 slabs have been rolled.

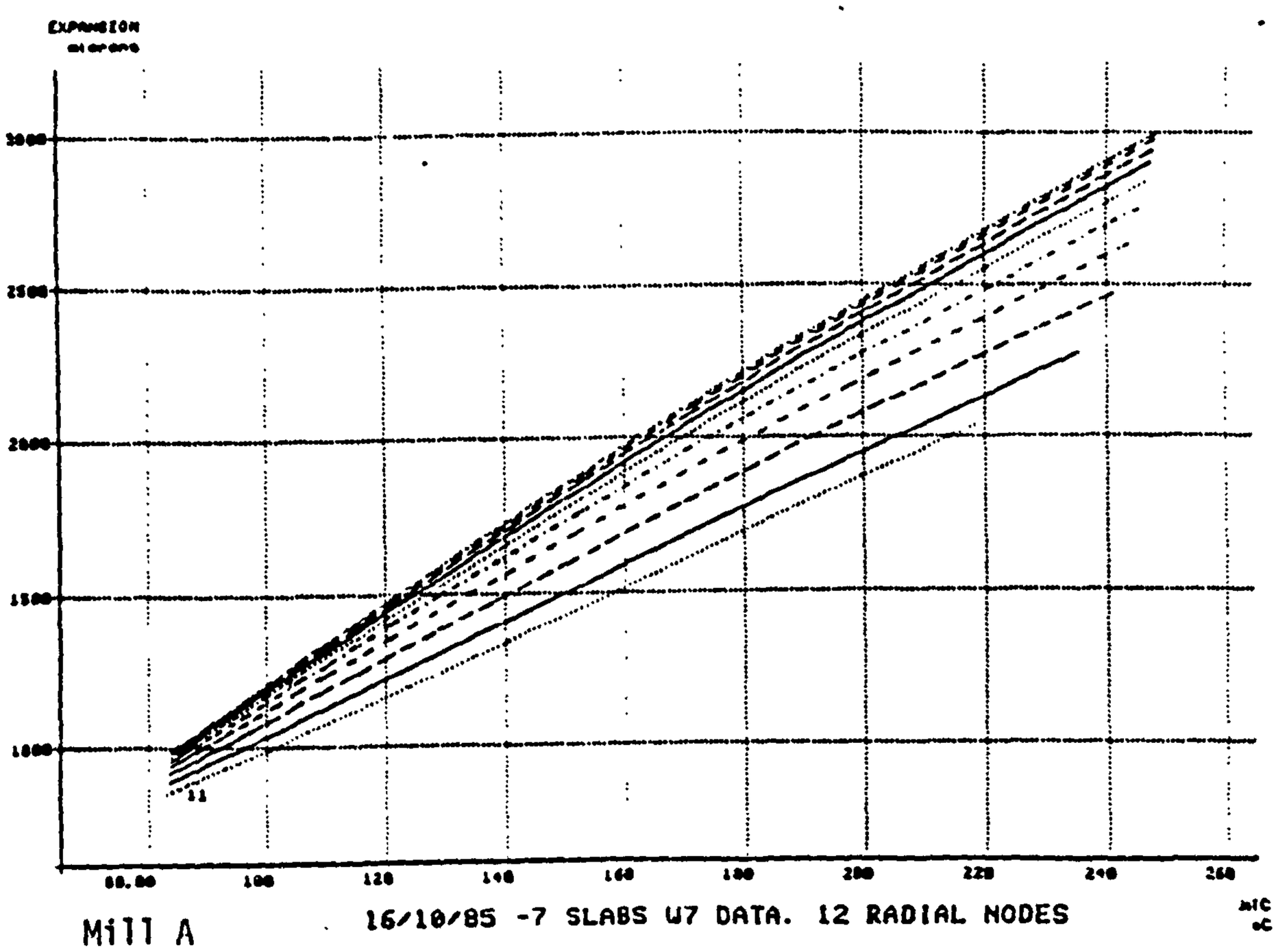

Fig. G18 Roll surface temperature v roll diametral expansion after two slabs have been rolled.

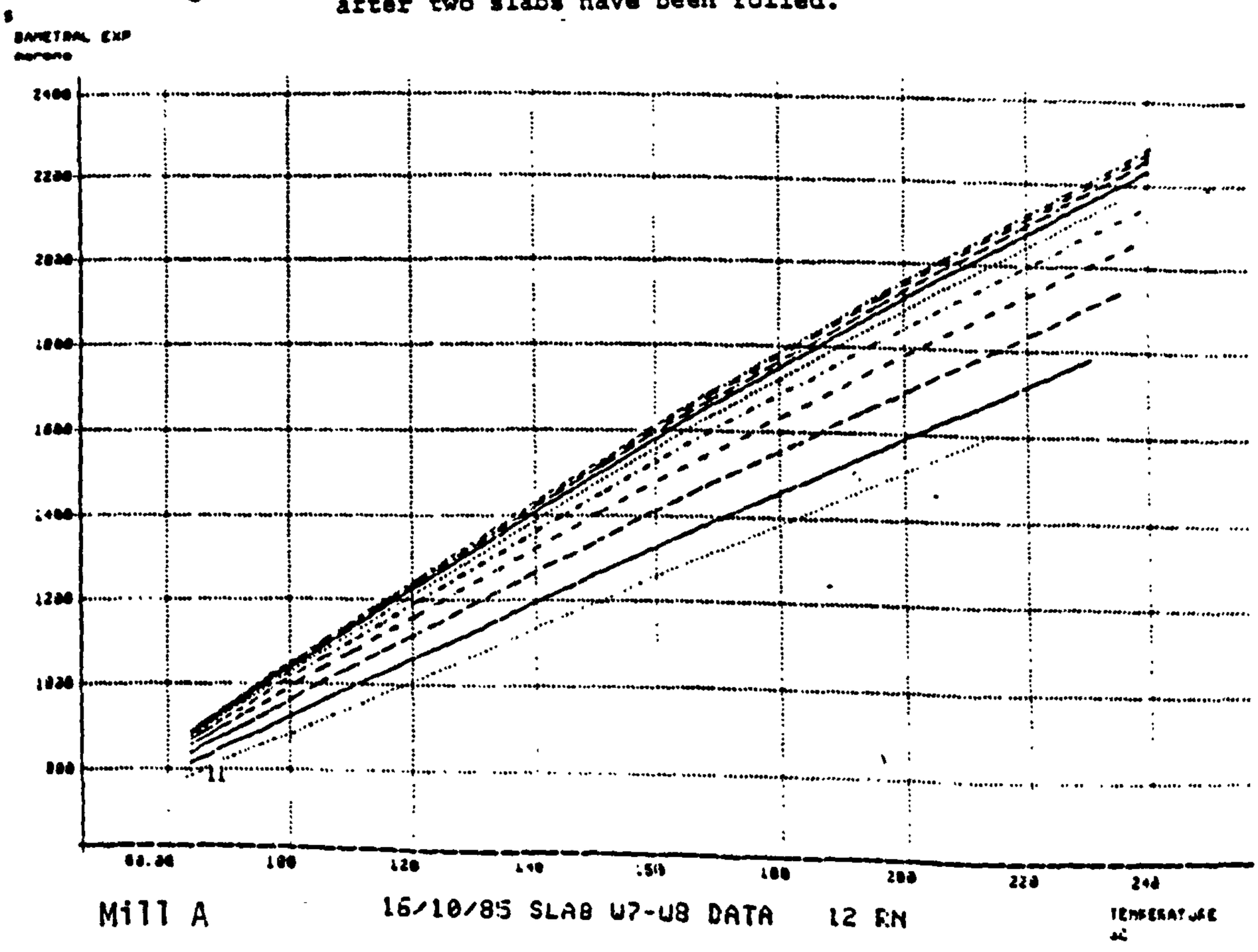

Fig. G19 Roll surface temperature v diametral expansion

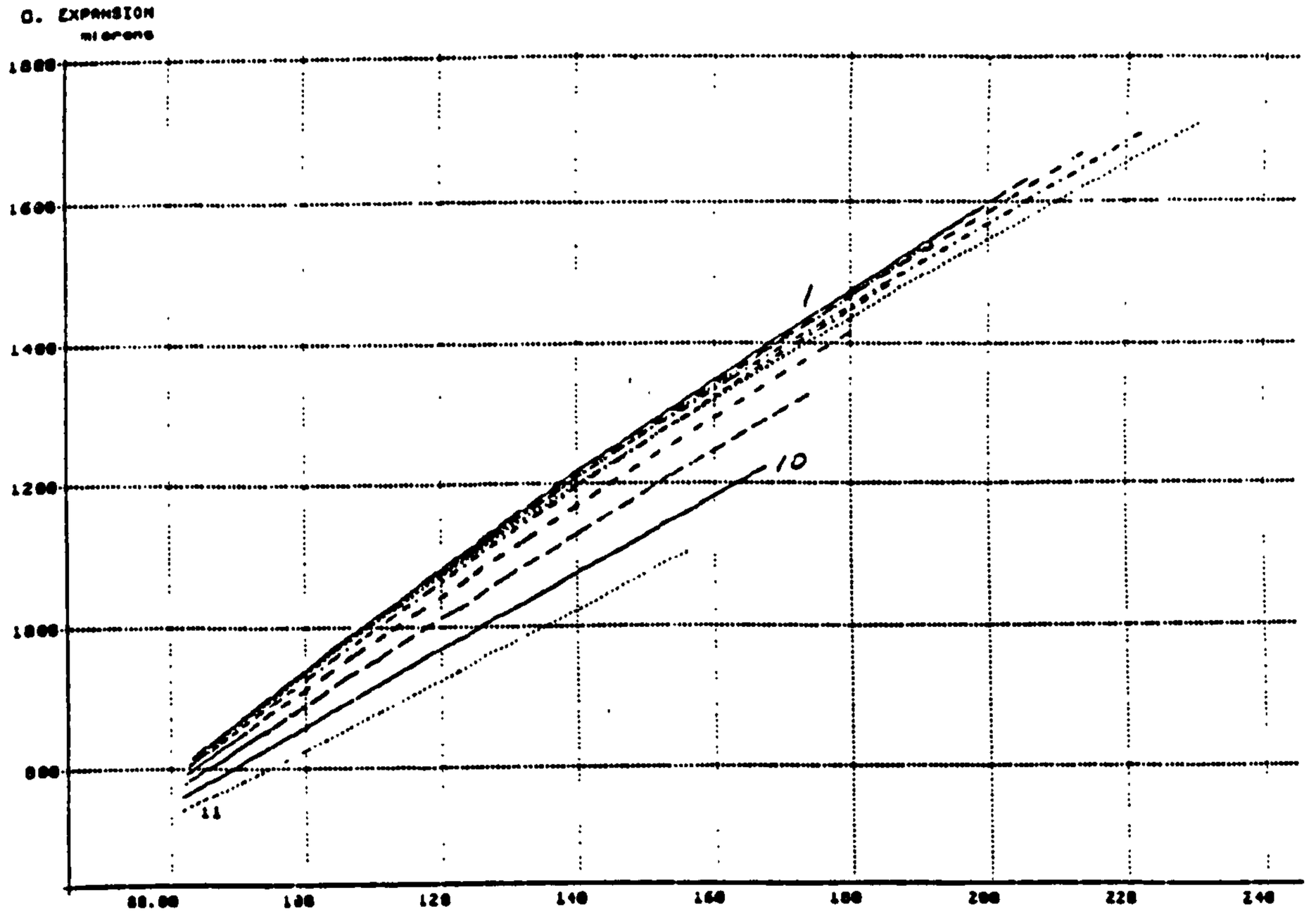

Mill A 16/10/85 SLAB W7 DATA HTC RAMPED 12 RN

APPENDIX H

GRAPHS SHOWING VARIATION OF STRIP CROWN WITH CHANGES IN SPRAY PATTERNS AND WORK ROLL BENDING FORCE

Fig.H1 . Roll thermal camber v. distance from roll centre line after 1 slab is rolled with spray levels:

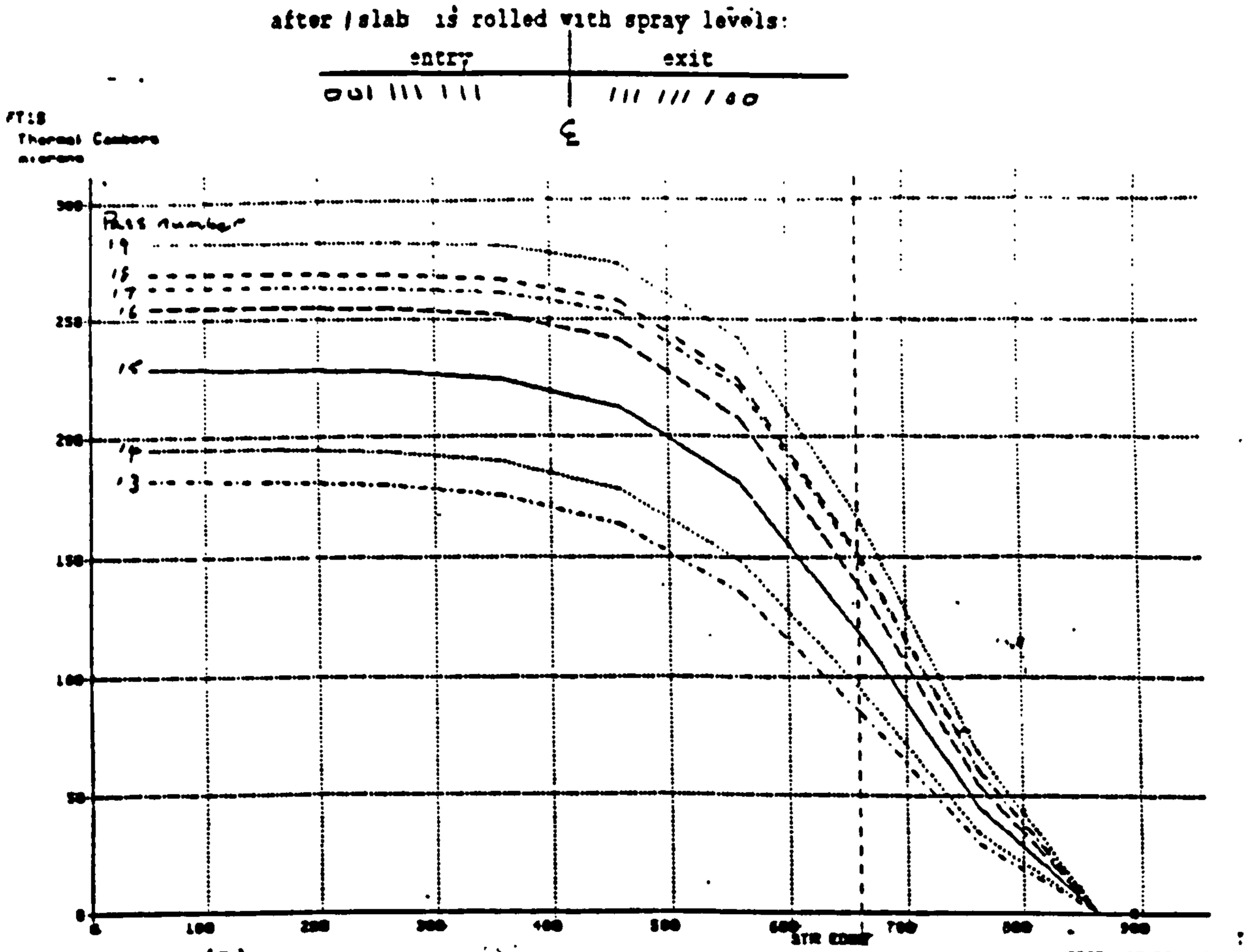

(B) HOT MILL. SLAB (3004) / 1 . 00IIIIIIIIIIIIII10@

Fig. H2 . Roll thermal camber v. distance from roll centre line after 2 slab is rolled with spray levels:

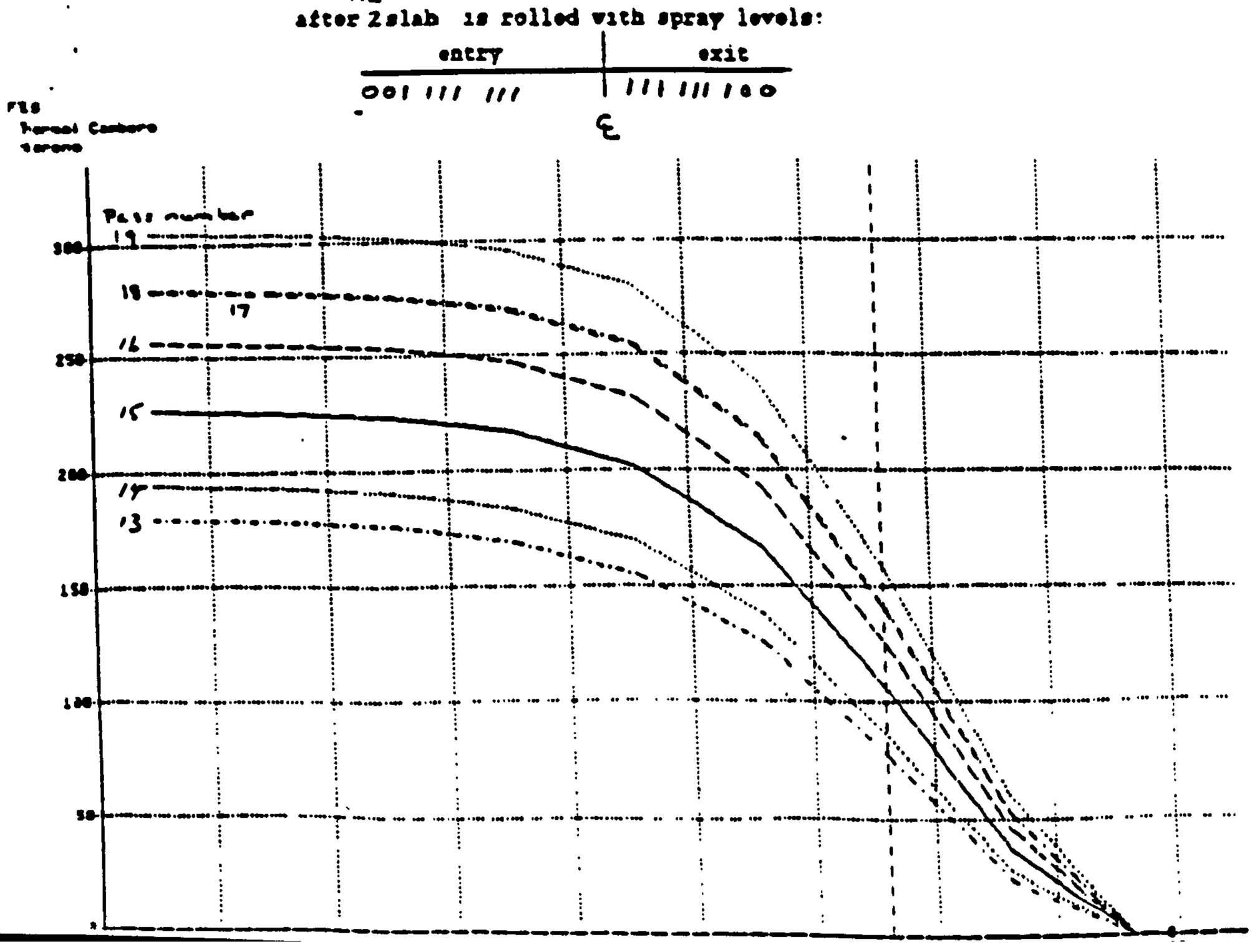

Fig. 44. Roll thermal camber v. distance from roll centre line after 4 slab is rolled with spray levels.

entry | exit

0 0 1 111 111 | 111 111 100

℄

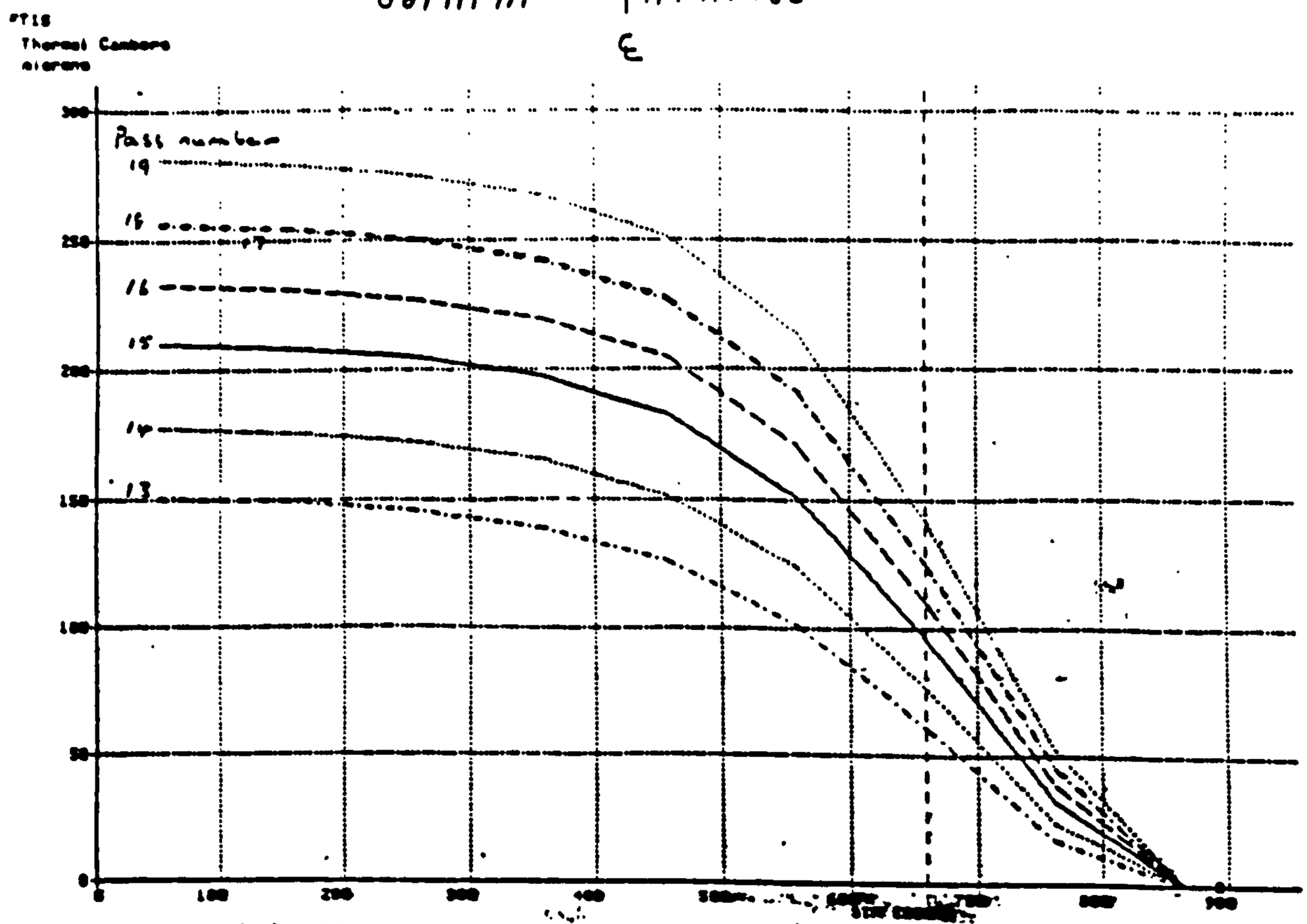

(B) HOT MILL. SLAB (3004) / 4 . 0 1 1 1 1 1 1 1 1 1 1 1 0

Fig. H3. Roll thermal camber v. distance from roll centre line after / slab is rolled with spray levels:

entry | exit

0 0 3 3 3 4 3 3 3 | 3 3 5 3 3 3 2 0

℄

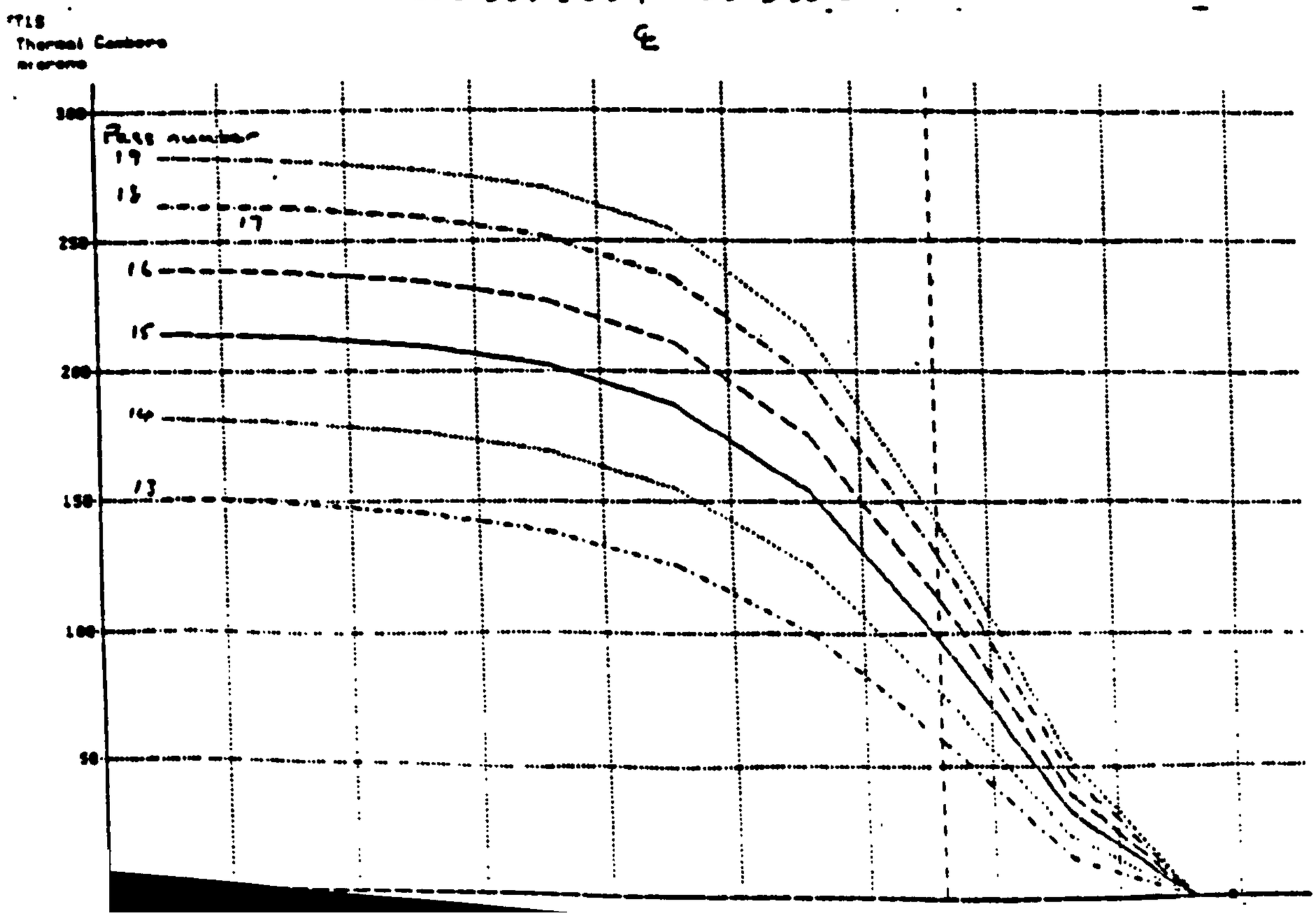

Fig.H5 . Predicted strip crown in half strip width.
1 slab rolled. spray levels

entry	exit
001 111 111	111 111 100

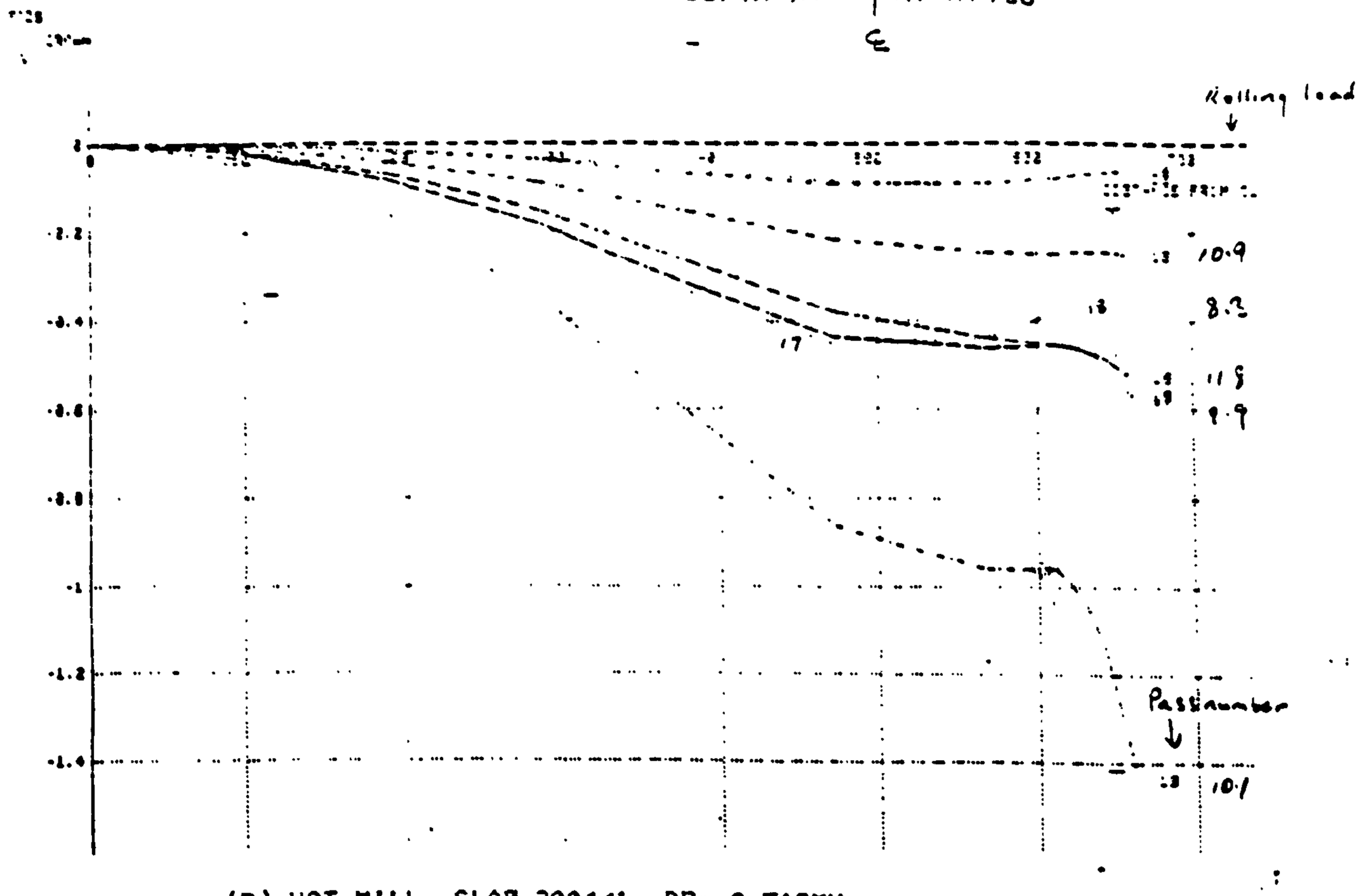

(B) HOT MILL SLAB 3004/1. RB: 0.512MN.

Fig H6 Predicted strip crown in half strip width.
2 slab rolled. Spray levels:

entry	exit
001 111 111	111 111 100

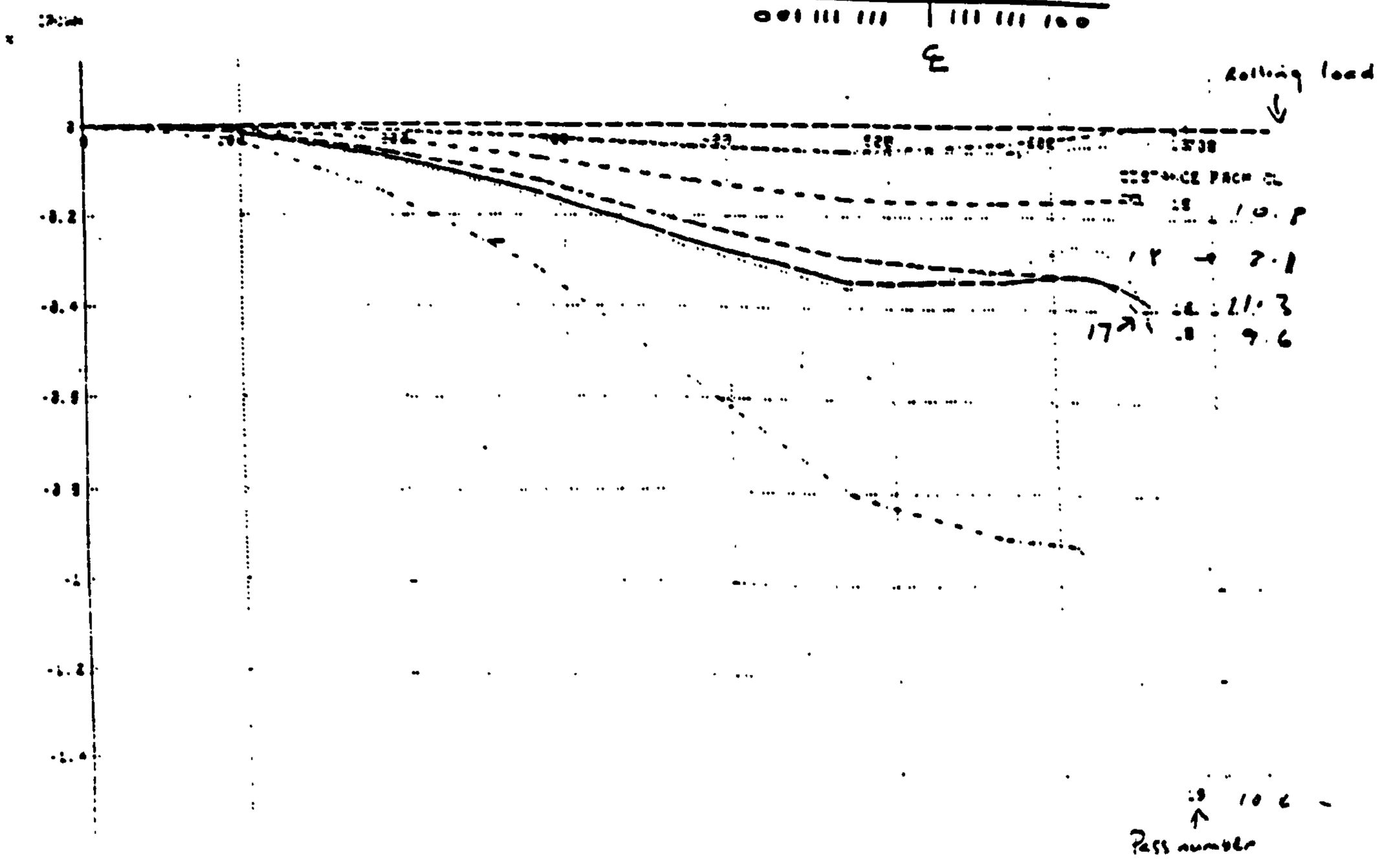

Fig H7 Predicted strip crown in half strip width
4 slab rolled Spray levels:

entry	exit
003 333 333	333 333 300

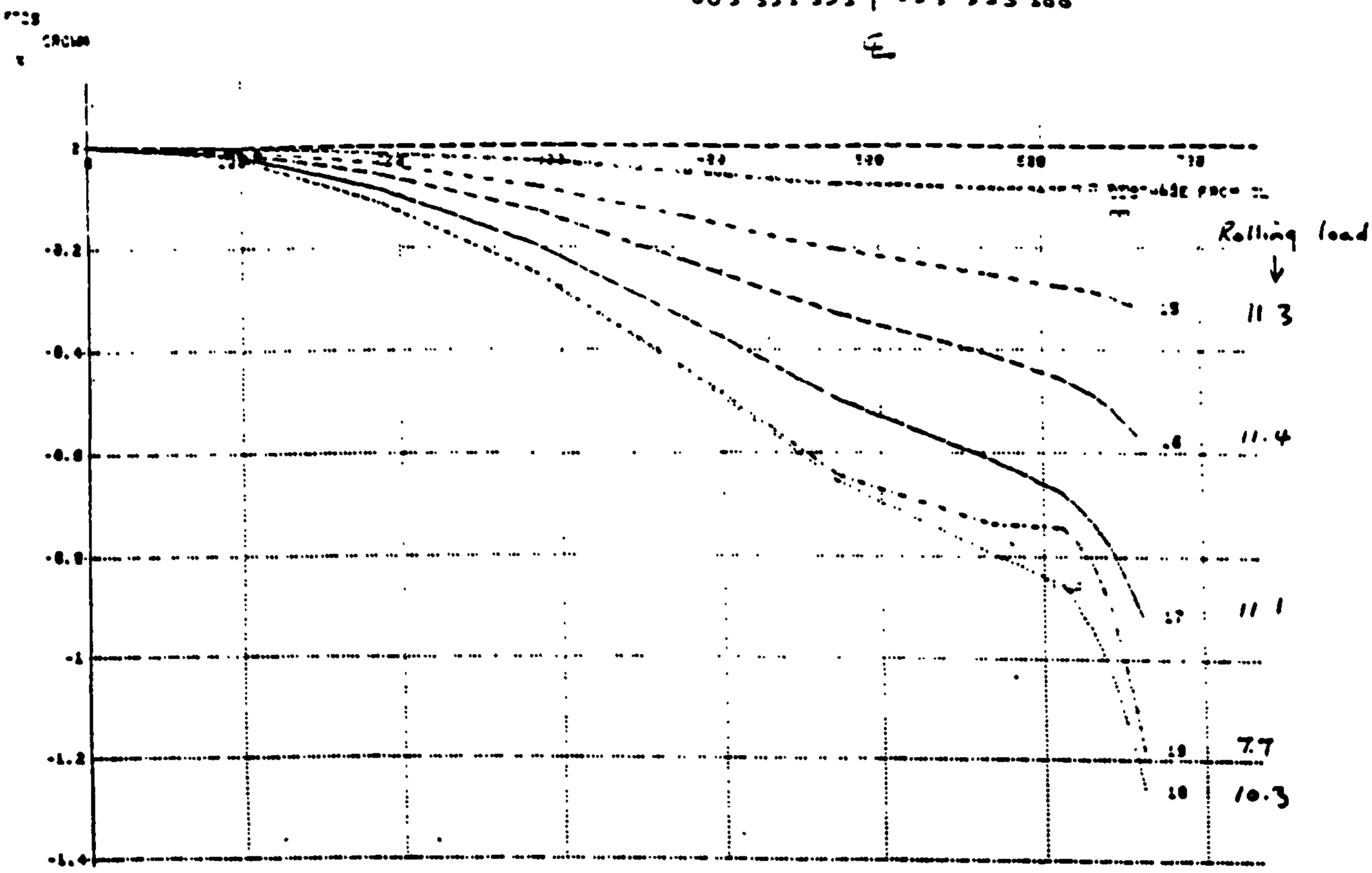

(B) HOT MILL SLAB 3004/4. RB: 0.512MN.

Fig. H8 . Predicted strip crown in half strip width.
4 slab rolled. Spray levels:

entry	exit
003 333 333	333 333 300

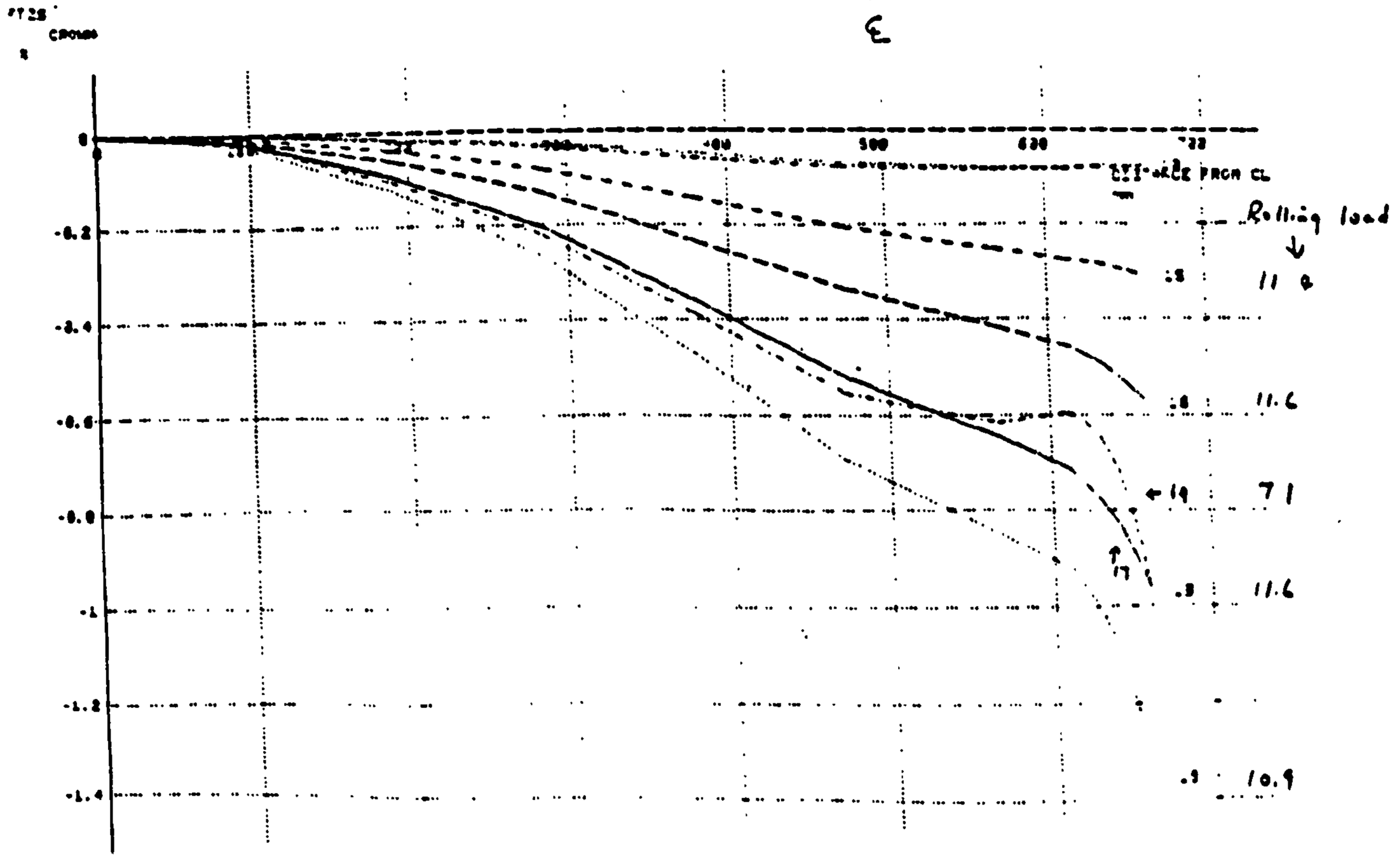

Fig.H9 . Predicted strip crown in half strip width.
/slab rolled. Spray levels

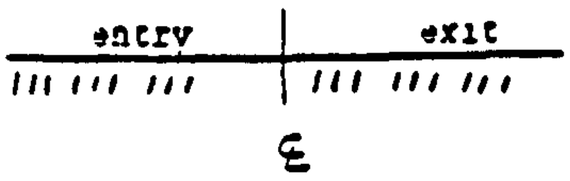

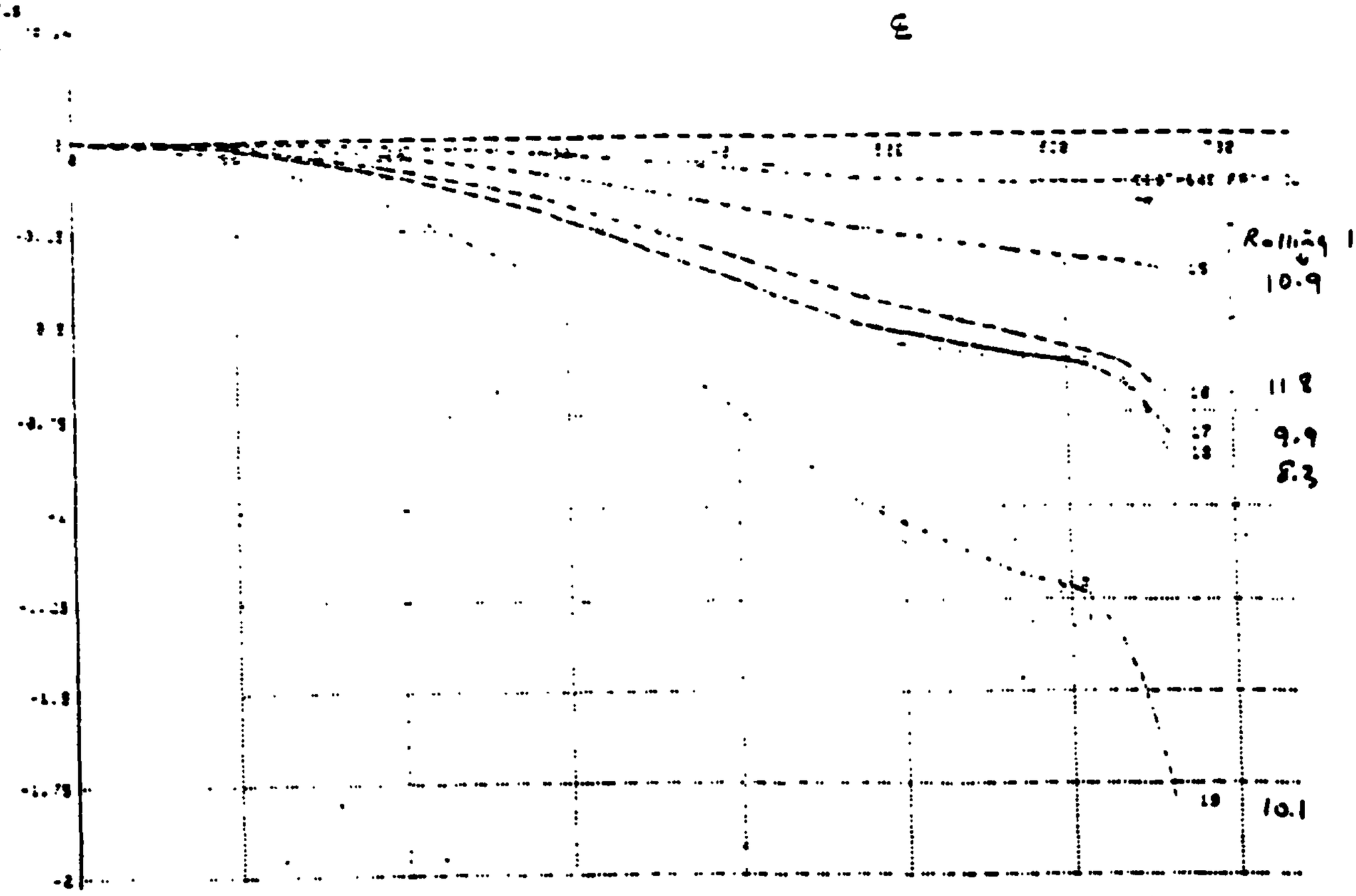

(B) HOT MILL SLAB 3004/1. RB: 0.512MN.

Fig. H10 . Predicted strip crown in half strip width.
2 slab rolled. Spray levels:

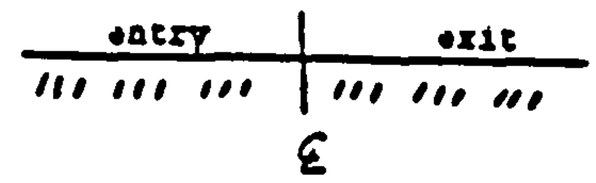

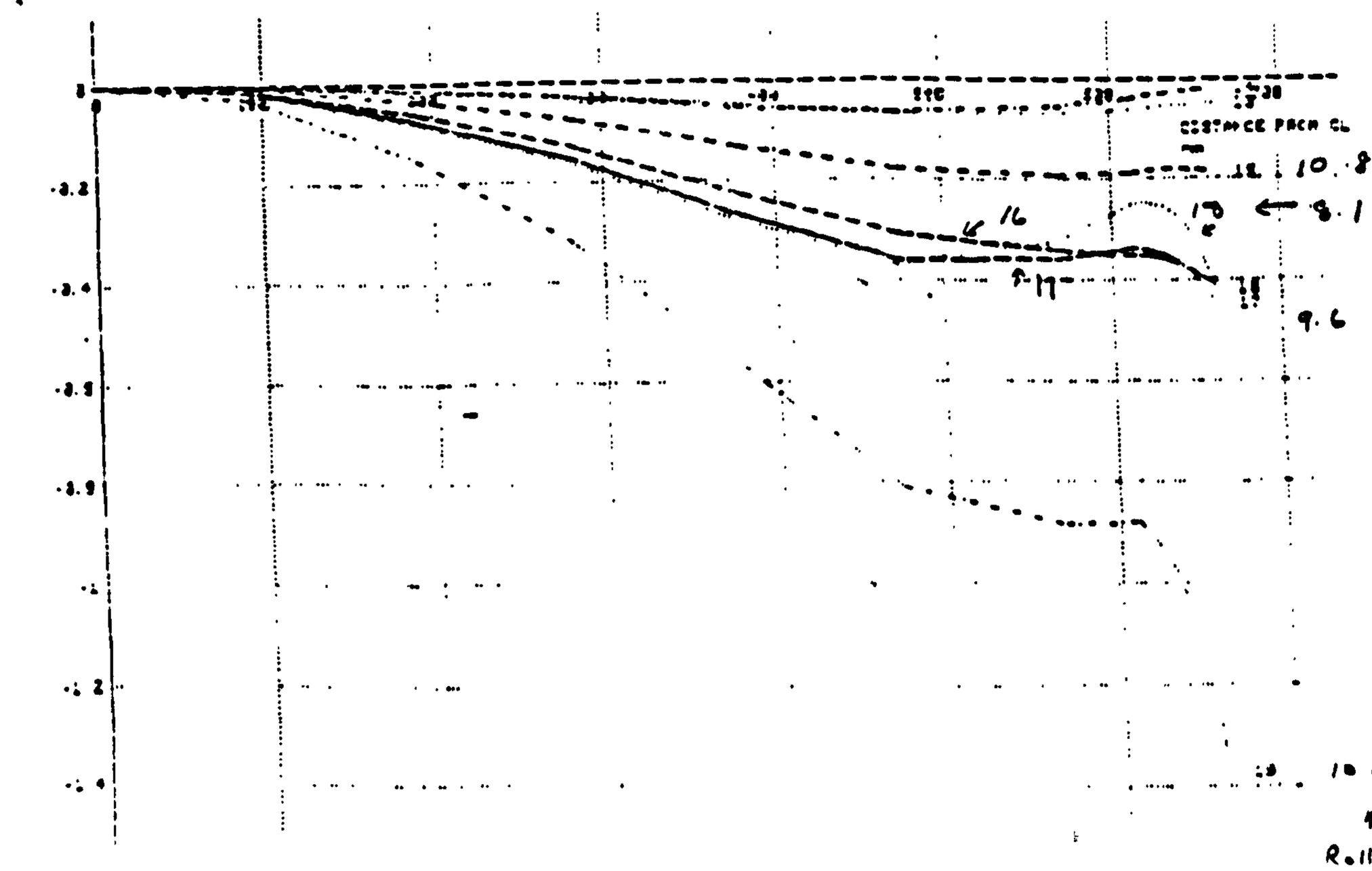

Fig H10 Predicted strip crown in half strip width
3slab rolled. Spray levels

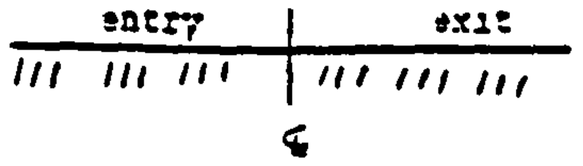

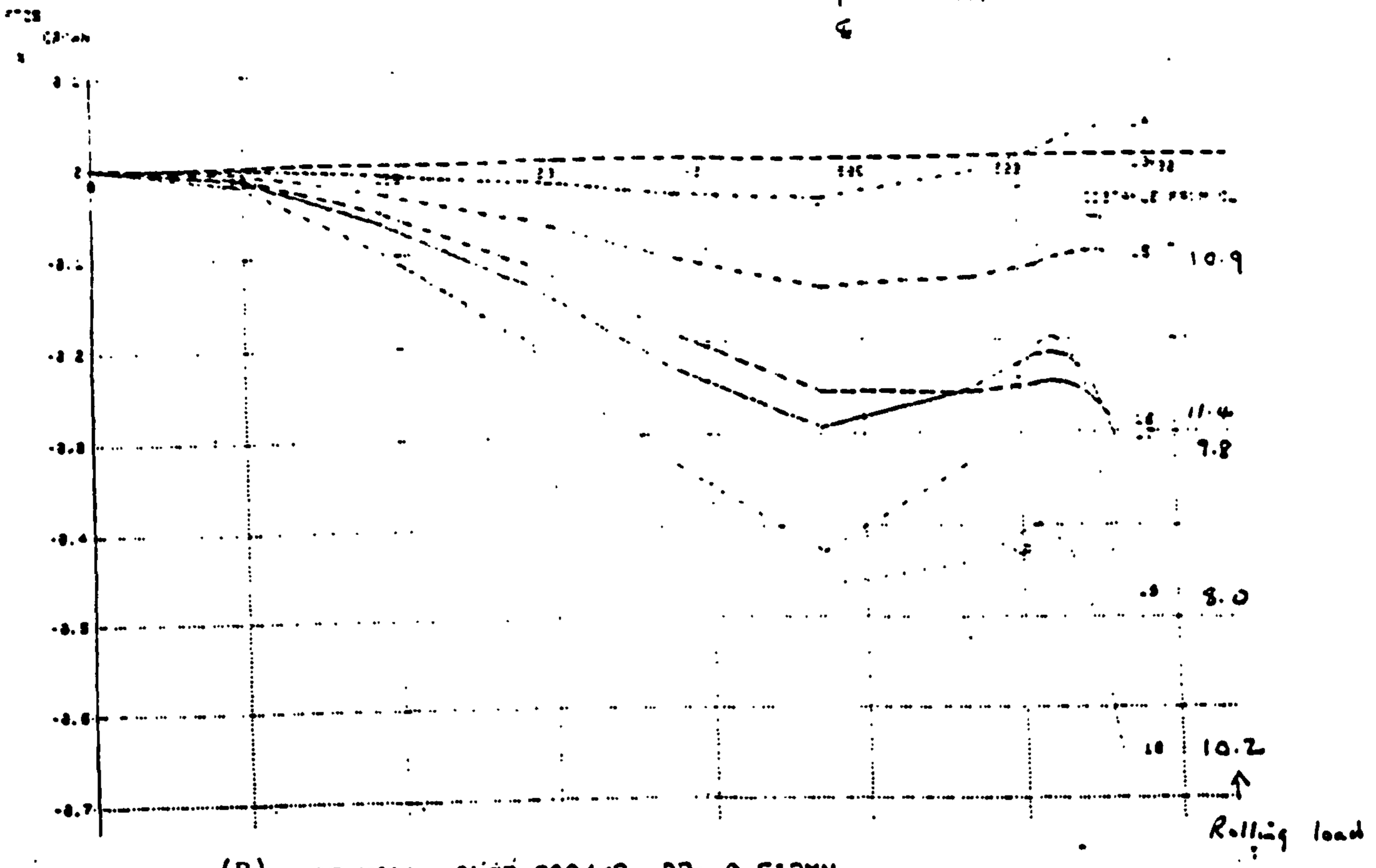

(B) HOT MILL SLAB 3004/3. RB: 0.512MN

Fig H11 Predicted strip crown in half strip width
7 slab rolled. Spray levels.

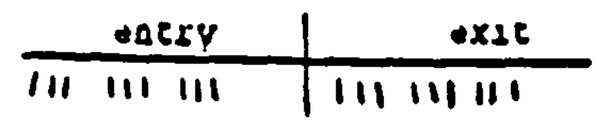

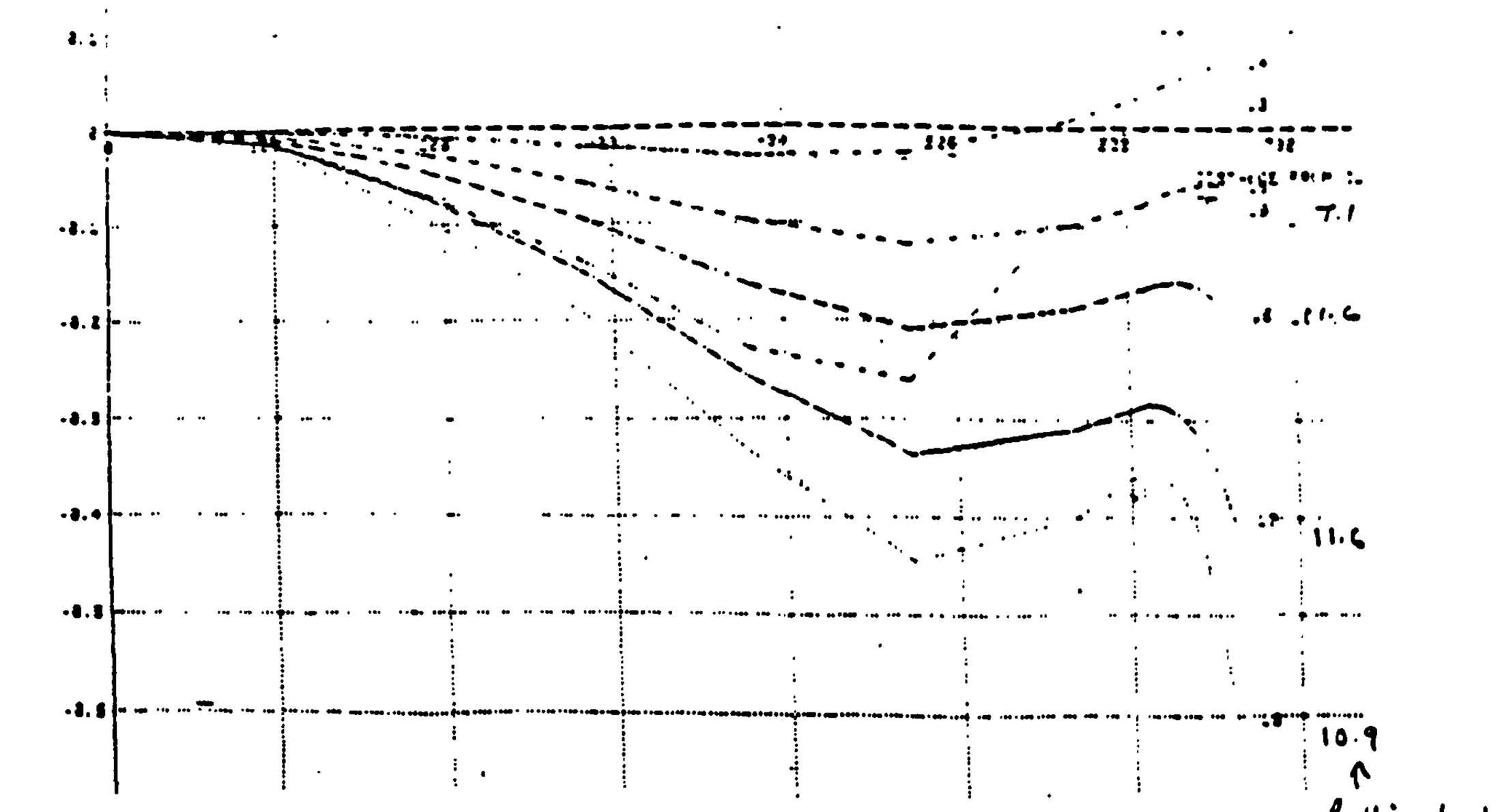

(B) HOT MILL SLAB 3004/9. RB: 0.512MN.

Fig.H12. Predicted strip crown in half strip width.
/slab rolled Spray levels:

entry	exit
ooo ooo ooo	/// /// /oo

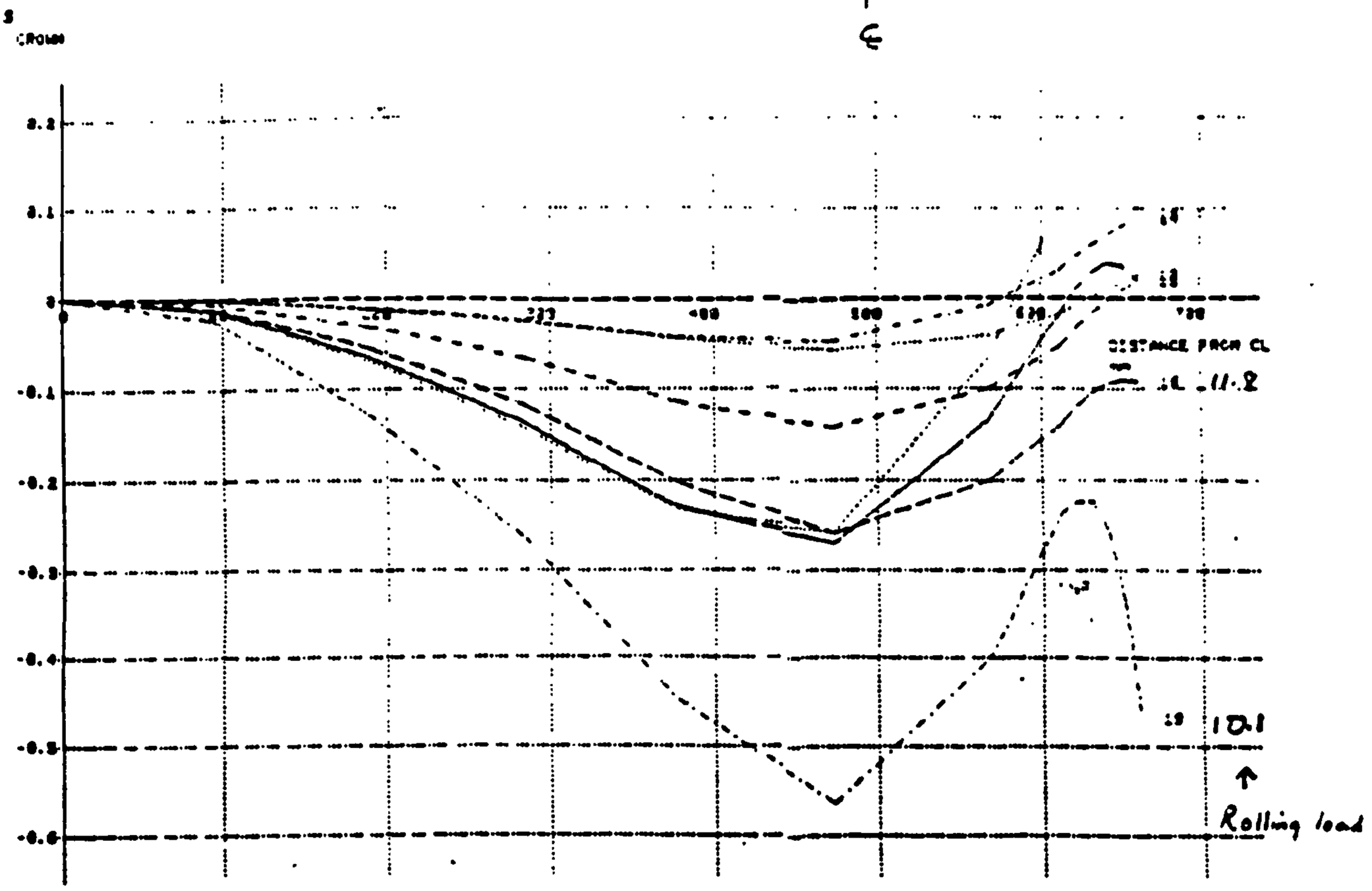

(B) HOT MILL SLAB 3004/1. RB: 0.1512MM.

Fig.H13. Predicted strip crown in half strip width.
Z slab rolled. Spray levels:

entry	exit
ooo ooo ooo	/// /// /oo

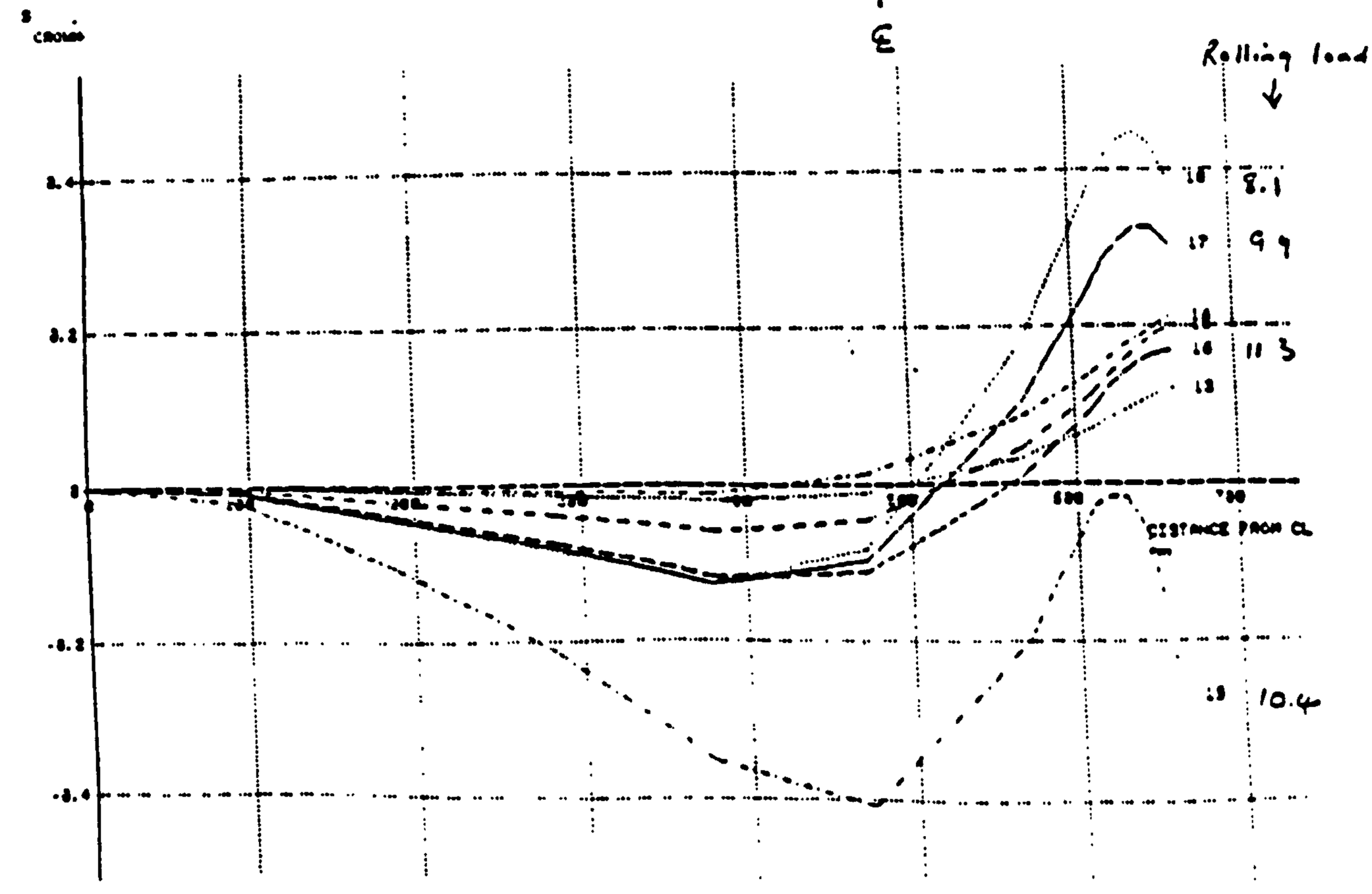

Fig H14 Predicted strip crown in half strip width
9 slab rolled. Spray levels:

entry	exit
ooo ooo ooo	/// /// /oo

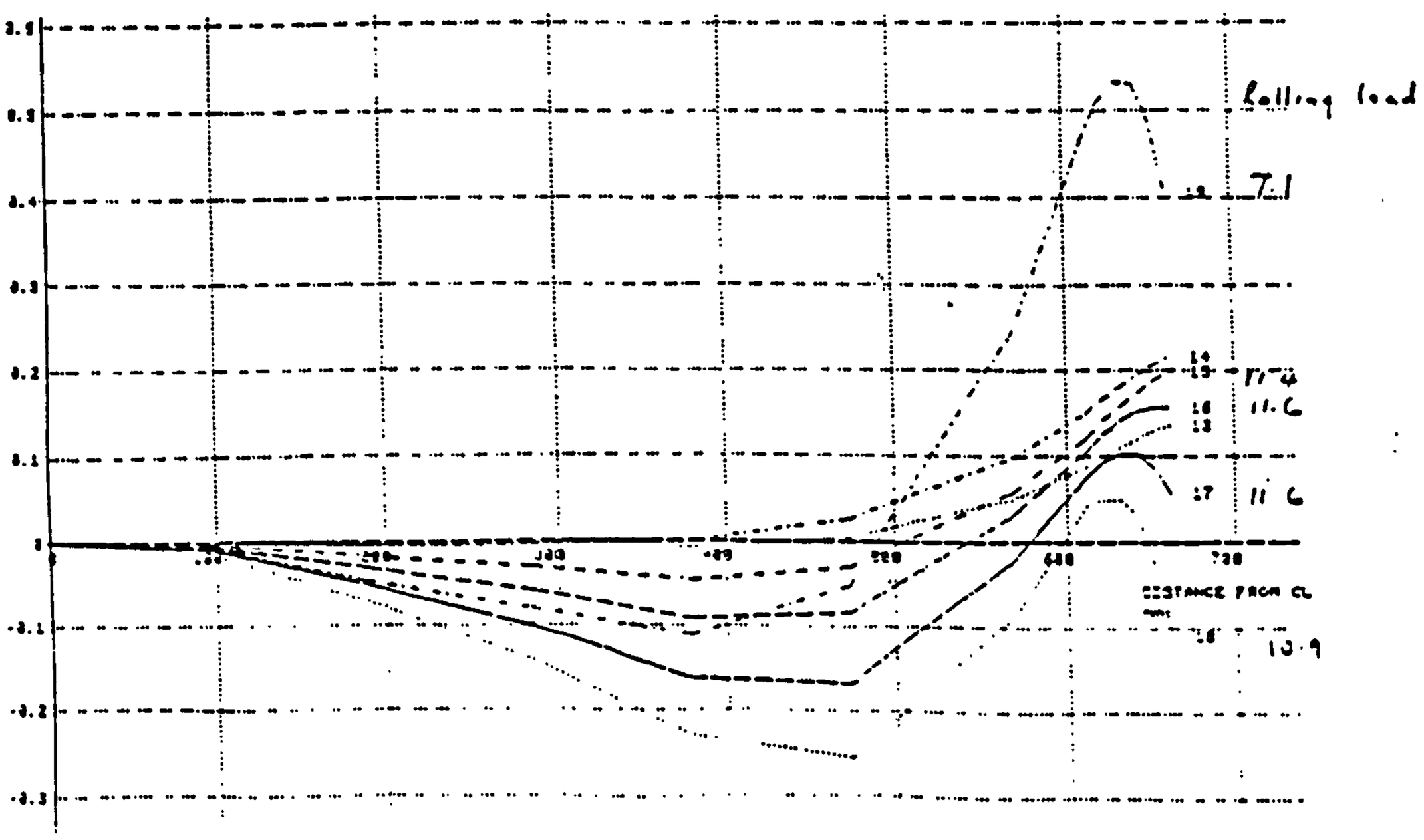

Fig H15 Predicted strip crown in half strip width
9 slab rolled. Spray levels.

entry	exit
000 000 000	222 333 333

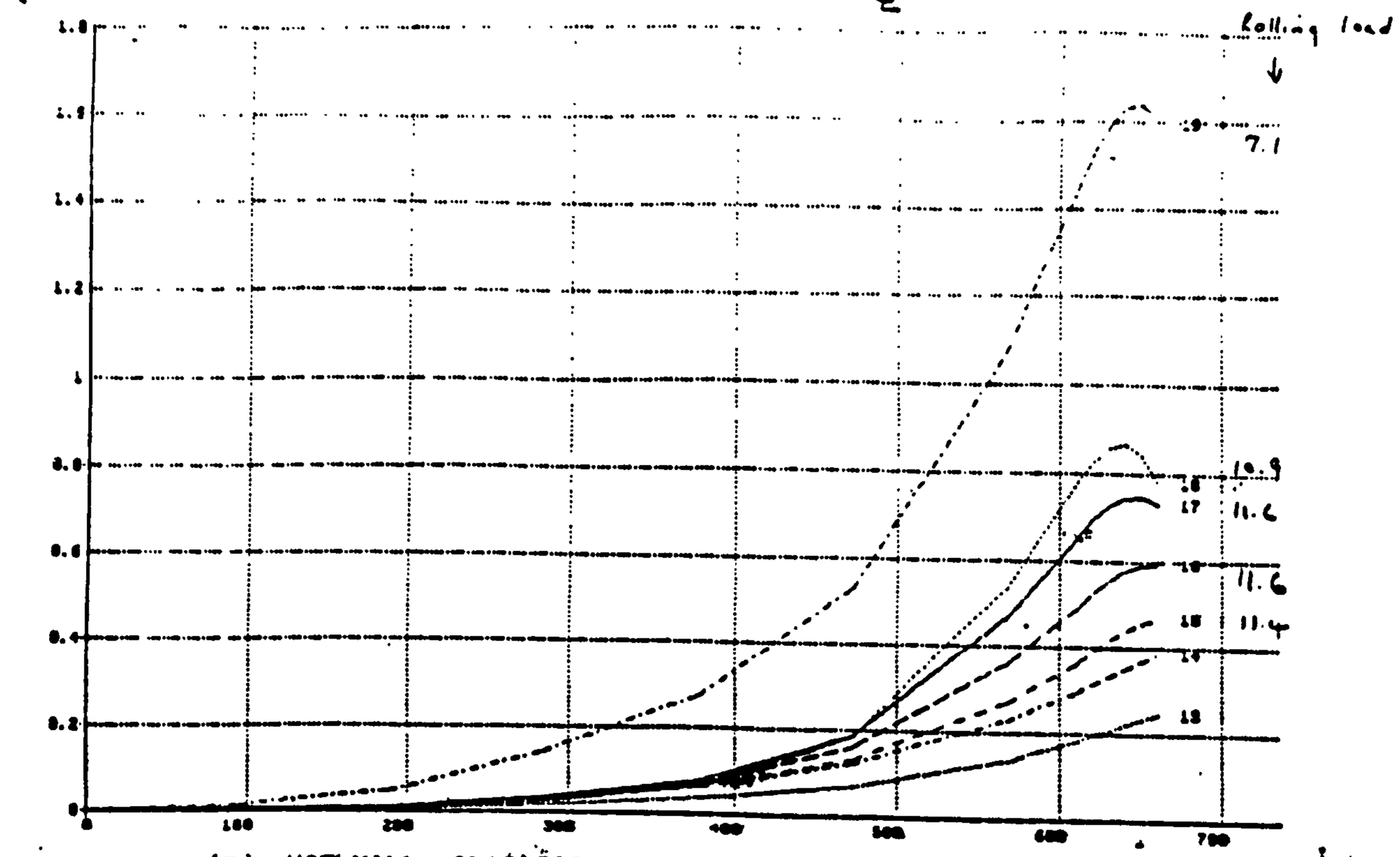

(B) HOT MILL SLAB 3004/9. RB: 0.512MN.

Fig. H16 Predicted strip crown in half strip width.
9 slab rolled. Spray levels:

entry	exit
000 000 000	222 333 300

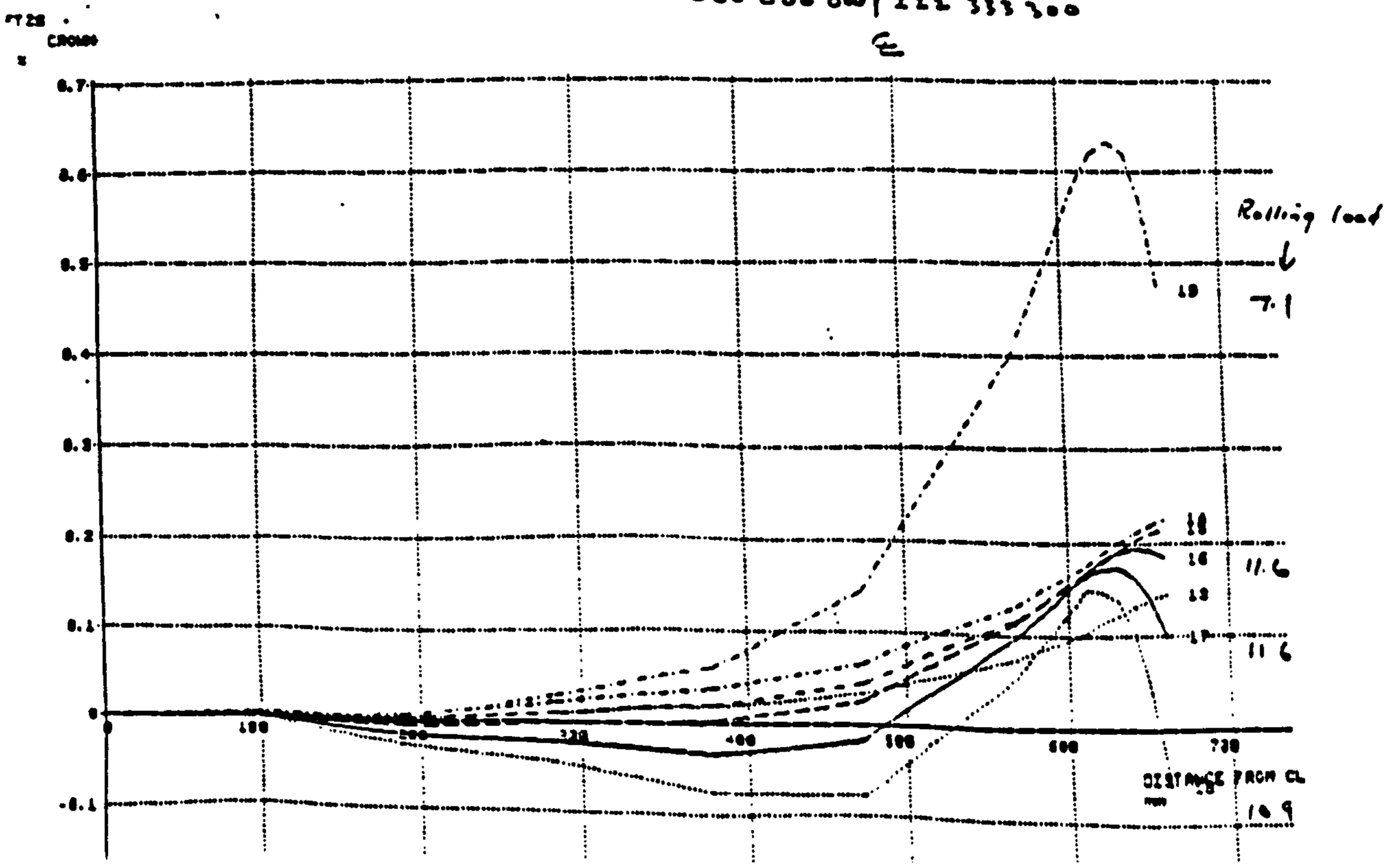

Fig. H17 Predicted strip crown in half strip width
4 slab rolled. Spray levels.

entry	exit
○○○ ○○○ ○○○	/// /// ///

℄

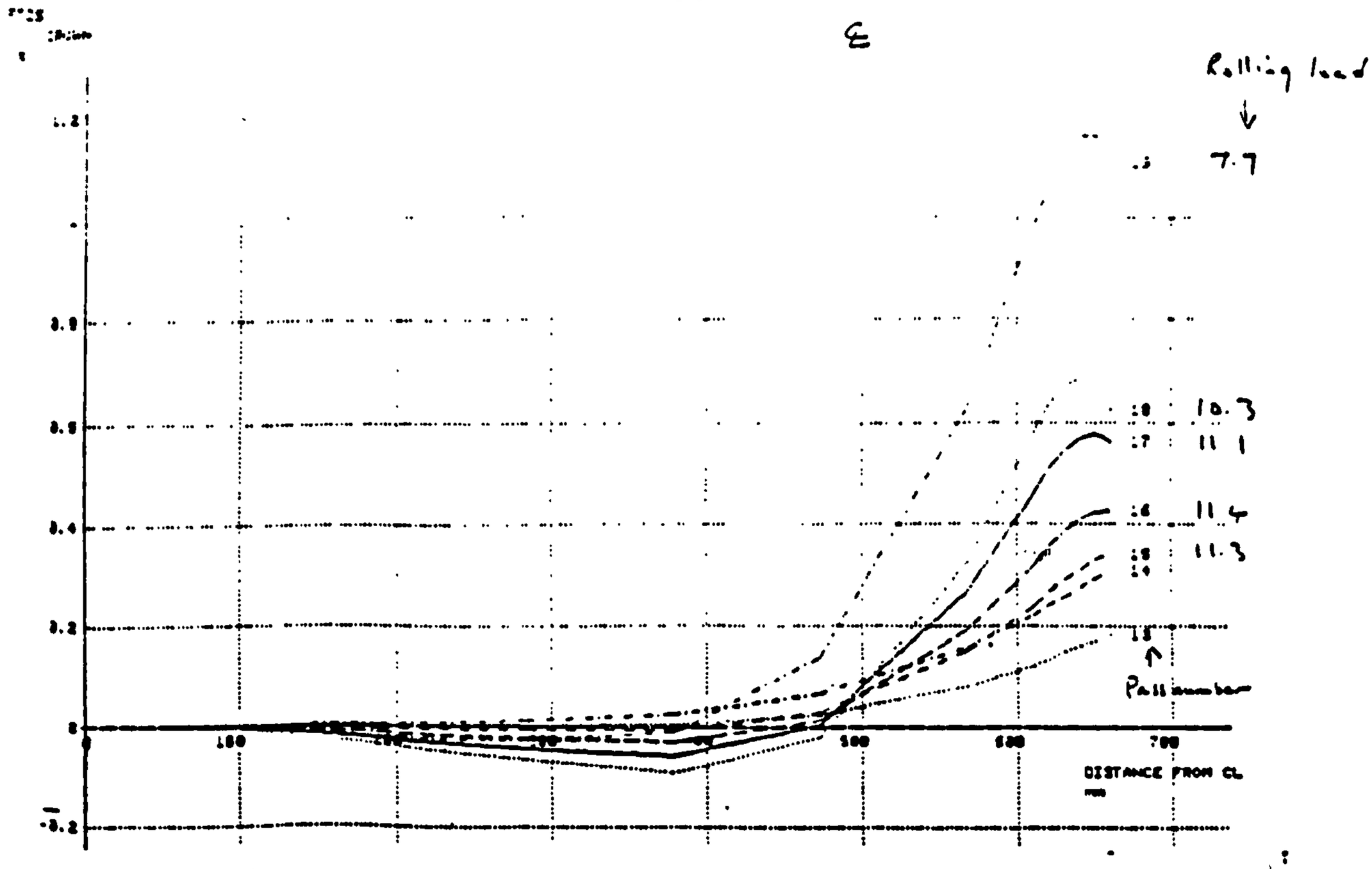

(B) HOT MILL SLAB 3004/4. RB: 0.512MN.

Fig H18 Predicted strip crown in half strip width.
9 slab rolled. Spray levels:

entry	exit
○○○ ○○○ ○○○	/// /// ///

℄

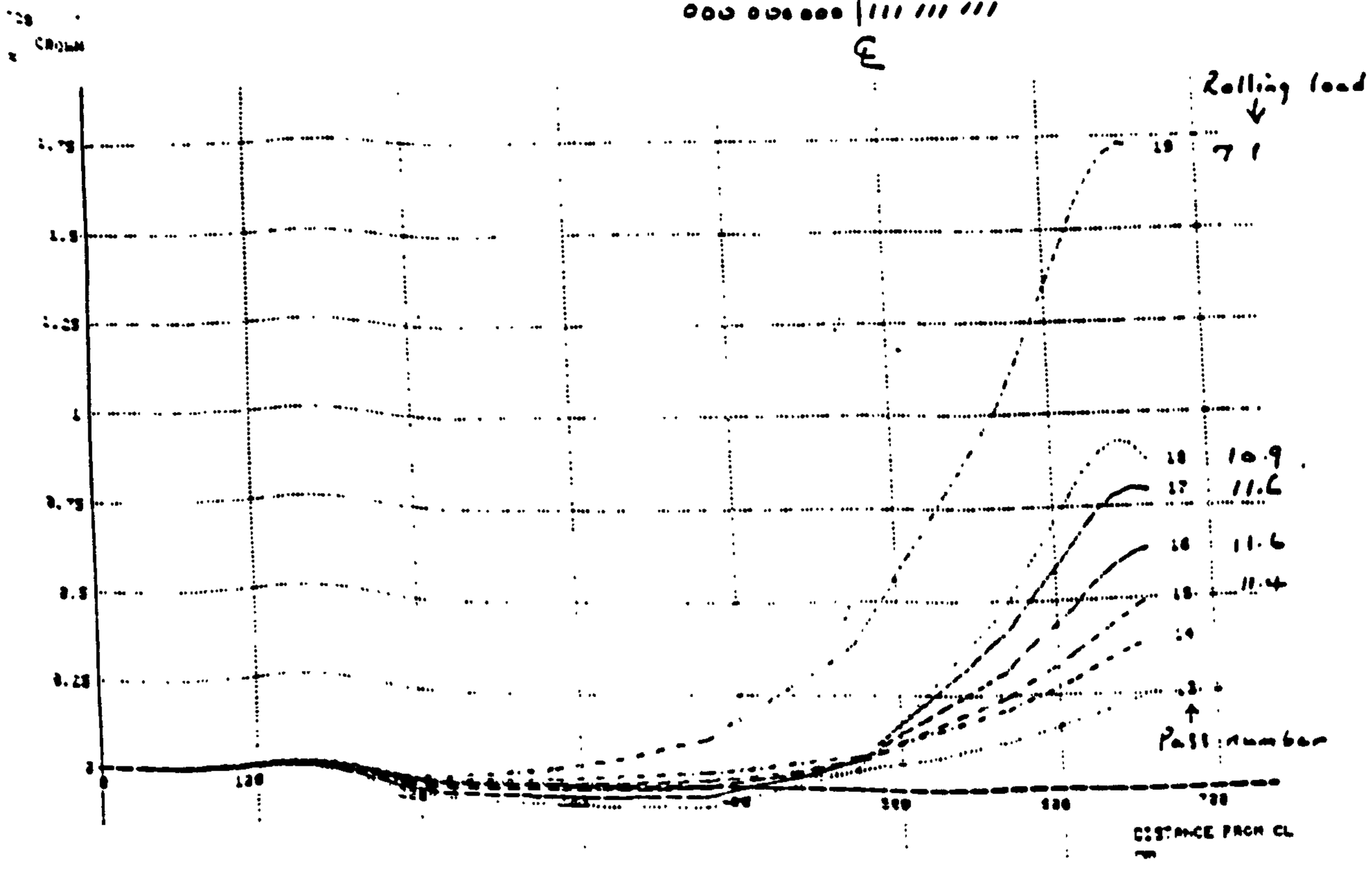

Fig. H19 General relationship between strip profile and work roll bending force at a particular location in the strip and fixed roll load.

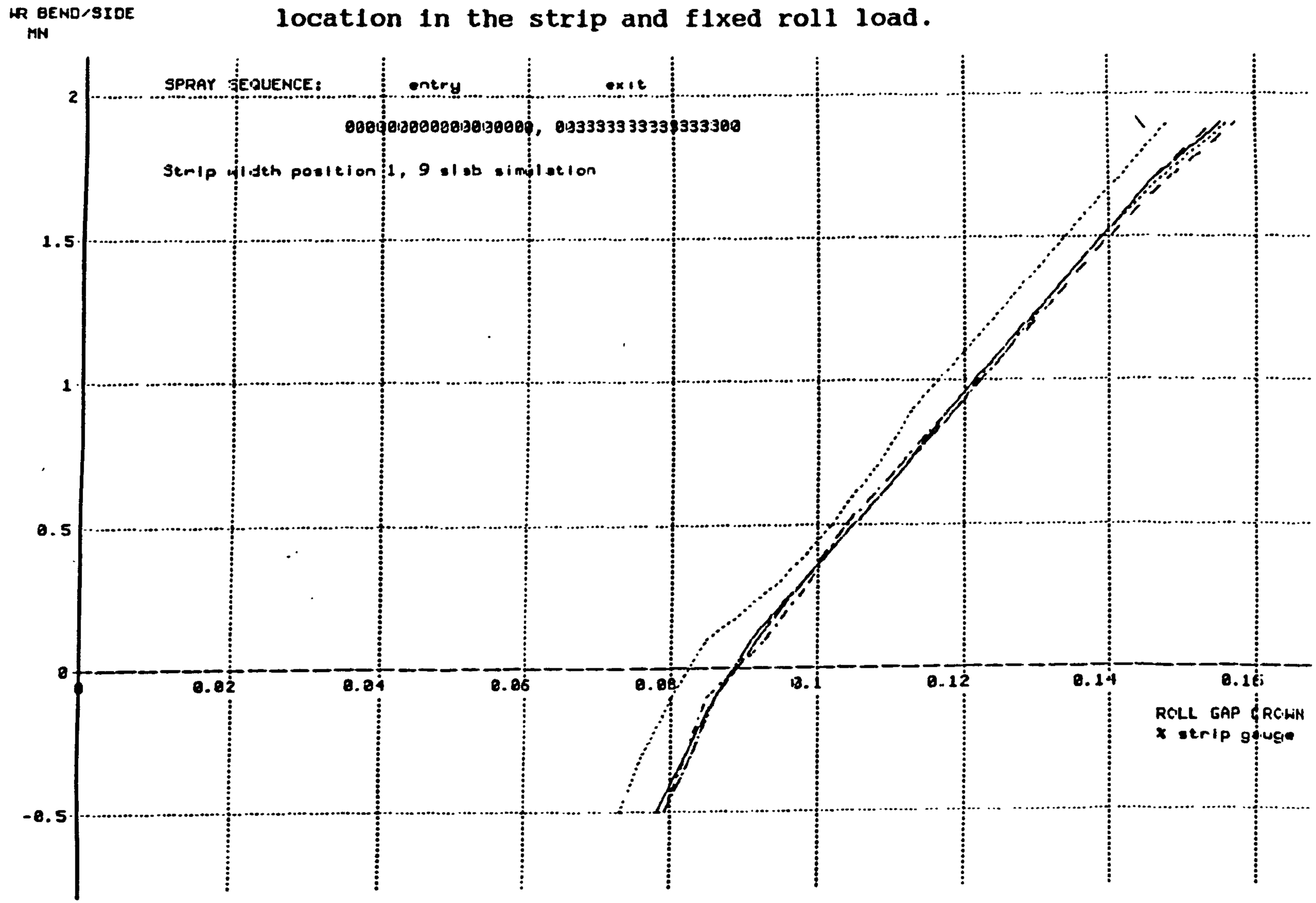

Mill B /3004 SLAB 1 /RL=10MN

Fig. H20 General relationship between strip profile and work roll bending force at a particular location in the strip and fixed roll load.

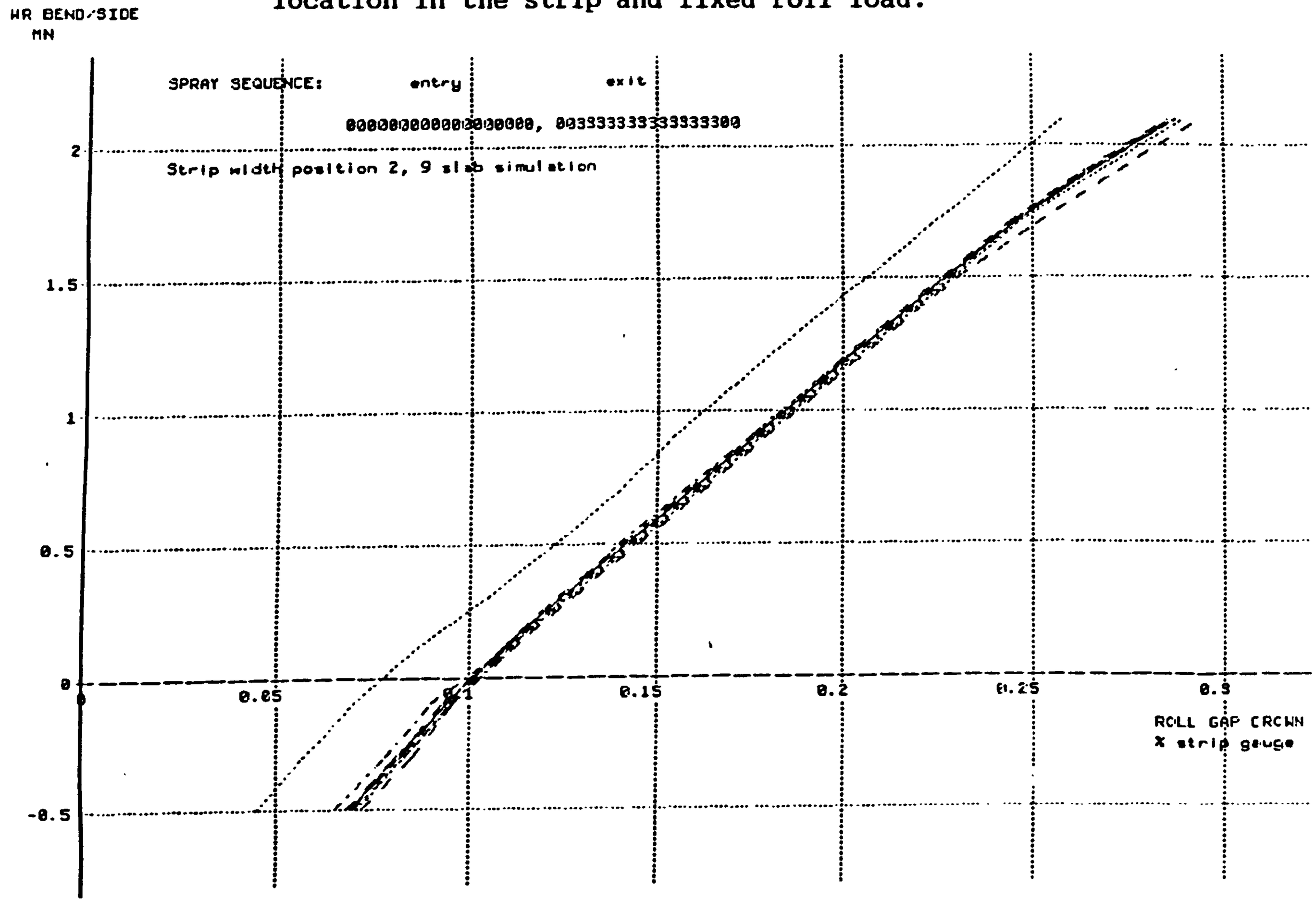

Mill B /3004 SLAB /RL=10MN

Fig. H21 General relationship between strip profile and work roll bending force at a particular location in the strip and fixed roll load.

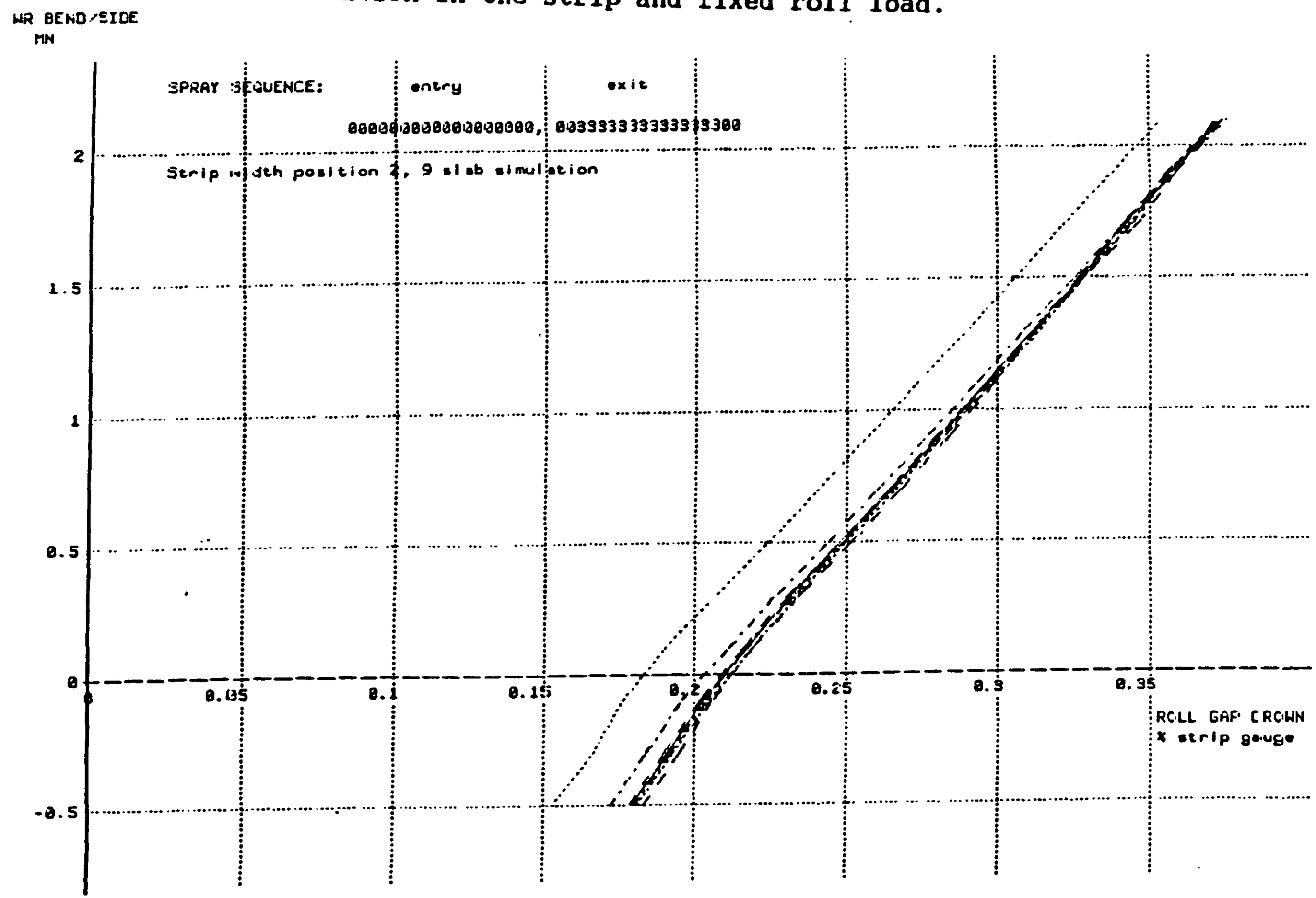

Mill B '3004 SLAB /RL=25MN

Fig. H22 General relationship between strip profile and work roll bending force at a particular location in the strip and fixed roll load.

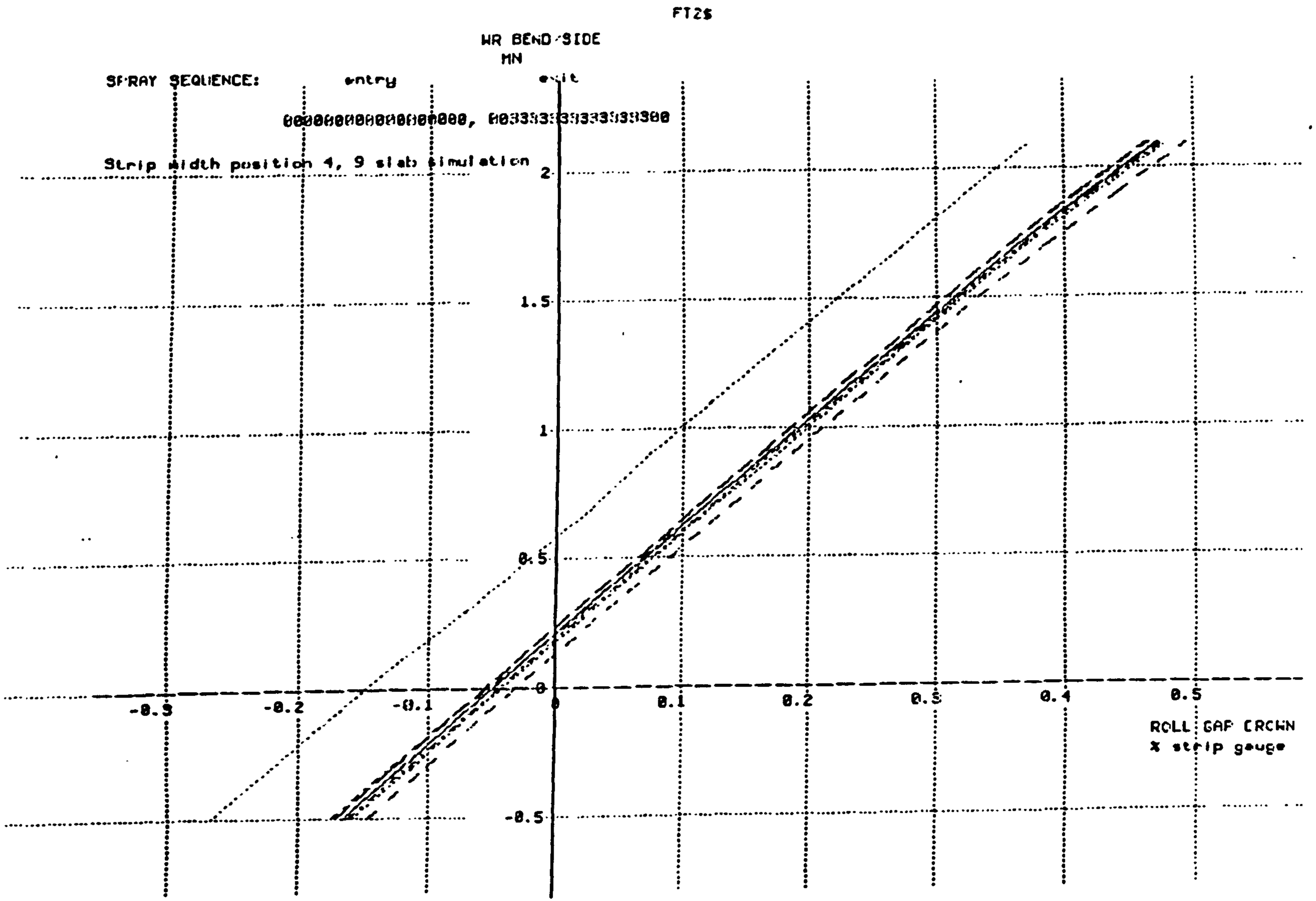

Mill B /3004 SLAB /RL=10MN

Fig. H23 The effect on Strip Profile caused by changes in work roll bending force at different strip positions (Slab 1). The Rolling load is set at 10 MN.

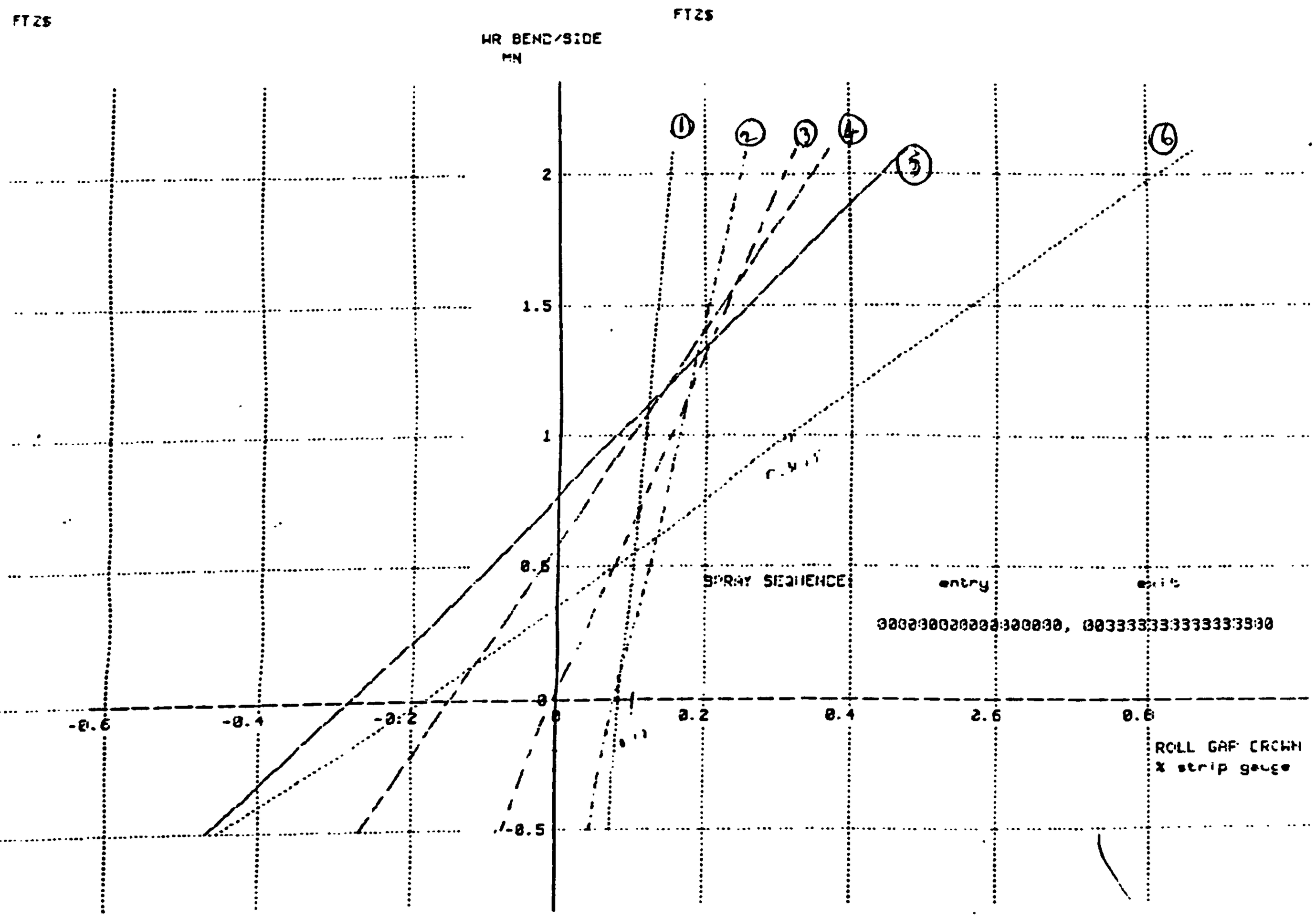

/3004 SLAB 1/RL=10MN

Fig. H24 The effect on Strip Profile caused by changes in work roll bending force at different strip positions (Slab 1). The Rolling load is set to 25 MN.